UNIVERSITAT POLITÈCNICA DE VALÈNCIA

INSTITUTO INTERUNIVERSITARIO DE INVESTIGACIÓN
DE RECONOCIMIENTO MOLECULAR
Y DESARROLLO TECNOLÓGICO

Smart microdevices for nutraceutical-controlled delivery

PhD Thesis

Submitted by

Elisa Poyatos Racionero

PhD Supervisors

Prof. María Dolores Marcos Martínez

Dra. Andrea Bernardos Bau

Dra. Elena Aznar Gimeno

Valencia, October 2020

MARÍA DOLORES MARCOS MARTÍNEZ, PhD in Chemistry and Professor at the *Universitat Politècnica de València*, ANDREA BERNARDOS BAU, PhD in Chemistry and ELENA AZNAR GIMENO, PhD in Chemistry

CERTIFY:

That the work "**Smart microdevices for nutraceutical-controlled delivery**" has been developed by Elisa Poyatos Racionero under their supervision in the Instituto Interuniversitario de Investigación de Reconocimiento Molecular y Desarrollo Tecnológico (IDM) of the *Universitat Politècnica de València* and the Centro de Investigación en Red (CIBER), as a Thesis Project in order to obtain the degree of PhD in Chemistry from the *Universitat Politècnica de València*.

Valencia, October 2020.

Prof. María Dolores Marcos Martínez Dra. Andrea Bernardos Bau Dra. Elena Aznar Gimeno

Ningún mar en calma
hizo experto a un marinero

Acknowledgements

Agradecimientos

Después de muchos años, llega el momento de escribir la parte de la Tesis en la que más he pensado desde el primer día que la comencé. Algo profundamente vocacional se convirtió en una búsqueda, y los giros de la vida me hicieron llegar a Valencia. Así que, en primer lugar, gracias a Ramón Martínez por brindarme la oportunidad y abrirme las puertas del IDM para conseguirlo. Gracias Félix por tu ayuda en los momentos que la he necesitado. Gracias a la Generalitat Valenciana por la financiación de mi tesis. Gracias por supuesto a mis directoras, Elena, Loles y Andrea, por vuestro tiempo y trabajo. Me siento muy halagada de haber tenido una tesis dirigida por mujeres, con lo que esto significa para la Ciencia en general. Loles, gracias por haber luchado por mí, gracias por el afecto que he recibido de ti siempre. Andrea, gracias por haber estado ahí siempre desde que te conozco, por haber aguantado los buenos y los malos momentos, y por haber zanjado cada uno de los malos con un abrazo, además de por tus consejos científicos. Has sido un apoyo fundamental durante estos años, y sobre todo en los últimos tramos.

Escribí los agradecimientos de mi tesis el último día que estuve en el laboratorio sola. Ese día despejé mi mesa, y me deshice de lo que ya no iba a volver a necesitar. Artículos que creí importantes, y que gracias a Mendeley nunca más volví a mirar, fueron a la papelera; y cientos de sólidos obsoletos y "porsiacasos" a residuos. Ese día sentí que se rompía un lazo y que terminaba una etapa, que decía adiós a un laboratorio del que espero llevarme tanto como creo que le he dado. Ese día decidí que era momento de dejar caer las lágrimas y escribir estas palabras. Para mí sin duda la parte más importante de la tesis, porque recoge los sentimientos más sinceros y no únicamente los resultados conseguidos.

Es difícil agradecer tanto y a tanta gente en solo unas páginas sin extenderse demasiado. Cuando el que defiende su tesis es alguien que nos importa, siempre leemos esta sección para ver nuestro nombre escrito y el recuerdo que se lleva de nosotros. Si, aunque no encuentres tu nombre en estas líneas, eres de los que mi marcha te apena, ten claro que yo también te echaré de menos y guardaré buen recuerdo de ti. Siempre tendrás mi confianza y si lo necesitas, mi consejo, no importa el tiempo que pase. *En Hogwarts siempre se prestará ayuda a quien la pida.*

Desde que tengo uso de razón, siempre quise investigar. Estudié Química porque la idea de trabajar en un laboratorio era lo que realmente me hacía feliz. Le agradezco al destino los compañeros que ahí tuve, y que a día de hoy siguen siendo una parte de mi vida: Diana, María Plana, Alberto, Arturo e Iván: gracias por estar ahí pese a la distancia y a los años que nos intentan separar; es siempre un placer volver a pasar tiempo con vosotros. Le agradezco también al primer contacto que tuve con la ciencia, donde encontré a Cristina Martín: agradezco lo que aprendí, la confianza y la cercanía que siempre me demostró y que guardo con cariño; gracias por mantener el contacto, y por seguir ayudándome a día de hoy. En otra etapa diferente, le agradezco a Félix Jalón los ratos lavando productos de reacción conmigo, gracias por alegrarme las tardes cuando entraba llamándome Elisita al laboratorio; siempre serás un ejemplo para mí. Y sobre todas esas cosas, le agradezco a Toledo el haberme brindado a dos personas excepcionales: Elo y María, de verdad sois un tesoro del que nunca me quiero desprender.

En el siguiente salto temporal, les agradezco ese magnífico año a todos los compañeros del máster en Biofísica de la Universidad Autónoma de Madrid. Le agradezco a Ricardo Arias la oportunidad que me dio de aprender sobre un mundo completamente nuevo para mí. A Sara y a Fer les agradezco el haberme escuchado en muchos momentos y haberme hecho reír en tantos otros. Por supuesto a Irene, además de todo eso, el haber sido otro gran ejemplo para mí; aprendí mucho a tu lado, como Química y como persona, y no de todo el mundo se puede decir lo mismo. A Antonio y a Alberto les agradezco el haber hecho del piso un lugar mejor; fue un placer convivir con vosotros. A Alberto le agradezco además los siguientes cuatro años de genial convivencia.

Mi etapa investigadora termina, de momento, en el doctorado. Un innumerable goteo de personas que sería difícil de cuantificar, y que es imposible nombrar por completo. Hay mucha gente a la que me ha alegrado ver cuando he entrado al laboratorio, pero quiero nombrar especialmente a Carmen, María Alfonso, Borja, Xente, Eva, Angy y Bea de Luis; Bea, aún tengo esa tarta grabada en mi mente, no creas que se me va a olvidar nunca tu sonriente presencia en

momentos críticos. Y cambiando de laboratorio a mi querida CPI, por supuesto Mar, Édgar, María Ruiz, Luis Pla, Adri y Santi; hemos compartido tantas horas y tantos recuerdos juntos, que es imposible no llevaros en el corazón. También a las chicas Fuentes de alimentos, Cristi y Ana, gracias por vuestra luz y vuestro carisma, ojalá en todos los sitios hubiese alguien como vosotras. Y finalmente, a Cris T, Sara, Carol, Nataly, Serena y Gemma. De verdad que habéis hecho brillar el sol en muchos días grises, habéis sido una parte fundamental de mi vida en Valencia y espero no perderos jamás, dé la vida las vueltas que dé.

No me gustaría acabar estas palabras sin agradecer a toda la gente del COMAV con la que he pasado tantos ratos en estos años. He aprendido muchísimo con vosotros, y me he reído aún más. Gracias por haberme hecho una más de este edificio. Gracias especialmente a Santi, Mariola, Pietro, Javi, Édgar, Estefanía, David y Carla. De verdad que ha sido un placer conoceros. Siempre recordaré con añoranza el cubo rojo.

In addition, I would like to thank all the people I met during my international stay in Italy. I never thought that I would feel part of a group only spending three months there. I want to thank Dr. Pier Paolo Pompa, for the opportunity of being part of the Nanobiointeractions group during that time, and also to all the teammates, Giuliet, Vale, Giusy, Leo, Paolo, Fabri, Fra... Thank you for your warmth and your unquantifiable help. Gracias especialmente a Paola y a Saúl, porque de verdad fuisteis un apoyo imprescindible durante esos tres meses, nada como reírse en tu idioma. Me alegra el alma cada vez que volvemos a ponernos en contacto.

Gracias al grupo de Alicante por ese mes que pasé con vosotros. De verdad no voy a olvidar el ambiente que se respiraba en ese laboratorio. Gracias a Marta, Alejandro y Bárbara por vuestra ayuda, a Emilio por su simpatía y la alegría que desprende, y a Isa, gracias por todo. Ha sido un auténtico placer conocerte y trabajar contigo. Es inspirador sentir que alguien ve la Ciencia con tus mismos ojos.

Como casi todo el mundo, dejo lo mejor para el final. **GRACIAS** a mi familia, por su apoyo incondicional pese a ver la vida tan dura que implica la investigación.

La distancia y las lágrimas deberían haber hecho que cualquier familia te recomendase otro camino, pero supongo que vosotros también habéis sido capaces de ver la vocación en este trabajo. Gracias a mis tíos por su cercanía e interés en mi bienestar en esta aventura. Gracias a mi padre, por su trabajo dedicado siempre a la familia y por esa forma de ser tan transparente que sin duda he heredado. Gracias a mi madre, por ser un ejemplo de comprensión, coraje y abnegación por los demás. Mamá, eres un referente para mí, por saber valorar las cosas importantes de la vida, y ser capaz de ver siempre el lado bueno de las personas de tu alrededor; no puedo hacer otra cosa, laboralmente hablando, que llevar tu apellido allí donde quiera que firme. Gracias Elena por quererme incondicionalmente, por aguantar mi carácter y mi sobreprotección a veces, desde que tú vives y yo tengo uso de razón; estoy muy orgullosa de ti, y quiero aprovechar la oportunidad que me brinda el escribir estas palabras para que quede reflejado. Y, por último, gracias Rubén. No podría haberme llevado mejor fortuna de todo este camino que a ti. Gracias por ver siempre lo bueno que hay en mí, y por haber sido mi luz en todos los momentos de oscuridad que me he encontrado durante los años que hemos compartido juntos. Y gracias por esa familia política que me has brindado y que me acogió desde el primer día.

Y finalmente, a las dos personas que nunca aparecen en esta lista de agradecimientos, pero que yo considero fundamentales. Gracias a *ti* y a *mí*. Gracias a mí misma por no haber tirado la toalla, por el afán de superación y consecución de las metas; recuerda tus cosas buenas, aunque tengas otras muchas que mejorar. Si alguna vez vuelves a leer estas palabras, no olvides ninguna de las dos facetas. Y a *ti* que lees esto, aparezca tu nombre o no en estas páginas, si alguna vez me has hecho sonreír, gracias. Nunca sobran sonrisas sinceras ni agradecimientos en la vida, y esa es una esencia que nunca deberíamos perder.

"La felicidad se puede hallar hasta en los más oscuros momentos,
si somos capaces de usar bien la luz". Albus Dumbledore

Resumen

La presente tesis doctoral, titulada "Microportadores inteligentes para la liberación controlada de sustancias de interés nutracéutico", se centra en el diseño y evaluación de sistemas híbridos orgánico-inorgánicos para la protección y liberación controlada de compuestos bioactivos. Dichos sistemas están basados en *(i)* materiales de sílice, principalmente partículas mesoporosas, como soporte inorgánico para almacenar y proteger la carga bioactiva; y *(ii)* en una capa externa de biomoléculas que regulan la liberación de dicha carga ante determinados estímulos.

El primer capítulo de la tesis trata sobre el empleo del *ácido oleico* como *puerta molecular* capaz de regular el confinamiento y salida de compuestos encapsulados mediante un determinado estímulo (surfactantes como las sales biliares). Este capítulo se subdivide a su vez en tres artículos diferentes, en los cuales se persiguen objetivos distintos para la misma puerta molecular.

En el primer artículo se ha desarrollado una nueva puerta molecular basada en ácido oleico, y se ha validado su capacidad de retener las moléculas cargadas en el interior de los poros y liberarlas exclusivamente en el intestino delgado. El sistema consta de un soporte inorgánico (SBA-15), cargado con la molécula modelo rodamina B, funcionalizado con grupos amina sobre los que se ancla el ácido oleico mediante enlace covalente. El material preparado es capaz de proteger la carga en las condiciones presentes en la boca y en el estómago, e inducir su liberación en el intestino. Finalmente, se ha validado el sistema para la liberación de vitamina B_2, demostrando así la utilidad del diseño para la protección y liberación controlada de moléculas bioactivas en las condiciones del intestino delgado.

El segundo artículo evalúa la efectividad de esta puerta molecular en diferentes tipos de partículas mesoporosas de sílice, con diversos tamaños y estructuras de poro (MCM-41, MCM-48, SBA-15 y UVM-7). En todos los sistemas estudiados, la puerta molecular es capaz de mantener protegidas las moléculas albergadas dentro de la estructura porosa, y liberarlas ante la presencia de sales

biliares, demostrándose además que el perfil de liberación depende de la estructura del material inorgánico empleado. Finalmente, el sólido basado en la estructura de UVM-7 se validó en un modelo *in vivo* con ratas Wistar, observándose un retraso en la absorción intestinal de la rodamina al administrarla empleando el sistema diseñado.

Por último, el tercer artículo incluido en este capítulo ha estudiado la posibilidad de incorporar puertas moleculares a filosilicatos. Estos materiales han sido empleados para liberación pasiva, pero no se habían protegido con puertas moleculares que permitiesen la liberación activa de las moléculas encapsuladas tras la acción de un estímulo específico. En este trabajo, se ha conseguido la protección y liberación controlada tanto de moléculas modelo (rodamina B) como de biomoléculas de gran tamaño implicadas en el metabolismo humano (vitamina B_{12} y hematina) empleando filosilicatos funcionalizados con ácido oleico como puerta molecular.

El segundo capítulo describe nuevos sistemas en los que se emplea por primera vez la proteína *zeína* (prolamina de maíz) como puerta molecular. Esta biomolécula, a pesar de su amplio uso en el ámbito alimentario, no ha sido empleada en el desarrollo de sistemas de liberación controlada basados en puertas moleculares. Se ha preparado una colección de partículas mesoporosas de sílice cargadas con diferentes componentes de aceites esenciales (EOCs, por sus siglas en inglés) y funcionalizadas con *zeína*. En los sistemas preparados, la presencia de la prolamina de maíz inhibe la salida de los EOCs encapsulados (timol, carvacrol y cinamaldehído) de manera que estos solo se liberan en presencia de las enzimas proteolíticas excretadas durante el crecimiento bacteriano, capaces de degradar la proteína que bloquea los poros. De todos los materiales desarrollados, el sistema cargado con cinamaldehído ha demostrado una inhibición del crecimiento de *E. coli* mucho mayor que el compuesto libre.

Finalmente, el tercer capítulo estudia la efectividad de la *lactosa* como puerta molecular capaz de proteger aceites esenciales y liberarlos solo en las condiciones presentes en el intestino delgado. Se han preparado tres materiales diferentes

basados en MCM-41, cargados con timol, eugenol y cinamaldehído y funcionalizados con lactosa para inhibir la salida de los EOCs. Así, solo la acción enzimática de la lactasa secretada por las microvellosidades intestinales es capaz de hidrolizar la puerta molecular en los correspondientes monosacáridos, eliminando el impedimento estérico que mantiene encapsulada la carga, y permitiendo así su liberación a lo largo del lumen intestinal. Los microdispositivos diseñados han sido validados en modelos *in vitro* con células Caco-2, donde se ha observado la internalización de las partículas por las células, y el aumento de la capacidad citotóxica del cinamaldehído gracias a su encapsulación. También se ha observado *in vitro* que la encapsulación de los EOCs en los microdispositivos protegidos con lactosa disminuye su permeabilidad a través de la membrana intestinal, aumentando así el tiempo de permanencia del compuesto en el lumen y su liberación progresiva con la acción de la lactasa secretada. Finalmente, el microdispositivo cargado con cinamaldehído se ha validado en un modelo *in vivo* (rata Wistar), ratificándose la disminución de la permeabilidad del cinamaldehído observada *in vitro* y una mayor permanencia del EOC en el lumen gastrointestinal.

Así, la presente tesis doctoral ha demostrado la posibilidad de emplear biomoléculas sencillas de grado alimentario como puertas moleculares sobre una amplia variedad de materiales de sílice. Estos nuevos sistemas han permitido encapsular diferentes compuestos nutracéuticos, tanto volátiles como de gran tamaño, para su protección y liberación controlada, mejorando así su bioactividad y biodisponibilidad. De este modo, se ha dado un paso más en el uso de la nanotecnología para potenciar las propiedades de biomoléculas naturales con fines farmacológicos.

Resum

La present tesi doctoral, titulada "Microportadors intel·ligents per l'alliberament controlat de substàncies d'interès nutracèutic", se centra en el disseny i avaluació de sistemes híbrids orgànic-inorgànics per a la protecció i alliberament controlat de compostos bioactius. Aquests sistemes estan basats en (i) materials de sílice, principalment partícules mesoporoses, com a suport inorgànic per emmagatzemar i protegir la càrrega bioactiva; i (ii) en una capa externa de biomolècules que regulen l'alliberament d'aquesta càrrega davant de determinats estímuls.

El primer capítol de la tesi tracta sobre l'ús de l'*àcid oleic* com a porta molecular capaç de regular el confinament i eixida de compostos encapsulats mitjançant un determinat estímul (surfactants com les sals biliars). Aquest capítol se subdivideix al seu torn en tres articles diferents, en els quals es persegueixen objectius diferents per a la mateixa porta molecular.

En el primer article s'ha desenvolupat una nova porta molecular basada en àcid oleic, i s'ha validat la seua capacitat de retenir les molècules carregades a l'interior dels porus i d'alliberar-les exclusivament a l'intestí prim. El sistema consta d'un suport inorgànic (SBA-15), carregat amb la molècula model rodamina B, funcionalitzat amb grups amina sobre els quals s'ancora l'àcid oleic mitjançant enllaç covalent. El material preparat és capaç de protegir la càrrega en les condicions presents a la boca i a l'estómac, i induir el seu alliberament a l'intestí. Finalment, s'ha validat el sistema per a l'alliberament de vitamina B_2, i s'ha demostrat així la utilitat del disseny per a la protecció i alliberament controlat de molècules bioactives en les condicions de l'intestí prim.

El segon article avalua l'efectivitat d'aquesta porta molecular en diferents tipus de partícules mesoporoses de sílice, amb diverses mides i estructures de porus (MCM-41, MCM-48, SBA-15 i UVM-7). En tots els sistemes estudiats, la porta molecular és capaç de mantenir protegides les molècules albergades dins de l'estructura porosa, i alliberar-les davant la presència de sals biliars. En el treball

s'ha demostrat que el perfil d'alliberament depèn de l'estructura del material inorgànic empleat. Finalment, el sòlid basat en l'estructura de UVM-7 es va validar en un model *in vivo* amb rates Wistar, i es va observar un retard en l'absorció intestinal de la rodamina a administrar-la emprant el sistema dissenyat.

Finalment, en el tercer article inclòs en aquest capítol s'ha estudiat la possibilitat d'incorporar portes moleculars a fil·losilicats. Aquests materials han estat emprats per alliberament passiu, però no s'havien protegit amb portes moleculars per tal d'aconseguir un alliberament actiu de les molècules encapsulades després de l'acció d'un estímul específic. En aquest treball, s'ha aconseguit la protecció i alliberament controlat tant de molècules model (rodamina B) com de biomolècules de grans dimensions implicades en el metabolisme humà (vitamina B_{12} i hematina) emprant fil·losilicats funcionalitzats amb àcid oleic com a porta molecular.

El segon capítol descriu nous sistemes en els quals s'empra per primera vegada la proteïna *zeïna* (prolamina de dacsa) com a porta molecular. Aquesta biomolècula, tot i el seu ampli ús en l'àmbit alimentari, no ha estat emprada en el desenvolupament de sistemes d'alliberament controlat basats en portes moleculars. S'ha preparat una col·lecció de partícules mesoporoses de sílice carregades amb diferents components d'olis essencials (EOCs, per les seues sigles en anglès) i funcionalitzades amb zeïna. En els sistemes preparats, la presència de la prolamina de dacsa inhibeix l'eixida dels EOCs encapsulats (timol, carvacrol i cinamaldèhid) de manera que aquests només s'alliberen en presència dels enzims proteolítics excretats durant el creixement bacterià, capaços de degradar la proteïna que bloqueja els porus. De tots els materials desenvolupats, el sistema carregat amb cinamaldèhid ha demostrat una inhibició del creixement d'*E. coli* molt major que el compost lliure.

Finalment, el tercer capítol estudia l'efectivitat de la *lactosa* com a porta molecular capaç de protegir olis essencials i alliberar-los només en les condicions presents en l'intestí prim. S'han preparat tres materials diferents basats en MCM-41, carregats amb timol, eugenol i cinamaldèhid i funcionalitzats amb lactosa per a

inhibir l'eixida dels EOCs. Així, només l'acció enzimàtica de la lactasa secretada per les microvellositats intestinals és capaç d'hidrolitzar la porta molecular en els corresponents monosacàrids, eliminant l'impediment estèric que manté encapsulada la càrrega, i permetent així el seu alliberament al llarg del lumen intestinal. Els microdispositius dissenyats han estat validats en models *in vitro* amb cèl·lules Caco-2, on s'ha observat la internalització de les partícules per les cèl·lules, i l'augment de la capacitat citotòxica del cinamaldèhid gràcies a la seua encapsulació. També s'ha observat *in vitro* que l'encapsulació dels EOCs en els microdispositius protegits amb lactosa disminueix la seua permeabilitat a través de la membrana intestinal, augmentant així el temps de permanència del compost en el lumen i el seu alliberament progressiu amb l'acció de la lactasa secretada. Finalment, el microdispositiu carregat amb cinamaldèhid s'ha validat en un model *in vivo* (rata Wistar), on s'ha pogut ratificar la disminució de la permeabilitat del cinamaldèhid observada *in vitro* i una major permanència de l'EOC al lumen gastrointestinal.

Així, la present tesi doctoral ha demostrat la possibilitat d'emprar biomolècules senzilles de grau alimentari com portes moleculars sobre una àmplia varietat de materials de sílice. Aquests nous sistemes han permès encapsular diferents compostos nutracèutics, tant volàtils com de grans dimensions, per a la seua protecció i alliberament controlat, millorant així la seua bioactivitat i biodisponibilitat. D'aquesta manera, s'ha donat un pas més en l'ús de la nanotecnologia per a potenciar les propietats de biomolècules naturals amb fins farmacològics.

Abstract

This PhD thesis, entitled "Smart microdevices for nutraceutical-delivery", is focused on the design and evaluation of organic-inorganic hybrid systems for the protection and controlled release of bioactive molecules. These systems are based on *(i)* silica materials, mainly mesoporous particles, as inorganic support to store and protect the bioactive cargo; and *(ii)* in an outer layer of biomolecules that regulate the payload release triggered by certain stimuli.

The first chapter of the thesis deals with the use of *oleic acid* as a molecular gate capable of regulating the confinement and release of the encapsulated compounds under the presence of a specific stimulus (surfactants like bile salts). This chapter is subdivided into three different articles, in which different objectives are pursued for the same molecular gate.

In the first article, a new molecular gate based on oleic acid has been developed, and its ability to entrap cargo molecules inside the pore voids and release them exclusively in the small intestine has been validated. The system consists of an inorganic support (SBA-15), loaded with the rhodamine B model molecule, and functionalized with amine groups on which oleic acid is anchored by covalent bonding. The designed material is capable of protecting the cargo under the conditions present in the mouth and stomach, and inducing its release in the small intestine. Finally, the system has been used for the release of vitamin B_2, thus demonstrating the validity of the system for the protection and controlled release of bioactive molecules in the conditions of the small intestine.

The second article evaluates the effectiveness of this molecular gate in different types of mesoporous silica particles, with different sizes and pore structures (MCM-41, MCM-48, SBA-15 and UVM-7). In all the systems studied, the molecular gate is able to keep the molecules confined and protected into the porous structure, and only release them in the presence of bile salts. Also, these experiments have evidenced the dependence of the release profile on the structure of the inorganic material used. Finally, the solid based on the structure of UVM-7

was validated in an *in vivo* model of Wistar rat, observing a delay in the intestinal absorption of rhodamine B when administered using the designed system compared with the administration of the free compound.

Lastly, the third article included in this chapter has studied the possibility of incorporating molecular gates onto phyllosilicates. These materials have been used for passive release, but they had not been protected with molecular gates that allow the payload's active release triggered by the action of a specific stimulus. In this work, the protection and controlled release of both model molecules (rhodamine B) and large biomolecules involved in human metabolism (vitamin B_{12} and hematin) have been achieved using phyllosilicates functionalized with oleic acid as molecular gate.

The second chapter describes new systems in which the protein *zein* (corn prolamin) is used for the first time as molecular gate. This biomolecule, despite its wide use in the food sector, has not been used in the development of controlled release systems based on molecular gates. A set of mesoporous silica particles loaded with different essential oil components (EOCs) and functionalized with zein has been prepared. In the designed systems, the presence of the corn prolamin inhibits the release of encapsulated EOCs (thymol, carvacrol and cinnamaldehyde), whose release is exclusively allowed in the presence of proteolytic enzymes excreted during bacterial growth, capable of degrading the protein that blocks the pores. Among all the developed materials, the cinnamaldehyde-loaded system has shown much greater inhibition of *E. coli* growth than the free compound.

Finally, the third chapter studies the effectiveness of lactose as a molecular gate capable of protecting essential oils and releasing them only in the conditions present in the small intestine. Three different materials have been prepared, based on MCM-41 inorganic support, loaded with thymol, eugenol and cinnamaldehyde and functionalized with lactose to inhibit the exit of EOCs. Thus, only the enzymatic action of the lactase secreted by the intestinal microvilli is capable of hydrolyzing the molecular gate into the corresponding monosaccharides, removing the steric hindrance that keeps the payload encapsulated, and thus allowing its release along

the intestinal lumen. The designed microdevices have been validated in *in vitro* models with Caco-2 cells, where the internalization of the particles by the cells has been observed, and the increase in the cytotoxic capacity of cinnamaldehyde thanks to its encapsulation. It has also been observed *in vitro* that the encapsulation of EOCs in the lactose-protected microdevices decreases their permeability through the intestinal membrane-model, thus increasing the residence time of the compound in the lumen and its progressive release with the triggering action of the secreted lactase. Finally, the cinnamaldehyde-loaded microdevice has been validated in an *in vivo* model (Wistar rat), which has confirmed the decrease in permeability of cinnamaldehyde previously observed *in vitro* and a greater permanence of the EOC in the gastrointestinal lumen.

Thus, the present PhD thesis has demonstrated the possibility of using simple food-grade biomolecules as gatekeepers on a wide variety of silica materials. These new systems have allowed the encapsulation of different nutraceutical compounds, both volatile and large, for their protection and controlled release, thus improving their bioactivity and bioavailability. In this way, a further step has been taken in the use of nanotechnology to enhance the properties of natural biomolecules for pharmacological purposes.

Abbreviations and Acronyms

A

ATCC	American Type Culture Collection
ACN	Acetonitrile
ap	Apical side (cell insert)
APTES	(3-Aminopropyl)triethoxysilane

B

B2	Riboflavin (vitamin B_2)
B12	Cyanocobalamin (vitamin B_{12})
BET	Brunauer, Emmett and Teller model
BJH	Barret, Joyner and Halenda model
bl	Basolateral side (cell insert)
BSA	Bovine Serum Albumin

C

C6	Coumarin 6
C_{max}	Maximum concentration of molecule
Caco-2	Human colon adenocarcinoma cells (*Ca*ncer *Co*li-2)
Car	Carvacrol
CECT	Spanish Type Culture Collection
CFU	Colony-forming unit
Cin	Cinnamaldehyde

CLSM Confocal Laser Scanning Microscopy

CTAB N-cetyltrimethylammonium bromide

D

DCC N,N'-dicyclohexylcarbodiimide

DLS Dynamic Light Scattering

DMEM Dulbecco's Modified Eagle's Medium

DMSO Dimethyl sulfoxide

E

EDC N-(3-dimethylaminopropyl)-N'-ethylcarbodiimide

EFSA European Food Safety Authority

EO(s) Essential oil(s)

EOC(s) Essential oil component(s)

EtOH Ethanol

Eug Eugenol

F

FBS Fetal Bovine Serum

FESEM Field Emission Scanning Electron Microscopy

FTIR Fourier Transform Infrared Spectroscopy

G

GIT Gastrointestinal tract

H

HBSS Hanks' Balanced Salt solution

HeLa Human cervix carcinoma cells

Hem Hematin

Hex Hexane

HPLC High liquid performance chromatography

I

IDA Iron deficiency anemias

IL-8 Interleukin 8 (cytokine)

IUPAC International Union of Pure and Applied Chemistry

K

K_F Kunipia F, natural refined montmorillonite

K-P Korsmeyer-Peppas model

L

Lac Lactose

LPS Lipopolysaccharide

LY Lucifer yellow

M

M41 *MCM*-41 calcined microparticles

M48 *MCM*-48 calcined microparticles

MBC Minimum bactericidal concentration

MCM Mobil Composition of Matter

MCP-1 Monocyte Chemoattractant Protein-1 (chemokine)

MeOH Methanol

MSNs Mesoporous silica nanoparticles

MSPs Mesoporous silica particles

MTT 3-(4,5-dimethylthiazol-2-yl)-2,5-diphenyltetrazolium bromide

N

NPs Nanoparticles

NSAIDs Nonsteroidal Anti-Inflammatory Drugs

O

OA Oleic acid

P

P123 Pluronic 123

PAF Paraformaldehyde

PBS Phosphate Buffer Solution

P/S Penicillin/Streptomycin antibiotic mixture

R

RhB Rhodamine B

ROS Reactive oxygen species

S

S15 *SBA*-15 calcined microparticles

SBA Santa Barbara Amorphous material

S_{BET} BET surface area

SDS Sodium Dodecyl Sulphate

SI Small Intestine

S_{SA} Sumecton SA, synthetic saponite

S_{SWN} Sumecton SWN, synthetic hectorite

T

TBX Tryptone bile x-glucuronide agar

$TEAH_3$ Triethanolamine

TEER Transepithelial electrical resistance

TEM Transmission electron microscopy

TEOS Tetraethyl orthosilicate

TFA Trifluoroacetic acid

TGA Thermogravimetric analysis

Thy Thymol

TSB Tryptic soy broth

U

U7 *UVM*-7 calcined microparticles

UV-Vis Ultraviolet-Visible

UVM-7	Universidad Valencia Material 7

W

WHO	World Health Organization

X

XRD	X-ray Diffraction

Z

Zein	α-zein protein from corn

β

β-gal	β-Galactosidase, Lactase

λ

λ_{em}	Emission wavelength
λ_{ex}	Excitation wavelength

TABLE OF CONTENTS

1. GENERAL INTRODUCTION

1. Brief Historical Background

From an informal perspective, the first evidence of a medical facet in humans was found in the oldest fossil of a welded bone. This fact, very simple *a priori*, denotes the existence of a community that provided the individual with the rest and care necessary to heal the injury. Whatever it was, this little brushstroke of human's History serves to illustrate an inherent essence of *Homo sapiens*: the constant search for a state of well-being and illness-cure. These aspects support the initial basis of medicine and drugs, the latter concept described as "any substance that is used to modify disease states for the benefit of the patient",[1] among other definitions.

From the beginning of plant-based medicine used by the first humans, to modern medicine, with scientifically improved technology and in continuous development, thousands of years of acquired knowledge and scientific method have elapsed. However, there is an essence that remains constant: the existence of active compounds, of natural or synthetic origin, which are able to treat the disease or to alleviate its symptoms. Many of these compounds, however, are labile under certain external conditions of pH, temperature, humidity, redox potential, enzymatic action or light irradiation.[2,3] Another drawback is that, frequently, many of these active compounds are poorly soluble in an aqueous media, what significantly reduces their absorption and hinders their therapeutic action.

These solubility and stability requirements, together with the need to exercise its therapeutic activity exclusively in specific action-places, have generated a well-defined field of research with constantly expanding limits: the encapsulation and controlled delivery of bioactive compounds. The origin of this discipline has not been a specific event in History, but rather a progressive evolution from the s. XIX onwards, with the appearance of tableting as administration form.[4] This field aims to improve certain aspects of the protected-compounds' administration, *i.e.* to decrease adverse side effects, to reduce the administration-doses thanks to the compound's increased bioavailability, and to extend the therapeutic effect by achieving gradual dosage while reducing concentration peaks, among others.[5]

Besides, the traditional methods of oral drug delivery are hindered by different aspects, such as limited control over the drug release rate, non-targeted delivery or possible drug-degradation. Therefore, diverse new controlled release strategies have emerged from the different scientific disciplines to overcome the obstacles, allowing the development of *organic*, *inorganic* and *hybrid* controlled release systems.

Although the oral route of administration for controlled release along the gastrointestinal tract (GIT) in the nutrition and biomedicine fields is the conceptual line addressed in this work, it should be noted that there are multiple areas where this kind of systems are applicable. The wide variety of devices covered by this classification, and the great versatility exhibited by some of them (*e.g.* mesoporous silica particles), offer a myriad of applications in other research fields such as sensors,[6–10] catalysis,[11,12] cosmetics[13] or agrology.[14–17] Moreover, focusing only on the biomedicine area, many other applications can be found, such as non-oral controlled release, bioimaging for diagnosis, biosensing, bio-catalysis or tissue-engineering.[18–23]

2. Systems for controlled release into the gastrointestinal tract

The route of administration of a compound directly influences the beginning and duration of its effect. Generally, the enteral route of administration (directly at some point in the GIT) is chosen when systemic absorption of cited compound is intended.[24] When possible, the oral route of administration is the first option to administer compounds, both pharmacological and obviously nutritional, due to its simplicity and scope. Even though some compounds are contemplated to exert their effect on the GIT itself, most enterally administered compounds are intended to be intestinally absorbed and then incorporated into the bloodstream, since the gut is naturally designed for nutrient absorption.[25] Therefore, the field of oral delivery represents an area of intense research and innovation in the pharmacological formulation, which seeks stomach protection, solubility modulation and bioavailability enhancement of the compounds of interest in order to improve their pretended function into the whole organism.

As previously stated, multiple systems for GIT controlled release can be found in the literature, and even in the current pharmacology administered to patients.[26] All systems have its own advantages and disadvantages, and therefore the mention of some of them seems necessary in this work. However, due to the objectives pursued in the present PhD thesis and the nature of the research-studies developed here, only controlled release systems based on silica materials, and especially mesoporous silica particles, will be detailed in depth.

2.1. Organic systems

2.1.1. Micro- and nano-emulsions

Micro- and nano-emulsions are encapsulation systems composed of oil and/or water domains which coexist in thermodynamic equilibrium. The conceptual basis of these systems resides on an enteric coating that protect the emulsion into the stomach, and the emulsion-disruption into the small intestine with or without the aid of bile salts as natural surfactant present in the GIT. Although emulsions can be used for duodenal release, they usually do not reach further areas of the GIT. Also,

these systems usually present low encapsulation efficiencies and low stability under physical and chemical attack (changes in temperature, dilution, ionic strength), what constitutes a major limitation.[27]

2.1.2. Liposomes and Niosomes

Liposomes are spherical structures which consist of an amphiphilic bilayer, mainly of phospholipids, that delimits two regions: *(i)* one within the bilayer of hydrophobic nature (where the lipid tails are found) and *(ii)* an internal core of hydrophilic nature. Therefore, liposomes can be used to harbor bioactive molecules of either hydrophobic or hydrophilic nature (in the interface region or in the core, respectively).[28] Although this double encapsulation capacity, in addition to its modulable size (from 30 nm to several microns) makes them partly versatile systems, their limited physical and chemical stability (they can suffer aggregation, coalescence, hydrolysis and/or oxidation) entails a restriction on their use.[29]

Otherwise, niosomes are conceptually similar to liposomes, since they are vesicles composed of a bilayer of non-ionic surfactants, which are biodegradable, low toxic and relatively stable, being a possible alternative to liposomes.[30] However, they present restrictions on loading efficiency and, like liposomes, have low stability under demanding physical and chemical conditions, what reduces their applicability.

2.1.3. Biopolymers

Polymers of natural origin, or their artificial modifications to improve their properties, are based on proteins and polysaccharides. They are compounds of high molecular weight built by the repeated binding (in a linear or branched sequence) of monomers, *i.e.* aminoacids or monosaccharides/disaccharides.[31] Due to their display of immunogenicity, biocompatibility and biodegradability, they have a potential role as controlled release systems.[32] However, too rapid biodegradability (causing leaks) coupled with poor binding capacity to bioactive compounds, poor mechanical resistance and high polydispersity,[33] make them less versatile for the cited application.

2.1.4. Polymeric micelles

Polymeric micelles are based on the same principle of hydrophobic-hydrophilic interactions that give rise to liposomes and niosomes. They are formed by self-assembling of amphiphilic block copolymers that build core-shell nanostructures in aqueous solutions.[34] During the self-assembling process, lipophilic (bio)molecules can be encapsulated into the structure's core. Although the properties of these systems have evolved since their origin, improving aspects like their cargo capacity, cargo release modulation or biocompatibility,[35] these systems still have low stability and cargo-leakage compared to other more-robust systems.

2.1.5. Dendrimers

Dendrimers are three-dimensional polymeric macromolecules synthetically assembled in a well-organized pattern, with globular shape and nanometric size. However, the most distinctive characteristic is their architecture, built by a huge number of ramifications.[36] In the hole structure, two main areas can be visualized, the inner core and the outer surface. Bioactive guest molecules can be attached by three different methods: entrapped into the void spaces, bonded to some branching points, or interacting with the outer surface.[37] Besides that, dendrimers are (in a general consideration) low water-soluble and relatively toxic, being these facets the challenges to overcome by this system for controlled release applications.[38]

2.1.6. Hydrogels

Hydrogels are three-dimensional networks of cross-linked polymers. They are made from any water-soluble polymer in a wide variety of physical forms, which offers several chemical compositions and physical properties. Their ability to control cargo's rate through the cross-links density and biocompatibility are indisputable advantages of these systems. However, to effectively place hydrogels into the organism without implantation, to prolong their cargo release kinetics and to increase the number of molecules able to be loaded in their structure are still challenges for this technique.[39,40]

2.2. Inorganic systems

2.2.1. Graphene oxide, carbon nanotubes and fullerenes

Each member of the carbon-based-structure family has its unique and inimitable characteristics, reason why they have been widely used in biological applications. Conceptually, the different structures are formed by the different folding possibilities of the basic form, the graphene sheet (*i.e.* a one-atom-thickness sheet of graphite).[41] Among all the structures, nanotubes have received special attention, since their morphology facilitates a non-invasive introduction across biological membranes. Usually, to design carriers from these structures the bioactive molecules are attached to the structural walls, both internal or external, through *(i)* covalent or *(ii)* electrostatic interactions. Covalent bonding provides higher stabilization of guest molecules, minimizing leakage, but also reduce cargo-release at the action place. On the other hand, electrostatic interactions maximize controlled release, but are unstable under pH changes. As intermediate measure, bioactive compounds are usually loaded in the nanotube cavity, but these systems are poorly biocompatible when the nanotube-walls are not modified.[42]

2.2.2. Gold nanoparticles

Generally, almost all the gold nanoparticles (NPs) are synthesized following the same synthesis scheme: reduction of gold salts to Au^0, normally in the presence of a stabilizing agent that prevents the particles from aggregating as they are formed. The amount and type of gold salts used, as well as the reducing agent, are the parameters that determine the size and uniformity of the synthesized particles. Gold particles have various optical and photothermal properties, and moreover, they can be modified to modulate their toxicity and biodistribution. These properties make them useful for drug delivery combined with photothermal treatments using hollow-gold particles as host-structure for cargo loading.[43]

However, to absorb radiation for these treatments, gold NPs must have an ideal size of 50-100 nm, but smaller particle sizes are required to accumulate into the tissues. Additionally, unmodified gold particles have other drawbacks, such as

their aggregation under acidic pH or their impossibility to be metabolized and hence, their tendency to be accumulate in spleen and liver.[44]

2.2.3. Iron-Oxide based structures

The iron oxide NPs are nanocrystals chemically composed of Fe_3O_4 or Fe_2O_3, with magnetic properties capable of interacting with external magnetic fields. Because of these properties, they have a particular field of application in magnetically triggered controlled release. Furthermore, when these NPs are smaller than approximately 20 nm, they are superparamagnetic, *i.e.* they are magnetized by applying a magnetic field, but exhibit zero magnetization when the field is removed. However, unmodified iron oxide NPs have poor colloidal stability and adverse interactions with biological systems, which requires chemical modifications for its applicability.

2.2.4. Silica based materials

Among all the possible inorganic material options, silica-based materials have a leading role due to the advantages conferred by a specific manufacturing technique: the sol-gel synthesis. The great advantage offered by this process lies in the production of ceramic materials under ambient conditions.[45] The sol-gel technique was extensively studied in the 1980s and 1990s, and is based on the use of silicon alkoxides as silica precursors. The reaction can be briefly schematized in two steps: first, the precursor forms a colloidal suspension of particles and is subjected to a hydrolysis reaction (acid or base catalyzed) that replaces the alkoxide groups with hydroxyl. Secondly, siloxane (Si-O-Si) bonds are formed during the subsequent condensation reaction into a new gel phase.[46,47]

Although this technique is not the only one to produce siliceous materials, it has marked a turning point that facilitates Si-materials' use and growth as systems for controlled release. Even among the silica-based materials for controlled release, systems such as hollow silica[48] or zeolites[49] are also found, the interest of this PhD thesis will be focused on the use and description of *clays* and *mesoporous silica particles* as base materials to develop controlled release systems.

2.2.4.1. Layered aluminosilicates: Clays

Clay minerals could be chemically described, in a simple form, as hydrous metallosilicates. Their structure is based on layers, each one composed of two types of structural sheets: octahedral and tetrahedral. The two tetrahedral sheets are composed of silicon bound to oxygen; and the octahedral sheet is usually composed of aluminium or magnesium coordinated with oxygen and with hydroxyl (see Figure 1 for a structure schematization view). Together, these three sheets form a layer. Both the tetrahedral and the octahedral sheets can experiment cationic substitution with metals of lower charge, giving rise to an excess of negative charge in the three-lamellar layer. This charge-excess is equilibrated with cations that are located between the layers, helping in the pillaring of the total structure.

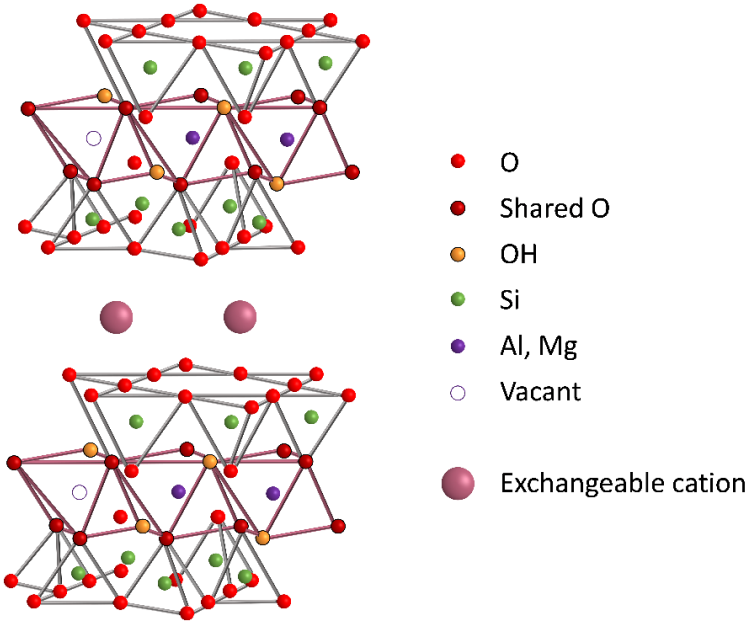

Figure 1. Representation of clay-laminar structure, where the Si tetrahedral and Al | Mg octahedral sheets that form the layers can be appreciated, as well as the exchangeable cations that hold them together.

Therefore, clay-hosts are composed of crystalline layers with strong covalent intralayer forces, but weak interlayer unions, such as electrostatic forces, hydrogen bonding and Van der Waals forces, among others.[50] These weak interactions allow the intercalation of compounds as interlayer guests, promoted by the feasibility of the interlaminar rearrangement to accommodate the loaded molecules.[44,51]

These types of loaded systems are called "intercalation compounds", and the term refers to the reversible exchange process, while maintaining the structural integrity of the original material. Guest compounds may include ions or even molecules (organic, organometallic and also biomolecules).[52,53] When the loaded molecules are incorporated into the interlaminar space, different structural changes may occur: *(i)* the interlaminar spacing is modified, *(ii)* the shape of the layers can change, *(iii)* intermediate phases of interlaminar loading can appear, especially at low cargo concentrations, in which mixtures between the original cations and the new guest compounds are produced.[51,54]

For the formation of intercalation compounds with clay minerals, the ion exchange method is the most useful technique for exchanging large ions or even molecules. This method replaces the original ion with a new molecule, for which appropriate solvents are required to assist the delaminating and re-laminating processes of the host structure.[54,55]

Traditionally, the most intended use of clays in the nanotechnology has been their incorporation into a polymer matrix in order to modify their properties. The obtained result is a hybrid material (called nanocomposite) with different properties from those of the initials clay or polymer.[13,56,57] Different processes can be performed to solubilize the clay within the polymer, including the formation of a previous “organoclay” by direct modification of the layers with silane groups.[58]

This fact suggests that it would be possible to design elaborate modifications of their layers, in order to obtain a hybrid-material capable of modulating the release rate of the intercalated molecules, resulting in “gated-organoclays”, conceptually equivalent to gated-MSPs (explained in section 2.3 and following).

2.2.4.2. Mesoporous silica particles

Mesoporous silica particles (MSPs) are materials chemically composed of silicon dioxide. The SiO_2 walls that structure the MSPs also delimit uniform porous cavities within the particles, with a pore diameter-dimensions in the range between 2 and 50 nm. The order in which these structural pores are distributed gives rise to the different types of mesoporous materials found in the literature. Some examples of these materials, generally named according to the initials of a descriptive phrase or the developing-institution, followed by the number of the specific material, temporarily ordered are FSM-16,[59] the M41S family (MCM-50, MCM-48, MCM-41),[60] HMS,[61] SBA-15,[62,63] TUD-1,[64] UVM-7,[65] AMS-6,[66] KIT-6,[67] NFM-1.[68] Among all these materials, traditionally the use of MCM-41 and SBA-15 has stood out in the field of controlled release, thanks to the advantages offered in the flow-rate uniformity due to their cylindrical and regularly ordered porous structure.

Since its first use in a controlled release application (as system to encapsulate and deliver Ibuprofen)[69] until nowadays, MSPs have been used not only to release drugs in a controlled way,[70–75] but also antimicrobials,[15,76,77] antioxidants,[78,79] bioactive peptides,[80] vitamins,[81–83] etc. Their use in oral controlled release has increased exponentially due to their properties, the most relevant detailed below.

- *Designable pore size and regular structure*. The structure and morphology of the particles, as well as of the porous matrix, are easily controllable by means of the synthesis parameters. The ability to design the pore size and to arrange them in an ordered pattern allows the regulation of the payload release rate.[84] A regular structure reduces the variability in the cargo release, which is essential for drug delivery systems.
- *High loading capacity*. The large amount of mesopores present in the particles gives these materials large specific surface areas (up to 1200 $m^2 g^{-1}$) and large values of pore sizes (2-10 nm) and volumes (0.6 - 1 $cm^3 g^{-1}$).[47,85] All these characteristics allow to harbor a high quantity of biomolecules with appropriate dimensions to fit into the pores.

- *Chemical, biological and thermal stability*. The silica walls that conform these structures are thick and resistant to thermal[86] and chemical[87] adverse conditions, also even under certain biological conditions.[88] This fact gives them an important advantage over organic devices such as those previously described, which are more susceptible to these attacks.

- *Cargo-protection against degradation*. The high denseness encapsulation of biomolecules into the porous cavities, and the inner stability of the material, allows cargo protection against adverse conditions, thus avoiding their degradation by pH, oxidation, temperature or enzymatic action.[89]

- *Improved dissolution rate of poorly water-soluble molecules*. The loading process increases the local payload-concentration, which disturbs the diffusion equilibrium by increasing the payload delivery towards the outside.[90] That process can benefit the delivery of compounds poorly-soluble in water by enhancing their solubility.

- *Biocompatibility*. The toxicity of MSPs in different biological models, both *in vitro* and *in vivo*, is a difficult parameter to evaluate, since there are numerous factors that can critically influence the result, such as: particle size,[91] tested concentration of particles and their stability in the growing medium,[92] the administration route into the organism,[93] and obviously the toxicity-effect of the loaded molecules to deliver. Despite all these factors, MSPs are considered a well-tolerated material by biological systems, and feasible to remove from the organism through different excretion mechanisms.[93–95]

- *Modifiable surface though easy chemistry reactions*. The siliceous composition of MSPs causes the presence of silanol groups along their surface, both internal and external.[96,97] The well-known chemistry of Si makes the surface easy to functionalize with organic molecules of several types.[98] This allows the formation of hybrid organic-inorganic compounds based on MSPs, whose joint-properties overcome those of the starting materials.

Due to the detailed versatility exhibited by MSPs materials, they have been frequently used as nucleus of hybrid materials, mainly powered by the aforementioned easy chemical modification of their external surface. The synthesis process of MSPs will be explained in section 3, as first synthesis step of gated-MSPs hybrid systems.

2.3. Hybrid materials

As any other scientific area, organic and inorganic delivery systems have their strengths and restrictions. Organic systems have been the most studied until recently, due to their drug-stabilizing effect *in vivo*, but their matrices are sometimes weak under pH, temperature and physical adverse conditions, and (in general) they do not have enough capacity to regulate the cargo's delivery-rate. On the other hand, inorganic systems are more robust and their characteristics allow modulating the drug's diffusion, but sometimes they present biocompatibility constraints.[89]

Aiming to unite the pros and reduce the cons of aforementioned systems, organic-inorganic hybrid materials appeared, as experts early realized that mixed devices could show better properties than their unadulterated counterparts.[45] As it can be noticed from the entire description above, there is a plethora of organic and inorganic materials studied to perform controlled release functions. Therefore, it is logical to assume that the number of hybrid materials is even higher, since they are the result of various intra- and intergroup combinations. However, between all the possible combinations, the aforementioned sol-gel synthesis caused the hybrid systems based on silica matrices to stand out. Furthermore, the selection of Si as the inorganic element with the main structural role is explained by the good processability and stability of the Si-C bond, which allows the organic modification of the network both during and after the synthesis process.[45]

Among hybrid silica materials, there is a specific category whose applications are growing abruptly in the recent decades: *hybrid MSPs*. These systems are engineered thanks to Supramolecular Chemistry, a discipline which "aims at developing highly complex chemical systems from components that interact by noncovalent intermolecular forces".[99] The potential of MSPs capped with molecules as devices for regulating payload delivery after stimulus-recognition, or *gated-MSPs,* was already glimpsed since their inception, because "they improve their supramolecular functions through pre-organized supports" and achieve a reduction in the release-rate variability by using homogeneous supports.[100]

3. Gated-MSPs

The two parts that shape the term *gated-MSPs* perfectly denominate the main components of these hybrid systems. On the one hand, a porous inorganic support based on MSPs, whose ordered structure maximizes the cargo-loading and allows its outflow-regulation. On the other hand, a molecular gate (also called gatekeeper), which is an organic, inorganic or biological ensemble able to establish supramolecular interactions with environmental stimuli, and thus regulate the enclosure or delivery of the entrapped payload. The conceptual essence of molecular gates lies in the fact that they are chemically designed to respond to a specific stimulus, *sine qua non* condition to allow the mass transport.[101] Due to the presence in the organism of a wide variety of biochemical phenomena able to be used as stimuli, the number of switchable moieties used to recognize them is vast and constantly growing.[96–98,102–105]

All the supramolecular interactions stablished between the components, add to the new hybrid material some "extra" properties over those that MSPs generally had. Among these properties, those detailed below can be highlighted.

- *Active release that minimizes leakage*. When MSPs-external surface is covered with a gatekeeper, the new system *(i)* actively allows the release of the entrapped cargo when a stimulus is applied, while *(ii)* prevents or minimizes its diffusion in the absence of cited conditions.[98] The “zero-release” behavior allows the confinement and protection of bioactive molecules within the pore voids, while the active release triggered by an specific stimulus allows the modulation of compound’s bioaccesibility in the desired place of the GIT.[106]
- *Increased biocompatibility*. Although MSPs are considered a biocompatible material, silanolate groups that cover their surface at neutral pH could cause under certain conditions unwanted reactivity or toxicity in biological models. This drawback is overcome thanks to the surface-functionalization with biocompatible molecules, which in turn increase the biocompatibility of the entire "superstructure.[107,108]

Therefore, and in order to summarize, gated-MSPs are nano or microdevices based on *(i)* a mesoporous material which acts as a cargo container, modulating the mass transport from the pore voids, *(ii)* a (bio)molecule wanted to be protected and delivered in its action place, which is loaded into the porous matrix and *(iii)* a molecular gate that avoids payload release in the absence of stimulus ("closed"), and allows its outflow when the stimulus is present ("open").

Both the structure of the porous matrix and the nature and behavior of the molecular gate are essential in the rate and profile of the payload's release. Thus, these parameters can be modified by changing any of the builder components. Additionally, the payload's interaction with the hole "superstructure" is an added factor that affects these parameters. Therefore, the synthesis of the mesoporous support, the cargo and its loading process, and the nature of the external functionalization and its attachment procedure are parameters that determine the properties of the final hybrid system.[23]

3.1. Inorganic support synthesis

As it has been explained, the MSPs synthesis is based on the sol-gel process that takes place through condensation and hydrolysis reactions of the corresponding precursors. The various modifications applied to this process give rise to the different silica-based materials, and in this case, the introduced changes lead to the obtention of the characteristic pore matrix. The synthesis of MSPs is achieved via supramolecular self-assembly of two main elements: *(i)* a structure-directing agent that is organized supramolecularly to form a highly ordered template in the form of a liquid crystal, and *(ii)* a silica precursor as in the traditional sol-gel reaction, which as described above, undergoes a hydrolysis and condensation reaction around the stablished template, resulting in a rigid structured material.

The procedure for obtaining MSPs in general (*e.g.* MCM-41) is described below, and schematized in Figure 2.[109] The hydrolysis and condensation reactions are carried out in aqueous solution, catalyzed by both acidic and basic pH, where

the silica precursor (*e.g.* tetraethyl orthosilicate) polymerizes around the previously stablished surfactant micelles (*e.g.* N-cetyltrimethylammonium bromide). The final mesoporous material is obtained after template removal, either by extraction or calcination, and the mesopores thus obtained have cylindrical shape, with a diameter of about 3 nm, and are neatly stacked with a hexagonal distribution.

As previously stated, several modifications can be introduced in the synthesis procedure (reaction time, temperature or pH; the type of silica precursor, the type of surfactant and/or the presence of co-surfactants, etc.). The introduction of these modifications markedly influences the final synthesized material, being the origin of the great variety of mesoporous materials existing in the literature.

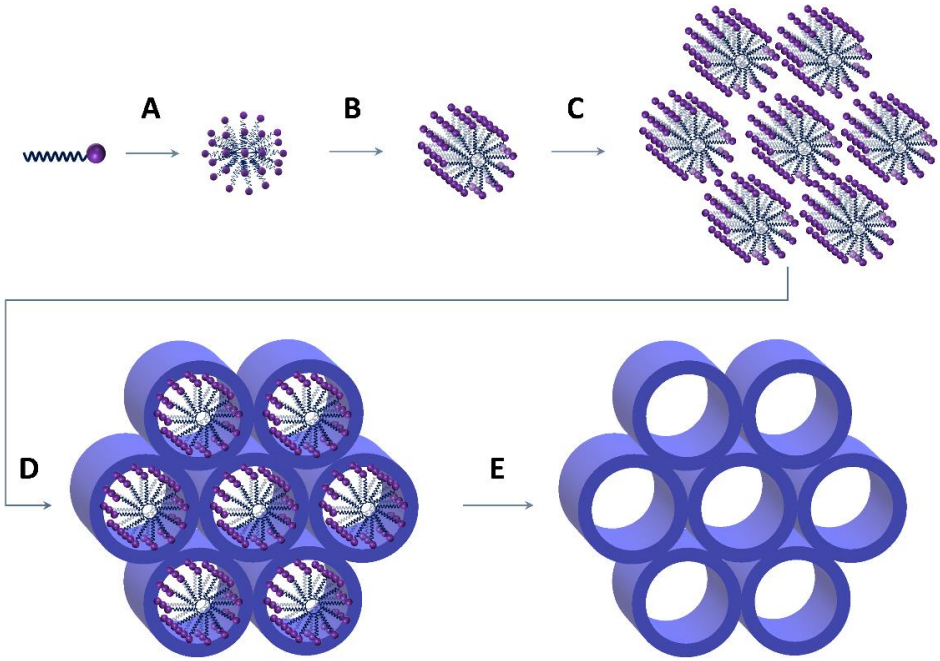

Figure 2. Representation of the synthesis process followed to obtain the mesoporous silica particles (e.g. MCM-41). The synthesis is developed in five steps: **A**, spherical micelle formation from surfactant molecules; **B**, tubular micelle formation; **C**, supra-micellar aggregate into hexagonal pattern (liquid crystal) which conforms the template; **D**, addition of the polymeric siliceous precursors and formation of the mesostructured phase; and **E**, surfactant-template removal to obtain the final mesoporous material.

3.2. Loading of guest molecules

The loading procedure of certain (bio)molecules into the MSPs pore voids is, conceptually, a quite simple process: maximum payload's incorporation must be achieved into the pores, while its presence on the external part must be reduced as possible, since this phenomenon could cause loss of control over the system's diffusion rate and homogeneity.[110] However, when the concept is translated from theory to practice, there are numerous factors that directly influence its effectiveness. These factors include, among others, the ratio between MSPs pores and (bio)molecule's dimensions, the charge of the encapsulated molecule and its possible reactivity with the matrix, the used solvent and the (bio)molecule's solubility in it, pH, temperature, time and loading method.[111] The influence of the most representative factors is outlined below.

3.2.1. Ratio between (bio)molecule and pore dimensions

The correct selection of the proper mesoporous material is an essential fact, since pore dimensions must be large enough for the guest (bio)molecule to fit inside. Usually, pore diameters slightly larger than the biomolecule's size ($Ø_{pore}/Ø_{(bio)molecule} > 1$) allow its adsorption within the material.[18] Besides that, other factors such as pore length, arrangement and morphology of the pores, particle morphology and the presence of organic molecules into the SiO_2 walls or attached to its surface, also influence the entrance capacity of the guest molecule.[112]

Besides being large enough to ensure guest molecules fitting, pore size also influences the profile and rate of the payload release. Small pore sizes have slower and more sustained releases over time, since supramolecular interactions between the host and the guest increase by proximity, delaying payload's outflow. On the other hand, the payload release from wider pores is more abrupt, which can be an advantage or a disadvantage depending on system's intention.[113] Moreover, when the molecular gate has small dimensions, large-pore materials may be insufficiently capped, which make them more prone to leakage.

3.2.2. Loading method

The payload's encapsulation process into the MSPs-pores is a diffusion balance between the outer and inner concentration. In order to maximize the number of molecules housed into the pores, the concentration on the MSPs-outside should be maximum as well. With this aim, different loading methods can be followed, but all must attempt good payload's solubility in the selected solvent. In fact, the possibility of carrying out this process without solvent (when guest molecules present a fluid state) supposes a great advantage, since the subsequent solvent-removal would not be necessary.

Although there are other methods for the encapsulation of (bio)molecules in addition to those that are explained below, its use is scarce or is far from the focus of interest of this thesis. Briefly, some of these methods are *(i) supercritical CO_2 fluid method*, where CO_2 above its critical temperature and pressure is used to solubilize poorly soluble guests, *(ii) one-step co-condensation method*, where the payload itself or entrapped into micelles is used as structure directing agent during the MSPs synthesis, or *(iii) incipient wetness impregnation method*, as modification of the general impregnation method where shorter loading times are used, offsetting the loading deficit with a hyper-concentrated payload's solution.[111]

The most commonly used methods, and also the most relevant for the development of this thesis, are indicated below in decreasing order of required solvent-volume.

3.2.2.1. Immersion

This technique is one of the most widely used due to its simplicity and reproducibility. The method consists of *(i)* the preparation of a concentrated solution of the guest molecule, followed by *(ii)* the immersion of the mesoporous material in it. The solution diffuses into the pores, so that both the cargo and the solvent are loaded. Therefore, the last step in this process *(iii)* is the solvent's removal by any technique (evaporation by heat or vacuum drying, filtration, etc.) so that only the payload remains in the pores.[85]

This method has great advantages, such as the possibility of being carried out at room temperature, which allows the encapsulation of thermolabile molecules, or the possibility to use a large number of solvents. However, poorly soluble molecules generally are not well encapsulated by this method, and there is also the possibility that solvent traces may persist within the pores.

3.2.2.2. Impregnation

This method consists of *(i)* preparing a solution of the (bio)molecule to be loaded, and then *(ii)* adding small volumes of it to a thin layer of MSPs, followed by *(iii)* the solvent's evaporation. The described process may be repeated several times in order to increase the loading yield.[106] This method offers several advantages, such as greater control of the amount of compound loaded and even greater effectiveness of the process.

Furthermore, lower amounts of payload are required, since low solution volumes are used, which is very advantageous for encapsulating expensive compounds. However, the payload tends to crystallize on the walls of the material, which can be a big problem for poorly soluble compounds, since the coating generated cannot be solubilized in successive synthesis steps, and prevents the effectively-loaded compound to outflow from the pore voids.[111]

3.2.2.3. Hot melt method (and vapor adsorption or vapor phase)

This process is carried out at a temperature above the melting point of the guest molecule, and in the absence of solvent. The host and guest are mixed together, and due to the fluent state of the guest compound at the process temperature, no solvent is required to introduce it into the pores.[114]

This method maximizes the loading effectiveness, since only payload is encapsulated into the pores, but it is restricted to thermally stable and low-viscous molecules. It is a useful method for molecules that reach vapor phases at low temperature, like essential oils,[115] since the absence of solvent and the increase in temperature could magnify the undesired reactivity between the (bio)molecules and the MSPs.[111]

3.3. Functionalization with organic moieties

The functionalization process is the synthesis step that properly gives rise to hybrid-MSPs materials. The presence of silanol groups around the entire material's surface allows its chemical modification with alkoxysilanes. Furthermore, a wide range of organo-alkoxysilanes can be adhered to the particle's surface, and then act as linker molecules. This implies that successive chemical reactions in order to bound other moieties to these linkers can be performed. There are two types of mechanisms that can be used to functionalize MSPs: *co-condensation* and *grafting*.

3.3.1. Co-condensation

Like the co-condensation loading method, co-condensation functionalization (also called one-pot synthesis) is performed during the synthetic process of the mesoporous material's matrix. The method consists of the incorporation of organo-alkoxysilanes into the synthesis mixture, so that the polymerization process makes the organic moieties to become part of the structure.[23,116] This process distributes the organic molecules more homogeneously throughout the material's structure, and both the external and internal surfaces (pores) are functionalized. Additionally, this method forces the surfactant-template removal by extraction, since the calcination process would also degrade the structural organic moieties.

3.3.2. Grafting

Another method to bind organic molecules to MSPs is the post-synthesis method, also denominated *grafting*. In this method, the same organo-alkoxysilanes previously cited are also used, but their incorporation to the MSPs is performed after the synthesis process. The addition of the alkoxysilanes can be performed both before or after the removal of the surfactant template.[85] Functionalizing the surface by this method do not modify the material's structure, and the specific surface to functionalize can be selected: the internal, the external, or both.[117] This method is immensely versatile due to the last described factor, which has resulted in a multitude of externally functionalized MSPs designed to use the anchored moieties as *molecular gates*.[77,98]

The selection of a molecular gate is generally not a random choice, and it requires a significant material's design in order to obtain the desired response to a specific stimulus. When a new drug delivery system is addressed, the biochemistry of the organism, at the cellular, tissue or systemic level, is the "defining entity" that stablishes the conditions that can be the possible stimuli. Based on this, molecules and even superstructures able to modify some of their properties (*i.e.* conformational or interaction change, able of being hydrolyzed or disassembled, etc.) under these conditions are selected or designed.

Stablishing these premises as a base, numerous molecules or bigger entities have been used as molecular gates or gatekeepers capable of presenting "open-closed" states,[118] such as polysaccharides,[119] proteins,[120,121] nucleic acids,[122–125] polymers,[126–129] graphene,[130,131] or even supramolecular assemblies.[132,133] These systems exercise their function when they are under a specific stimulus among a wide variety such as pH,[81,106,134] temperature,[135–137] light irradiation and/or redox potential,[138–141] and the presence of certain biomolecules, such as enzymes[104,142] or selected antibodies.[143] A schematic representation of the gated-MSPs preparation from the starting MSPs inorganic structure, and the "open-close" gatekeeper performance under an external stimulus is shown in Figure 3.

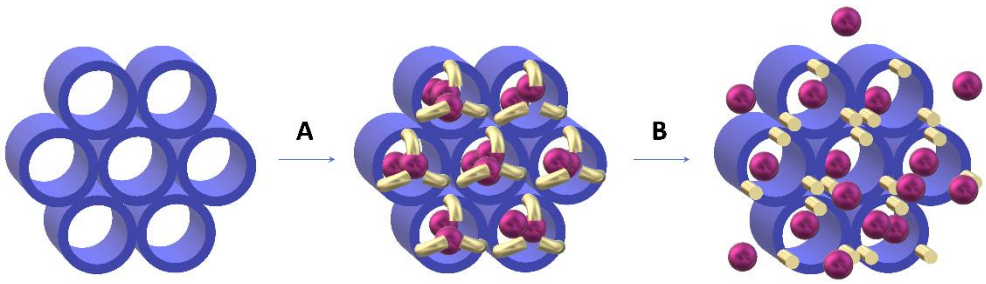

Figure 3. Gated-MSPs synthesis and working principle: **A**) loading and functionalization processes carried out to obtain the gated-MSPs, which remains closed at standard conditions. **B**) recognition of an external stimulus that "opens" the molecular gate and triggers the cargo release.

3.4. Gated-MSPs for gastrointestinal controlled delivery: triggering stimuli

As indicated before, the presence throughout the body of a wide variety of biochemical phenomena contributes to the technology of gated-MSPs with a series of stimuli capable of triggering the release of the payload. The number of stimuli present along the gastrointestinal tract (GIT) is vast and varied, due to the changing conditions of pH and enzymes, the lasts secreted both by the organism and by its sheltered microbiota.

3.4.1. pH variations

One of the most marked characteristics of the digestive system is the abrupt pH changes throughout the entire tract. From the neutral pH of the oral cavity, through the strongly acidic pH of the stomach, to the neutral-slightly basic pH in the intestine, this characteristic strongly determines the biochemistry of the GIT, such as the presence of microorganisms and the enzymes they excrete, the enzymes produced by the body and its optimal pK, the degradation of food (and drugs) and its absorption.[25]

Therefore, it is not surprising that numerous examples of molecular gates for release in the GIT are designed to be pH-targeted.[144–146] One of the most frequent strategies is to use molecules capable of being protonated in the stomach and deprotonated in the intestine, so that their change between their molecular interactions (attraction-repulsion) defines the closed state in the stomach, and the open state in the intestine, thus regulating the payload's release.[81,106,145]

3.4.2. Enzyme secretion

Apart from pH changes along the GIT, a second relevant feature is the presence of specific enzymes in each organ on the digestive system. Enzymatic actions are much more selective stimuli than pH variations, and also their presence is strategic at every point of the GIT. Starting with enzymes directly involved in the absorption of nutrients, such as amylases, peptidases/proteases, and lipases, and ending with bacterial-origin enzymes secreted by the symbiotic microorganisms that shape the

intestinal microbiota, enzyme production is specific to the place where their action is required. In order to use their action as stimulus, numerous molecular gates have been developed, which can be classified into two categories:

- First, capping-moieties constituted by the primary source of energy molecules, such as polysaccharides, peptides, and proteins, that are hydrolyzed in the early stages of GIT (mouth, stomach, and small intestine -mainly duodenum and jejunum-).[104,147–152]
- Second, molecules hydrolyzed by the exogenous enzymes present in the large intestine, principally in the colon due to the high presence of microorganisms. This strategy is usually pursued for colon-targeting (mainly for drug delivery), and several examples can be found in the literature.[102,153–155]

3.4.3. Other stimuli: redox potential, bile salts and hormones

Although changes in pH and the different enzymes present throughout the GIT are the most frequent stimuli used to design gated-MSP, there are other conditions which can also be considered, such as

- *Changes in redox potential*, since the higher concentration of microorganisms and their metabolic action leads to a reducing environment in the cited area.[156]
- *Hormones*, whose supramolecular interaction with the molecular gate may be the triggering stimulus for payload release, thanks to a molecular recognition.[157]
- *Bile salts*, which are produced by the liver and dosed into the small intestine by the gallbladder, their surfactant action could be a stimulus for lipid gates since they are able to emulsify fats.[158]

A graphical summary of the wide variety of conditions present in the GIT[159,160] that can be used as triggering stimuli for controlled release applications, is shown in Figure 4.

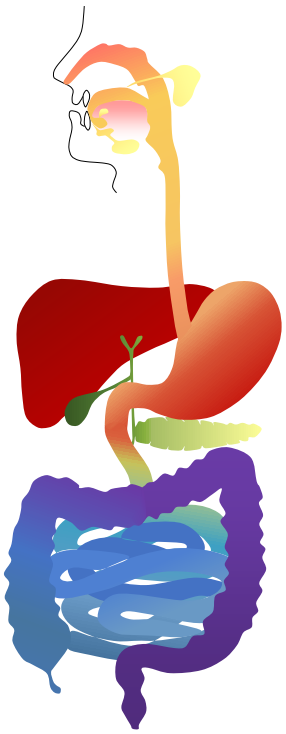

MOUTH

pH ≈ 6.2 – 7.4

t_R ≈ up to 1 min

Enzymes

- Amylase
- Salivary Lipase

STOMACH

pH ≈ 2 – 3 (HCl secretion)

t_R ≈ *4 h* (2 – 6 h)

Redox potential *= +150 mV*

Enzymes

- Pepsin
- Renin
- Gastric lipase

PANCREAS

- Pancreatin cocktail
- Proteases *(Trypsin, Chymotrypsin, Carboxypeptidase)*
- Pancreatic lipase
- Pancreatic amylase
- Ribo- and deoxyribonucleases
- Elastase
- Cholesterol esterase
- H_2CO_3 neutralizes gastric HCl

LIVER AND GALLBLADDER

- Bile salts (emulsifier)
- H_2CO_3

SMALL INTESTINE

pH ≈ 5.7 – 7.5 (gradually increases from stomach)

t_R ≈ 2 – 5 h

Redox potential*:* from *-50 mV* to *-150 mV*, due to increasing number of microorganisms.

Enzymes (in addition to pancreatic enzymes)

- Saccharidases *(Lactase, Sucrase, Maltase)*
  Peptidases
- Nucleases

Hormones

LARGE INTESTINE

pH ≈ 6 – 7.1

t_R ≈ 12 – 24 h (up to 72 h)

Redox potential*: -200 mV*

Enzymes (colonic microbiota)

- Esterases
- Azoreductases
- Oxidoreductases
- Ureases
- Dextranases
- Saccharidases
- …

Figure 4. Summary of the biochemical conditions generated by the different organs or regions of the gastrointestinal tract able to be used as triggering stimuli of gated-MSPs.[159,160]

4. Gated-MSPs to protect and/or deliver nutraceutical molecules

One of the most aimed objectives in Food research is to increase the nutritional value of food by supplementing compounds towards improving human health. The boundary line between nutrition and medicine is narrow, since (as it was already said) a drug is considered as "any substance that is used to modify the disease state for the benefit of the patient".[1] Such broad definition can perfectly accommodate any food-compound beneficial to health, or that prevents or even cures certain disease. At this point, the term *"nutraceutical"* appears. Although the nutraceutical concept and definition are not worldwide accepted, it can be defined as "a food (or part of a food) that provides medical or health benefits, including the prevention and/or treatment of a disease".[161] As further specification, a nutraceutical "must not only supplement the diet but should also aid in the prevention and/or treatment of disease and/or disorder"[161]

Within this term, numerous compounds of natural origin, present in multiple foods (usually vegetables) with beneficial properties for health, *e.g.* antioxidant, anti-inflammatory or anti-carcinogenic, can be considered nutraceuticals. From those that are focused on improving the organoleptic properties of foods, to those considered potential alternatives to current pharmacological treatments, the nutraceuticals described below have been reported to have preventive and/or curative properties.

4.1. Use of MSPs to improve food aspects of nutraceuticals

Although the fundamental requirement of food is its safety, *i.e.* to be free of any contaminant (both chemical and biological), there are other attributes related to its quality. Among these attributes, organoleptic properties (texture, flavor, color…) and nutritional value can be found.[162] Industrial processing and food's aging cause the deterioration of many of the nutraceutical compounds related to these properties. To avoid quality loss and increase food properties (both organoleptic and nutritional), the inclusion of aforementioned compounds into MSPs for their protection has been one of the followed strategies in the food industry.[111]

4.1.1. Color

Although color is not one of the main properties to be improved in food using gated-MSPs, there are certain molecules with other desired organoleptic properties that absorb visible light, and therefore have color, which are easily degraded with the irradiation of light (*i.e.* photolabile compounds). Among these types of molecules, examples as anthocyanins or curcumin can be found.

- *Anthocyanins*

These molecules are red, blue or purple pigments that can be found in several plants, especially in flowers and fruits (grapes, berries, etc.) Anthocyanins are natural dyes highly sensitive to pH, temperature and light conditions.[163] Due to these labile properties, but especially due to their antioxidant effect and potential improvement of visual and neurological health, the encapsulation of anthocyanins into MSPs is intended in food industry.[164]

- *Curcumin*

Although curcumin is an orange pigment used as a spice and food-coloring, its incorporation in functional foods is intended because its anti-inflammatory and anticancer properties. Curcumin's direct inclusion into food matrix is low effective, since it is poorly soluble. Its encapsulation and controlled release in MSPs increase its solubility and bioavailability.[165,166]

4.1.2. Flavor and aroma

Flavor and aroma, due to their close relationship, are two of the most important characteristics of food's quality. The loss of aroma and the appearance of unwanted odors are directly related to food aging and loss of freshness, even food spoilage.[162] Actually, low concentrations of certain compounds can induce intense aromas, both pleasant and unpleasant. Therefore, their encapsulation in gated-MSPs, and even only in inorganic matrices, can decrease the volatility of the compounds, allowing their properties to remain protected and their aroma to be released at the appropriate time. As in the case of color, the number of compounds

intended to be encapsulated because of their odor properties is scarce. Rather, their encapsulation aims to improve other properties, being their odor (pleasant or not) a secondary characteristic. One of the clearest examples where encapsulation reduces unpleasant odors is the *organosulfur* family.

- *Organosulfurs*

The organosulfur family includes compounds such as diallyl sulfide, diallyl disulfide, allicin, allixin… coming from A*llium* vegetables, whose proven antibiotic, antioxidant and even anticancer properties are the reason for their use as guest molecules.[167,168] However, their high volatility and pungent odor reduce their opportunities of being incorporated into functional foods. This fact is diminished thanks to the encapsulation in gated-MSPs, where the gate prevents the compound's outflow and its odor, and allows its release at the action place, where its organoleptic characteristics are indifferent.[169]

4.2. Use of MSPs for nutraceutical-controlled delivery. A health-related goal

The number of hybrid-MSPs systems focused exclusively into the upgrading of food's organoleptic properties is scarce. Usually, the objective of food improvement is not only to enhance the aroma or color of certain product, but rather to increase the bioavailability of nutraceuticals to develop a healthier product with added value. Moreover, any of the above-mentioned compounds that have been encapsulated for their antioxidant, anti-inflammatory, anti-cancer or any other health-related properties could also be in this section.

The use of antioxidants in food technology, as scavengers of reactive oxygen species (ROS), avoids fat oxidation while extends the product's self-life.[170] However, an antioxidant can be defined as any molecule able to prevent oxidation processes that affect other molecules, not only lipids but also proteins or nucleic acids, which explains their huge potential as nutraceuticals for human health.[171] Among the possible antioxidant molecules related to food and natural-sources, *phenolic antioxidants* and *essential oil components* can be specially highlighted.

4.2.1. Phenolic antioxidants

They are a wide variety of organic molecules synthesized and accumulated by higher plants in their secondary metabolism. The secondary metabolism of plants is not vital to them (as the primary metabolism), but allows the synthesis of compounds that, for example, protect them against pests and tissue-damaging, or attract insects to promote pollination.[172] These metabolites are used for human benefit as medicines, fragrances, flavors, insecticides or dyes. Plants production of polyphenols has the aim of protect them against tissue injuries produced by the free radicals and ROS generated in the photosynthetic process.[171,173] Phenolic compounds stand out especially for their properties and wide presence in different plants. Some phenolic antioxidants whose characteristics have been improved by being encapsulated in MSPs are described below.

- *Gallic acid*

Gallic acid (Figure 5A) is one of the most abundant phenolic acids in the plant kingdom, naturally found in grapes, pomegranates, rose flowers or green tea. This molecule and its derivatives, *e.g.* lauryl gallate, propyl gallate or octyl gallate, are able to inhibit the oxidation process and subsequent rancidity of oils as additives in the food industry. Besides the potential uses of these phytochemicals as preservatives and/or flavoring agents in the food industry, their pharmacological activities have also been reported, emphasizing their antimicrobial, anti-inflammatory, anticancer, antioxidant and tissue-protective effects.[174] In order to use it as an anticancer agent in controlled release systems, gallic acid has been encapsulated in MSPs in several studies, demonstrating the ability of these systems to protect the semi-stable antioxidant and to allow the payload to exert its action.[175–177]

- *Resveratrol*

Resveratrol (Figure 5B) is present in more than 70 species of plants, especially in the skin and seeds of grapes, and therefore also in red wines at discrete levels. Its high antioxidant action, combined with its antimicrobial and antitumor activity,

makes resveratrol a molecule with potential use in prevention and treatment of different types of cancer.[178] Besides, it presents many other properties, such as vasorelaxant, cardio- and neuroprotective or anti-inflammatory. However, its low water-solubility, hence low bioavailability, its photosensitivity and its adverse effects reduce its applicability in pharmaceutical treatments.[179] However, resveratrol encapsulation into MSPs systems improves its stability and dissolution rate.[180–182]

- *Quercetin*

Quercetin (Figure 5C) is a flavonoid from plant sources commonly found in buckwheat, citrus fruits and onions. Traditionally, it has been used for prevention or treatment of several diseases such as chronic inflammation, obesity, cardiovascular and nervous disorders, or even cancer. Although the specific action mechanism is still unknown, quercetin's molecular structure suggests a key action related with its antioxidant and/or anti-inflammatory effects through several routes as mitochondrial mechanism or modulation of oxidative enzymes.[183]

However, their use as nutraceuticals is limited due to their instability and low water-solubility. Therefore, they are potential candidates to be guest molecules of MSPs. Various studies in which this compound has been encapsulated in gated-MSPs systems have shown high encapsulation efficiency, stabilization of the compound against irradiation, and improvement of its antioxidant properties compared to the free compound.[184–188]

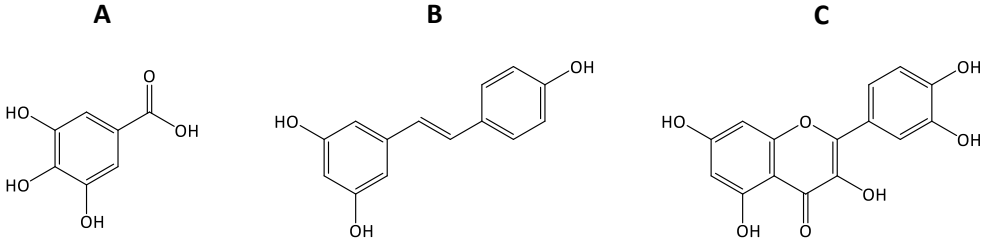

Figure 5. Chemical structure of the aforementioned antioxidants: **A**) gallic acid, **B**) resveratrol, **C**) quercetin.

4.2.2. Essential oil components

Essential oils (EO) are complex volatile mixtures of even more than 300 molecules, which are denominated essential oil components (EOCs).[189] EOCs are bioactive compounds included in the subproducts produced in the secondary metabolism of aromatic and medicinal plants. The diverse and powerful properties of EOCs make of them, in addition to antioxidants, potential nutraceuticals to be an alternative to synthetic chemical compounds currently used in the pharmaceutical and food industry.[190–192]

Despite their potential benefits, EOCs lipophilic nature makes them poorly water-soluble and therefore poorly bioavailable, limiting their applicability.[115,193] Their encapsulation in gated-MSPs is one of the diverse strategies that have emerged to increase the use of these compounds in different sectors.[15,194,195] The selection of MSPs systems as possible solution is related to their already described ability to protect labile compounds and to increase the solubility of poorly soluble compounds.[89,90] Some of the powerful properties that make EOCs possible candidates to MSPs-guest molecules are described below.

4.2.2.1. Antimicrobial properties

The EOCs antimicrobial action is related to diverse reactions that sooner or later lead to cell death.[196] Among the different described mechanisms to elucidate the antimicrobial action of EOCs, one of the most important is related to their lipophilic character. This behavior allows EOCs to disseminate and destabilize the cell membrane and the mitochondria, triggering a destruction mechanism that forces the cellular content to spill outside.[195] However, there are other mechanisms related to the destabilization of cellular metabolism that induce the microorganism-death in the long term. Among these destabilizations, several examples can be found, such as: the increased membrane-permeability, the damage to membrane proteins, the inhibition of the electron transport chain, the disruption of the proton-motive force or the ATP-synthesis reduction.[196]

Numerous examples in the literature can be found where the antimicrobial effects of EOCs are enhanced by their combination with silica materials, not only loaded into MSPs but also anchored to the silica particle's surface,[17,197–199] or by means of intercalation compounds with clays.[14,114] Focusing exclusively on the incorporation of EOCs into the MSPs pore voids, there are also numerous examples in the literature where the high efficiency of the loading process, the decrease in the compound's volatility and the improvement of its activity are evidenced.[77,114,200] Furthermore, these benefits are enhanced by the incorporation of a molecular gate onto the system, since the system leakage in normal conditions is reduced, and the payload's release occurs only when the specific stimulus is present.[201]

4.2.2.2. Anti-inflammatory properties

The inflammation process is a normal response of the damaged tissues to a possible attack, whether physical, chemical or biological, with the aim of destroying the irritating agent. However, endless processes or inadequately executed, lead to chronic inflammation and subsequent associated diseases, such as hepatic damage, cancer, arthritis, diabetes, Alzheimer's or Parkinson's disease.[202,203] During chronic inflammation, a large number of biochemical responses occur within the organism, including high oxygen uptakes that lead to the accumulation of ROS. Under normal conditions, cells have their own enzymes as defense mechanisms against these species, but when ROS production is greater than the antioxidant capacity of the cell, this oxidative stress can severely damage proteins, lipids, and DNA.[203]

The anti-inflammatory properties of EOCs have been a key role in the search of new effective compounds with fewer side effects. Many research works have been carried out with these compounds, obtaining satisfactory results.[204] Depending on the specific compound, the mechanism of action may be different, but in general terms, the antioxidant capacity of EOCs: reduces ROS levels, sequesters free radicals or the produced superoxide, increases the activity of antioxidant enzymes, or reduces the amount of nitric oxide and other toxic compounds generated. Any one of these mechanisms contributes to reduce tissue inflammation.[204–206]

4.2.2.3. Anti-tumoral properties

Due to the relationship of inflammatory processes with cancer,[207] the anti-inflammatory capacity of EOCs also makes them potential anti-cancer compounds. In addition to its antioxidant effect, EOCs interfere with the various mechanisms involved in cancer, such as an antiproliferative effect on tumor cells, an enzyme induction to degrade toxins and, or an antimutagenic effect, among others. The antimutagenic effect of EOCs is attributed to several mechanisms, such as the inhibition of the passage of mutagens to cells, the direct sequestration of mutagens or the free radicals they produce, or the enhancement of the immune action.[202,208]

Despite their anti-inflammatory and anti-cancer properties, almost all the works on the literature that report the use of EOCs encapsulated in MSPs are mainly focused on their antimicrobial action. One of the objectives of this PhD thesis has been the encapsulation of different EOCs molecules into gated-MSPs, not only to protect them and to reduce their volatility, but also to enhance their activity at the desired action site by means an active-release process triggered by a specific stimulus. The synthesized microdevices have been intended to enhance not only the antimicrobial action, but also the anticancer activity of different EOCs, such as those described below.

- *Thymol*

Thymol (Figure 6A), one of the major components of all essential oils of *Thymus* species, has numerous pharmacological properties that have made it part of traditional medicine for centuries. In addition to the antimicrobial, anti-inflammatory, and anticancer characteristics common for almost all the EOCs, thymol has antihyperlipidemic, analgesic, and antispasmodic properties.[209–212] It has therapeutic action against cardiovascular, neurological, gastrointestinal and rheumatological diseases, among others.[212] Focusing on the possibility of harboring it in gated-MSPs, thymol has been effectively encapsulated in MSPs in previous research works in the literature, where an enhancement of its antimicrobial properties was demonstrated.[114,200,201]

- *Eugenol*

Eugenol (Figure 6B) is a volatile phenolic compound principally found in clove, but also in other plant-sources like soybeans, coffee and herbs. To the properties commonly attributed to EOCs, eugenol also has been reported to have anesthetic properties.[213] The effective encapsulation of eugenol into MSPs with the aim of enhancing its antimicrobial capacity has been previously reported.[114,200,214]

- *Carvacrol*

Carvacrol (Figure 6C) is a phenolic compound produced by a large number of aromatic plants, especially thyme and oregano. Traditionally, it has been used as flavoring and preservative compound in the food and cosmetic industries. Furthermore, its properties make its use feasible for other clinical applications, since in addition to the properties common to the rest of EOCs (antimicrobial, anti-inflammatory and anticancer), eugenol has hepatoprotective, vasorelaxant and spasmolytic properties.[202,215,216]

- *Cinnamaldehyde*

Cinnamaldehyde, specifically the trans-isomer (Figure 6D), is the main component in the cinnamon's essential oil. Cinnamaldehyde is an organic compound with different pharmacologic properties, such as antidiabetic, anti-obesity and neuroprotective properties, in addition to the EOCs-general features. This compound has been reported to have preventive and therapeutic effects on nervous, cardiovascular, diabetes and cancer diseases, among others.[202,217–220]

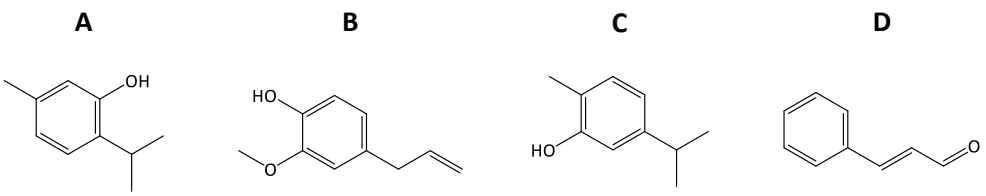

Figure 6. Chemical structure of the aforementioned essential oil components: **A**) thymol, **B**) eugenol, **C**) carvacrol, **D**) trans-cinnamaldehyde.

5. Gated-MSPs for treatment of nutraceutical deficits and their related diseases

Although the action of all nutraceuticals is by definition focused on the prevention and even cure of several diseases, some of these compounds are directly involved in human metabolism. Maintaining balanced levels of these compounds is a crucial factor for the correct state of well-being, and their deregulation (both their deficit and their excess) can lead to metabolic disorders and even diseases. This is the case of the nutraceuticals described below.

5.1. Vitamins

Vitamins are a wide group of organic molecules normally acquired through food, since only vitamin D can be synthesized by the human body. Vitamins are essential for the correct metabolism and development of the organism, and their severe dysregulation can become a cause of disease. Vitamin-related disorders can be summarized in *(i)* avitaminosis, when there is a total loss of one or more vitamins, *(ii)* hypovitaminosis, when this loss is partial, or *(iii)* hypervitaminosis, when there is an accumulation of one or more vitamins. Depending on their solubility, vitamins can be water-soluble (vitamins B and C) and lipid-soluble (vitamins A, D, E, and K). The accumulation of vitamins is more related to lipid-soluble vitamins, since water-soluble can be easily excreted in the urine.[221]

The bioaccesibility of vitamins is conditioned by their general labile and unstable nature, in addition to their solubility. Frequently, vitamins are degraded with temperature and oxidation, so the processes carried out in the food industry can reduce (and even deplete) vitamins from food. In addition, conditions present in the GIT such as aggressive pH, digestive enzymes or other nutrients that interact with them, may hinder their absorption.[222] In order to increase the nutritional value of foods, they have traditionally been supplemented directly with vitamins, but due to the facts described above, this technique does not guarantee the viability and durability of the added molecules. For this reason, better designs in which these molecules are more protected, such as gated-MSPs, would be a good option to improve vitamin supplementation.[145,223]

5.1.1. β-carotene (provitamin A)

The molecules included in the vitamin A group (or vitamers) are retinol (vitamin A_1) and dehydroretinol (A_2). However, several compounds called pro-vitamins (such as β-carotene, Figure 7A), are rapidly converted to retinol upon intestinal absorption. Vitamin A is involved in cell division cycles, and therefore in the tissue formation and regeneration processes (sperm production, embryonic development, tissue differentiation, bone growth, etc.) as well as in the regulation of vision and the immune system. After a hypothetical suppression of its intake, the liver of an adult accumulates sufficient levels of this vitamin over a period of 1 to 2 years. However, this fact is different in children and especially in underdeveloped countries, where it can cause vulnerability to infections, various types of blindness, keratinization and even death.[221]

Foods with aqueous nature are difficult to enrich with this vitamin due to its hydrophobic character. Furthermore, its sensitivity to oxidation, light and heat requires an extra protection in order to increase its bioavailability. β-carotene inclusion in MSPs has been carried out satisfactorily, reducing its degradation and controlling the payload's release.[224,225]

5.1.2. Riboflavin (vitamin B_2)

Riboflavin (Figure 7B) and its derivates, flavin mononucleotide (FMN, or riboflavin-5'-phosphate) and flavin adenine dinucleotide (FAD, obtained from FMN adenylation), have a key role in human metabolism, since they are redox cofactors of hundreds of enzymes, called flavoenzymes. Riboflavin is crucial for the oxidative metabolism of the relevant metabolites of mammal diet (lipids, carbohydrates and some aminoacids) since the flavoenzymes are involved in mitochondrial reactions and respiratory chain. Because of the riboflavin relation with the biosynthesis of heme, its deficit is related with some types of anemia.[226] Also, critically low levels of this vitamin are associated with other diseases as intestinal disorders,[227,228] hypertension[229] or cancer.[230]

Dietary supplementation with riboflavin could be effective for the treatment or palliation of these diseases.[229] Considering that the absorption of riboflavin and the other water-soluble vitamins occurs in the small intestine via carrier-mediated processes,[231] gated-MSPs triggered by GIT-stimulus can protect this photosensitive vitamin and release it effectively in its action place.[81] One of the objectives of this PhD Thesis has been the design, synthesis and validation of an organic-inorganic hybrid system for the controlled release of this vitamin.[81]

5.1.3. Folic acid (vitamin B_9)

Folic acid is a common name of the biologically active tetrahydrofolic acid (Figure 7C), which has a similar function to that performed by cobalamins (vitamin B12, explained below). Vitamin B_9 is a donor of methyl groups, reason why is implicated in the DNA synthesis of developing tissues. Therefore, it is essential during pregnancy in the formation of the neural tube of the fetus and hence, folic acid deficiency during pregnancy may produce neural tube defects as spina bifida and even anencephaly. Vitamin B_9 deficit is related to macrocytic anemia, cardiovascular disorders and Alzheimer's disease.[221]

Folic acid's general supplementation, and especially in specific situations such as pregnancy, is recommended by the EFSA (European Food Safety Authority) and widely developed.[232] However, high levels of folic acid in the blood are also associated with possible cardiovascular risks and cancer,[233–235] so adequate supplementation methods able to regulate the bioavailability of vitamin B_9 are necessary. Gated-MSPs have been one of the options developed to protect this photosensitive vitamin and release it in a controlled way in the intestine, demonstrating its ability to modulate folic acid's bioavailability.[106,145]

5.1.4. Cobalamin (vitamin B_{12})

Cobalamin is the cofactor with the most complex structure present in the nature (Figure 7D),[236] similar to chlorophyll or *heme*-group of hemoglobin due to the presence of the protoporphyrin IX ring. The vitamers of vitamin B_{12} have an activity closely related to folic acid and the methylation cycle in DNA synthesis. Due

to this, its deficit causes alterations in cell division, especially in the bone marrow, which trigger abnormal erythrocytes and the denominated megaloblastic anemia, among other diseases.[237–240] Although they are not common, vitamin B_{12} deficits are related with absorption problems or low-cobalamin content foods (like in vegetarian and vegan diets),[241,242] the latter produced because this vitamin is only obtained from animal-source foods.[243,244]

Although the parenteral route is often used to treat severe and specific deficits,[245,246] oral supplementation with cyanocobalamin is also indicated,[247] and has been shown to be effective in several studies.[236,248] However, this vitamin is labile and shows low stability under pH, light and temperature unfavorable conditions,[249,250] hindering food supplementation. Therefore, more protective systems that ensure the bioavailability of the molecule at the site of action, such as gated-MSPs or similar, could be a good administration alternative. As in the case of vitamin B_2, one of the objectives of this PhD thesis has been the design, synthesis and validation of an organic-inorganic hybrid system for the controlled release of cyanocobalamin.

5.1.5. Ascorbic acid (vitamin C)

L-ascorbic acid (Figure 7E) and dehydroascorbic acid are the vitamers of vitamin C, and their role is essential in metabolic processes such as the synthesis of collagen. The enzyme involved in this production requires iron as cofactor, and vitamin C as co-substrate to maintain the iron atom in the active form. This fact explains why vitamin C is associated with the correct absorption of iron, favoring it and promoting the regulation of *Fe* levels. In addition, vitamin C is an important antioxidant that acts in synergy with vitamin E, hence it is essential to reduce ROS and their related diseases. Its severe deficiency leads to scurvy, a disease in which capillary breaks and soft tissue hemorrhage occurs.[221]

As a consequence of its antioxidant nature, ascorbic acid is a sensitive molecule to the environmental exposure, where it is easily oxidized. To avoid this

degradation, different nanotechnological strategies have been carried out, among which the encapsulation into MSPs for different applications is included.[251]

5.1.6. α-tocopherol (vitamin E)

Biologically, α-tocopherol (Figure 7F) is the most active vitamer of vitamin E. This vitamin is the most important of the fat-soluble vitamins present in the body, and has a fundamental role in protecting polyunsaturated fatty acids from cell membranes thanks to its antioxidant action. It is one of the body's intrinsic antioxidant mechanisms, so its role against oxidative stress and ROS generated by the cell-metabolism prevents premature aging, cardiovascular diseases, arthritis or cancer. Vitamin E exhibits the most effective antioxidant role in the body, and its deficit is associated with fat malabsorption, even neuromuscular dysfunction.[221]

Due to its powerful antioxidant activity, vitamin E has been widely used in the food industry to increase the shelf life of food, both as food and packaging additive. Furthermore, in order to enhance its properties through nanotechnology, it has also been encapsulated into MSPs,[252] and used not only for food and nutritional applications,[253–255] but also as a possible anticancer agent.[256]

5.2. Inositol

Inositol (Figure 7G) is a polyol isomer of glucose, which can exist as 9 different stereoisomers depending on the orientation of its 6 hydroxyl groups. Myo-inositol and D-chiro-inositol stereoisomers are the most frequent ones, and they are involved in numerous metabolic pathways within the organism, such as insulin mediators or calcium metabolism. Furthermore, myo-inositol is essential for the maturation of oocytes and has important roles in the correct function of the male gonads.[257]

In healthy conditions, the human body is able to produce inositol from glucose derivatization, and a western diet also provides an average of 1 g/day of this compound, mainly from animal-sources and several plant-sources such as fresh fruit and seeds. However, the different processes that these products undergo in the food industry, such as baking or fermentation, reduce inositol's amount. In addition, more than 66% of the quantity ingested is degraded in the stomach and in the large intestine due to bacterial action. All these factors can lead to an inositol's deficiency, which is associated with several metabolic disorders, such as diabetes, hypertension, dyslipidemia, or polycystic ovary syndrome.[257,258]

Several studies in which supplementation with myo-inositol and D-chiro-inositol to patients with these metabolic disorders have been carried out, obtaining satisfactory results.[259–263] However, taking into account the high percentage of inositol degraded under the GIT conditions and the possible side effects of its overdose, the administration of this compound through gated-MSP systems would serve to increase its bioavailability in a more efficient way.

5.3. Iron coordinated to protoporphyrin IX (heme-iron)

Iron is a redox metal actively present in numerous enzymes, energy mechanisms and oxygen transport reactions. The absorption mechanism of iron is complex, and depends on how it reaches the intestine. Iron from inorganic-sources is fundamentally Fe^{3+}, and is enzymatically reduced on the surface of the duodenal enterocytes to Fe^{2+}, which is actively transported through the intestinal membrane. On the other hand, iron from animal-sources (or *heme* iron, which is coordinated to protoporphyrin IX like in hematin -Figure 7H-) is transported directly from the intestinal lumen through the membrane, and then separated from protoporphyrin IX ring and reduced to Fe^{2+}.[264,265] Absorption of heme iron is quite efficient, around 15 – 35%, while the absorption of non-heme iron is significantly lower, around 2 – 20%. This fact is due to the absorption mechanism, since heme iron is already chelated in the porphyrin ring and then directly absorbed, while non-heme iron is susceptible to the presence in the lumen of iron chelating ligands that hinder its absorption.[265–267]

Regulation of iron levels is essential in all organisms. Its deficit causes iron deficiency anemias (IDA),[268] but its redox nature makes its excess highly toxic, and systemic overloads can cause brain degeneration and liver, endocrine or cardiac damage.[269] Therefore, its supplementation for the treatment of anemias using systems that modulate its bioavailability, such as gated-MSPs or the like, could help control overdoses. Furthermore, if such administration were in a more efficiently absorbed form, such as heme iron, supplementation would be more effective. The latter has recently been proposed to EFSA, that has considered it positively although further research is needed before approving it.[270]

One of the objectives of this PhD thesis has been the design, synthesis and validation of an organic-inorganic hybrid system for the controlled release of *heme*-iron.

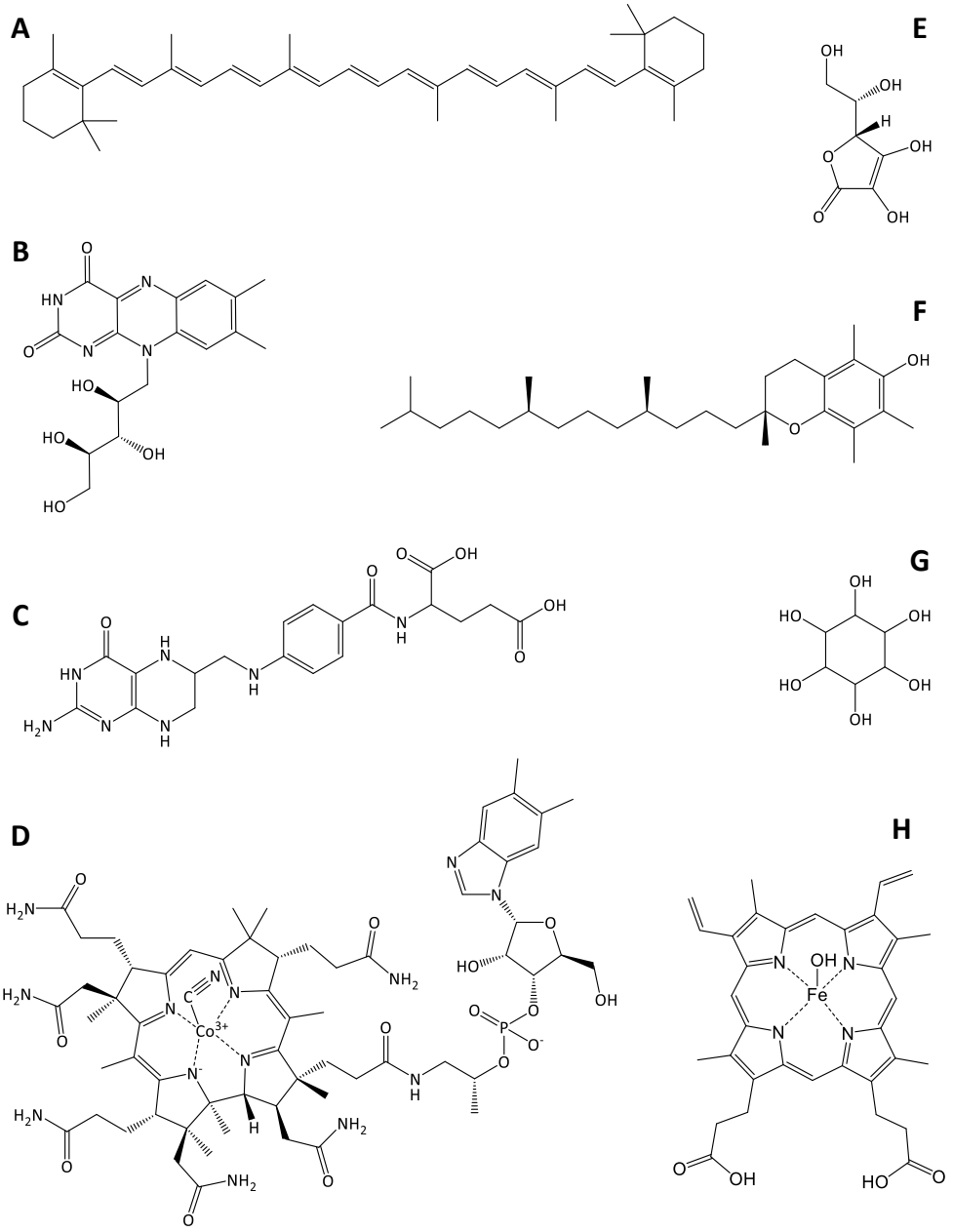

Figure 7. Chemical structure of the aforementioned nutraceuticals: **A**) β-carotene, **B**) riboflavin, **C**) tetrahydrofolic acid, **D**) cyanocobalamin, **E**) L-ascorbic acid, **F**) α-tocopherol, **G**) inositol, **H**) hematin (*heme*-iron).

6. References

1. Bruschi ML, ed. General considerations. In: *Strategies to Modify the Drug Release from Pharmaceutical Systems*. Elsevier; 2015:1-14. doi:10.1016/B978-0-08-100092-2.00001-1
2. Briscoe CJ, Hage DS. *Factors Affecting the Stability of Drugs and Drug Metabolites in Biological Matrices*. Vol 1.; 2009. doi:10.4155/bio.09.20
3. Vyas SS, Surana AP, Patravale VB. Preformulation studies. Role in Pharmaceutical Product Development. In: Patravale VB, Disouza JI, Rustomjee M, eds. *Pharmaceutical Product Development*. 1st ed. CRC Press; 2016:163-184. doi:10.1016/S0149-6395(01)80007-6
4. Florence AT. A Short History of Controlled Drug Release and an Introduction. In: Wilson CG, Crowley PJ, eds. *Controlled Release in Oral Drug Delivery*. Springer US; 2011:1-26. doi:10.1007/978-1-4614-1004-1_1
5. Bruschi ML, ed. Modification of drug release. In: *Strategies to Modify the Drug Release from Pharmaceutical Systems*. Elsevier; 2015:15-28. doi:10.1016/b978-0-08-100092-2.00002-3
6. Pla L, Lozano-Torres B, Martínez-Máñez R, Sancenón F, Ros-Lis J V. Overview of the evolution of silica-based chromo-fluorogenic nanosensors. *Sensors (Switzerland)*. 2019;19(23):5138. doi:10.3390/s19235138
7. Sancenón F, Pascual L, Oroval M, Aznar E, Martínez-Máñez R. Gated Silica Mesoporous Materials in Sensing Applications. *ChemistryOpen*. 2015;4(4):418-437. doi:10.1002/open.201500053
8. El-Safty SA, Shenashen MA. Optical mesosensor for capturing of Fe(III) and Hg(II) ions from water and physiological fluids. *Sensors Actuators, B Chem*. 2013;183:58-70. doi:10.1016/j.snb.2013.03.041
9. Kuswandi B, Wicaksono Y, Jayus, Abdullah A, Heng LY, Ahmad M. Smart packaging: Sensors for monitoring of food quality and safety. *Sens Instrum Food Qual Saf*. 2011;5(3-4):137-146. doi:10.1007/s11694-011-9120-x
10. Prado M, Espiña B, Fernandez-Argüelles MT, et al. Detection of Foodborne Pathogens Using Nanoparticles. Advantages and Trends. In: *Antimicrobial Food Packaging*. Elsevier Inc.; 2016:183-201. doi:10.1016/B978-0-12-800723-5.00014-0
11. Shang L, Bian T, Zhang B, et al. Graphene-supported ultrafine metal nanoparticles encapsulated by mesoporous silica: Robust catalysts for oxidation and reduction reactions. *Angew Chemie - Int Ed*. 2014;53(1):250-254. doi:10.1002/anie.201306863
12. Taguchi A, Schüth F. Ordered mesoporous materials in catalysis. *Microporous Mesoporous Mater*. 2005;77(1):1-45. doi:10.1016/j.micromeso.2004.06.030
13. Patel HA, Somani RS, Bajaj HC, Jasra R V. Nanoclays for polymer nanocomposites, paints, inks, greases and cosmetics formulations, drug delivery vehicle and waste water treatment. *Bull Mater Sci*. 2006;29(2):133-145. doi:10.1007/BF02704606

14. Bernardos A, Bozik M, Alvarez S, et al. The efficacy of essential oil components loaded into montmorillonite against Aspergillus niger and Staphylococcus aureus. *Flavour Fragr J*. 2019;34(3):151-162. doi:10.1002/ffj.3488

15. Bernardos A, Piacenza E, Sancenón F, et al. Mesoporous Silica-Based Materials with Bactericidal Properties. *Small*. 2019;15(24):1-34. doi:10.1002/smll.201900669

16. Park SY, Barton M, Pendleton P. Mesoporous silica as a natural antimicrobial carrier. In: Sabliov CM, Chen H, Yada RY, eds. *Colloids and Surfaces A: Physicochemical and Engineering Aspects*. Vol 385. Elsevier B.V.; 2011:256-261. doi:10.1016/j.colsurfa.2011.06.021

17. Ruiz-Rico M, Pérez-Esteve É, Bernardos A, et al. Enhanced antimicrobial activity of essential oil components immobilized on silica particles. *Food Chem*. 2017;233:228-236. doi:10.1016/j.foodchem.2017.04.118

18. Vallet-Regí M, Balas F, Arcos D. Mesoporous materials for drug delivery. *Angew Chemie - Int Ed*. 2007;46(40):7548-7558. doi:10.1002/anie.200604488

19. Bharti C, Gulati N, Nagaich U, Pal A. Mesoporous silica nanoparticles in target drug delivery system: A review. *Int J Pharm Investig*. 2015;5(3):124. doi:10.4103/2230-973x.160844

20. Oshiro JA, Abuçafy MP, Manaia EB, Da Silva BL, Chiari-Andréo BG, Chiavacci LA. Drug delivery systems obtained from silica based organic-inorganic hybrids. *Polymers (Basel)*. 2016;8(4). doi:10.3390/polym8040091

21. Ahn H, Park JH. Liposomal delivery systems for intestinal lymphatic drug transport. *Biomater Res*. 2016;20(1). doi:10.1186/s40824-016-0083-1

22. Santos HA, Canham LT, Salonen J, et al. Porous Silicon for Biomedical Applications. In: *Porous Silicon for Biomedical Applications*.; 2014:xiii-xvi. doi:10.1016/b978-0-85709-711-8.50023-4

23. Salonen J, Lehto VP. Fabrication and chemical surface modification of mesoporous silicon for biomedical applications. *Chem Eng J*. 2008;137(1):162-172. doi:10.1016/j.cej.2007.09.001

24. Ruiz ME, Scioli Montoto S. Routes of drug administration. In: Telavi A, Quiroga P, eds. *ADME Processes in Pharmaceutical Sciences*. Springer International Publishing; 2007:614-638. doi:10.1017/CBO9780511544828.035

25. Wilson CG. The Organization of the Gut and the Oral Absorption of Drugs: Anatomical, Biological and Physiological Considerations in Oral Formulation Development. In: Wilson CG, Crowley PJ, eds. *Controlled Release in Oral Drug Delivery*. Springer US; 2011:27-48. doi:10.1007/978-1-4614-1004-1_2

26. Dungan SR. Interfacial science and the creation of nanoparticles. In: Sabliov CM, Chen H, Yada RY, eds. *Nanotechnology and Functional Foods*. John Wiley & Sons, Ltd; 2015:52-68. doi:10.1002/9781118462157.ch4

27. Garti N, Yuli-Amar I. Micro- and nano-emulsions for delivery of functional food

ingredients. In: Garti NBT-D and CR of B in F and N, ed. *Delivery and Controlled Release of Bioactives in Foods and Nutraceuticals*. Woodhead Publishing; 2008:149-183. doi:https://doi.org/10.1533/9781845694210.2.149

28. Liu W, Liu W, Ye A, Liu C, Singh H. Liposomes as food ingredients and nutraceutical delivery systems. *Agro Food Ind Hi Tech*. 2013;24(2):68-71. doi:10.1533/9780857095909.3.287

29. Jambrak AR, Škevin D. Lipids. In: Galanakis CM, ed. *Nutraceutical and Functional Food Components*.; 2017:103-128. doi:10.1016/B978-0-12-805257-0.00004-1

30. Moghassemi S, Hadjizadeh A. Nano-niosomes as nanoscale drug delivery systems: An illustrated review. *J Control Release*. 2014;185(1):22-36. doi:10.1016/j.jconrel.2014.04.015

31. Luo Y, Hu Q. Food-derived biopolymers for nutrient delivery. In: *Nutrient Delivery*. ; 2017:251-291. doi:10.1016/B978-0-12-804304-2.00007-X

32. Jacob J, Haponiuk JT, Thomas S, Gopi S. Biopolymer based nanomaterials in drug delivery systems: A review. *Mater Today Chem*. 2018;9:43-55. doi:10.1016/j.mtchem.2018.05.002

33. Gopi S, Amalraj A, Sukumaran NP, Haponiuk JT, Thomas S. Biopolymers and Their Composites for Drug Delivery: A Brief Review. *Macromol Symp*. 2018;380(1):1800114. doi:10.1002/masy.201800114

34. Ahmad Z, Shah A, Siddiq M, Kraatz HB. Polymeric micelles as drug delivery vehicles. *RSC Adv*. 2014;4(33):17028-17038. doi:10.1039/c3ra47370h

35. Xu W, Ling P, Zhang T. Polymeric Micelles, a Promising Drug Delivery System to Enhance Bioavailability of Poorly Water-Soluble Drugs. *J Drug Deliv*. 2013;2013:1-15. doi:10.1155/2013/340315

36. Madaan K, Kumar S, Poonia N, Lather V, Pandita D. Dendrimers in drug delivery and targeting: Drug-dendrimer interactions and toxicity issues. *J Pharm Bioallied Sci*. 2014;6(3):139-150. doi:10.4103/0975-7406.130965

37. Chauhan AS. Dendrimers for Drug Delivery. *Molecules*. 2018;23(4). doi:10.3390/molecules23040938

38. Markowicz-Piasecka M, Mikiciuk-Olasik E. Dendrimers in drug delivery. In: *Nanobiomaterials in Drug Delivery: Applications of Nanobiomaterials*. Elsevier Inc.; 2016:39-74. doi:10.1016/B978-0-323-42866-8.00002-2

39. Hoare TR, Kohane DS. Hydrogels in drug delivery: Progress and challenges. *Polymer (Guildf)*. 2008;49(8):1993-2007. doi:10.1016/j.polymer.2008.01.027

40. Ghasemiyeh P, Mohammadi-Samani S. Hydrogels as Drug Delivery Systems; Pros and Cons. *Trends Pharm Sci*. 2019;5(1):7-24. doi:10.30476/TIPS.2019.81604.1002

41. Prasek J, Drbohlavova J, Chomoucka J, et al. Methods for carbon nanotubes synthesis - Review. *J Mater Chem*. 2011;21(40):15872-15884. doi:10.1039/c1jm12254a

42. Maiti D, Tong X, Mou X, Yang K. Carbon-Based Nanomaterials for Biomedical

Applications: A Recent Study. *Front Pharmacol*. 2019;9:1-16. doi:10.3389/fphar.2018.01401

43. Xiong C, Lu W, Zhou M, Wen X, Li C. Cisplatin-loaded hollow gold nanoparticles for laser-triggered release. *Cancer Nanotechnol*. 2018;9(1). doi:10.1186/s12645-018-0041-9

44. Zhang X, Cresswell M. Alternative Inorganic Systems for Controlled Release Applications. In: Zhang X, Cresswell M, eds. *Inorganic Controlled Release Technology*. Butterworth-Heinemann; 2016:189-219. doi:10.1016/b978-0-08-099991-3.00007-7

45. Kickelbick G. Introduction to Hybrid Materials. In: Kickelbick G, ed. *Hybrid Materials: Synthesis, Characterization, and Applications*. John Wiley and Sons; 2007:1-48. doi:10.1002/9783527610495.ch1

46. Brinker CJ, Scherer GW. *Sol-Gel Science: The Physics and Chemistry of Sol-Gel Processing*. Elsevier Inc.; 2013. doi:10.1016/C2009-0-22386-5

47. Zhang X, Cresswell M. Silica-Based Amorphous Drug Delivery Systems. In: Zhang X, Cresswell M, eds. *Inorganic Controlled Release Technology*. Butterworth-Heinemann; 2016:93-137. doi:10.1016/b978-0-08-099991-3.00004-1

48. Li ZZ, Wen LX, Shao L, Chen JF. Fabrication of porous hollow silica nanoparticles and their applications in drug release control. *J Control Release*. 2004;98(2):245-254. doi:10.1016/j.jconrel.2004.04.019

49. Khodaverdi E, Soleimani HA, Mohammadpour F, Hadizadeh F. Synthetic Zeolites as Controlled-Release Delivery Systems for Anti-Inflammatory Drugs. *Chem Biol Drug Des*. 2016;87(6):849-857. doi:10.1111/cbdd.12716

50. Uddin F. Clays, nanoclays, and montmorillonite minerals. *Metall Mater Trans A Phys Metall Mater Sci*. 2008;39(12):2804-2814. doi:10.1007/s11661-008-9603-5

51. Cao G, Wang Y. Special Nanomaterials. In: *Nanostructures and Nanomaterials*. WORLD SCIENTIFIC; 2011:297-368. doi:10.1142/9789814340571_0006

52. Choi SJ, Kim YR. Bioinspired layered nanoclays for nutraceutical delivery system. *ACS Symp Ser*. 2013;1143:207-220. doi:10.1021/bk-2013-1143.ch012

53. Akbari Alavijeh M, Sarvi MN, Ramazani Afarani Z. Properties of adsorption of vitamin B12 on nanoclay as a versatile carrier. *Food Chem*. 2017;219:207-214. doi:10.1016/j.foodchem.2016.09.140

54. Solin SA. Clays and clay intercalation compounds: Properties and physical phenomena. *Annu Rev Mater Sci*. 1997;27(1):89-115. doi:10.1146/annurev.matsci.27.1.89

55. Constantino VRL, Barbosa CAS, Bizeto MA, Dias PM. Intercalation compounds involving inorganic layered structures. *An Acad Bras Cienc*. 2000;72(1):45-49. doi:10.1590/s0001-37652000000100006

56. Jawaid M, Qaiss A el K, Bouhfid R. Nanoclay Reinforced Polymer Composites : Natural Fibre/Nanoclay Hybrid Composites. *Eng Mater*. 2016;(July):301. doi:10.1007/978-

981-10-0950-1

57. Shankar S, Jaiswal L, Rhim JW. Gelatin-Based Nanocomposite Films: Potential Use in Antimicrobial Active Packaging. In: *Antimicrobial Food Packaging*. Elsevier Inc.; 2016:339-348. doi:10.1016/B978-0-12-800723-5.00027-9

58. Zhu J, Wilkie CA. Intercalation Compounds and Clay Nanocomposites. In: Kickelbick G, ed. *Hybrid Materials: Synthesis, Characterization, and Applications*. John Wiley and Sons; 2007:151-173. doi:10.1002/9783527610495.ch4

59. Yanagisawa T, Shimizu T, Kuroda K, Kato C. The preparation of alkyltrimethylammonium-kanemite complexes and their conversion to microporous materials. *Bull Chem Soc Jpn*. 1990;63(4):988-992. doi:10.1246/bcsj.63.988

60. Beck JS, Vartuli JC, Roth WJ, et al. A New Family of Mesoporous Molecular Sieves The method of Horvath and Kawazoe18 was used to de. *J Am Chem Soc*. 1992;114(27):10834-10843. doi:10.1021/ja00053a020

61. Tanev PT, Pinnavaia TJ. A neutral templating route to mesoporous molecular sieves. *Science (80-)*. 1995;267(5199):865-867. doi:10.1126/science.267.5199.865

62. Zhao D, Huo Q, Feng J, Chmelka BF, Stucky GD. Nonionic triblock and star diblock copolymer and oligomeric sufactant syntheses of highly ordered, hydrothermally stable, mesoporous silica structures. *J Am Chem Soc*. 1998;120(24):6024-6036. doi:10.1021/ja974025i

63. Zhao D, Feng J, Huo Q, et al. Triblock Copolymer Syntheses of Mesoporous Silica with Periodic 50 to 300 Angstrom Pores. *Science*. 1998;279(5350):548-552. http://science.sciencemag.org/content/279/5350/548.abstract

64. Jansen JC, Shan Z, Marchese L, Zhou W, Puil N V.D., Maschmeyer T. A new templating method for three-dimensional mesopore networks. *Chem Commun*. 2001;(8):713-714. doi:10.1039/b101000j

65. El Haskouri J, de Zárate DO, Guillem C, et al. Silica-based powders and monoliths with bimodal pore systems. *Chem Commun*. 2002;2(4):330-331. doi:10.1039/b110883b

66. Garcia-Bennett AE, Terasaki O, Che S, Tatsumi T. Structural Investigations of AMS-n Mesoporous Materials by Transmission Electron Microscopy. *Chem Mater*. 2004;16(5):813-821. doi:10.1021/cm035074z

67. Kim TW, Kleitz F, Paul B, Ryoo R. MCM-48-like large mesoporous silicas with tailored pore structure: Facile synthesis domain in a ternary triblock copolymer-butanol-water system. *J Am Chem Soc*. 2005;127(20):7601-7610. doi:10.1021/ja042601m

68. Zhou C, Garcia-Bennett AE. Release of folic acid in mesoporous NFM-1 silica. *J Nanosci Nanotechnol*. 2010;10(11):7398-7401. doi:10.1166/jnn.2010.2823

69. Vallet-Regi M, Rámila A, Del Real RP, Pérez-Pariente J. A new property of MCM-41: Drug delivery system. *Chem Mater*. 2001;13(2):308-311. doi:10.1021/cm0011559

70. Xu X, Wu C, Bai A, Liu X, Lv H, Liu Y. Folate-Functionalized Mesoporous Silica Nanoparticles as a Liver Tumor-Targeted Drug Delivery System to Improve the

Antitumor Effect of Paclitaxel. *J Nanomater*. 2017;2017. doi:10.1155/2017/2069685

71. Murugan C, Rayappan K, Thangam R, et al. Combinatorial nanocarrier based drug delivery approach for amalgamation of anti-tumor agents in bresat cancer cells: An improved nanomedicine strategies. *Sci Rep*. 2016;6(1):1-22. doi:10.1038/srep34053

72. García-Fernández A, García-Laínez G, Ferrándiz ML, et al. Targeting inflammasome by the inhibition of caspase-1 activity using capped mesoporous silica nanoparticles. *J Control Release*. 2017;248:60-70. doi:10.1016/j.jconrel.2017.01.002

73. Shi X, Wang Y, Ren L, Zhao N, Gong Y, Wang DA. Novel mesoporous silica-based antibiotic releasing scaffold for bone repair. *Acta Biomater*. 2009;5(5):1697-1707. doi:10.1016/j.actbio.2009.01.010

74. Cheng CA, Deng T, Lin FC, Cai Y, Zink JI. Supramolecular nanomachines as stimuli-responsive gatekeepers on mesoporous silica nanoparticles for antibiotic and cancer drug delivery. *Theranostics*. 2019;9(11):3341-3364. doi:10.7150/thno.34576

75. Nairi V, Medda L, Monduzzi M, Salis A. Adsorption and release of ampicillin antibiotic from ordered mesoporous silica. *J Colloid Interface Sci*. 2017;497:217-225. doi:10.1016/j.jcis.2017.03.021

76. Park SY, Pendleton P. Mesoporous silica SBA-15 for natural antimicrobial delivery. *Powder Technol*. 2012;223:77-82. doi:10.1016/j.powtec.2011.08.020

77. Martínez-Carmona M, Gun'ko YK, Vallet-Regí M. Mesoporous silica materials as drug delivery: "the nightmare" of bacterial infection. *Pharmaceutics*. 2018;10(4). doi:10.3390/pharmaceutics10040279

78. Gargiulo N, Attianese I, Buonocore GG, et al. α-Tocopherol release from active polymer films loaded with functionalized SBA-15 mesoporous silica. *Microporous Mesoporous Mater*. 2013;167:10-15. doi:10.1016/j.micromeso.2012.07.037

79. Popova M, Szegedi A, Mavrodinova V, et al. Preparation of resveratrol-loaded nanoporous silica materials with different structures. *J Solid State Chem*. 2014;219:37-42. doi:10.1016/j.jssc.2014.07.002

80. Luo Z, Deng Y, Zhang R, et al. Peptide-laden mesoporous silica nanoparticles with promoted bioactivity and osteo-differentiation ability for bone tissue engineering. *Colloids Surfaces B Biointerfaces*. 2015;131:73-82. doi:10.1016/j.colsurfb.2015.04.043

81. Bernardos A, Aznar E, Coll C, et al. Controlled release of vitamin B2 using mesoporous materials functionalized with amine-bearing gate-like scaffoldings. *J Control Release*. 2008;131(3):181-189. doi:10.1016/j.jconrel.2008.07.037

82. Mai Z, Chen J, Hu Y, et al. Novel functional mesoporous silica nanoparticles loaded with Vitamin E acetate as smart platforms for pH responsive delivery with high bioactivity. *J Colloid Interface Sci*. 2017;508:184-195. doi:10.1016/j.jcis.2017.07.027

83. Rashidi L, Vasheghani-Farahani E, Rostami K, Gangi F, Fallahpour M. Mesoporous silica nanoparticles as a nanocarrier for delivery of vitamin C. *Iran J Biotechnol*.

2013;11(4):209-213. doi:10.5812/ijb.14279

84. Huang X, Young NP, Townley HE. Characterization and comparison of mesoporous silica particles for optimized drug delivery. *Nanomater Nanotechnol*. 2014;4(1). doi:10.5772/58290

85. Li Z, Zhang Y, Feng N. Mesoporous silica nanoparticles: synthesis, classification, drug loading, pharmacokinetics, biocompatibility, and application in drug delivery. *Expert Opin Drug Deliv*. 2019;16(3):219-237. doi:10.1080/17425247.2019.1575806

86. Matsumoto A, Sasaki T, Nishimiya N, Tsutsumi K. Thermal stability and hydrophobicity of mesoporous silica FSM-16. *Colloids Surfaces A Physicochem Eng Asp*. 2002;203(1-3):185-193. doi:10.1016/S0927-7757(01)01105-0

87. El Mourabit S, Guillot M, Toquer G, Cambedouzou J, Goettmann F, Grandjean A. Stability of mesoporous silica under acidic conditions. *RSC Adv*. 2012;2(29):10916-10924. doi:10.1039/c2ra21569a

88. Izquierdo-Barba I, Colilla M, Manzano M, Vallet-Regí M. In vitro stability of SBA-15 under physiological conditions. *Microporous Mesoporous Mater*. 2010;132(3):442-452. doi:10.1016/j.micromeso.2010.03.025

89. Zhang X, Cresswell M. Materials for Inorganic Controlled Release Technology. In: Zhang X, Cresswell M, eds. *Inorganic Controlled Release Technology*. Butterworth-Heinemann; 2016:1-16. doi:10.1016/b978-0-08-099991-3.00001-6

90. Van Speybroeck M, Mellaerts R, Martens JA, Annaert P, Van den Mooter G, Augustijns P. Ordered Mesoporous Silica for the Delivery of Poorly Soluble Drugs. In: Wilson CG, Crowley PJ, eds. *Controlled Release in Oral Drug Delivery*. Springer US; 2011:203-219. doi:10.1007/978-1-4614-1004-1_10

91. Kim IY, Joachim E, Choi H, Kim K. Toxicity of silica nanoparticles depends on size, dose, and cell type. *Nanomedicine Nanotechnology, Biol Med*. 2015;11(6):1407-1416. doi:10.1016/j.nano.2015.03.004

92. Yazdimamaghani M, Barber ZB, Hadipour Moghaddam SP, Ghandehari H. Influence of Silica Nanoparticle Density and Flow Conditions on Sedimentation, Cell Uptake, and Cytotoxicity. *Mol Pharm*. 2018;15(6):2372-2383. doi:10.1021/acs.molpharmaceut.8b00213

93. Fu C, Liu T, Li L, Liu H, Chen D, Tang F. The absorption, distribution, excretion and toxicity of mesoporous silica nanoparticles in mice following different exposure routes. *Biomaterials*. 2013;34(10):2565-2575. doi:10.1016/j.biomaterials.2012.12.043

94. He Q, Shi J. Mesoporous silica nanoparticle based nano drug delivery systems: Synthesis, controlled drug release and delivery, pharmacokinetics and biocompatibility. *J Mater Chem*. 2011;21(16):5845-5855. doi:10.1039/c0jm03851b

95. Kupferschmidt N, Xia X, Labrador RH, Atluri R, Ballell L, Garcia-Bennett AE. In vivo oral toxicological evaluation of mesoporous silica particles. *Nanomedicine*. 2013;8(1):57-64. doi:10.2217/nnm.12.77

96. Asefa T, Tao Z. Mesoporous silica and organosilica materials-Review of their synthesis and organic functionalization. *Can J Chem*. **2012**;90(12):1015-1031. doi:10.1139/v2012-094

97. Añón E, Costero AM, Gaviña P, et al. Not always what closes best opens better: mesoporous nanoparticles capped with organic gates. *Sci Technol Adv Mater*. **2019**;20(1):699-709. doi:10.1080/14686996.2019.1627173

98. Aznar E, Oroval M, Pascual L, Murguía JR, Martínez-Máñez R, Sancenón F. Gated Materials for On-Command Release of Guest Molecules. *Chem Rev*. **2016**;116(2):561-718. doi:10.1021/acs.chemrev.5b00456

99. Steed JW, Atwood JL, Gale PA. Definition and Emergence of Supramolecular Chemistry. In: Gale PA, Steed JW, eds. *Supramolecular Chemistry: From Molecules to Nanomaterials*.; **2012**:3-8. doi:10.1002/9780470661345.smc002

100. Descalzo AB, Martínez-Máñez R, Sancenón F, Hoffmann K, Rurack K. The supramolecular chemistry of organic-inorganic hybrid materials. *Angew Chemie - Int Ed*. **2006**;45(36):5924-5948. doi:10.1002/anie.200600734

101. Aznar E, Martínez-Máñez R, Sancenón F. Controlled release using mesoporous materials containing gate-like scaffoldings. *Expert Opin Drug Deliv*. **2009**;6(6):643-655. doi:10.1517/17425240902895980

102. González-Alvarez M, Coll C, Gonzalez-Alvarez I, et al. Gated Mesoporous Silica Nanocarriers for a "two-Step" Targeted System to Colonic Tissue. *Mol Pharm*. **2017**;14(12):4442-4453. doi:10.1021/acs.molpharmaceut.7b00565

103. Coll C, Bernardos A, Martínez-Máñez R, Sancenón F. Gated Silica Mesoporous Supports for Controlled Release and Signaling Applications. *Acc Chem Res*. **2013**;46(2):339-349. doi:10.1021/ar3001469

104. Llopis-Lorente A, Lozano-Torres B, Bernardos A, Martínez-Máñez R, Sancenón F. Mesoporous silica materials for controlled delivery based on enzymes. *J Mater Chem B*. **2017**;5(17):3069-3083. doi:10.1039/c7tb00348j

105. Manzano M, Vallet-Regí M. New developments in ordered mesoporous materials for drug delivery. *J Mater Chem*. **2010**;20(27):5593-5604. doi:10.1039/b922651f

106. Pérez-Esteve É, Fuentes A, Coll C, et al. Modulation of folic acid bioaccessibility by encapsulation in pH-responsive gated mesoporous silica particles. *Microporous Mesoporous Mater*. **2015**;202(C):124-132. doi:10.1016/j.micromeso.2014.09.049

107. Tang F, Li L, Chen D. Mesoporous silica nanoparticles: Synthesis, biocompatibility and drug delivery. *Adv Mater*. **2012**;24(12):1504-1534. doi:10.1002/adma.201104763

108. Seré S, De Roo B, Vervaele M, et al. Altering the Biodegradation of Mesoporous Silica Nanoparticles by Means of Experimental Parameters and Surface Functionalization. *J Nanomater*. **2018**;2018. doi:10.1155/2018/7390618

109. Beck JS, Vartuli JC, Roth WJ, et al. A New Family of Mesoporous Molecular Sieves Prepared with Liquid Crystal Templates. *J Am Chem Soc*. **1992**;27(114):10834-10843.

doi:10.1021/ja00053a020

110. Salonen J, Kaukonen AM, Hirvonen J, Vesa-Pekka L. Mesoporous Silicon in Drug Delivery Applications. *J Pharm Sci*. 2008;97(2):632-653. doi:10.1002/jps

111. Pérez-Esteve É, Ruiz-Rico M, Martínez-Máñez R, Barat JM. Mesoporous silica particles as encapsulation and delivery systems for food ingredients and nutraceuticals. In: Sen S, Pathak Y, eds. *Nanotechnology in Nutraceuticals: Production to Consumption*. 1st Editio. CRC Press; 2016:397-438. doi:https://doi.org/10.1201/9781315370859

112. Nieto A, Balas F, Colilla M, Manzano M, Vallet-Regí M. Functionalization degree of SBA-15 as key factor to modulate sodium alendronate dosage. *Microporous Mesoporous Mater*. 2008;116(1-3):4-13. doi:10.1016/j.micromeso.2008.03.025

113. Pérez-Esteve É, Ruiz-Rico M, De La Torre C, et al. Encapsulation of folic acid in different silica porous supports: A comparative study. *Food Chem*. 2016;196:66-75. doi:10.1016/j.foodchem.2015.09.017

114. Bernardos A, Marina T, Žáček P, et al. Antifungal effect of essential oil components against Aspergillus niger when loaded into silica mesoporous supports. *J Sci Food Agric*. 2015;95(14):2824-2831. doi:10.1002/jsfa.7022

115. Laird K, Phillips C. Vapour phase: A potential future use for essential oils as antimicrobials? *Lett Appl Microbiol*. 2012;54(3):169-174. doi:10.1111/j.1472-765X.2011.03190.x

116. Zucchetto N, Brühwiler D. Strategies for Localizing Multiple Functional Groups in Mesoporous Silica Particles through a One-Pot Synthesis. *Chem Mater*. 2018;30(20):7280-7286. doi:10.1021/acs.chemmater.8b03603

117. Brühwiler D. Postsynthetic functionalization of mesoporous silica. *Nanoscale*. 2010;2(6):887-892. doi:10.1039/c0nr00039f

118. Wen J, Yang K, Liu F, Li H, Xu Y, Sun S. Diverse gatekeepers for mesoporous silica nanoparticle based drug delivery systems. *Chem Soc Rev*. 2017;46(19):6024-6045. doi:10.1039/c7cs00219j

119. Andreani T, Fangueiro JF, Severino P, et al. The influence of polysaccharide coating on the physicochemical parameters and cytotoxicity of silica nanoparticles for hydrophilic biomolecules delivery. *Nanomaterials*. 2019;9(8). doi:10.3390/nano9081081

120. Zhao G, Chen Y, He Y, et al. Succinylated casein-coated peptide-mesoporous silica nanoparticles as an antibiotic against intestinal bacterial infection. *Biomater Sci*. 2019;7(6):2440-2451. doi:10.1039/c9bm00003h

121. Song Y, Zhu P, Wu Y, et al. Epsilon-poly-L-lysine decorated ordered mesoporous silica contributes to the synergistic antifungal effect and enhanced solubility of a lipophilic drug. *Mater Sci Eng C*. 2019;99:231-240. doi:10.1016/j.msec.2019.01.077

122. Zhang Y, Hou Z, Ge Y, et al. DNA-Hybrid-Gated Photothermal Mesoporous Silica

Nanoparticles for NIR-Responsive and Aptamer-Targeted Drug Delivery. *ACS Appl Mater Interfaces*. 2015;7(37):20696-20706. doi:10.1021/acsami.5b05522

123. Oroval M, Climent E, Coll C, et al. An aptamer-gated silica mesoporous material for thrombin detection. *Chem Commun*. 2013;49(48):5480-5482. doi:10.1039/c3cc42157k

124. Zhang Y, Hou Z, Ge Y, et al. DNA-Hybrid-Gated Photothermal Mesoporous Silica Nanoparticles for NIR-Responsive and Aptamer-Targeted Drug Delivery. *ACS Appl Mater Interfaces*. 2015;7(37):20696-20706. doi:10.1021/acsami.5b05522

125. Zhu CL, Lu CH, Song XY, Yang HH, Wang XR. Bioresponsive controlled release using mesoporous silica nanoparticles capped with aptamer-based molecular gate. *J Am Chem Soc*. 2011;133(5):1278-1281. doi:10.1021/ja110094g

126. Bernardos A, Mondragõn L, Javakhishvili I, et al. Azobenzene polyesters used as gate-like scaffolds in nanoscopic hybrid systems. *Chem - A Eur J*. 2012;18(41):13068-13078. doi:10.1002/chem.201200787

127. Palanikumar L, Choi ES, Cheon JY, Joo SH, Ryu JH. Noncovalent polymer-gatekeeper in mesoporous silica nanoparticles as a targeted drug delivery platform. *Adv Funct Mater*. 2015;25(6):957-965. doi:10.1002/adfm.201402755

128. Baliś A, Wolski K, Zapotoczny S. Thermoresponsive polymer gating system on mesoporous shells of silica particles serving as smart nanocontainers. *Polymers (Basel)*. 2020;12(4):888. doi:10.3390/POLYM12040888

129. Asghar K, Qasim M, Dharmapuri G, Das DD. Thermoresponsive polymer gated and superparamagnetic nanoparticles embedded hollow mesoporous silica nanoparticles as smart multifunctional nanocarrier for targeted and controlled delivery of doxorubicin. *Nanotechnology*. 2020;Accepted M. doi:10.1088/1361-6528/ab8b0e

130. Wang TT, Lan J, Zhang Y, et al. Reduced graphene oxide gated mesoporous silica nanoparticles as a versatile chemo-photothermal therapy system through pH controllable release. *J Mater Chem B*. 2015;3(30):6377-6384. doi:10.1039/c5tb00824g

131. Gao Y, Zhong S, Xu L, et al. Mesoporous silica nanoparticles capped with graphene quantum dots as multifunctional drug carriers for photo-thermal and redox-responsive release. *Microporous Mesoporous Mater*. 2019;278:130-137. doi:10.1016/j.micromeso.2018.11.030

132. Cheng CA, Deng T, Lin FC, Cai Y, Zink JI. Supramolecular nanomachines as stimuli-responsive gatekeepers on mesoporous silica nanoparticles for antibiotic and cancer drug delivery. *Theranostics*. 2019;9(11):3341-3364. doi:10.7150/thno.34576

133. Llopis-Lorente A, Díez P, Sánchez A, et al. Interactive models of communication at the nanoscale using nanoparticles that talk to one another. *Nat Commun*. 2017;8(1):1-7. doi:10.1038/ncomms15511

134. Peng S, Yuan X, Lin W, Cai C, Zhang L. pH-responsive controlled release of

mesoporous silica nanoparticles capped with Schiff base copolymer gatekeepers: Experiment and molecular dynamics simulation. *Colloids Surfaces B Biointerfaces*. 2019;176:394-403. doi:10.1016/j.colsurfb.2019.01.024

135. Yu Z, Li N, Zheng P, Pan W, Tang B. Temperature-responsive DNA-gated nanocarriers for intracellular controlled release. *Chem Commun*. 2014;50(26):3494-3497. doi:10.1039/c3cc49183h

136. Aznar E, Mondragõn L, Ros-Lis J V., et al. Finely Tuned Temperature-Controlled Cargo Release Using Paraffin-Capped Mesoporous Silica Nanoparticles. *Angew Chemie - Int Ed*. 2011;50(47):11172-11175. doi:10.1002/anie.201102756

137. De La Torre C, Agostini A, Mondragón L, et al. Temperature-controlled release by changes in the secondary structure of peptides anchored onto mesoporous silica supports. *Chem Commun*. 2014;50(24):3184-3186. doi:10.1039/c3cc49421g

138. Chai S, Guo Y, Zhang Z, Chai Z, Ma Y, Qi L. Cyclodextrin-gated mesoporous silica nanoparticles as drug carriers for red light-induced drug release. *Nanotechnology*. 2017;28(14):145101. doi:10.1088/1361-6528/aa5e74

139. Hernández Montoto A, Montes R, Samadi A, et al. Gold Nanostars Coated with Mesoporous Silica Are Effective and Nontoxic Photothermal Agents Capable of Gate Keeping and Laser-Induced Drug Release. *ACS Appl Mater Interfaces*. 2018;10(33):27644-27656. doi:10.1021/acsami.8b08395

140. Cheng B, He H, Huang T, et al. Gold nanosphere gated mesoporous silica nanoparticle responsive to near-infrared light and redox potential as a theranostic platform for cancer therapy. *J Biomed Nanotechnol*. 2016;12(3):435-449. doi:10.1166/jbn.2016.2195

141. Yang Y, Lin Y, Di D, et al. Gold nanoparticle-gated mesoporous silica as redox-triggered drug delivery for chemo-photothermal synergistic therapy. *J Colloid Interface Sci*. 2017;508:323-331. doi:10.1016/j.jcis.2017.08.050

142. Liu J, Zhang B, Luo Z, et al. Enzyme responsive mesoporous silica nanoparticles for targeted tumor therapy in vitro and in vivo. *Nanoscale*. 2015;7(8):3614-3626. doi:10.1039/c5nr00072f

143. Climent E, Bernardos A, Martínez-Máñez R, et al. Controlled delivery systems using antibody-capped mesoporous nanocontainers. *J Am Chem Soc*. 2009;131(39):14075-14080. doi:10.1021/ja904456d

144. Gisbert-Garzarán M, Manzano M, Vallet-Regí M. pH-responsive mesoporous silica and carbon nanoparticles for drug delivery. *Bioengineering*. 2017;4(1):3. doi:10.3390/bioengineering4010003

145. Ruiz-Rico M, Daubenschüz H, Pérez-Esteve É, et al. Protective effect of mesoporous silica particles on encapsulated folates. *Eur J Pharm Biopharm*. 2016;105:9-17. doi:10.1016/j.ejpb.2016.05.016

146. Florek J, Caillard R, Kleitz F. Evaluation of mesoporous silica nanoparticles for oral drug delivery-current status and perspective of MSNs drug carriers. *Nanoscale*.

2017;9(40):15252-15277. doi:10.1039/c7nr05762h

147. Bernardos A, Aznar E, Marcos MD, et al. Enzyme-responsive controlled release using mesoporous silica supports capped with lactose. *Angew Chemie - Int Ed*. 2009;48(32):5884-5887. doi:10.1002/anie.200900880

148. Bernardos A, Mondragón L, Aznar E, et al. Enzyme-Responsive Intracellular Controlled Release Using Nanometric Silica Mesoporous Supports Capped with "Saccharides." *ACS Nano*. 2010;4(11):6353-6368. doi:10.1021/nn101499d

149. Candel I, Aznar E, Mondragón L, et al. Amidase-responsive controlled release of antitumoral drug into intracellular media using gluconamide-capped mesoporous silica nanoparticles. *Nanoscale*. 2012;4(22):7237-7245. doi:10.1039/c2nr32062b

150. Coll C, Mondragón L, Martínez-Máñez R, et al. Enzyme-mediated controlled release systems by anchoring peptide sequences on mesoporous silica supports. *Angew Chemie - Int Ed*. 2011;50(9):2138-2140. doi:10.1002/anie.201004133

151. Popat A, Jambhrunkar S, Zhang J, et al. Programmable drug release using bioresponsive mesoporous silica nanoparticles for site-specific oral drug delivery. *Chem Commun*. 2014;50(42):5547-5550. doi:10.1039/c4cc00620h

152. Popat A, Liu J, Lu GQ, Qiao SZ. A pH-responsive drug delivery system based on chitosan coated mesoporous silica nanoparticles. *J Mater Chem*. 2012;22(22):11173-11178. doi:10.1039/c2jm30501a

153. Teruel AH, Pérez-Esteve É, González-Álvarez I, et al. Smart gated magnetic silica mesoporous particles for targeted colon drug delivery: New approaches for inflammatory bowel diseases treatment. *J Control Release*. 2018;281(May):58-69. doi:10.1016/j.jconrel.2018.05.007

154. Ferri D, Gaviña P, Parra M, et al. Mesoporous silica microparticles gated with a bulky azo derivative for the controlled release of dyes/ drugs in colon. *R Soc Open Sci*. 2018;5(8). doi:10.1098/rsos.180873

155. Teruel AH, Coll C, Costero AM, et al. Functional magnetic mesoporous silica microparticles capped with an azo-derivative: A promising colon drug delivery device. *Molecules*. 2018;23(2):1-13. doi:10.3390/molecules23020375

156. Luca SV, Macovei I, Bujor A, et al. Bioactivity of dietary polyphenols: The role of metabolites. *Crit Rev Food Sci Nutr*. 2020;60(4):626-659. doi:10.1080/10408398.2018.1546669

157. Li S, Zhang D, Sheng S, Sun H. Targeting thyroid cancer with acid-triggered release of doxorubicin from silicon dioxide nanoparticles. *Int J Nanomedicine*. 2017;12:5993-6003. doi:10.2147/IJN.S137335

158. Ijare OB, Somashekar BS, Gowda GAN, Sharma A, Kapoor VK, Khetrapal CL. Quantification of Glycine and Taurine Conjugated Bile Acids in Human Bile Using H NMR Spectroscopy. *Magn Reson Med*. 2005;53:1441-1446. doi:10.1002/mrm.20513

159. Pérez-Esteve É, Ruiz-Rico M, Martínez-Máñez R, Barat JM. Mesoporous Silica-Based

Supports for the Controlled and Targeted Release of Bioactive Molecules in the Gastrointestinal Tract. *J Food Sci*. 2015;80(11):E2504-E2516. doi:10.1111/1750-3841.13095

160. Mohn ES, Johnson EJ. Nutrient absorption in the human gastrointestinal tract. In: Sabliov CM, Chen H, Yada RY, eds. *Nanotechnology and Functional Foods*. John Wiley & Sons, Ltd; 2015:3-34. doi:10.1002/9781118462157.ch2

161. Kalra EK. Nutraceutical - Definition and introduction. *AAPS J*. 2003;5(3):25. doi:10.1208/ps050325

162. Fennema O, Tannenbaum S. *Fennema's Food Chemistry*. 5th ed. (Damodaran S, Parkin KL, eds.). CRC Press; 2017. doi:10.1201/9781315372914

163. Khoo HE, Azlan A, Tang ST, Lim SM. Anthocyanidins and anthocyanins: Colored pigments as food, pharmaceutical ingredients, and the potential health benefits. *Food Nutr Res*. 2017;61:1-21. doi:10.1080/16546628.2017.1361779

164. Paun N, Niculescu V, Tamaian R, Miricioiu M. Functionalized mesoporous silica nanoparticles as novel systems for natural anthocyanins stability enhancement. *Int Multidiscip Sci GeoConference Surv Geol Min Ecol Manag SGEM*. 2017;17(61):149-156. doi:10.5593/sgem2017/61/S24.020

165. Bernardos A, Kourimská L. Applications of mesoporous silica materials in food - A review. *Czech J Food Sci*. 2013;31(2):99-107. doi:10.17221/240/2012-cjfs

166. Choi YL, Jaworski J, Seo ML, Lee SJ, Jung JH. Controlled release using mesoporous silica nanoparticles functionalized with 18-crown-6 derivative. *J Mater Chem*. 2011;21(22):7882-7885. doi:10.1039/c1jm11334h

167. Viswanathan V, Phadatare A, Mukne A. Antimycobacterial and antibacterial activity of Allium sativum bulbs. *Indian J Pharm Sci*. 2014;76(3):256-261. Accessed June 24, 2020. /pmc/articles/PMC4090836/?report=abstract

168. Block E, Calvey EM, Gillies CW, Gillies JZ, Uden P. Peeling the Onion. In: *Functionality of Food Phytochemicals*. Springer US; 1997:1-30. doi:10.1007/978-1-4615-5919-1_1

169. Acosta C, Pérez-Esteve E, Fuenmayor CA, et al. Polymer composites containing gated mesoporous materials for on-command controlled release. In: *ACS Applied Materials and Interfaces*. Vol 6. American Chemical Society; 2014:6453-6460. doi:10.1021/am405939y

170. Alfonso Valenzuela B, Sanhueza J, Nieto S. Natural antioxidants in functional foods: From food safety to health benefits. *Grasas y Aceites*. 2003;54(3):295-303. doi:10.3989/gya.2003.v54.i3.245

171. San Miguel-Chávez R. Phenolic Antioxidant Capacity: A Review of the State of the Art. In: Soto-Hernández M, Palma-Tenango M, García-Mateos R, eds. *Phenolic Compounds - Biological Activity*. InTech; 2017:59-74. doi:10.5772/66897

172. Van Der Fits L, Memelink J. ORCA3, a jasmonate-responsive transcriptional regulator of plant primary and secondary metabolism. *Science (80)*. 2000;289(5477):295-297.

doi:10.1126/science.289.5477.295

173. Cvejić JH, Krstonošić MA, Bursác M, Miljić U. Polyphenols. In: Galanakis CM, ed. *Nutraceutical and Functional Food Components*.; 2017:203-258. doi:10.1016/B978-0-12-805257-0.00007-7

174. Kahkeshani N, Farzaei F, Fotouhi M, et al. Pharmacological effects of gallic acid in health and disease: A mechanistic review. *Iran J Basic Med Sci*. 2019;22(3):225-237. doi:10.22038/ijbms.2019.32806.7897

175. Iraji S, Ganji F, Rashidi L. Surface modified mesoporous silica nanoparticles as sustained-release gallic acid nano-carriers. *J Drug Deliv Sci Technol*. 2018;47:468-476. doi:10.1016/j.jddst.2018.08.008

176. Rashidi L, Vasheghani-Farahani E, Rostami K, Ganji F, Fallahpour M. Mesoporous silica nanoparticles with different pore sizes for delivery of pH-sensitive gallic acid. *Asia-Pacific J Chem Eng*. 2014;9(6):845-853. doi:10.1002/apj.1832

177. Rashidi L, Vasheghani-Farahani E, Soleimani M, et al. A cellular uptake and cytotoxicity properties study of gallic acid-loaded mesoporous silica nanoparticles on Caco-2 cells. *J Nanoparticle Res*. 2014;16(3):2285. doi:10.1007/s11051-014-2285-6

178. Gambini J, Inglés M, Olaso G, et al. Properties of Resveratrol: In Vitro and In Vivo Studies about Metabolism, Bioavailability, and Biological Effects in Animal Models and Humans. *Oxid Med Cell Longev*. 2015;2015:13. doi:10.1155/2015/837042

179. Salehi B, Mishra AP, Nigam M, et al. Resveratrol: A double-edged sword in health benefits. *Biomedicines*. 2018;6(3). doi:10.3390/biomedicines6030091

180. Popova M, Szegedi A, Mavrodinova V, et al. Preparation of resveratrol-loaded nanoporous silica materials with different structures. *J Solid State Chem*. 2014;219:37-42. doi:10.1016/j.jssc.2014.07.002

181. Summerlin N, Qu Z, Pujara N, et al. Colloidal mesoporous silica nanoparticles enhance the biological activity of resveratrol. *Colloids Surfaces B Biointerfaces*. 2016;144:1-7. doi:10.1016/j.colsurfb.2016.03.076

182. Chaudhary Z, Subramaniam S, Khan GM, et al. Encapsulation and Controlled Release of Resveratrol Within Functionalized Mesoporous Silica Nanoparticles for Prostate Cancer Therapy. *Front Bioeng Biotechnol*. 2019;7:225. doi:10.3389/fbioe.2019.00225

183. Zhang M, Swarts SG, Yin L, et al. Antioxidant Properties of Quercetin. In: LaManna JC, Puchowicz MA, Xu K, Harrison DK, Bruley DF, eds. *Oxygen Transport to Tissue XXXII. Advances in Experimental Medicine and Biology*. Vol 701. Springer US; 2011:283-289. doi:10.1007/978-1-4419-7756-4_38

184. Popova M, Trendafilova I, Szegedi Á, et al. Experimental and theoretical study of quercetin complexes formed on pure silica and Zn-modified mesoporous MCM-41 and SBA-16 materials. *Microporous Mesoporous Mater*. 2016;228:256-265. doi:10.1016/j.micromeso.2016.04.001

185. Ugazio E, Gastaldi L, Brunella V, et al. Thermoresponsive mesoporous silica nanoparticles as a carrier for skin delivery of quercetin. *Int J Pharm*. 2016;511(1):446-454. doi:10.1016/j.ijpharm.2016.07.024

186. Popova M, Trendafilova I, Tsacheva I, et al. Amino-modified KIT-6 mesoporous silica/polymer composites for quercetin delivery: Experimental and theoretical approaches. *Microporous Mesoporous Mater*. 2018;270:40-47. doi:10.1016/j.micromeso.2018.05.002

187. Rasyidah Abdul Rahim A, Hidayatul Nazirah Kamarudin N, Najiha Timmiati S, Jusoh R, Fatien Muhamad Salleh N. Polyethylene Oxide Functionalized Mesoporous Silica Nanoparticles for pH- Responsive Quercetin Release. *Mater Today Proc*. 2019;19:1673-1681. doi:10.1016/j.matpr.2019.11.196

188. Yang TS, Liu TT, Liu HI. Nanostructured lipid carriers complexed with mesoporous silica nanoparticles in encapsulating lipid-insoluble functional substances or volatile compounds. *LWT*. 2020;120. doi:10.1016/j.lwt.2019.108947

189. Tajkarimi MM, Ibrahim SA, Cliver DO. Antimicrobial herb and spice compounds in food. *Food Control*. 2010;21(9):1199-1218. doi:10.1016/j.foodcont.2010.02.003

190. Lingan K. A Review on Major Constituents of Various Essential Oils and its Application. *Transl Med*. 2018;8(1):1-5. doi:10.4172/2161-1025.1000201

191. Bakkali F, Averbeck S, Averbeck D, Idaomar M. Biological effects of essential oils - A review. *Food Chem Toxicol*. 2008;46(2):446-475. doi:10.1016/j.fct.2007.09.106

192. Inoue M, Hayashi S, E. Craker L. Role of Medicinal and Aromatic Plants: Past, Present, and Future. In: *Pharmacognosy - Medicinal Plants*.; 2019:1-13. doi:10.5772/intechopen.82497

193. Suhr KI, Nielsen P V. Antifungal activity of essential oils evaluated by two different application techniques against rye bread spoilage fungi. *J Appl Microbiol*. 2003;94(4):665-674. doi:10.1046/j.1365-2672.2003.01896.x

194. Asbahani A El, Miladi K, Badri W, et al. Essential oils: From extraction to encapsulation. *Int J Pharm*. 2015;483(1-2):220-243. doi:10.1016/j.ijpharm.2014.12.069

195. Chouhan S, Sharma K, Guleria S. Antimicrobial Activity of Some Essential Oils—Present Status and Future Perspectives. *Medicines*. 2017;4(4):58. doi:10.3390/medicines4030058

196. Nazzaro F, Fratianni F, De Martino L, Coppola R, De Feo V. Effect of essential oils on pathogenic bacteria. *Pharmaceuticals*. 2013;6(12):1451-1474. doi:10.3390/ph6121451

197. Ruiz-Rico M, Moreno Y, Barat JM. In vitro antimicrobial activity of immobilised essential oil components against Helicobacter pylori. *World J Microbiol Biotechnol*. 2020;36(1):1-9. doi:10.1007/s11274-019-2782-y

198. Polo L, Díaz de Greñu B, Della Bella E, et al. Antimicrobial activity of commercial

calcium phosphate based materials functionalized with vanillin. *Acta Biomater*. 2018;81:293-303. doi:10.1016/j.actbio.2018.09.033

199. Peña-Gómez N, Ruiz-Rico M, Pérez-Esteve É, Fernández-Segovia I, Barat JM. Novel antimicrobial filtering materials based on carvacrol, eugenol, thymol and vanillin immobilized on silica microparticles for water treatment. *Innov Food Sci Emerg Technol*. 2019;58:102228. doi:10.1016/j.ifset.2019.102228

200. Janatova A, Bernardos A, Smid J, et al. Long-term antifungal activity of volatile essential oil components released from mesoporous silica materials. *Ind Crops Prod*. 2015;67:216-220. doi:10.1016/j.indcrop.2015.01.019

201. Shahriarinour M, Divsar F, Eskandari Z. Synthesis, characterization, and antibacterial activity of thymol loaded SBA-15 mesoporous silica nanoparticles. *Inorg Nano-Metal Chem*. 2019;49(6):182-189. doi:10.1080/24701556.2019.1624569

202. Bhalla Y, Gupta VK, Jaitak V. Anticancer activity of essential oils: A review. *J Sci Food Agric*. 2013;93(15):3643-3653. doi:10.1002/jsfa.6267

203. Chen L, Deng H, Cui H, et al. Inflammatory responses and inflammation-associated diseases in organs. *Oncotarget*. 2018;9(6):7204-7218. doi:10.18632/oncotarget.23208

204. de Lavor ÉM, Cavalcante Fernandes AW, de Andrade Teles RB, et al. Essential oils and their major compounds in the treatment of chronic inflammation: A review of antioxidant potential in preclinical studies and molecular mechanisms. *Oxid Med Cell Longev*. 2018;2018. doi:10.1155/2018/6468593

205. Amorim JL, Simas DLR, Pinheiro MMG, et al. Anti-inflammatory properties and chemical characterization of the essential oils of four Citrus species. *PLoS One*. 2016;11(4). doi:10.1371/journal.pone.0153643

206. Miguel MG. Antioxidant and anti-inflammatory activities of essential oils: A short review. *Molecules*. 2010;15(12):9252-9287. doi:10.3390/molecules15129252

207. Coussens LM, Werb Z. Inflammation and cancer. *Nature*. 2002;420(6917):860-867. doi:10.1038/nature01322

208. Bayala B, Bassole IHN, Scifo R, et al. Anticancer activity of essential oils and their chemical components - A review. *Am J Cancer Res*. 2014;4(6):591-607. Accessed June 29, 2020. www.ajcr.us/

209. Omonijo FA, Liu S, Hui Q, et al. Thymol Improves Barrier Function and Attenuates Inflammatory Responses in Porcine Intestinal Epithelial Cells during Lipopolysaccharide (LPS)-Induced Inflammation. *J Agric Food Chem*. 2019;67(2):615-624. doi:10.1021/acs.jafc.8b05480

210. Liu DM, Zhou CY, Meng XL, Wang P, Li W. Thymol exerts anti-inflammatory effect in dextran sulfate sodium-induced experimental murine colitis. *Trop J Pharm Res*. 2018;17(9):1803-1810. doi:10.4314/tjpr.v17i9.18

211. Islam MT, Khalipha ABR, Bagchi R, et al. Anticancer activity of thymol: A literature-

based review and docking study with Emphasis on its anticancer mechanisms. *IUBMB Life*. 2019;71(1):9-19. doi:10.1002/iub.1935

212. Nagoor Meeran MF, Javed H, Taee H Al, Azimullah S, Ojha SK. Pharmacological properties and molecular mechanisms of thymol: Prospects for its therapeutic potential and pharmaceutical development. *Front Pharmacol*. 2017;8(JUN). doi:10.3389/fphar.2017.00380

213. Mohammadi Nejad S, Özgüneş H, Başaran N. Pharmacological and Toxicological Properties of Eugenol. *Turkish J Pharm Sci*. 2017;14(2):201-206. doi:10.4274/tjps.62207

214. Melendez-Rodriguez B, Figueroa-Lopez KJ, Bernardos A, et al. Electrospun antimicrobial films of poly(3-hydroxybutyrate-co-3-hydroxyvalerate) containing eugenol essential oil encapsulated in mesoporous silica nanoparticles. *Nanomaterials*. 2019;9(2):227. doi:10.3390/nano9020227

215. Suntres ZE, Coccimiglio J, Alipour M. The Bioactivity and Toxicological Actions of Carvacrol. *Crit Rev Food Sci Nutr*. 2015;55(3):304-318. doi:10.1080/10408398.2011.653458

216. Liu S, Song M, Yun W, et al. Effects of oral administration of different dosages of carvacrol essential oils on intestinal barrier function in broilers. *J Anim Physiol Anim Nutr (Berl)*. 2018;(April):1-9. doi:10.1111/jpn.12944

217. Mateen S, Rehman MT, Shahzad S, et al. Anti-oxidant and anti-inflammatory effects of cinnamaldehyde and eugenol on mononuclear cells of rheumatoid arthritis patients. *Eur J Pharmacol*. 2019;852:14-24. doi:10.1016/j.ejphar.2019.02.031

218. Hong SH, Ismail IA, Kang SM, Han DC, Kwon BM. Cinnamaldehydes in Cancer Chemotherapy. *Phyther Res*. 2016;30(5):754-767. doi:10.1002/ptr.5592

219. Thompson M, Schmelz EM, Bickford L. Anti-Cancer Properties Of Cinnamon Oil And Its Active Component, Trans-Cinnamaldehyde. *J Nutr Food Sci*. 2019;09(01). doi:10.4172/2155-9600.1000750

220. Hagenlocher Y, Satzinger S, Civelek M, et al. Cinnamon reduces inflammatory response in intestinal fibroblasts in vitro and in colitis in vivo leading to decreased fibrosis. *Mol Nutr Food Res*. 2017;61(9):1-9. doi:10.1002/mnfr.201601085

221. Gironés-Vilaplana A, Villanõ D, Marhuenda J, Moreno DA, Garciá-Viguera C. Vitamins. In: Galanakis CM, ed. *Nutraceutical and Functional Food Components*.; 2017:159-201. doi:10.1016/B978-0-12-805257-0.00006-5

222. Fathima SJ, Nallamuthu I, Khanum F. 12 – Vitamins and minerals fortification using nanotechnology: bioavailability and Recommended Daily Allowances. In: *Nutrient Delivery*.; 2017:457-496. doi:10.1016/B978-0-12-804304-2.00012-3

223. Karunaratne DN, Surandika Siriwardhana DA, Ariyarathna IR, Indunil Rajakaruna RMP, Banu FT, Karunaratne V. Nutrient delivery through nanoencapsulation. In: *Nutrient Delivery* ; 2017:653-680. doi:10.1016/B978-0-12-804304-2.00017-2

224. Clifford NW, Iyer KS, Raston CL. Encapsulation and controlled release of nutraceuticals using mesoporous silica capsules. *J Mater Chem*. 2008;18(2):162-165. doi:10.1039/b715100d

225. Kohno Y, Kato Y, Shibata M, et al. Fixation and stability enhancement of beta-carotene by organo-modified mesoporous silica. *Microporous Mesoporous Mater*. 2016;220:1-6. doi:10.1016/j.micromeso.2015.08.019

226. Barile M, Giancaspero TA, Leone P, Galluccio M, Indiveri C. Riboflavin transport and metabolism in humans. *J Inherit Metab Dis*. 2016;39(4):545-557. doi:10.1007/s10545-016-9950-0

227. Said HM, Ortiz A, Moyer MP, Yanagawa N. Riboflavin uptake by human-derived colonic epithelial NCM460 cells. *Am J Physiol Cell Physiol*. 2000;278(2):C270-C276.

228. Nakano E, Mushtaq S, Heath PR, et al. Riboflavin depletion impairs cell proliferation in adult human duodenum: Identification of potential effectors. *Dig Dis Sci*. 2011;56(4):1007-1019. doi:10.1007/s10620-010-1374-3

229. Thakur K, Tomar SK, Singh AK, Mandal S, Arora S. Riboflavin and health: A review of recent human research. *Crit Rev Food Sci Nutr*. 2017;57(17):3650-3660. doi:10.1080/10408398.2016.1145104

230. Li S-S, Xu Y-W, Wu J-Y, et al. Plasma Riboflavin Level is Associated with Risk, Relapse, and Survival of Esophageal Squamous Cell Carcinoma. *Nutr Cancer*. 2017;69(1):21-28. doi:10.1080/01635581.2017.1247890

231. Said HM. Intestinal absorption of water-soluble vitamins in health and disease. *Biochem J*. 2011;437(3):357-372. doi:10.1042/BJ20110326

232. Turck D, Bresson J, Burlingame B, et al. Dietary Reference Values for riboflavin. *EFSA J*. 2017;15(8). doi:10.2903/j.efsa.2017.4919

233. Pieroth R, Paver S, Day S, Lammersfeld C. Folate and Its Impact on Cancer Risk. *Curr Nutr Rep*. 2018;7(3):70-84. doi:10.1007/s13668-018-0237-y

234. Stevens VL, McCullough ML, Sun J, Jacobs EJ, Campbell PT, Gapstur SM. High levels of folate from supplements and fortification are not associated with increased risk of colorectal cancer. *Gastroenterology*. 2011;141(1):98-105.e1. doi:10.1053/j.gastro.2011.04.004

235. Sauer J, Mason JB, Choi SW. Too much folate: A risk factor for cancer and cardiovascular disease? *Curr Opin Clin Nutr Metab Care*. 2009;12(1):30-36. doi:10.1097/MCO.0b013e32831cec62

236. Fedosov SN. Physiological and Molecular Aspects of Cobalamin Transport. In: Stanger O, ed. *Water Soluble Vitamins. Subcellular Biochemistry, Vol 56*. Springer; 2012:347-367. doi:10.1007/978-94-007-2199-9

237. Wolffenbuttel BHR, Wouters HJCM, Heiner-Fokkema MR, van der Klauw MM. The Many Faces of Cobalamin (Vitamin B12) Deficiency. *Mayo Clin Proc Innov Qual Outcomes*. 2019;3(2):200-214. doi:10.1016/j.mayocpiqo.2019.03.002

238. Shipton MJ, Thachil J. Vitamin B12 deficiency - A 21st century perspective. *Clin Med (Northfield Il)*. 2015;15(2):145-150.

239. Oh RC, Brown DL. Vitamin B 12 Deficiency Clinical Manifestations of Vitamin B 12 Deficiency. *Am Fam Physician*. 2003;67(5):979-986. Accessed March 18, 2020. www.aafp.org/afp

240. Kozyraki R, Cases O. Vitamin B12 absorption: Mammalian physiology and acquired and inherited disorders. *Biochimie*. 2013;95(5):1002-1007. doi:10.1016/j.biochi.2012.11.004

241. Green R, Allen LH, Bjørke-Monsen A-L, et al. Vitamin B12 deficiency. *Nat Rev Dis Prim*. 2017;3(17040):17040. 1-19. doi:10.1038/nrdp.2017.40

242. Andrès E, Loukili NH, Noel E, et al. Vitamin B12 (cobalamin) deficiency in elderly patients. *Cmaj*. 2004;171(3):251-259. doi:10.1503/cmaj.1031155

243. Tucker KL, Rich S, Rosenberg I, et al. Plasma vitamin B-12 concentrations relate to intake source in the framingham offspring study. *Am J Clin Nutr*. 2000;71(2):514-522. doi:10.1093/ajcn/71.2.514

244. Rizzo G, Laganà AS, Rapisarda AMC, et al. Vitamin B12 among vegetarians: Status, assessment and supplementation. *Nutrients*. 2016;8(12). doi:10.3390/nu8120767

245. Festen HPM. Intrinsic factor secretion and cobalamin absorption: Physiology and pathophysiology in the gastrointestinal tract. *Scand J Gastroenterol*. 1991;26(S188):1-7. doi:10.3109/00365529109111222

246. Lane LA, Rojas-Fernández C. Treatment of vitamin B12 deficiency anemia: Oral versus parenteral therapy. *Ann Pharmacother*. 2002;36(11):1268-1272. doi:10.1345/aph.1A122a

247. Rychen G, Aquilina G, Azimonti G, et al. Safety and efficacy of vitamin B 12 (in the form of cyanocobalamin) produced by Ensifer spp. as a feed additive for all animal species based on a dossier submitted by VITAC EEIG. *EFSA J*. 2018;16(7). doi:10.2903/j.efsa.2018.5336

248. Andrès E, Kaltenbach G, Noel E, et al. Efficacy of short-term oral cobalamin therapy for the treatment of cobalamin deficiencies related to food-cobalamin malabsorption: A study of 30 patients. *Clin Lab Haematol*. 2003;25(3):161-166. doi:10.1046/j.1365-2257.2003.00515.x

249. Komaromy-Hiller G, Nuttall KL, Ashwood ER. Effect of storage on serum vitamin B12 and folate stability. *Ann Clin Lab Sci*. 1997;27(4):249-253.

250. Chalella Mazzocato M, Thomazini M, Favaro-Trindade CS. Improving stability of vitamin B12 (Cyanocobalamin) using microencapsulation by spray chilling technique. *Food Res Int*. 2019;126(108663):1-11. doi:10.1016/j.foodres.2019.108663

251. Caritá AC, Fonseca-Santos B, Shultz JD, Michniak-Kohn B, Chorilli M, Leonardi GR. Vitamin C: One compound, several uses. Advances for delivery, efficiency and stability. *Nanomedicine Nanotechnology, Biol Med*. 2020;24:102117.

doi:10.1016/j.nano.2019.102117

252. Chandrasekar G, Vinu A, Murugesan V, Hartmann M. Adsorption of vitamin E on mesoporous silica molecular sieves. In: *Studies in Surface Science and Catalysis*. Vol 158 B. Elsevier Inc.; 2005:1169-1176. doi:10.1016/s0167-2991(05)80462-8

253. Buonocore GG, Gargiulo N, Verdolotti L, Liguori B, Lavorgna M, Caputo D. Mesoporous silica as carrier of antioxidant for food packaging materials. In: *AIP Conference Proceedings*. Vol 1599. American Institute of Physics Inc.; 2014:430-433. doi:10.1063/1.4876870

254. Li C, Qiu XL, Lu LX, Tang YL, Long Q, Dang JG. Preparation of low-density polyethylene film with quercetin and α-tocopherol loaded with mesoporous silica for synergetic-release antioxidant active packaging. *J Food Process Eng*. 2019;42(5). doi:10.1111/jfpe.13088

255. Sun LN, Lu LX, Wang LQ, Qiu XL, Ge C. Influence of α-tocopherol/MCM-41 assembly on physical and antioxidant release properties of low-density polyethylene antioxidant active films. *Polym Eng Sci*. 2018;58(10):1710-1716. doi:10.1002/pen.24768

256. Qu Q, Ma X, Zhao Y. Anticancer Effect of α-Tocopheryl Succinate Delivered by Mitochondria-Targeted Mesoporous Silica Nanoparticles. *ACS Appl Mater Interfaces*. 2016;8(50):34261-34269. doi:10.1021/acsami.6b13974

257. Caputo M, Bona E, Leone I, et al. Inositols and metabolic disorders: From farm to bedside. *J Tradit Complement Med*. 2020. doi:10.1016/j.jtcme.2020.03.005

258. Minozzi M, Nordio M, Pajalich R. The combined therapy myo-inositol plus D-Chiro-inositol, in a physiological ratio, reduces the cardiovascular risk by improving the lipid profile in PCOS patients. *Eur Rev Med Pharmacol Sci*. 2013;17:537-540. Accessed June 11, 2020. http://repositorio.unan.edu.ni/2986/1/5624.pdf

259. Iuorno MJ, Jakubowicz DJ, Baillargeon JP, et al. Effects of D-chiro-inositol in lean women with the polycystic ovary syndrome. *Endocr Pract*. 2002;8(6):417-423.

260. Bradford EM, Thompson CA, Goretsky T, et al. Myo-inositol reduces β-catenin activation in colitis. *World J Gastroenterol*. 2017;23(28):5115-5126. doi:10.3748/wjg.v23.i28.5115

261. Giordano D, Corrado F, Santamaria A, et al. Effects of myo-inositol supplementation in postmenopausal women with metabolic syndrome: A perspective, randomized, placebo-controlled study. *Menopause*. 2011;18(1):102-104. doi:10.1097/gme.0b013e3181e8e1b1

262. Tabrizi R, Ostadmohammadi V, Lankarani KB, et al. The effects of inositol supplementation on lipid profiles among patients with metabolic diseases: A systematic review and meta-analysis of randomized controlled trials. *Lipids Health Dis*. 2018;17(123):1-11. doi:10.1186/s12944-018-0779-4

263. Mendoza N, Galan MI, Molina C, et al. High dose of d-chiro-inositol improves oocyte quality in women with polycystic ovary syndrome undergoing ICSI: a randomized

controlled trial. *Gynecol Endocrinol*. 2020;36(5):398-401. doi:10.1080/09513590.2019.1681959

264. Waldvogel-Abramowski S, Waeber G, Gassner C, et al. Physiology of iron metabolism. *Transfus Med Hemotherapy*. 2014;41(3):213-221. doi:10.1159/000362888

265. Sharp P, Srai SK. Molecular mechanisms involved in intestinal iron absorption. *World J Gastroenterol*. 2007;13(35):4716-4724. doi:10.3748/wjg.v13.i35.4716

266. Hallberg L, Björn-Rasmussen E, Howard L, Rossander L. Dietary heme iron absorption: A discussion of possible mechanisms for the absorption-promoting effect of meat and for the regulation of iron absorption. *Scand J Gastroenterol*. 1979;14(7):769-779. doi:10.3109/00365527909181403

267. Shayeghi M, Latunde-Dada GO, Oakhill JS, et al. Identification of an intestinal heme transporter. *Cell*. 2005;122(5):789-801. doi:10.1016/j.cell.2005.06.025

268. Camaschella C. New insights into iron deficiency and iron deficiency anemia. *Blood Rev*. 2017;31(4):225-233. doi:10.1016/j.blre.2017.02.004

269. Hider RC, Kong X. Iron: Effect of Overload and Deficiency. In: Sigel A, Sigel H, Sigel R, eds. *Metal Ions in Life Sciences*. Vol 13. Springer, Dordrecht; 2013:229-294. doi:10.1007/978-94-007-7500-8_8

270. EFSA. Scientific Opinion on the safety of heme iron (blood peptonates) for the proposed uses as a source of iron added for nutritional purposes to foods for the general population, including food supplements. *EFSA J*. 2010;8(4):1-31. doi:10.2903/j.efsa.2010.1585

2. OBJECTIVES

The main objective of this PhD thesis was to find simple molecules of diverse nature which can act as capping agents of different silica materials (mostly mesoporous silica particles), in order to protect nutraceuticals into their pore voids and properly deliver them, thus performing the function of molecular gates. This process aims to achieve the controlled release of the entrapped payload, which in turn will improve its activity and bioavailability. To achieve this main objective, this PhD Thesis is divided into three chapters, depending on the nature of the molecules used as molecular gates.

Lipid-gated microdevices. This is addressed to use the hydrophobic interaction between lipid molecules as gate closing force, and the subsequent action of surfactant molecules as triggering stimulus to exert the payload release. Bile salts are specifically highlighted as delivery stimulus as they are the surfactants naturally present in the gastrointestinal tract. Therefore, the specific objectives of this chapter are:

I. Find a lipid molecule capable of acting as molecular gate, i.e. confining the entrapped cargo and delivering it in a controlled way only when surfactant molecules are present.

II. Synthesize several delivery microdevices using the chosen lipid moiety in order to encapsulate different payload molecules. Hence, to assess the capability of the chosen functionality to act as molecular gate on different inorganic materials, and to correlate cargo-dimensions with the different pore dimensions of the specific inorganic support.

III. Characterize the synthesized microdevices, and to study their release kinetics as a function of the inorganic structure. Therefore, to be able to modulate the payload release by selecting the appropriate inorganic support.

IV. Evaluate the efficiency of the synthesized microdevices to improve the properties of nutraceutical molecules through the encapsulation and controlled release processes. Specifically, to protect labile nutraceuticals which could be degraded under light irradiation, aggressive pH values or enzymatic action.

Protein-gated microdevices. This chapter is addressed to use common proteins as molecular gates, without using designed polypeptides and the inherent cost in time and resources that it implies. The hydrolytic action carried out by proteolytic enzymes was intended to be the triggering stimulus for payload release. Hence, the specific objectives of this subject are:

V. Design, synthesize, characterize and validate a new protein-capped microdevice, capable of confining the loaded cargo and releasing it under proteolytic stimuli.

VI. Enhance the properties of naturally-derived molecules with antimicrobial capability through their encapsulation in the designed protein-capped microdevice.

VII. Apply the developed system in bacterial cultures as antimicrobial microdevice, using the inherent protease secretion derived from bacterial growth as triggering stimulus for the antimicrobial payload release.

Saccharide-gated microdevices. This chapter is addressed to use the carbohydrate-hydrolytic enzymes present throughout the gastrointestinal tract as stimulus to release the encapsulated payload. Therefore, the specific objectives of this chapter are:

VIII. Synthesize and characterize a lactose-protected microdevice and validate it under gastrointestinal conditions, triggered by the enzymatic action of lactase, which is secreted along the small intestine lumen.

IX. Apply the designed microdevice for the protection and intestinal controlled delivery of natural-origin molecules with described anticancer effect.

X. Study and visualize the interaction of aforementioned microdevices with different *in vitro* and *in vivo* gastrointestinal models, with the aim of developing new alternatives for cancer-treatment

3. CHAPTER 1

Lipid-gated Microdevices

Article 1

New oleic acid-capped mesoporous silica particles as surfactant-responsive delivery systems *(Communication)*

Elisa Poyatos-Racionero,[a,b] Édgar Pérez-Esteve,[a,c] M. Dolores Marcos,[a,b,d,f,g],* José M. Barat,[c,e] Ramón Martínez-Máñez,[a,b,d,f,g],* Elena Aznar,[a,b,f,g] and Andrea Bernardos,[a,b,g]

[a] Instituto Interuniversitario de Investigación de Reconocimiento Molecular y Desarrollo Tecnológico (IDM), Universitat Politècnica de València, Universitat de València. Camino de Vera s/n, 46022, Valencia (Spain).

[b] CIBER de Bioingeniería, Biomateriales y Nanomedicina (CIBER-BBN) (Spain)

[c] Grupo de Investigación e Innovación Alimentaria (CUINA). Universitat Politècnica de València Camino de Vera s/n, 46022, Valencia (Spain).

[d] Departamento de Química, Universitat Politècnica de València. Camino de Vera s/n, 46022, Valencia (Spain).

[e] Departamento de Tecnología de Alimentos, Universitat Politècnica de València. Camino de Vera s/n, 46022, Valencia (Spain)

[f] Unidad Mixta de Investigación en Nanomedicina y Sensores Universitat Politècnica de València, IIS La Fe de Valencia. 46026, Valencia (Spain)

[g] Unidad Mixta UPV-CIPF Investigación de Mecanismos Enfermedad y Nanomedicina, Universitat Politècnica de València, Centro de Investigación Príncipe Felipe. 46100, Valencia (Spain).

* Correspondence: mmarcos@upv.es (M.D.M.); rmaez@qim.upv.es (R.M-M.)

ChemistryOpen **2019**, *8*, 1052.

Abstract

A new delivery microdevice, based on hydrophobic oleic acid-capped SBA mesoporous silica particles, able to payload release in the presence of surfactants, has been developed. The oleic acid functionalization confers to the system a high hydrophobic character, which avoids cargo release unless surfactant molecules are present. The performance of this oleic-acid capped microdevice in the presence of different surfactants is presented and its zero-release operation in the absence of surfactants is demonstrated.

Keywords: mesoporous materials • oleic acid • surfactants • controlled delivery • molecular gate

1. Communication

Controlled delivery has become an essential field of research for the design of systems able to liberate a cargo upon the application of specific stimuli, as stimuli-responsive systems allow to minimize side effects caused by non-controlled administration.[1] Traditionally, the delivery systems were based on polymers that released the cargo by diffusion-controlled processes or through degradation of the polymer container.[2,3] In the last years, porous hybrid organic-inorganic materials have merged as a noteworthy and large class of materials.[4–7] These materials show high surface area, tunable pore size and versatility in their framework composition, which confer them an outstanding performance in many fields such as drug delivery, species adsorption and sensing applications among others.[8–12] In particular, a promising alternative for controlled delivery systems are mesoporous silica particles (MSPs) due to their versatile properties such as low toxicity, high internal volume and easy chemical functionalization.[13] The opportunity of functionalizing the external surface of the MSPs with capping agents and uncap them with predefined stimuli makes these supports ideal candidates for controlled delivery applications. A number of examples able to payload deliver in the presence of physical, chemical and biochemical stimuli have been widely described.[14–18]

Despite these reported examples, the design of MSPs gated materials able to control the delivery through the action of surfactants is still emerging. To the best of our knowledge, only one example involving surfactant-responsive mesoporous silica particles has been recently described.[19] In that work, mesoporous materials loaded with a dye and capped with a lipid bilayer was prepared. The solid was opened by the rupture of the lipid bilayer induced by the presence of the surfactant DTABr (dodecyltrimethylammonium bromide). However, and despite the appeal of this attractive stimuli-responsible strategy on MSPs, no more examples of surfactant triggers have been reported.

Surfactant nature of bile salts from the duodenum has been thoroughly reported in literature. In addition to play an important role in cholesterol elimination route, in hormone secretion or in the stimulation of intestinal immune

system, bile contains surfactant molecules that emulsify ingested fats facilitating their intestinal absorption.[17,18] However, this character of bile salts has not yet been explored as a possible trigger for capped MSPs to deliver certain molecules in the small intestine. The small intestine is a relevant place where controlled release is needed, being the site where the bioactive molecules absorption takes place.[20] Traditionally, the particles developed to deliver active molecules in the small intestine use pH changes and the presence of enzymes as external stimuli, despite the inconvenience that these stimulus can be also present in other parts of the digestive tract.[21,22]

In this scenario, with the aim of exploring the surfactant properties of bile salts, we present here MSPs capped with strong hydrophobic lipid molecules (oleic acid) and loaded with a reporter, rhodamine B (RhB). Our original approach relies on proving that using lipid-capped silica mesoporous particles a remarkable delivery control can be obtained as only surfactants should trigger the release of the cargo, whereas in their absence, zero release should be maintained.

Lipid molecules have been widely used as carriers of bioactive molecules, but their use as capping molecules is scarce in the literature.[23,24] The attachment of lipid molecules on the MSPs surface originates a hydrophobic layer around the particles that avoids the release of the loaded cargo. In our case, oleic acid was selected as capping agent, which confers the aforementioned hydrophobic character and increases the bioapplicability of the particles.[25] The presence of oleic acid in capped-mesoporous silica particles has been described but, as far as we know, its use as capping system for surfactant-responsive controlled release has not been reported yet. The presence of surfactant molecules (as bile salts) was expected to allow the release of the cargo entrapped into the MSPs, via the emulsifier action of surfactants on the hydrophobic layer (oleic acid). The novelty of this work relies on the remarkable effect of the surfactant nature of bile salts in the controlled release of the cargo loaded inside the pores of the oleic acid-capped mesoporous silica particles. As far as we know, this is the first example of bile salts surfactant-responsive-induced delivery using lipid-capped silica mesoporous particles.

SBA-15 microparticles were chosen as support in the envisioned functional MSPs system. SBA-15 was prepared using Pluronic 123 as micellar template and tetraethylortosilicate (TEOS) as inorganic precursor. The as-made solid was calcined at 550 ℃ for 5 h in order to remove the organic template, and the resulted porous solid was loaded with RhB (solid **S0**). Solid **S0** was functionalized firstly with (3-aminopropyl)triethoxysilane (APTES) to produce the coating of the surface with amino groups (solid **S1**) and then with oleic acid by means of amidation reaction, giving the final solid **S2**, see Scheme 1. All the solids were then characterized using standard techniques (see Supporting information for details).[26] Powder X-ray diffraction (PXRD), transmission electron microscopy (TEM) and N_2 adsorption-desorption isotherms carried out on the initial SBA-15 mesoporous particles, clearly showed a mesoporous structure that remained in solid **S2** regardless of the loading process and further functionalization with APTES and oleic acid. DLS measurements pointed out an average particle size of 1 μm for the prepared solids. FTIR spectra was used to follow the functionalization process through the anchoring of the APTES moieties in **S1** and the formation of the amide bond between the anchored amines and the oleic acid to form the gating system in solid **S2.** Measurements of ζ potential of the different materials were in agreement with the functionalization process reaching a value of 44.43 mV in **S2**, indicative of a stable final material. Thermogravimetric analysis (TGA) and elemental analysis (EA) showed an organic matter content of 43.1 mg RhB g^{-1} SiO_2 and 84.7 mg molecular gate g^{-1} SiO_2 in **S2**.

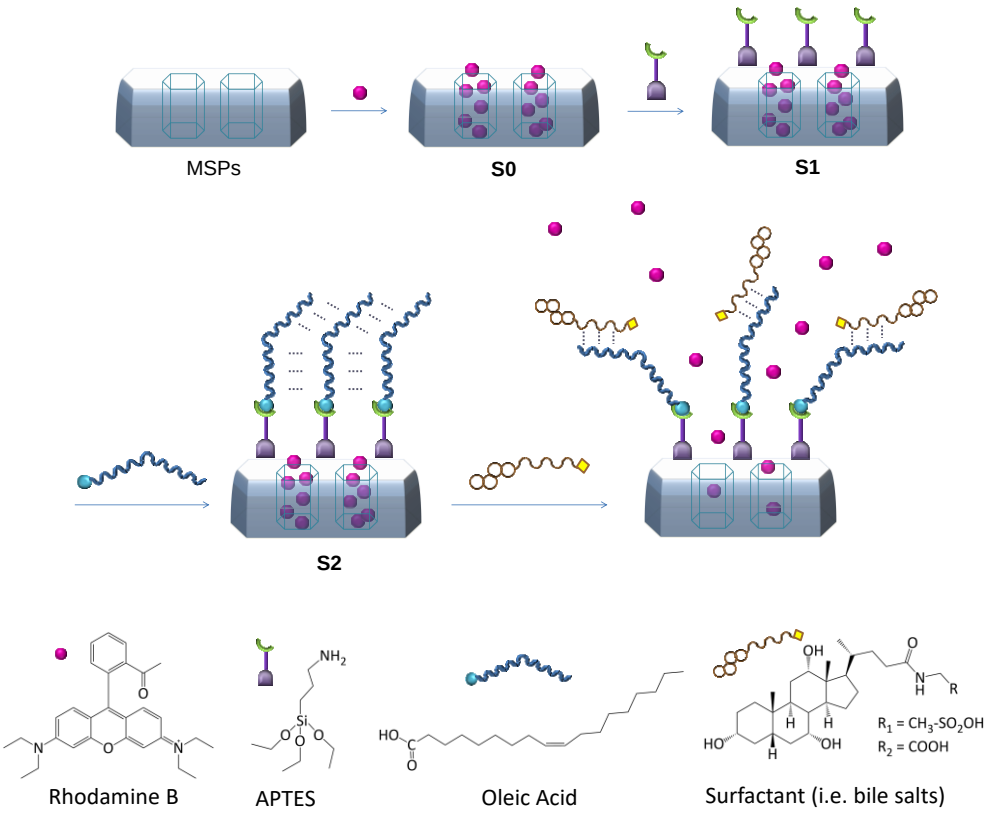

Scheme 1. Representation of mesoporous silica material encapsulated with a cargo molecule (RhB) and capped with APTES and the oleic acid layer attached to the free amine of the APTES. Addition of surfactant (i.e. bile salts) to S2 would uncap the mesopores via emulsifier action.

In addition to the characterization process applied to all solids,26 the release profile of RhB from solid S2 was studied in the presence and absence of bile salts at 37 ºC. In a typical experiment, 5 mg of S2 were suspended in 10 mL of PBS or in 10 mL of a bile extract solution. At different times an aliquot was taken, filtered, and the fluorescence signal of RhB measured (λ_{ex} = 555 nm, λ_{em} = 572 nm). As depicted in Figure 1 no cargo release was observed when the solid was suspended in PBS. In contrast, a remarkable delivery was achieved when bile salts were present. After 4 hours of the experiment, almost 80% of the total cargo release was reached.

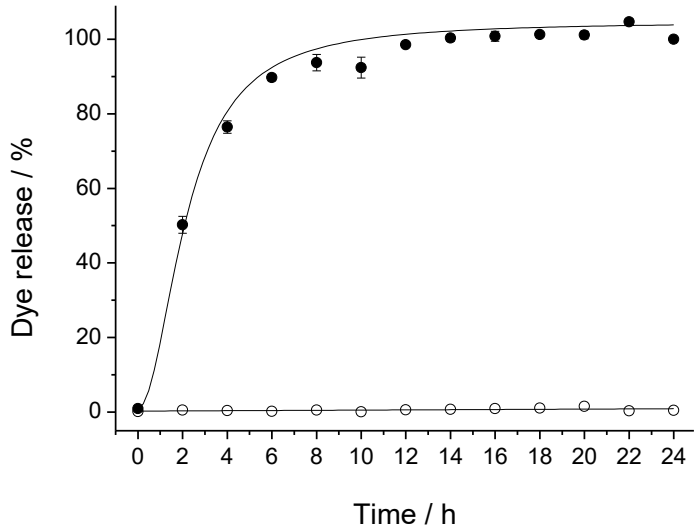

Figure 1. Kinetic release profile of RhB dye from **S2** in a PBS suspension without bile salts (○) and when bile salts are present (●)

In order to study the surfactant-responsive controlled-release protocol in detail, several experiments of RhB release from **S2** in the presence of bile salts, different gastrointestinal enzymes (pepsin, pancreatin, pronase, and esterase) and different surfactants (CTAB, SDS, Triton™ X-100) were carried out. For this purpose, 5 mg of **S2** were suspended in 10 mL of the corresponding solution, and the suspension was stirred for 10 h to allow maximum cargo delivery. Figure 2 shows

no RhB release when **S2** was suspended in water, PBS or solutions containing enzymes. However, a high cargo release was induced when surfactants were present. Comparing the effect of different surfactants, the release achieved with CTAB, SDS or Triton™ X-100 was higher than that found with bile salts. It is tentatively attributed to the fact that the surfactant concentration on bile extract used is between 3 and 8×10^{-3} M, lower than the one used for CTAB, SDS or Triton™ X-100. These experiments demonstrated that only surfactant molecules were able to open the **S2** system, while the solid remains capped when surfactants are not present.

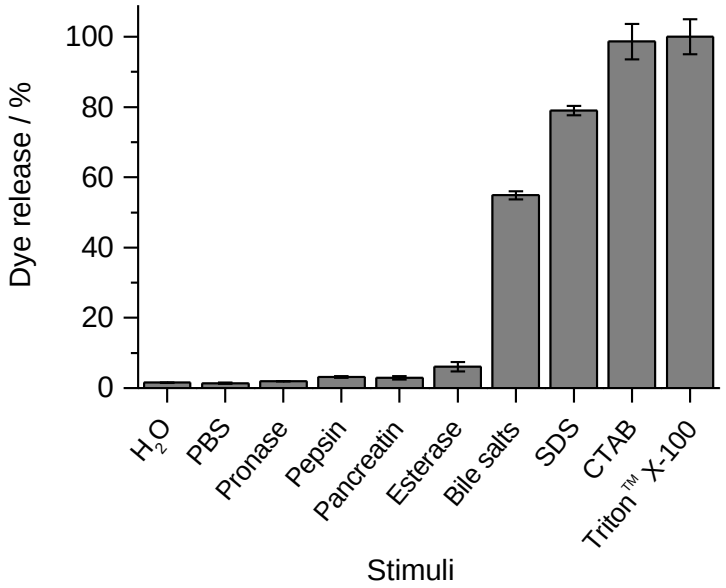

Figure 2. Percentages of dye released from **S2** with different stimuli. Enzymes solutions were prepared in PBS at their optimal pH (7.5 for pancreatin, pronase and esterase; and 2 for pepsin), in the same concentration as the one of bile extract (10 mg/mL). Surfactants concentration was 10^{-2} M.

Having this in mind and taking into account that active molecules are absorbed in the small intestine,[20] **S2** was tested in an *in vitro* digestion. The assay was carried out simulating the digestive steps and conditions of mouth, stomach and small intestine (see Figure 3). In this experiment, the corresponding fluids were added after certain times to 5 mg of **S2** (3, 6 and 9 mL of simulated saliva, gastric and intestinal fluids, respectively). Aliquots were taken at different times to measure the fluorescence signal of the RhB release over 5 hours.[26] Figure 3 shows no cargo release from **S2** during the mouth and stomach digestion (saliva and gastric fluid addition), while in the small intestine, when bile salts were added, the signal of the cargo increased. This difference is in agreement with the selective opening of **S2** in the presence of the bile salts acting as surfactant.

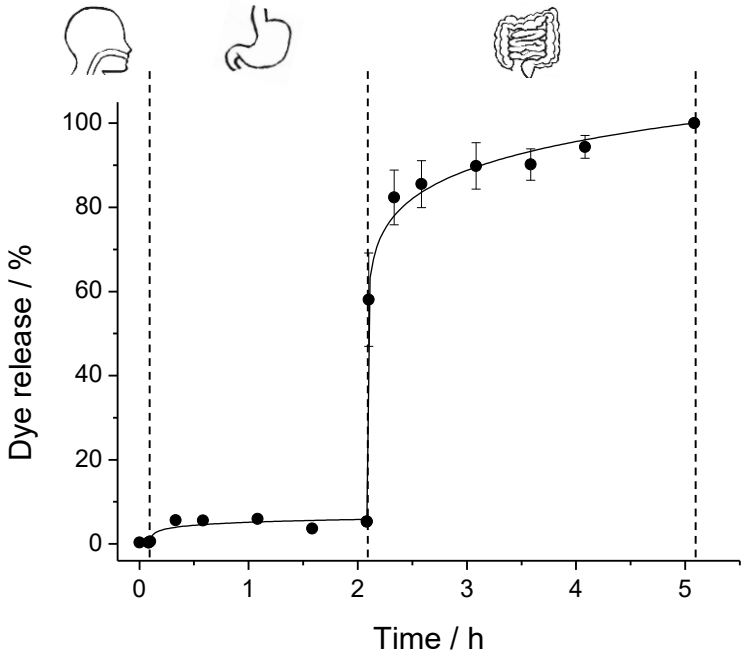

Figure 3. *In vitro* digestion of **S2**, in saliva, gastric fluid and small intestine for 5 hours.

Finally, in order to validate the system for biological or nutritional application, the bioactive molecule riboflavin-5P, one of the vitamers of vitamin B_2, was loaded into the pores of MSPs. Riboflavin plays important roles in energy metabolism and is required in the metabolism of amino acids, fatty acids and carbohydrates. Moreover, it is well established that water-soluble vitamins, as riboflavin, are absorbed in the intestine via specific carrier-mediated processes.[27] Interference with absorption, which occurs in a variety of conditions (e.g. congenital defects in the digestive or absorptive system, intestinal disease/resection, drug interaction and chronic alcohol use), leads to the development of deficiency (and sub-optimal status) and results in clinical abnormalities.[27] Riboflavin deficit is related with different diseases as migraine and hypertension,[28] anemia,[29] brain injury,[30] intestinal disorders[31,32] and also cell carcinomas.[33] A dietary supplementation with riboflavin could be an effective therapy for these diseases, or serve as palliative treatment to decrease the symptoms.[28]

Based on the above-mentioned facts, encapsulation and controlled release of riboflavin appears to be an important approach. Then, SBA-15 was loaded with riboflavin-5P, and afterwards functionalized in two steps with APTES and oleic acid to obtain the final solid **S3** (ζ potential 39.71 mV, 50.0 mg Riboflavin-5P g^{-1} SiO_2 and 167.2 mg molecular gate g^{-1} SiO_2). Solid **S3** release was tested in similar conditions than solid **S2**, using water as blank and a surfactant solution as stimulus, and an analogous behavior was observed. The riboflavin-5P release in the blank solution was negligible compared with the one achieved in the presence of surfactant.[26]

In summary, although several controlled release systems based on mesoporous silica particles have been described, none of them uses bile salts or other surfactant as opening stimulus for gastrointestinal delivery. Lipid systems have been used as carriers of bioactive molecules, but its performance as release controllers in the presence of specific stimuli has not been reported yet. The microdevice presented here has many advantages such as the high loading capacity typical of mesoporous silica materials, an expected good biocompatibility due to the external lipid coating, and specific controlled release in the presence of

surfactants. In conclusion, the synthesis of new oleic acid-capped mesoporous silica particles as surfactant-responsive delivery systems for on-command delivery applications has been described. The zero-release system's behavior in the absence of surfactant molecules could make it a useful protective support for sensitive molecules, and its selective response to surfactant molecules can be used as specific trigger for both controlled delivery and sensory applications. In fact, very good performance of bile salts, similar to that of commercial surfactants, in the controlled release of the cargo loaded inside the pores of the oleic acid-capped mesoporous silica particles was demonstrated. As far as we know, this is the first example of surfactant-responsive-induced delivery using lipid-capped silica mesoporous particles. We believe that our microdevice presented here, possesses high potential for finding application in the food and pharmaceutical industry.

2. Experimental Section

2.1. Solids synthesis

In a typical synthesis, 300 mg of SBA-15 were suspended in 20 mL of an aqueous solution of RhB (115 mg, 0.24 mol) and stirred during 24 h to obtain the loaded solid **S0**. After that, an excess of APTES (1.75 mL, 7.48 mmol) was added to the previous mixture, and the mixture was stirred during 5.5 h. Solid **S1** was isolated by centrifugation and was dried at 37 ℃ overnight.

Then, 300 mg of **S1** were added to a mixture of 50 mg of EDC and 5 mL of oleic acid in 18 mL of ethanol in order to obtain the final loaded and functionalised solid **S2**. This solid was washed twice with an ethanol:water (2:1) mixture and dried at 37 ℃ overnight.

In order to obtain the riboflavin loaded and functionalized solid (**S3**), 150 mg of SBA-15 were suspended in a riboflavin solution [75 mg in 6 mL of a water:methanol (2:1) mixture] and stirred during 24 h. After that, the solid was centrifuged and promptly re-suspended in 5 mL of acetone. Then an excess of

APTES (0.876 mL, 3.74 mmol) was added. The reaction was stirred during 5.5 h, centrifuged and dried at 37 ℃ overnight. 50 mg of the dried solid were added to a mixture of oleic acid (1 mL) and DCC (17 mg) in acetone (10 mL), and the reaction was stirred overnight. The final solid **S3** was centrifuged, washed twice with ethanol:water (2:1) and dried at 37 ℃ overnight.

Acknowledgements

The authors want to thank the Spanish Government (projects MAT2015-64139-C4-1-R, AGL2015-70235-C2-1-R and AGL2015-70235-C2-2-R (MINECO/FEDER)) and the Generalitat Valenciana (project PROMETEO/2018/024) for support. E.P-R. thanks the Generalitat Valenciana for her predoctoral fellowship. A.B. wants to acknowledge the Spanish Government for the financial support Juan de la Cierva Incorporación IJCI-2014-21534. The authors also thank the Electron Microscopy Service at the UPV for support.

References

1 K. Harrison, in *Biomedical Polymers.*, ed. M. Jenkins, Cambridge: Woodhead Publishing, UK, 2007, pp. 33–56.

2 G. Shankar and Y. K. Agrawal, *Int. J. Pharm. Sci. Res.*, 2017, **8**, 4983–4991.

3 V. Bourganis, T. Karamanidou, O. Kammona and C. Kiparissides, *Eur. J. Pharm. Biopharm.*, 2017, 111, 44–60.

4 S. A. El-Safty, M. A. Shenashen and A. A. Ismail, *Chem. Commun.*, 2012, **48**, 9652–9654.

5 S. A. El-Safty, M. Khairy, M. A. Shenashen, E. Elshehy, W. Warkocki and M. Sakai, *Nano Res.*, 2015, **8**, 3150–3163.

6 S. A. El-Safty, M. A. Shenashen, M. Ismael and M. Khairy, *Adv. Funct. Mater.*, 2012, **22**, 3013–3021.

7 M. A. Shenashen, A. Shahat and S. A. El-Safty, *J. Hazard. Mater.*, 2013, **244–245**, 726–735.

8 S. A. El-Safty, M. A. Shenashen, M. Ismael and M. Khairy, *Chem. Commun.*, 2012, **48**, 6708–6710.

9 S. A. El-Safty, M. A. Shenashen and A. Shahat, *Small*, 2013, **9**, 2288–2296.

10 S. A. El-Safty and M. A. Shenashen, *Sensors Actuators, B Chem.*, 2013, **183**, 58–70.

11 I. M. El-Sewify, M. A. Shenashen, A. Shahat, H. Yamaguchi, M. M. Selim, M. M. H. Khalil and S. A. El-Safty, *J. Lumin.*, 2018, **198**, 438–448.

12 M. Y. Emran, S. A. El-Safty, M. A. Shenashen and T. Minowa, *Sensors Actuators, B Chem.*, 2019, **284**, 456–467.

13 G. Kickelbick, *Angew. Chemie - Int. Ed.*, 2004, **43**, 3102–3104.

14 E. Aznar, M. Oroval, L. Pascual, J. R. Murguía, R. Martínez-Máñez and F. Sancenón, *Chem. Rev.*, 2016, **116**, 561–718.

15 I. Candel, E. Aznar, L. Mondragón, C. De La Torre, R. Martínez-Máñez, F. Sancenón, M. D. Marcos, P. Amorós, C. Guillem, E. Pérez-Payá, A. Costero, S. Gil and M. Parra, *Nanoscale*, 2012, **4**, 7237–7245.

16 P. Díez, A. Sánchez, M. Gamella, P. Martínez-Ruíz, E. Aznar, C. De La Torre, J. R. Murguía, R. Martínez-Máñez, R. Villalonga and J. M. Pingarrón, *J. Am. Chem. Soc.*, 2014, **136**, 9116–9123.

17 C. De La Torre, A. Agostini, L. Mondragón, M. Orzáez, F. Sancenón, R. Martínez-Máñez, M. D. Marcos, P. Amorós and E. Pérez-Payá, *Chem. Commun.*, 2014, **50**, 3184–3186.

18 É. Pérez-Esteve, A. Fuentes, C. Coll, C. Acosta, A. Bernardos, P. Amorós, M. D. Marcos, F. Sancenón, R. Martínez-Máñez and J. M. Barat, *Microporous Mesoporous Mater.*, 2015, **202**, 124–132.

19 M. González-Alvarez, C. Coll, I. Gonzalez-Alvarez, C. Giménez, E. Aznar, M. C. Martínez-Bisbal, I. Lozoya-Agulló, M. Bermejo, R. Martínez-Máñez and F. Sancenón, *Mol. Pharm.*, 2017, **14**, 4442–4453.

20 M. Shimizu, *Biosci. Biotechnol. Biochem.*, 2010, **74**, 232–241.

21 A. Bernardos, E. Aznar, C. Coll, R. Martínez-Mañez, J. M. Barat, M. D. Marcos, F. Sancenón, A. Benito and J. Soto, *J. Control. Release*, 2008, **131**, 181–189.

22 A. Bernardos, E. Aznar, M. D. Marcos, R. Martínez-Máñez, F. Sancenón, J. Soto, J. M. Barat and P. Amorós, *Angew. Chemie - Int. Ed.*, 2009, **48**, 5884–5887.

23 N. Han, Y. Wang, J. Bai, J. Liu, Y. Wang, Y. Gao, T. Jiang, W. Kang and S. Wang, *Microporous Mesoporous Mater.*, 2016, **219**, 209–217.

24 J. Zhang, D. Desai and J. M. Rosenholm, *Adv. Funct. Mater.*, 2014, **24**, 2352–2360.

25 M. M. Van Schooneveld, E. Vucic, R. Koole, Y. Zhou, J. Stocks, D. P. Cormode, C. Y. Tang, R. E. Gordon, K. Nicolay, A. Meijerink, Z. A. Fayad and W. J. M. Mulder, *Nano Lett.*, 2008, **8**, 2517–2525.

26 See Supporting information for details, .

27 H. M. Said, *Biochem. J.*, 2011, **437**, 357–372.

28 K. Thakur, S. K. Tomar, A. K. Singh, S. Mandal and S. Arora, *Crit. Rev. Food Sci. Nutr.*, 2017, **57**, 3650–3660.

29 M. Lane and C. P. Alfrey Jr, *Blood J.*, 1965, **25**, 432–442.

30 A. M. Bosch, N. G. G. M. Abeling, L. Ijlst, H. Knoester, W. L. Van Der Pol, A. E. M. Stroomer, R. J. Wanders, G. Visser, F. A. Wijburg, M. Duran and H. R. Waterham, *J. Inherit. Metab. Dis.*, 2011, **34**, 159–164.

31 H. M. Said, A. Ortiz, M. P. Moyer and N. Yanagawa, *Am. J. Physiol. Cell Physiol.*, 2000, **278**, C270–C276.

32 E. Nakano, S. Mushtaq, P. R. Heath, E. S. Lee, J. P. Bury, S. A. Riley, H. J. Powers and B. M. Corfe, *Dig. Dis. Sci.*, 2011, **56**, 1007–1019.

33 S.-S. Li, Y.-W. Xu, J.-Y. Wu, H.-Z. Tan, Z.-Y. Wu, Y.-J. Xue, J.-J. Zhang, E.-M. Li and L.-Y. Xu, *Nutr. Cancer*, 2017, **69**, 21–28.

34 D. Zhao, J. Feng, Q. Huo, N. Melosh, G. H. Fredrickson, B. F. Chmelka and G. D. Stucky, *Science (80-.).*, 1998, **279**, 548–552.

35 C. H. M. Versantvoort, A. G. Oomen, E. Van De Kamp, C. J. M. Rompelberg and A. J. A. M. Sips, *Food Chem. Toxicol.*, 2005, **43**, 31–40.

SUPPORTING INFORMATION

New oleic acid-capped mesoporous silica particles as surfactant-responsive delivery systems

Elisa Poyatos-Racionero,[a,b] Édgar Pérez-Esteve,[a,c] M. Dolores Marcos,[a,b,d,f,g],* José M. Barat,[c,e] Ramón Martínez-Máñez,[a,b,d,f,g],* Elena Aznar,[a,b,f,g] and Andrea Bernardos,[a,b,g]

[h] Instituto Interuniversitario de Investigación de Reconocimiento Molecular y Desarrollo Tecnológico (IDM), Universitat Politècnica de València, Universitat de València. Camino de Vera s/n, 46022, Valencia (Spain).

[i] CIBER de Bioingeniería, Biomateriales y Nanomedicina (CIBER-BBN) (Spain)

[j] Grupo de Investigación e Innovación Alimentaria (CUINA). Universitat Politècnica de València Camino de Vera s/n, 46022, Valencia (Spain).

[k] Departamento de Química, Universitat Politècnica de València. Camino de Vera s/n, 46022, Valencia (Spain).

[l] Departamento de Tecnología de Alimentos, Universitat Politècnica de València. Camino de Vera s/n, 46022, Valencia (Spain)

[m] Unidad Mixta de Investigación en Nanomedicina y Sensores Universitat Politècnica de València, IIS La Fe de Valencia. 46026, Valencia (Spain)

[n] Unidad Mixta UPV-CIPF Investigación de Mecanismos Enfermedad y Nanomedicina, Universitat Politècnica de València, Centro de Investigación Príncipe Felipe. 46100, Valencia (Spain).

* Correspondence: mmarcos@upv.es (M.D.M.); rmaez@qim.upv.es (R.M-M.)

ChemistryOpen **2019**, *8*, 1052.

General techniques for characterization

Powder X-ray diffraction (PXRD), transmission electron microscopy (TEM), N_2 adsorption-desorption, thermogravimetric analysis (TGA), elemental analysis, Dynamic Light Scattering (DLS), ζ potential, UV-visible (UV-vis) and fluorescence spectroscopy were employed to characterize synthesized materials. PXRD measurements were taken on a D8 Advance diffractometer using CuKα radiation (Philips, Amsterdam, The Netherlands). TEM images were obtained with a 100 kV CM10 microscope (Philips). N_2 adsorption-desorption isotherms were recorded with a Tristar II Plus automated analyzer (Micromeritics, Norcross, GA, USA). The samples were degassed at 120℃ in vacuum overnight. Specific surface areas were calculated from the adsorption data within the low-pressure range using the Brunauer, Emmett and Teller (BET) model. Pore size was determined following the Barret, Joyner and Halenda (BJH) method. Thermogravimetric analyses were carried out on a TGA/SDTA 851e balance (Mettler Toledo, Columbus, OH, USA) in an oxidizing atmosphere (air, 80 mL min^{-1}) with a heating program which consist of a gradient of 393-1273 K at 10℃ min^{-1}, followed by an isothermal heating step at 1273℃ for 30 min. ζ potential of the particles was measured in Ethanol 96% at 20 ºC by Zetasizer Nano ZS equipment (Malvern Instruments, Malvern, UK) and their size was measured by DLS in a Malvern Mastersizer 2000 (Malvern Instruments, Malvern, UK). Fluorescence spectroscopy measurements were taken on a JASCO FP-8500 fluorimeter and UV-Visible spectra were recorder with a JASCO V-650 spectrophotometer.

Chemicals

Tetraethylortosilicate (TEOS), Pluronic 123 (P123), Hydrochloric acid 37% (HCl), N-cetyltrimethylammonium bromide (CTABr), (3-aminopropyl)triethoxysilane (APTES), N-(3-dimethylaminopropyl)-N'-ethylcarbodiimide (EDC), N,N'-dicyclohexylcarbodiimide (DCC), Rhodamine B (RhB), oleic acid, the employed surfactants (SDS, LAS, Triton™-X100), all the chemicals for the digestive fluids (bile extract included) and enzymes (pancreatin, pronase, pepsin and esterase) were provided by Sigma (Sigma-Aldrich Química S.L., Madrid,

Spain). Riboflavin 5-Phosphate was provided from Proquimac (Barcelona, Spain); and ethanol (extra pure and 96%), methanol and acetone were purchased from Scharlau (Barcelona, Spain). Bile extract from Sigma Aldrich had bile salts concentration between 3 and 8×10^{-3} M.

Mesoporous silica particles synthesis

SBA-15 microparticles were synthesized following the method described by Zhao et al.[1] P123 was used as structure-directing agent. Molar ratio of the reagents was fixed to 0.017 P123:1.0 TEOS:6 HCl:196 H_2O. The preparation was performed by mixing an aqueous solution of 4 g of P123 with HCl 37%, and stirring for 2 h, after which the silica source, TEOS, was added dropwise. This final mixture was stirred for a further 24 h, and it was aged in an autoclave at 100 ℃ for 24 h. The mixture was filtered, the obtained white solid was washed with deionized water until neutral pH and dried at 70 ℃ overnight. The final SBA-15 particles were obtained by calcination of the as-synthesized solid at 550 ℃ during 5 h in oxidant atmosphere with the aim of removing the surfactant template.

Characterization

All the solids were characterized using standard techniques, as powder X-Ray diffraction (PXRD), transmission electron microscopy (TEM), N_2 adsorption–desorption isotherms (N_2 ads-des), thermogravimetric analysis (TGA) and elemental analysis (EA).

The PXRD (Figure S1 a-d) of all solids show a sharp peak and two minor ones indexed as (100), (110) and (200) Bragg reflections, respectively, indicating that the porous structure is preserved during the loading and functionalization processes. The mesoporous structure of all the solids was confirmed from TEM analysis, in which the typical channels of the SBA-15 matrix were visualized as alternate black and white stripes (see Figure S1 e-g for TEM images of solids **S0** and **S2**, and **S3** respectively).

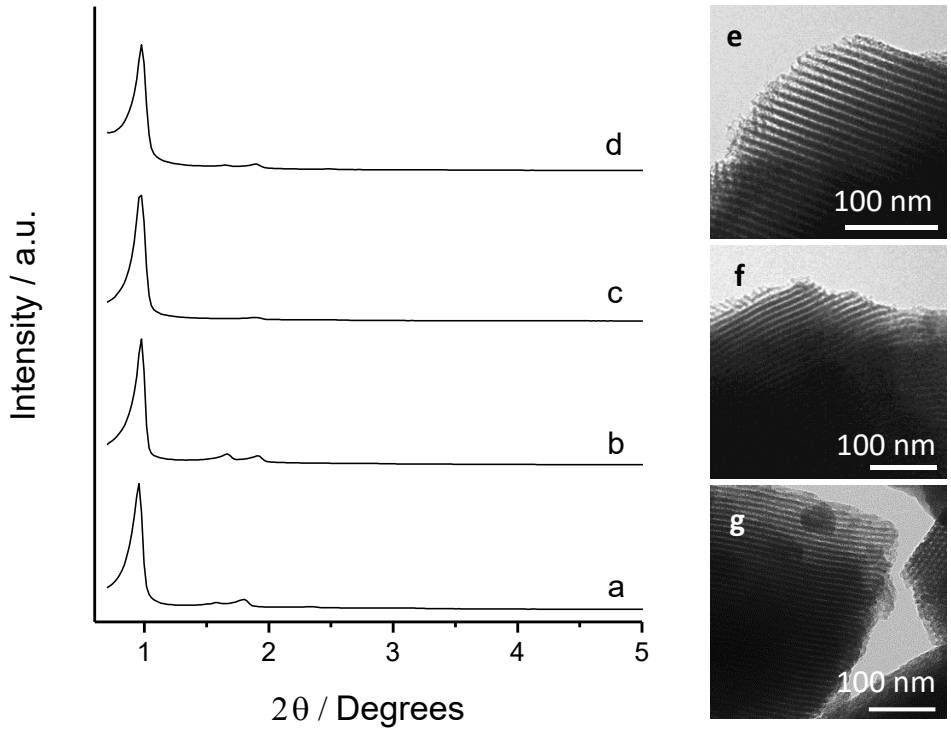

Figure S1. Left: powder X-ray diffraction (PXRD) patterns of solids (**a**) SBA-15 particles as made, (**b**) SBA-15 calcined and (**c**) **S2**, (d) **S3** Right: TEM images of (**e**) SBA-15 calcined, (**f**) **S2** and (**g**) **S3**, showing the typical porosity of the mesoporous silica matrix.

The N_2 adsorption-desorption isotherms of the microparticles SBA-15 calcined material is shown in Figure S2. A typical curve for these mesoporous solids consisting of an adsorption step at intermediate P/P_0 value (0.1-0.3) can be observed. This curve corresponds to a type IV isotherm, in which the observed step corresponds with nitrogen condensation inside the mesopores. The pore diameter (5.3 nm) and pore volume (0.82 $cm^3\ g^{-1}$) values were calculated using the BJH model on the adsorption branch of the isotherm. The application of the BET model resulted in a value of 678.6 m^2/g for the total specific surface (**Table S1**).

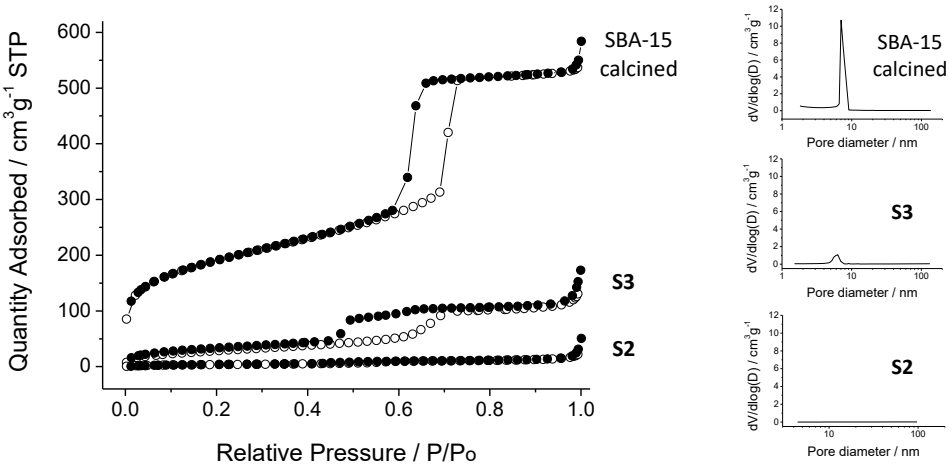

Figure S2. Left: nitrogen adsorption (○) – desorption (●) isotherms for SBA-15 mesoporous materials: SBA-15 calcined (top), loaded and functionalized solid S3 (middle) and loaded and functionalized solid S2 (bottom). Right: pore volumes of SBA-15 calcined, **S3** and **S2** (top, middle and bottom, respectively).

The N_2 adsorption-desorption isotherm of solids **S2** and **S3** is typical of mesoporous systems with practically filled mesopores (see Figure S2). Consequently, relatively low N_2 adsorbed volume and surface area (see **Table S1**) values were calculated. In fact, these solids show flat or almost flat curves when compared to those of the SBA-15 parent material, which indicates significant pore blocking and the subsequent absence of appreciable mesoporosity.

Table S1. BET specific surface values, pore volumes and pore sizes calculated from the N_2 adsorption–desorption isotherms for selected materials.

	S_{BET} ($m^2\ g^{-1}$)	Pore Volume ($cm^3\ g^{-1}$)	Pore size [c] (nm)
calcined SBA-15	678.6	0.82	5.32
S2	14.3	0.03	-
S3	108.0	0.19	-

[a]Pore volumes and pore sizes were estimated by using the BJH model applied on the adsorption branch of the isotherm. Data were restricted to intraparticle mesopores.

Thermogravimetric analysis (TGA) and elemental analysis (EA) indicated an organic matter content of 43.1 mg RhB g^{-1} SiO_2 and 84.7 mg molecular gate g^{-1} SiO_2 in **S2**; and 50.0 mg Riboflavin-5P g^{-1} SiO_2 and 167.2 mg molecular gate g^{-1} SiO_2 in **S3.** The proportion in mmol of all the moieties is summarized in Table S2.

Table S2. Content of RhB/Riboflavin-5P, APTES and oleic acid in the solids **S2** and **S3**.

Solid	α_{RhB} (mmol g^{-1} SiO_2)	α_{APTES} (mmol g^{-1} SiO_2)	$\alpha_{Oleic\ acid}$ (mmol g^{-1} SiO_2)
S2	0.09	1.23	0.08
S3	0.11	1.09	0.40

[a]Pore volumes and pore sizes were estimated by using the BJH model applied on the adsorption branch of the isotherm. Data were restricted to intraparticle mesopores.

The size of the particles was measured in ethanol 96%. A distribution of particles between 0.5 and 5 μm (mainly 1 μm) was obtained. The functionalization process gave smaller particles' size due to the repulsion effect between the charged moieties around the material's surface, which avoids the aggregation between particles (see Figure S3).

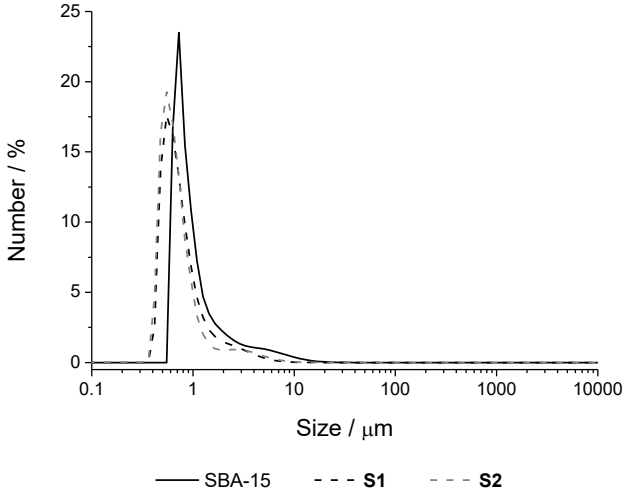

Figure S3. Size distribution of solids SBA-15, **S1** and **S2**.

Infrared spectroscopy and ζ potential were also used for following the functionalization process leading to solids **S2** and **S3**. In all the FTIR spectra the dominant bands are those due to the silica matrix (1060, 790 and 450 cm^{-1}). However, some changes in minor bands can be related with the presence of functionalized groups in solids **S2** and **S3.** Thus, it is possible to observe the decrease of the band at 960cm^{-1} assignable to the silanol group vibration when the APTES group is anchored to the surface of the silica matrix. Also, it is visible the appearance two bands at 2930 cm^{-1} and 2850 cm^{-1} assignable to the bending C–H vibrations, that increase as the functionalization process proceeds (see Figure S4).

On the other hand, the region that would have told us about the formation of the amide group shows an important number of bands due to the complex structure of the loaded molecules. Though it is difficult to unambiguously assign the bands between 1700 cm^{-1} and 1250 cm^{-1} many changes can be observed with the functionalization process as for example the decrease of the bands at 1330 cm^{-1} and 1270 cm^{-1} that could be assigned to the C-N vibration of the propylamine when anchoring the oleic acid to get the final gating moiety.

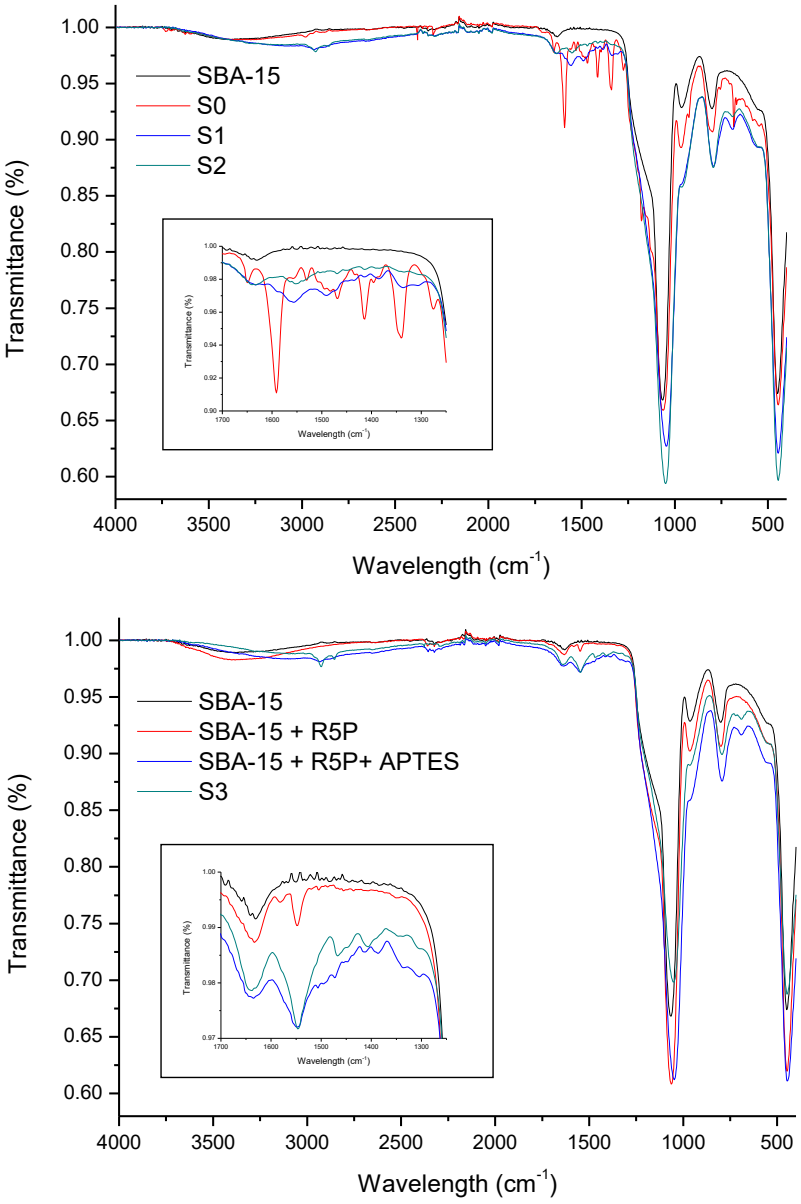

Figure S4. Top: Infrared spectra of the synthesis process of solids with RhB (**S0**, **S1**, **S2**). Bottom: Infrared spectra of the synthesis process of solids with Riboflavin-5P (SBA-15 + Riboflavin-5P, SBA-15 + Riboflavin-5P + APTES, **S3**).

ζ potential values are in agreement with the expected values for the external moieties. The starting material SBA-15 has a negative value of -27.45 mV which is still negative when the solids are loaded (**S0** and SBA-15 + Riboflavin-5P). The value changes to positive when APTES is added, due to the external amine groups (41.48 and 23.68 mv for **S1** and SBA-15 + Riboflavin-5P + APTES, respectively), and the values are still positive when oleic acid is added, due to the amide groups in the surface (see Figure S5).

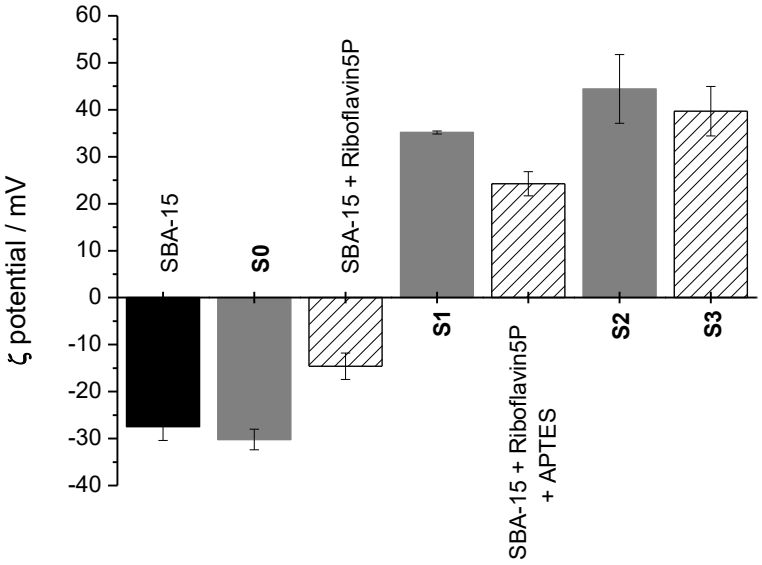

Figure S5. ζ potential values of the different solids synthesized from SBA-15 (black). The solids loaded with Rhodamine B are represented with solid gray bars, and solids loaded with Riboflavin-5P are represented with white striped bars.

Cargo release kinetics

In a typical experiment, 5 mg of solid **S2** were placed in 10 mL of PBS, simulating a general aqueous medium, and 10 mL of bile salts suspension (100 mg of bile salts in 10 mL of PBS), simulating conditions at the small intestine. At certain times aliquots were taken and filtered. Delivery of RhB from the pore voids to the different solutions was analyzed via the fluorescence emission band of this molecule at 572 nm (excitation at 555 nm, see Figure S6 left).

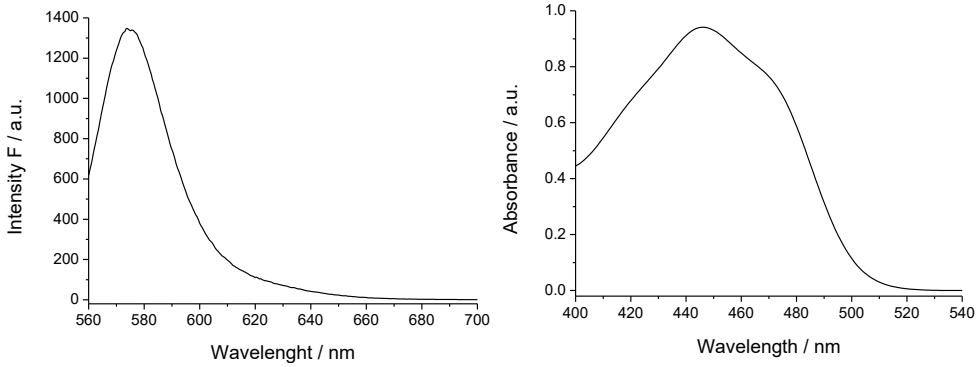

Figure S6. Left: fluorescence spectrum of Rhodamine B in water or bile solution. Right: Absorption spectrum of Riboflavin-5P in water or CTAB solution.

The procedure was repeated with some variations for the delivery of riboflavin from solid **S3**. In this experiment, 5 mg of solid **S3** were placed in 10 mL of distilled water and 10 mL of a CTAB 10^{-2} M solution as surfactant (to avoid the redox and pH effects of a complex matrix like bile salts on a sensible molecule like riboflavin-5P). The cargo release profiles are shown in Figure S7. Riboflavin-5P release was followed and quantified by means of its absorption band at 451 nm (see Figure S6 right).

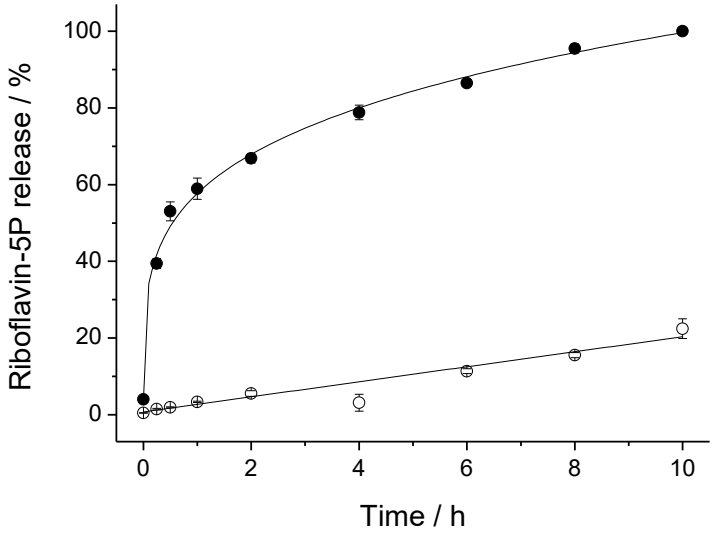

Figure S7. Kinetic release profile of riboflavin-5P from solid **S3** in aqueous medium without surfactant molecules (○), and when CTAB molecules are present (●).

***In vitro* digestion**

An *in vitro* digestion model consisting of mouth, gastric and intestinal phases was used to simulate the typical chemical composition, pH and residence time periods of each of the three main compartments of the gastrointestinal tract (GIT), in order to monitor the cargo release in the different sections of the GIT.[2] The pH values of the digestive juices were checked and, if necessary, adjusted to the appropriate interval with $NaHCO_3$ (1 M) or HCl (37% w/w).

In a typical experiment, 10 mg of solid **S2** were added to three vials (A, B and C) with the specified volume of simulated fluids (saliva, gastric fluid and intestinal fluid respectively). 3 mL of saliva fluid were added to the three vials, and aliquots were taken from vial A. Once the permanence time in the mouth was achieved, 6 mL of gastric fluid were added to vials B and C, and the respective aliquots were taken from vial B. Finally, when the two hours of gastric permanence were

completed, 12 mL of intestinal fluid and 1 mL of $NaHCO_3$ 1M (to adjust the pH value) were added to the last vial, C; and the pertinent aliquots where taken from it.

The aliquots taken at the stipulated times (0 and 5 min for saliva; 0, 15, 30, 60, 90 and 120 min for gastric fluid; and 0, 15, 30, 60, 90, 120 and 180 min for intestinal fluid) were filtered and its fluorescence (λ_{ex} = 555 nm, λ_{em} = 572 nm) was measured in order to register the amount of rhodamine B released from the pore voids.

References

1 D. Zhao, J. Feng, Q. Huo, N. Melosh, G. H. Fredrickson, B. F. Chmelka and G. D. Stucky, Science., 1998, 279, 548–552.

2 C. H. M. Versantvoort, A. G. Oomen, E. Van De Kamp, C. J. M. Rompelberg and A. J. A. M. Sips, Food Chem. Toxicol., 2005, 43, 31–40.

Article 2

Surfactant-Triggered Molecular Gate Tested on Different Mesoporous Silica Supports for Gastrointestinal Controlled Delivery

Elisa Poyatos-Racionero,[a,b] Isabel González-Álvarez,[c] Marta González-Álvarez,[c] Ramón Martínez-Máñez,[a,b,d,e,f] M. Dolores Marcos[a,b,d,e,f]*, Andrea Bernardos[b,a,e]* and Elena Aznar[a,b,d,e]

[a] CIBER de Bioingeniería, Biomateriales y Nanomedicina (CIBER-BBN) (Spain)

[b] Instituto Interuniversitario de Investigación de Reconocimiento Molecular y Desarrollo Tecnológico (IDM), Universitat Politècnica de València, Universitat de València. Camino de Vera s/n, 46022, Valencia (Spain).

[c] Departamento de Ingeniería, Sección de Farmacia y Tecnología Farmacéutica, Universidad Miguel Hernández. 03550, Alicante, Spain

[d] Unidad Mixta de Investigación en Nanomedicina y Sensores Universitat Politècnica de València, IIS La Fe de Valencia. 46026, Valencia (Spain)

[e] Unidad Mixta UPV-CIPF Investigación de Mecanismos de Enfermedad y Nanomedicina, Universitat Politècnica de València, Ctr Invest Príncipe Felipe. 46100, Valencia (Spain).

[f] Departamento de Química, Universitat Politècnica de València. Camino de Vera s/n, 46022, Valencia (Spain).

* Correspondence: mmarcos@upv.es (M.D.M.); anberba@upv.es (A.B.)

Nanomaterials **2020**, *10*, 1290

Abstract

In recent decades, the versatility of mesoporous silica particles and their relevance to develop controlled release systems have been demonstrated. Within them, gated materials able to modulate payload delivery represent great advantages. However, the role played by the porous matrix in this kind of systems is scarce. In this work, different mesoporous silica materials (MCM- 41, MCM-48, SBA-15 and UVM-7) are functionalized with oleic acid as a molecular gate. All systems are fully characterized and their ability to confine the entrapped cargo and release it in the presence of bile salts is validated with release assays and in vitro digestion experiments. The cargo release profile of each synthesized support is studied, paying attention to the inorganic scaffold. Obtained release profiles fit to Korsmeyer–Peppas model, which explains the differences among the studied supports. Based on the results, UVM-7 material was the most appropriate system for duodenal delivery and was tested in an in vivo model of the Wistar rat. Payload confinement and its complete release after gastric emptying is achieved, establishing the possible use of mesoporous silica particles as protection and direct release agents into the duodenum and, hence, demonstrating that these systems could serve as an alternative to the administration methods employed until now.

Keywords: mesoporous silica • oleic acid • molecular gate • MCM-41 • MCM-48 • SBA-15 • UVM-7 • controlled release • kinetic modelling • gastrointestinal delivery

1. Introduction

The use of mesoporous silica particles (MSPs) as delivery systems of bioactive molecules has been reinforced during recent years. The great loading capacity in their ordered pore matrix, low toxicity levels and high stability in biological conditions, especially when organic moieties are attached to the external surface,[1–3] make them ideal supports for passive release supports. In these systems, cargo molecules are released from the pores of the particles by diffusion mechanisms.[4] Moreover, MSPs also become ideal candidates for active (or controlled) release, where a stimulus-triggered mechanism regulates cargo delivery.[4,5] The combination of a suitable pore size, together with an appropriate external functionalization to control payload delivery,[6] gives them versatile uses in different fields, such as catalysis,[7,8] controlled drug release,[9–13] sensing,[14–17] communication[18,19] and protection and controlled administration of molecules with nutraceutical interest.[20–23]

Within the wide field of MSPs, microparticles present a special interest for the controlled release in the lumen of the gastrointestinal tract (GIT), since their large size makes their internalization in healthy epithelial tissues difficult.[24–26] In the field of MSPs, it is possible to find a wide diversity of structures with different morphology, composition or pore pattern.[27,28] Despite this wide range and versatility, the influence of inorganic support on the cargo release has been only thoroughly examined in passive release systems.[4,29–31] Generally, on active release works, the triggered opening of the molecular gate is the main pursued objective with the aim of minimizing the non-specific payload release. Studies of active release in which the importance of inorganic support is evaluated are rarely found;[32–34] however, the release process can strongly depend on the utilized support.

Another aspect to be considered in delivery systems based on MSPs is that sustained release over time is usually the most common objective in drug administration into the organism, in order to promote the progressive incorporation of the components into the blood stream.[35] However, this statement,

although true for many substances, is not applicable to the entire spectrum of drugs currently administered. There are drugs that require different action times, from an overtime sustained activity to an immediate one, or even the ability to combine both sustained and immediate action depending on the organism requirements, as in the case of insulin.[36] There are also processes in which a massive release is needed after a protection stage, such as intestinal absorption after protection from the stomach environment. This is the case of patients with gastric problems, or drugs that suffer from gastric malabsorption because of pH or the enzymes present in this organ.

Slightly detailing these last two examples, several drawbacks are found. On the one hand, patients with severe gastric diseases such as ulcers, bariatric surgery or gastrectomy undergo significant modifications of the stomach pH or the reconstructed area,[37] as well as a variation of the intestinal microbiota.[38] The aforementioned aspects highly influence the patient administration of medications that require strict pH conditions for their correct absorption.[39,40] On the other hand, there are drugs that suffer from degradation by the pH of the gastric juice and the exposition time to the enzymes secreted in the gastric and intestinal mucosa.[41] Due to these inconveniences, the direct intraduodenal perfusion is selected in some cases as an alternative administration route. With this system, the immediate absorption of the drug in blood is achieved and concentration fluctuations are decreased.[42,43] However, this kind of administration is dependent on surgery and on an intraduodenal pump that injects the selected drug continuously.[44,45]

In cases like these, an immediate release system in the duodenum would be the recommended solution to protect the drug and the stomach in equal parts. Additionally, with this solution, the dose of bioactive molecule that will reach the duodenum will not be reduced. These facts show that different modes of release could be necessary, and the possibility of having different systems that deliver their cargo in a sustained, immediate or combined way is an important aspect to be considered.

In this context, the objective of this research focuses on the controlled release performance of a chosen molecular gate, equally effective when it is functionalized on different MSPs, and on the role of the several supports in managing payload delivery. Thus, the release process in different inorganic structures perfectly protected by the same capping organic moiety would be determined by the properties of the loaded molecule and the material's pore structure. This fact allows one to have a set of microdevices with perfectly defined release profiles which enable the selection of the ideal one for a desired application.

Oleic acid (OA) has been demonstrated to be a good gating entity when functionalized onto MSPs for cargo delivery in the small intestine, avoiding cargo release when no bile salts (or surfactants) are present.[46] Its good behavior in both open and closed state was the reason why it was chosen as model to act as the molecular gate for the different mesoporous systems under this study. The main objective of this work is to survey the release profiles of different MSPs capped with OA in the presence of bile salts with the aim of finding the best one for cargo protection from the adverse conditions of the stomach and maximum release into the duodenum.

2. Materials and Methods

2.1. Chemicals and Cell Culture Media

Tetraethylortosilicate (TEOS), triethanolamine ($TEAH_3$), sodium hydroxide (NaOH), N-cetyltrimethylammonium bromide (CTAB), Pluronic 123 (P123), hydrochloric acid 37% (HCl), aqueous ammonia 28% (NH_4OH), trifluoroacetic acid (TFA), (3-aminopropyl)triethoxysilane (APTES), N-(3-dimethylaminopropyl)-N'-ethylcarbodiimide (EDC), rhodamine B (RhB), oleic acid (OA) and all the chemicals for the digestive fluids (bile salts included) were provided by Sigma (Sigma-Aldrich Química S.L., Madrid, Spain). Ethanol (extra pure), dimethyl sulfoxide (DMSO), acetonitrile (ACN) and acetone were purchased from Scharlab (Scharlab S.L., Barcelona, Spain). 3-(4,5-dimethylthiazol-2-yl)-2,5-diphenyltetrazolium bromide

(MTT) was provided by ThermoFisher (Thermo Fisher Scientific Inc., Madrid, Spain). Phosphate Buffer Solution (PBS), Dulbecco's Modified Eagle's Medium (DMEM), Fetal Bovine Serum (FBS), penicillin/streptomycin antibiotic (P/S), non- essential amino acids and all the needed mediums for cell culture were provided by Labclinics (Labclinics S.A., Barcelona, Spain).

2.2. Mesoporous Silica Particles Synthesis

MCM-41 microparticles (M41) were synthesized following the "atrane route" according to the method described by Cabrera et al.[47] CTAB was used as the structure-directing agent, and the molar ratio of the reagents was fixed to 7 $TEAH_3$:2 TEOS:0.52 CTAB:0.5 NaOH:180 H_2O. CTAB was added to a solution of $TEAH_3$ containing NaOH and TEOS at 118 °C. After dissolving CTAB in the solution, water was slowly added with vigorous stirring at 70 °C. The resultant white suspension formed after a few minutes was stirred for 1 h at room temperature, and then aged in an autoclave at 100 °C for 24 h.

MCM-48 microparticles (M48) were made applying the method described by Meléndez-Ortiz.[48] The molar ratio of the reagents was 0.11 CTAB:100 H_2O:13.1 EtOH:1.3 NH_4OH:0.2 TEOS. CTAB was dissolved in a mixture of H_2O:EtOH, and then NH_4OH was poured. Then, TEOS was immediately added into the solution under vigorous stirring for 16 h at room temperature.

SBA-15 (S15) microparticles were synthesized following the method described by Zhao et al.[49] P123 was used as a template of the mesoporous structure. The molar ratio of the reagents was 0.017 P123:1.0 TEOS:6 HCl:196 H_2O. For the microparticle synthesis, an aqueous solution of 4 g of P123 was mixed with HCl 37%, and this liquor was stirred for 2 h, after which the silica source (TEOS) was added dropwise. This final mixture was stirred for a further 24 h, and it was aged in an autoclave at 100 °C for another 24 h.

UVM-7 particles (U7) were synthesized following the method presented by El Haskoury et al,[50] based also on the "atrane route". The molar ratio of the reagents was fixed at 7 $TEAH_3$:2 TEOS:0.52 CTAB:180 H_2O. The $TEAH_3$/TEOS mixture was

heated to 150 °C in a Dean–Stark apparatus until no condensation of ethanol was observed. The reaction was cooled to 90 °C and CTAB was gradually added in small portions, followed by water addition. The reaction was aged for 24 h at room temperature.

In all synthesis, the resulting powder was isolated from the mother liquor by filtration (M41, M48 and S15) or by centrifugation (U7), washed with deionized water until neutral pH was achieved and dried at 70 °C overnight. The final mesoporous materials were obtained by calcination of the as- synthesized solids at 550 °C for 5 h in an oxidant atmosphere with the aim of removing the surfactant template.

2.3. Synthesis of Solids Loaded with RhB and Capped with OA Solids

Solids were synthesized following the procedure described in previous works of the group with slight modifications [41]. In a typical synthesis, 500 mg of the initial materials (M41, M48, S15 or U7) were suspended in 15 mL of an aqueous solution of RhB (192 mg, 0.4 mol) and stirred for 24 h to obtain the loaded solids (M41-RhB, M48-RhB, S15-RhB and U7-RhB, respectively), which were centrifuged and dried under vacuum.

In the next step, 500 mg of the loaded solids were suspended in 20 mL of ethanol, and an excess of APTES (2.34 mL, 10 mmol) was added to the previous mixture. The reaction was stirred for 5.5 h to obtain the APTES-functionalized solids (M41-APTES, M48-APTES, S15-APTES and U7-APTES), which were isolated by centrifugation and dried under vacuum.

To obtain the final solids, 500 mg of the APTES-functionalized solids were added to a solution of EDC (50 mg) and OA (5 mL) previously dissolved in 30 mL of ethanol. The reaction was stirred at room temperature during 24 h. The final solids, functionalized with OA (M41-OA, M48-OA, S15-OA and U7-OA, respectively, or MSP-OA in general), were isolated by centrifugation, washed with a mixture of EtOH:H_2O (1:2) and dried at 37 °C for 24 h.

2.4. Methods Used for Characterization

Powder X-ray diffraction (XRD), transmission electron microscopy (TEM), N_2 adsorption–desorption isotherms, FTIR, thermogravimetric analysis (TGA) and fluorescence spectroscopy were employed to characterize the synthesized solids. XRD was performed on a Bruker D8 Advance diffractometer (Bruker, Coventry, UK) using Cu Kα radiation. TEM images were obtained with a JEOL JEM-1010 (JEOL Europe SAS, Croissysur-Seine, France). N_2 adsorption–desorption isotherms were recorded with a Micromeritics TriStar II Plus automated analyzer (Micromeritics Instrument Corporation, Norcross, GA, USA). The samples were degassed at 120 °C in vacuum overnight. The specific surface areas were calculated from the adsorption data in the low-pressure range using the BET model. Pore size was determined by following the BJH method.

The functionalization process of all the solids was followed by infrared spectroscopy in a Bruker Tensor 27 FTIR spectrometer. The composition of loaded and functionalized particles was determined by TGA. Thermogravimetric analyses were carried out on a TGA/SDTA 851e Mettler Toledo balance (Mettler Toledo Inc., Schwarzenbach, Switzerland) using an oxidant atmosphere (air, 80 mL/min) with a heating program consisting of a heating ramp of 10 °C per minute from 393 to 1273 K and an isothermal heating step at this temperature of 30’. Fluorescence spectroscopy was carried out on a JASCO FP-8300 Spectrofluorometer (JASCO, Easton, OH, United States).

2.5. Cargo Delivery

In a typical experiment, 5 mg of each final solid (M41-OA, M48-OA, S15-OA and U7-OA respectively) were placed in 10 mL of PBS (pH 7.5) as general aqueous fluid, and 10 mL of bile salts suspension (100 mg of bile salts in 10 mL of PBS, pH 7.5), simulating and simplifying the conditions at the duodenum. At certain times aliquots were taken and filtered. The delivery of RhB from the pore voids to the different solutions was analyzed via the fluorescence emission band of this molecule at 572 nm (excitation at 555 nm).

2.6. Cargo release

The payload release kinetics from the pore system of all the inorganic supports were calculated using different mathematical models. The employed models are:[51]

Zero order: *Cargo release* (%) = $k_0 \cdot t$ [1]

First order: *log Cargo release* (%) = $\log C_0 + (k_1 \cdot t)/2.303$ [2]

Higuchi: *Cargo release* (%) = $K_H \cdot t^{½}$ [3]

Korsmeyer – Peppas: *log Cargo release* (%) = $K \cdot t^n + b$ [4]

2.7. In Vitro Digestion

An in vitro digestion was performed to all the solids according to the method described by Versantvoort et al.[52] The procedure was followed to simulate the chemical composition and pH of the different gastrointestinal (GI) steps (mouth, stomach and duodenum). The residence times of each organ were also based on this protocol. The pH of the fluids (saliva pH 7.5, gastric fluid pH 1.5–2, duodenal fluid pH 7.8–8) was checked and adjusted to the appropriate value when necessary with NaOH (1M) or HCl (37%).

2.8. Cell Culture Conditions

Caco-2 human colon adenocarcinoma cells were grown in DMEM medium supplemented with 10% FBS, 1% P/S and 1% non-essential amino acids. Cells were maintained at 37 °C in an atmosphere of 5% CO_2 and 95% air and underwent passage when 80% confluence was reached.

2.9. MTT Cell Viability Assay

Caco-2 cells were cultured in sterile 96-well plates at density of 2×10^4 cells/well and were incubated 24 h in the atmosphere conditions previously reported. Then, all the tested MSPs were suspended in final concentrations and each one was tested in 8 wells; control cells were absent of any MSP. After 24 h of incubation, cells were washed with PBS in order to remove MSPs and then 100 µL

of MTT solution in non-supplemented DMEM medium (0.5 mg/mL) were added to each well, and the plates were incubated for another 2 h. After incubation, supernatant DMEM-MTT medium was removed, and 100 µL of DMSO were added to each well and the plate was softly shacked until complete solution of formazan crystals to ensure homogeneous distribution of violet color. Then, the absorbance was measured at λ_{exc} = 550 nm. The reported results are given as average of the results of two independent experiments.

2.10. In Vivo Pharmacokinetic Studies

To assess the in vitro results, in vivo experiments with U7-OA (which showed the best performance in the in vitro studies) in rats were carried out and RhB concentration in plasma was studied. The experimental protocol was approved by the Ethics Committee for Animal Experimentation of the University in accordance with the 2010/63/EU directive of 22 September 2010 (Spain, code A1330354541263). A cannula was implanted in the jugular vein 24 h before administration to take blood samples (0.5 mL). A dose of 2 mL of RhB solution (0.84 mg/mL) was administrated orally in group 1 and the same dose of a suspension of U7-OA (containing 150 mg of solid which releases 1.67 mg of RhB, in 2 mL) was administered in group 2. Blood samples were withdrawn at 15', 30', 45', 1 h, 1.5 h, 2 h, 3 h, 4 h, 5 h, 6 h, 7 h and 8 h and plasma was immediately separated by centrifugation (10,000 rpm for 10') and then proteins were precipitated with methanol (4 °C). Samples were analyzed by HPLC with Novapack C18 (Waters Alliance® e2695, Milford, MA, USA), mobile phase ACN:H_2O 30:70 v/v with 1% of TFA and fluorescence detector using λ_{exc} = 555 and λ_{em} = 572 nm. 200 mL of volume injection were used and a flow of 1 mL/min was fixed. The method was previously validated with adequate linearity, precision and accuracy (R > 0.99 and coefficient of variation < 5%).

3. Results and Discussion

3.1. Design, Synthesis and Characterization of the Solids

In the present project, RhB was encapsulated into different mesoporous silica materials, which were finally capped with OA. The capacity of OA to effectively cap the pores and the ability of the materials to deliver the cargo in different conditions were evaluated. Four different porous silica supports (MCM-41, MCM-48, SBA-15 and UVM-7) with similar micrometric particle size, but with different shape, pore size and pore distribution were subjected to study. In this work, the cargo release mode of the different microdevices was evaluated in the presence of bile salts, which act as emulsifiers. The action mechanism of OA as a molecular gate was described in previous works of the group.[46] The interaction forces between the hydrophobic tails of the lipid molecules anchored to the MSPs surface act as closing forces, which avoid cargo release from the system to an aqueous environment. When surfactant molecules, like bile salts, are present in the particles' surroundings, this interaction is interrupted, and the encapsulated payload is then allowed to diffuse.

The synthesized solids were characterized using usual techniques. Normalized powder X-ray patterns of all solids (as made, calcined, loaded and functionalized) are shown in Figure 1. The observed changes in the shapes of peaks and positions in the diffractograms were independently evaluated for each mesoporous material. The MCM-41 solids' diffractograms show four low-angle peaks characteristic of a hexagonal arrangement, indexed from left to right as (1 0 0), (1 1 0), (2 0 0) and (2 1 0) Bragg reflections, respectively. It can be observed that the (1 0 0) peak is notably shifted to higher 2θ values in the calcined material curve (M41) with respect to the as made one. This shift is related to cell contraction due to the condensation of silanols during the calcination process. Finally, it can also be observed that, in the curves corresponding to the final solid (M41-OA), the reflections (1 1 0), (2 0 0) and (2 1 0) have almost disappeared because of a decrease in the contrast due to the external functionalization and pore filling. However, the

clear presence of the (1 0 0) peak at all synthesis stages demonstrates that neither calcination nor pore filling followed by external functionalization modify the material's mesoporous structure.

All these arguments are also applicable to the materials based on the structures of SBA-15 and UVM-7, with slight differences. On the one hand, SBA-15 materials exhibit peaks narrower than the MCM-41 ones due to a more ordered structure and smaller 2θ values corresponding to a larger unit cell related to their larger pore size. On the other hand, the diffractograms of the UVM-7 family solids are broader than those of the aforementioned materials due to the less ordered structure of their pore matrix. The different porous structure presented by solids based on the MCM-48 material makes the peaks of their diffractograms markedly different from those previously detailed. MCM-48 peaks positions are in agreement with the values reported already in literature, and, assuming a cubic three-dimensional mesostructure, the main peaks for MCM-48 can be indexed as (2 1 1), (2 2 0), (3 2 1), (4 2 0) and (3 3 2). Moreover, displacement of peaks positions to higher values after calcination and the order loss after loading and functionalization processes are phenomena that also occur with this material.

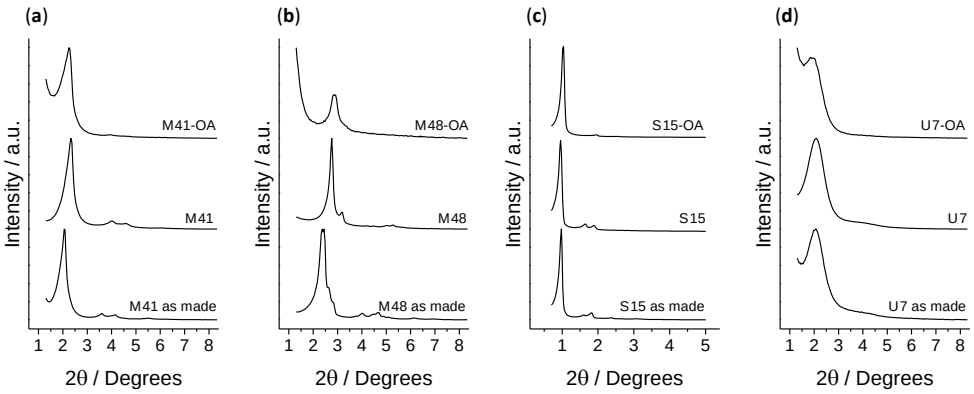

Figure 1. Normalized powder X-ray patterns of all the synthesized solids. From left to right, (**a**) MCM- 41, (**b**) MCM-48, (**c**) SBA-15 and (**d**) UVM-7 materials. From bottom to top: as made, calcined, and the loaded and functionalized final material (MSP-OA), respectively.

The presence of the mesoporous structure in the final functionalized solids was also confirmed by TEM analysis. Typical pores and channels of the MSP matrix are visualized as alternate black and white stripes (see Figure 2, top) or white circles, even with the loss of contrast produced by the presence of organic matter in loaded and functionalized solids (see Figure 2, bottom). In the case of the UVM-7, the different intraparticle structure of this material that can be considered as made of fussed irregular mesoporous nanoparticles, giving rise to a textural-intraparticle secondary pore system, can also be observed in Figure 2 (d and h).

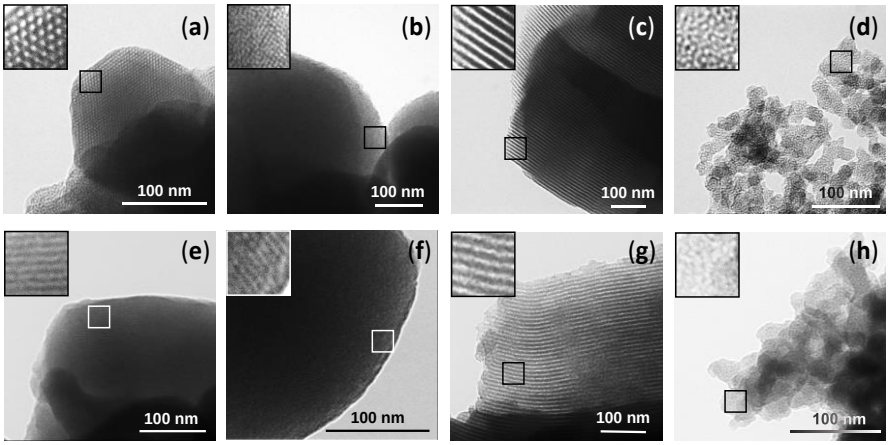

Figure 2. TEM images of calcined solids (top) (**a**) M41, **b**) M48, **c**) S15, **d**) U7) and loaded and functionalized solids (bottom) (**e**) M41-OA, **f**) M48-OA, **g**) S15-OA, **h**) U7-OA). Insets correspond to a 3× magnification of the respective selected zones.

The N_2 adsorption–desorption isotherms of the calcined microparticles are shown in Figure 3. A typical curve for these mesoporous solids consisting of an adsorption step at intermediate P/P_0 value (0.1–0.3) can be observed. These curves correspond to a type IV isotherm, in which the produced step deals with nitrogen condensation inside the mesopores of each structure. The absence of a hysteresis loop in this interval in MCM-41, MCM-48 and UVM-7 structures and the narrow BJH pore distribution (Figure 3, bottom), suggest the existence of uniform cylindrical mesopores. The presence of hysteresis loop in SBA-15 solids indicates adsorption and desorption processes carried out in different ways, which is related with the

high pore size of this material. Furthermore, it is important to point out that the large N_2 adsorption at high P/P_0 values for UVM-7 material correspond to the filling of the textural intraparticle pores. The N_2 adsorption–desorption isotherm of MSP-OA solids is typical of mesoporous systems with practically filled mesopores (see Figure 3). For all the loaded and functionalized solids, the N_2 adsorbed is negligible due to the inability of the gas to condense into the blocked pores.

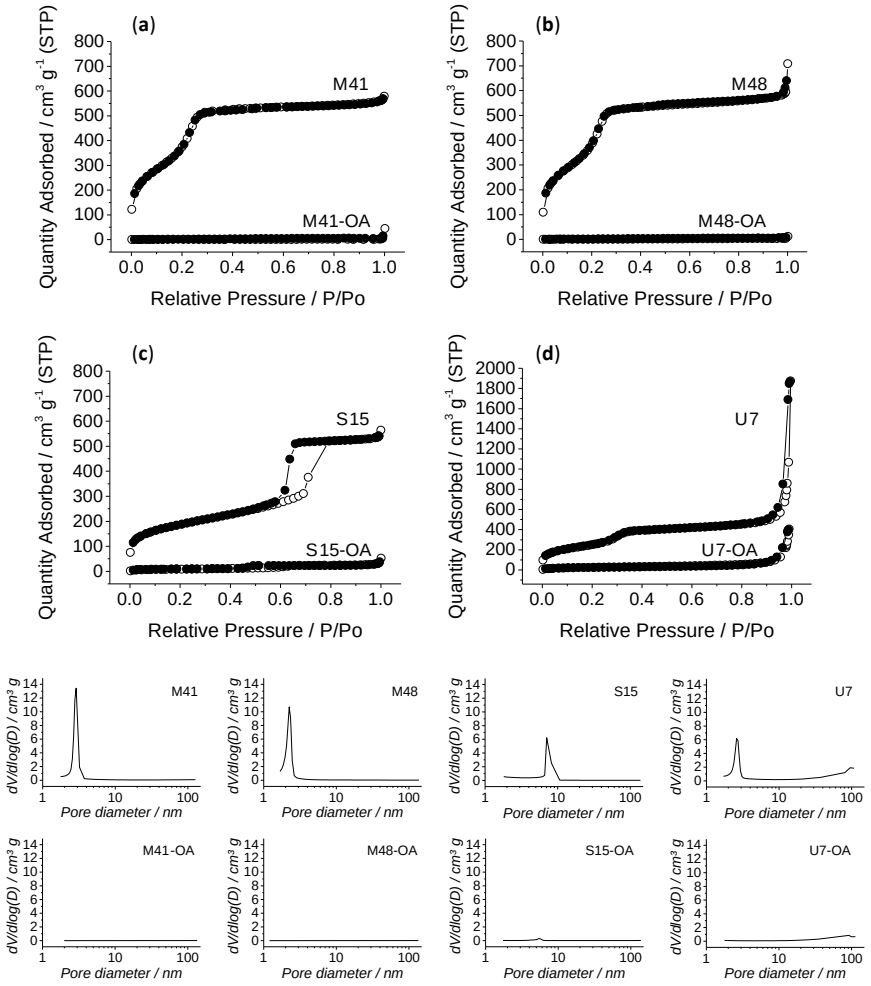

Figure 3. Top: Nitrogen adsorption (○)–desorption (●) isotherms for all the calcined and final solids (**a**) MCM-41, **b**) MCM-48, **c**) SBA-15, **d**) UVM-7). Bottom: Pore distribution graphs of all the calcined and final solids (MSP-OA), indicated in its own graph.

Consequently, relatively low N_2 adsorbed volume and surface area (see Table 1) values were calculated. In fact, these solids show flat curves when compared to those of the calcined parent material, which indicates significant pore blocking and the subsequent absence of appreciable mesoporosity. Only in the case of the U7-OA material, some textural-intraparticle porosity is maintained after loading and functionalization processes.

Table 1. BET specific surface values, pore volumes and pore sizes calculated from the N_2 adsorption–desorption isotherms for selected materials.

	S_{BET} ($m^2\ g^{-1}$)	Pore Volume ($cm^3\ g^{-1}$)	Pore size [c] (nm)
M41	1074.0	1.0	3.0
M41-OA	2.4	0.0	-
M48	1355.4	1.0	2.3
M48-OA	0.1	0.0	-
S15	670.7	0.8	5.4
S15-OA	31.3	0.0	-
U7	922.1	0.7 [a] (0.8) [b]	2.6 [a] (32) [b]
U7-OA	96.4	0.07 [a] (0.4) [b]	-[a] (34) [b]

[a] Pore volumes and pore sizes corresponding to "surfactant-templated" mesopores. [b] Pore volumes and pore sizes corresponding to textural intraparticle porosity. [c] Pore size was estimated using the BJH model applied on the adsorption branch of the isotherm.

Infrared spectroscopy (FTIR) was also employed to follow the loading and functionalization processes leading to solids MSP-OA (see Figure 4). In all the FTIR spectra, the dominant bands are those due to the silica matrix (1060, 800 and 450 cm^{-1}) giving rise to very similar spectra between them. However, some changes in minor bands can be related with the presence of specific organic groups in solids functionalized with APTES or OA.

Consequently, it can be observed the decrease of the band around 950 cm^{-1} assignable to the silanol groups of the inorganic surface when the APTES group is anchored. Furthermore, it is visible the appearance of two bands at approximately 2900 cm^{-1} and 2850 cm^{-1} assignable to C–H bending vibrations. It can also be observed that these two bands increase as the amount of functionalized organic groups increase.

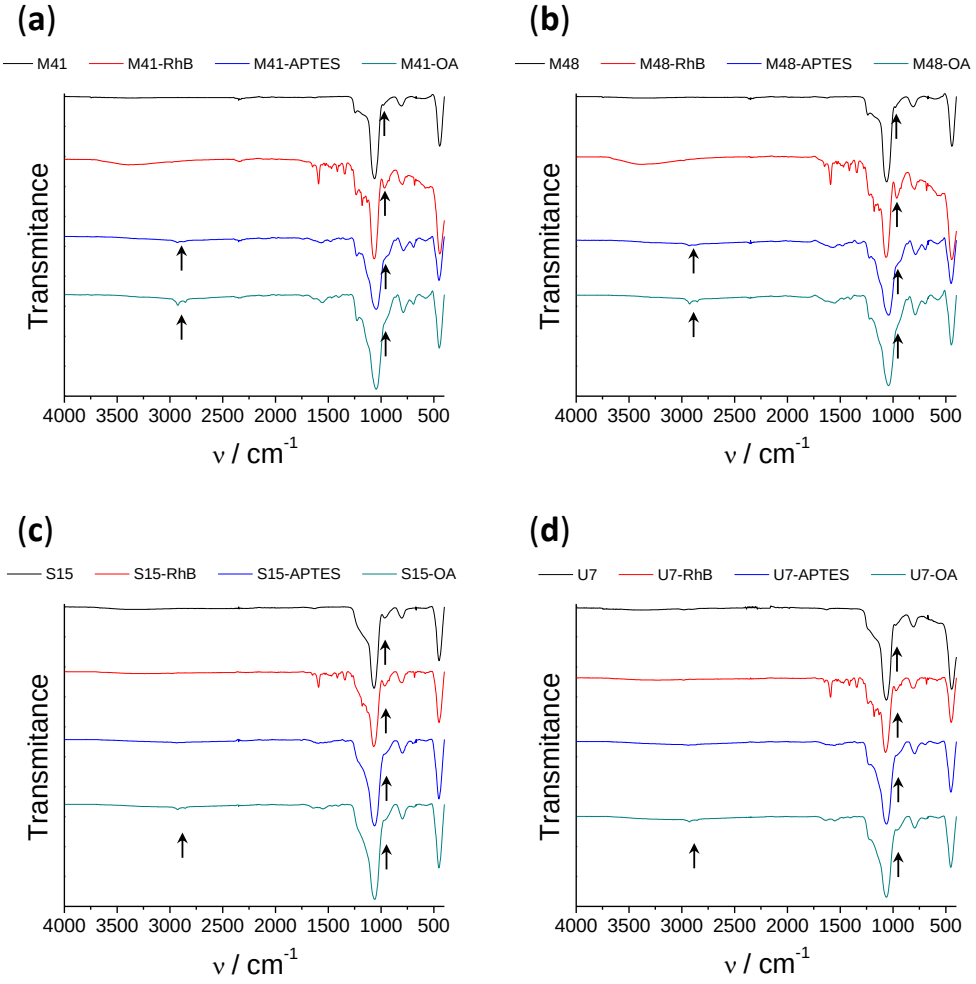

Figure 4. Infrared spectra of the consecutive steps of synthesis of the different solids: a) M41, b) M48, c) S15 and d) U7.

The contents of OA and RhB in MSP-OA solids were determined using TGA. TGA indicated an organic matter content of 72.75, 72.28, 133.64 and 46.14 mg RhB g^{-1} SiO_2 in M41-OA, M48-OA, S15-OA and U7-OA respectively. The content of OA in the loaded and functionalized solids was 164.70, 119.86, 85.55 and 122.0 mg OA g^{-1} SiO_2 in M41-OA, M48-OA, S15-OA and U7-OA respectively**.** The proportion in mmol per gram of SiO_2 of all the moieties is summarized in Table 2.

Table 2. Content (α) in mmol g^{-1} SiO_2 of RhB, APTES and OA in the loaded and functionalized solids (MSP-OA).

Solid	α_{RhB}	α_{APTES}	α_{OA}
M41-OA	0.15	6.30	0.59
M48-OA	0.15	6.17	0.43
S15-OA	0.28	3.57	0.30
U7-OA	0.10	3.59	0.44

3.2. Cargo Controlled Release

As stated above, the aim of this work was to test the ability of OA to maintain the cargo loaded into different MSP supports, and to ascertain the release profile of that cargo from the different supports under different conditions. In this section, several experiments were carried out with the objective of studying the bile-responsive controlled-release behavior of each capped material in detail.

The performance of the microdevices along the GIT was evaluated in an in vitro digestion, where a batch assay was carried out simulating the digestive steps and conditions of the mouth, the stomach and the duodenum (Figure 5). In this experiment, the particles are subjected to changes in pH, salinity and biomolecules (including enzymes) as well as residence times in the different steps of the GIT. Maximum quantity of released cargo from each loaded and functionalized MSP-OA solid (μg RhB mg^{-1} MSP-OA) at each digestion step (saliva, gastric and duodenal fluids) is detailed in Table 3. From this experiment, we can conclude that cargo

released in the first digestion steps (saliva and gastric fluid) is negligible compared with the signal appreciated in the first section of the small intestine, where the presence of the bile salts inhibits the hydrophobic interaction in the outer layer of the solid and provokes an important cargo release. Apart from the different behavior of each device, it can be derived that all of them can produce the release of the cargo in the first section of the small intestine where the bile salts appear (Figure 5).

In order to remove the influence of the complex matrix conditions in the cargo release profiles, and also to verify the action of bile salts as triggering stimulus, a simplified release assay was carried out. Thus, delivery studies of all the loaded and functionalized solids (M41-OA, M48-OA, S15-OA and U7-OA) were performed in PBS medium and in the presence of bile salts, resulting in the cargo delivery, presenting each material a different release profile (Figure 6). Comparing both experiments, the release profile for each functionalized material along the two first hours of the in vitro digestion's intestinal stage is similar to the one obtained during the delivery performed exclusively with bile extract and, hence, these data can be used as representative of the cargo release process for each material.

Since the aim of this work was to maximize cargo delivery into the duodenum as the action place, the cargo release assay was restricted to the first two hours. However, since the action of bile salts is not exclusively reduced to the duodenum, but is prolonged to farthest sections of the small intestine (jejunum and/or ileum), the maximum amounts of released cargo from each MSP-OA system under the presence of bile extract after a 24 h action have also been included in Table 3. These data add extra information to the synthesized systems' performance, indicating that a different behavior is observed for longer release times, which may be useful for other applications not contemplated in this work (such as (bio)molecules release in more distant absorption places of the small intestine or even in the large intestine).

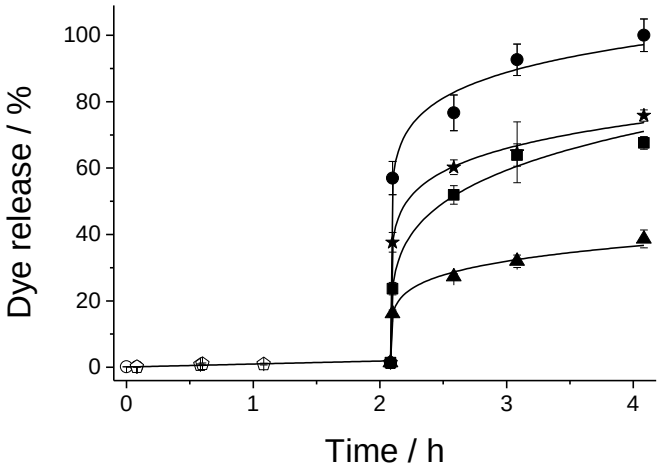

Figure 5. *In vitro* digestion of all the loaded and functionalized solids; saliva (○) and gastric (⬠) fluids show zero release for all the solids, and cargo release is produced when bile salts are present (▲ M41-OA, ■ S15-OA, ★ M48-OA, ● U7-OA).

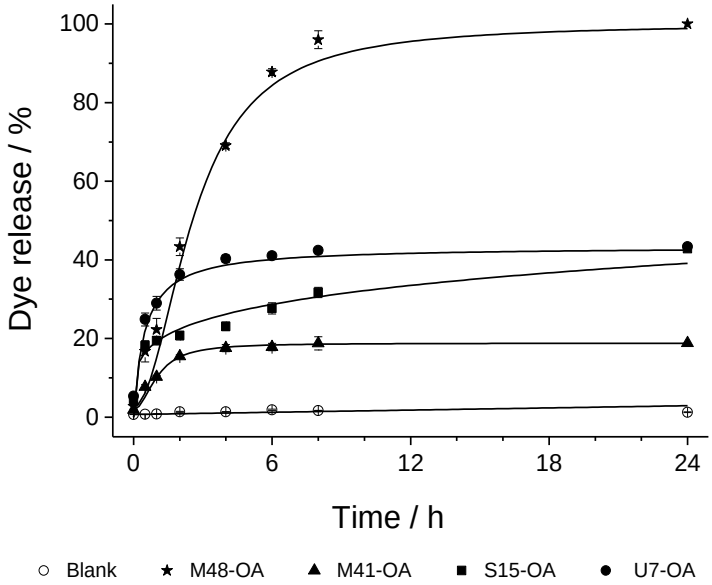

Figure 6. Release profile of RhB dye from all solids in a PBS suspension (○), showing zero release for all of them, and when bile extract is added (▲ M41-OA, ★ M48-OA, ■ S15-OA, ● U7-OA).

Table 3. Maximum quantity of released cargo from each MSP-OA solid (μg RhB mg^{-1} MSP-OA) in each digestion fluid (saliva, gastric and duodenal) compared to the maximum quantity reached in the cargo release assay using bile extract exclusively for 24 h.

Digestive fluid	M41-OA	M48-OA	S15-OA	U7-OA
Saliva	$0.01 \pm 3 \cdot 10^{-4}$	$0.02 \pm 9 \cdot 10^{-4}$	$0.01 \pm 7 \cdot 10^{-4}$	$0.01 \pm 4 \cdot 10^{-4}$
Gastric	0.10 ± 0.01	0.16 ± 0.01	0.16 ± 0.02	0.07 ± 0.02
Duodenal	3.35 ± 0.23	6.58 ± 0.15	5.86 ± 0.16	8.68 ± 0.39
Bile extract 24 h	4.84 ± 0.24	25.71 ± 0.38	11.02 ± 0.33	11.15 ± 0.20

3.3. Cargo Release Kinetics

In addition to achieving a notable cargo release triggered by the surfactant action of bile salts, it is also an important objective of this work to evaluate the ability of the studied systems to control the payload release, and distinguish whether it is bulk or sustained over time. For this purpose, the release kinetics data of the first 60% of the payload (data in Figure 6) were adjusted to four different mathematical models: zero order, first order, Higuchi and Korsmeyer–Peppas (K–P). All mathematical equations (Equations [1] to [4]) are detailed in section 2.6 in Materials and Methods.

In each of these models, certain premises are assumed, and different parameters are taken into account to describe the release process. The zero-order model describes immediate and constant time release processes, usually of very soluble drugs in aqueous media. The first order model considers the change in concentration of the payload over time, associated with a decrease in the concentration of the drug in the initial support. Higuchi's model, developed in the 1960s, marked a revolution in the modeling and understanding of drug release, since the matrix from which cargo is released was considered for the first time. This model is based on the premise of a uniform insoluble matrix with a cargo concentration much higher than the one released. Additionally, in this model, it is contemplated that the external medium penetrates to dissolve the loaded drug,

which is unidirectional and constantly released. Finally, the semi-empirical model of K–P or "power law" consists of a modification of the Higuchi model with the aim of making it more general. It is applied for drug release from matrices in which several phenomena occur simultaneously, not only diffusion. Two parameters are obtained from the mathematical adjustment of the data to this equation: *K*, which is the constant related to the cargo's diffusion velocity, and *n*, which is related to the type of diffusion and can be $n = 0.45$ in case of Fickian diffusion from cylindrical shaped pores, or $0.45 < n \leq 0.89$ if the diffusion is non-Fickian.[51]

As it can be seen in Table 4, data fit correctly to more than one equation. However, the model that best explains all the data as a whole is K–P, since it assesses in its formula different types of diffusion from the matrix.

Table 4. Parameters and coefficients of determination (r^2) obtained by adjusting the data to each model equation {(1), (2), (3), (4)}.

System	**Zero order Equation** (1)		**First order Equation** (2)			**Higuchi Equation** (3)		**Korsmeyer – Peppas Equation** (4)			
	k_0 (min)	r^2	k_1 (min)	C_0	r^2	K_H ($min^{-½}$)	r^2	K (min^{-n})	n	b	r^2
M48-OA	0.3	0.98	0.0	7.4	0.7	4.01	0.97	0.99	0.77	1.76	0.995
M41-OA	0.1	0.8	0.0	4.3	0.6	1.25	0.97	1.52	0.45	0.71	0.97
S15-OA	0.1	0.6	0.0	9.2	0.5	1.8	0.8	1.71	0.45	5.50	0.87
U7-OA	0.2	0.7	0.0	27.9	0.5	3.08	0.90	3.21	0.45	6.36	0.92

From the mathematical adjustment to this model the parameters *K*, *n* and *b* can be obtained (see Table 4). The values of these parameters allow us to better understand the process by which the cargo is released in the studied systems. If we compare *n*, which is forced by definition to be equal or bigger than 0.45,[53] it can be seen that from M41-OA, S15-OA and U7-OA the cargo is released by Fickian diffusion, as defined by the model for matrices with cylindrical structure. However, M48-OA releases the cargo with non-Fickian diffusion since the porous structure is not cylindrical but three-dimensional. On the other hand, the *y*-interception values correspond to the parameter *b*, which represents a phenomenon called "burst

release" by which the load is immediately released in the medium with the triggered stimulus. Burst release is an unfavorable phenomenon in the processes of sustained release, but it is favorable in the present work since the pursued objective is the immediate payload release when the specific stimulus (bile salts) appears.

There are some articles that attempt to explain the mechanism of burst release,[54] relating it to the structure of the guest molecules, their interaction with the host material, and especially with the structural characteristics of the support. The results obtained in this research are in agreement with data in the literature,[33] where it was concluded that among different studied supports, the higher burst release was reached by the materials with textural-intraparticle pores in addition to the "surfactant-templated" mesopores, followed by the materials with larger mesopores, and finally those with smaller pore size.

The results of the kinetic models are related with those of the N_2 adsorption-desorption isotherms (see Figure 3, bottom, and Table 1). It can be observed that the highest burst release is reached by the U7-OA system, which has completely filled mesopores and partially filled textural pores. Then, the next highest *b* value is achieved by the S15-OA system, since among the supports that only have "surfactant-templated" mesopores, S15 is the one with the largest pore size. Finally, although the solid M41 has a pore size slightly larger than M48, the complex internal structure of this last solid might be the cause of the difference between M41-OA and M48-OA burst release.

Consequently, all the parameters were obtained, and their explanations lead to the conclusion that U7-OA is the system with the biggest payload release in the first hours of stimulus and with highest velocity. This explanation is also applicable to the obtained *K*-values. The cargo diffuses with greater velocity from the systems with textural-intraparticle pores (U7), then systems with large pores (S15), followed by systems with smaller pores (M41) and finally from porous matrices with complex structures (M48) (see Table 4).

3.4. In Vitro Biocompatibility Test: Interaction with Cells of the GIT

In addition to the cargo release experiments from the four different supports, it was also an objective of this study to assess the biocompatibility of the developed microsystems. Therefore, studies with all the bare MSPs and final loaded-and-functionalized solids (MSP-OA) were performed employing Caco-2 human colon adenocarcinoma cells in order to exclude any toxic effect of microparticles.

Other studies in the literature reported low toxicity levels for similar mesoporous materials at low particle concentrations,[55] reason why cells in this work where exposed to higher— even critical—particle concentrations. Thus, cells were treated with the corresponding system for 24 h at final concentrations of 50, 100, 250, 500, 750 and 1000 μg/mL. After this time, a cell viability assay using MTT was performed, which is based in the absorbance measurement of formazan produced by oxidoreductase enzymes of viable cells.[56] The formazan crystals generated are insoluble in the growing medium, so DMSO solvent must be added after medium-removal in order to solubilize the generated compound. The absorbance of the resulting purple solution was measured at λ_{exc} 550 nm and compared with the one achieved by control cells. The obtained results are depicted in Figure 7.

As it can be seen, MTT cell viability assay indicated that even at concentrations as high as 1 mg/mL the level of cell viability is quite high (approximately 85–75%). Although the functionalized particles are slightly more toxic than the starting MSPs, this difference is very low. Furthermore, unlike the bare starting materials, it can be seen that cell viability did not decrease by increasing particle concentration, even at values as high as 1 mg/mL. This fact might be related to the differences on particle stability in the culture medium.

It has been reported in the literature that cell viability decreased when cell cultures were exposed to increasing particle concentrations, as these particles precipitate on the cell monolayer. However, stable suspensions with increasing concentration of the same particles maintained constant cell viability.[57] After this,

it could be assumed that the functionalization of the MSPs with OA produces more stable suspensions and that, then, the increase of the particle concentration might not affect the cell-viability. In conclusion, the assay suggested that the developed systems loaded with RhB and functionalized with OA were well-tolerated by the cells.

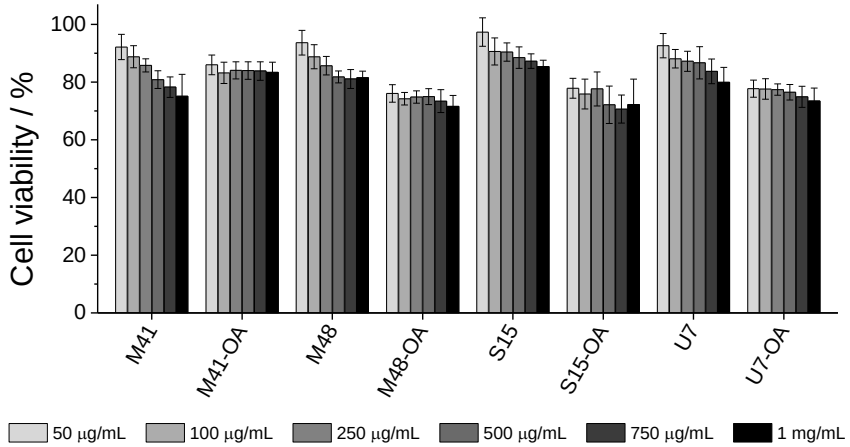

Figure 7. MTT cell viability assay. Caco-2 cells were treated with the bare MSPs and the final solids (MSPs-OA) at concentrations of 50, 100, 250, 500, 750 and 1000 μg/mL (increasing from light grey to black) for 24 h. After incubation, cell viability was quantified using MTT reagent and solubilization of formazan crystals into DMSO.

3.5. In Vivo Pharmacokinetic Studies

The difficulty of many physiological factors (such as exact pH and composition of GIT fluids, enzymes, gastric emptying, GIT motility, etc.) to be incorporated into the in vitro models requires the use of in vivo models to evaluate the final performance of a dispositive when these factors are crucial. Therefore, to prove the specific opening of the gated material in the SI and quantify cargo release in plasma, in vivo pharmacokinetic studies were carried out. U7-OA solid was the chosen to be tested because, although its biocompatibility and ability to protect the cargo are the same as all the other solids, its payload release and velocity in the first section

of the small intestine in simulated conditions (vide ante) are the highest ones. These reasons make of it an ideal system for immediate payload release in the duodenum after protecting the cargo from the adverse stomach conditions.

To perform the pharmacokinetic studies, male Wistar rats were divided into two groups (see section 2.10 in Materials and methods). The subjects in group 1 were treated with 2 mL of RhB solution (0.84 mg/mL), and rats from group 2 were treated with 2 mL of a suspension of U7-OA microparticles (containing 150 mg of solid, which release 1.67 mg of RhB). RhB concentration in plasma as a function of time for both groups of rats is shown in Figure 8. As it could be seen, subjects from group 1 (that received the RhB solution) showed maximum concentration of the molecule (C_{max}) at 45' after administration (black line); however, rats in group 2 presented maximum RhB levels at 1.5 h (gray line). Due to the high permeability of RhB through the intestinal membrane, the delay of the maximum concentration of this molecule in plasma can be related to the retard of its delivery in the duodenum. Thus, in group 1, the RhB absorption is almost immediate after gastric emptying, while RhB encapsulated into the U7-OA microdevice will only be adsorbed after the bile salts have produced the opening of the microdevice and the dye release. Then, we can assume that the RhB is effectively encapsulated and protected during the initial steps of the GIT (i.e., the mouth and the stomach). This strategy can be useful for drug administration, in order to avoid stomach damage or degradation of the compound.

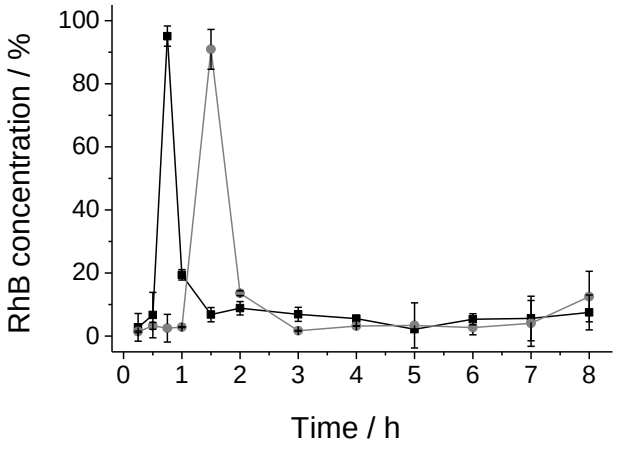

Figure 8. RhB concentration (%) in plasma for subjects of group 1 (RhB solution, black ■) and group 2 (U7-OA suspension, gray ●).

4. Conclusions

A set of different MSPs functionalized with oleic acid (MSP-OA) have been developed. The prepared materials are able to confine and protect their entrapped cargo in an aqueous environment and release it effectively only when bile salts are present. The release profiles of the different supports have been studied, emphasizing the role of the inorganic scaffold in active delivery regulated by oleic acid acting as a molecular gate. Thereby, the different behavior of the MSP-OA during the cargo delivery has been modeled using four different mathematical models: zero order, first order, Higuchi and Korsmeyer–Peppas (K–P). Among all, the K–P model gives the best adjustment for all solids and allows to distinguish between Fickian diffusion in solids M41-OA, S15-OA and U7-OA and the non-Fickian diffusion in M48-OA material. In order to test these MSP-OA materials as cargo release devices, in vitro cell viability experiments with Caco-2 adenocarcinoma cells were performed, showing that MSP-OA materials are non-toxic even at high particle concentrations. Based on the solids' release kinetics, the U7-OA material was selected to essay duodenal bulk delivery in an in vivo model of Wistar rat. The results show a delay in the RhB absorption when using the U7-OA

microdevice instead of the direct dosage of this model molecule. This delay indicates that the arrival of the RhB to the duodenum is retarded when using the U7-OA and corroborates the operation of the oleic acid functionalized MSPs. Payload discharge after gastric emptying achieved with this system stablishes an example of the possibility of using MSPs as protection and direct release agents into the duodenum. This fact makes of MSPs a good alternative to the existing administration methods employed until now.

Author Contributions: Conceptualization, E.P.-R., M.G.-A., M.D.M. and A.B; methodology, E.P.-R., I.G.-A., M.G.-A. and A.B.; validation, E.P.-R., I.G.-A., M.G.-A., R.M.-M., M.D.M., A.B. and E.A.; formal analysis, E.P.-R, I.G.-A.; investigation, E.P-R., I.G.-A., M.G.-A. and A.B.; data curation, E.P.-R., I.G.-A.; writing—original draft, E.P.-R. and A.B.; writing—review and editing, E.P.-R., I.G.-A., M.G.-A., R.M.M., M.D.M., A.B. and E.A.; visualization, E.P.-R., I.G.-A., M.G.-A., R.M.M., M.D.M., A.B. and E.A.; supervision, R.M.M., M.D.M., A.B. and E.A.; project administration, M.D.M.; and funding acquisition, R.M.M., M.D.M. and E.A. All authors have read and agreed to the published version of the manuscript.

Funding: This research was funded by the Spanish Government (projects RTI2018-100910-B-C41 and RTI2018-101599-B-C22-AR (MCUI/FEDER, EU)) and the Generalitat Valenciana (project PROMETEO/2018/024 and ACIF/2016/023 grant).

Acknowledgments: The authors want to thank the Electron Microscopy Service at the UPV for support.

References

1. Pérez-Esteve É, Ruiz-Rico M, De La Torre C, et al. Stability of different mesoporous silica particles during an in vitro digestion. Microporous Mesoporous Mater. 2016;230:196-207. doi:10.1016/j.micromeso.2016.05.004
2. Di Pasqua AJ, Sharma KK, Shi YL, et al. Cytotoxicity of mesoporous silica nanomaterials. J Inorg Biochem. 2008;102(7):1416-1423. doi:10.1016/j.jinorgbio.2007.12.028
3. Izquierdo-Barba I, Colilla M, Manzano M, Vallet-Regí M. In vitro stability of SBA-15 under physiological conditions. Microporous Mesoporous Mater. 2010;132(3):442-452. doi:10.1016/j.micromeso.2010.03.025
4. Arruebo M. Drug delivery from structured porous inorganic materials. Wiley Interdiscip Rev Nanomedicine Nanobiotechnology. 2012;4(1):16-30. doi:10.1002/wnan.132
5. Vallet-Regí M, Balas F, Arcos D. Mesoporous materials for drug delivery. Angew Chemie - Int Ed. 2007;46(40):7548-7558. doi:10.1002/anie.200604488
6. Descalzo AB, Martínez-Máñez R, Sancenón F, Hoffmann K, Rurack K. The supramolecular chemistry of organic-inorganic hybrid materials. Angew Chemie - Int Ed. 2006;45(36):5924-5948. doi:10.1002/anie.200600734
7. Shang L, Bian T, Zhang B, et al. Graphene-supported ultrafine metal nanoparticles encapsulated by mesoporous silica: Robust catalysts for oxidation and reduction reactions. Angew Chemie - Int Ed. 2014;53(1):250-254. doi:10.1002/anie.201306863
8. Taguchi A, Schüth F. Ordered mesoporous materials in catalysis. Microporous Mesoporous Mater. 2005;77(1):1-45. doi:10.1016/j.micromeso.2004.06.030
9. Angelos S, Liong M, Choi E, Zink JI. Mesoporous silicate materials as substrates for molecular machines and drug delivery. Chem Eng J. 2008;137(1):4-13. doi:10.1016/j.cej.2007.07.074
10. García-Fernández A, Aznar E, Martínez-Máñez R, Sancenón F. New Advances in In Vivo Applications of Gated Mesoporous Silica as Drug Delivery Nanocarriers. Small. 2020;16(3):1-62. doi:10.1002/smll.201902242
11. Barbé C, Bartlett J, Kong L, et al. Silica particles: A novel drug-delivery system. Adv Mater. 2004;16(21):1959-1966. doi:10.1002/adma.200400771
12. Llopis-Lorente A, Lozano-Torres B, Bernardos A, Martínez-Máñez R, Sancenón F. Mesoporous silica materials for controlled delivery based on enzymes. J Mater Chem B. 2017;5(17):3069-3083. doi:10.1039/c7tb00348j
13. Mas N, Arcos D, Polo L, et al. Towards the development of smart 3D "gated scaffolds" for on-command delivery. Small. 2014;10(23):4859-4864. doi:10.1002/smll.201401227

14. Santos-Figueroa LE, Giménez C, Agostini A, et al. Selective and sensitive chromofluorogenic detection of the sulfite anion in water using hydrophobic hybrid organic-inorganic silica nanoparticles. Angew Chemie - Int Ed. **2013**;52(51):13712-13716. doi:10.1002/anie.201306688

15. Poyatos-Racionero E, Ros-Lis JV, Vivancos J-LL, Martínez-Máñez R. Recent advances on intelligent packaging as tools to reduce food waste. J Clean Prod. **2018**;172:3398-3409. doi:10.1016/j.jclepro.2017.11.075

16. Coll C, Casasús R, Aznar E, et al. Nanoscopic hybrid systems with a polarity-controlled gate-like scaffolding for the colorimetric signalling of long-chain carboxylates. Chem Commun. **2007**;(19):1957-1959. doi:10.1039/b617703d

17. Perez-Esteve E, Bernardos A, Martinez-Manez R, M. Barat J. Nanotechnology in the Development of Novel Functional Foods or their Package. An Overview Based in Patent Analysis. Recent Pat Food Nutr Agric. **2013**;5(1):35-43. doi:10.2174/2212798411305010006

18. Lamprecht A, Schäfer U, Lehr Cl-MM. Size-dependent bioadhesion of micro- and nanoparticulate carriers to the inflamed colonic mucosa. Pharm Res. **2001**;18(6):788-793. doi:10.1023/A:1011032328064

19. de Luis B, Llopis-Lorente A, Rincón P, et al. An Interactive Model of Communication between Abiotic Nanodevices and Microorganisms. Angew Chemie - Int Ed. **2019**;58(42):14986-14990. doi:10.1002/anie.201908867

20. Bernardos A, Marina T, Žáček P, et al. Antifungal effect of essential oil components against Aspergillus niger when loaded into silica mesoporous supports. J Sci Food Agric. **2015**;95(14):2824-2831. doi:10.1002/jsfa.7022

21. Barat J, Pérez-Esteve É, Bernardos A, Martínez-Mañez R. Nutritional effects of folic acid controlled release from mesoporous materials. Procedia Food Sci. **2011**;1:1828-1832. doi:10.1016/j.profoo.2011.09.268

22. Ruiz-Rico M, Daubenschüz H, Pérez-Esteve É, et al. Protective effect of mesoporous silica particles on encapsulated folates. Eur J Pharm Biopharm. **2016**;105:9-17. doi:10.1016/j.ejpb.2016.05.016

23. Bernardos A, Piacenza E, Sancenón F, et al. Mesoporous Silica-Based Materials with Bactericidal Properties. Small. **2019**;15(24):1-34. doi:10.1002/smll.201900669

24. Awaad A, Nakamura M, Ishimura K. Imaging of size-dependent uptake and identification of novel pathways in mouse Peyer's patches using fluorescent organosilica particles. Nanomedicine Nanotechnology, Biol Med. **2012**;8(5):627-636. doi:10.1016/j.nano.2011.08.009

25. Hussain N, Jaitley V, Florence AT. Recent advances in the understanding of uptake of microparticulates across the gastrointestinal lymphatics. Adv Drug Deliv Rev. **2001**;50(1-2):107-142. doi:10.1016/S0169-409X(01)00152-1

26. Fu C, Liu T, Li L, Liu H, Chen D, Tang F. The absorption, distribution, excretion and toxicity of mesoporous silica nanoparticles in mice following different exposure routes. Biomaterials. 2013;34(10):2565-2575. doi:10.1016/j.biomaterials.2012.12.043

27. Alothman ZA. A review: Fundamental aspects of silicate mesoporous materials. Materials (Basel). 2012;5(12):2874-2902. doi:10.3390/ma5122874

28. Asefa T, Tao Z. Mesoporous silica and organosilica materials-Review of their synthesis and organic functionalization. Can J Chem. 2012;90(12):1015-1031. doi:10.1139/v2012-094

29. Li Y, Li N, Pan W, Yu Z, Yang L, Tang B. Hollow mesoporous silica nanoparticles with tunable structures for controlled drug delivery. ACS Appl Mater Interfaces. 2017;9(3):2123-2129. doi:10.1021/acsami.6b13876

30. Legnoverde MS, Basaldella EI. Influence of particle size on the adsorption and release of cephalexin encapsulated in mesoporous silica SBA-15. Mater Lett. 2016;181:331-334. doi:10.1016/j.matlet.2016.06.053

31. Popova M, Szegedi A, Mavrodinova V, et al. Preparation of resveratrol-loaded nanoporous silica materials with different structures. J Solid State Chem. 2014;219:37-42. doi:10.1016/j.jssc.2014.07.002

32. Martín A, Morales V, Ortiz-Bustos J, et al. Modelling the adsorption and controlled release of drugs from the pure and amino surface-functionalized mesoporous silica hosts. Microporous Mesoporous Mater. 2018;262:23-34. doi:10.1016/j.micromeso.2017.11.009

33. Pérez-Esteve É, Ruiz-Rico M, De La Torre C, et al. Encapsulation of folic acid in different silica porous supports: A comparative study. Food Chem. 2016;196:66-75. doi:10.1016/j.foodchem.2015.09.017

34. Silveira GQ, Da Silva RS, Franco LP, Vargas MD, Ronconi CM. Redox-responsive nanoreservoirs: The effect of different types of mesoporous silica on the controlled release of doxorubicin in solution and in vitro. Microporous Mesoporous Mater. 2015;206(C):226-233. doi:10.1016/j.micromeso.2014.12.026

35. Wang S. Ordered mesoporous materials for drug delivery. Microporous Mesoporous Mater. 2009;117(1-2):1-9. doi:10.1016/j.micromeso.2008.07.002

36. Donner T, Sarkar S. Insulin – Pharmacology, Therapeutic Regimens, and Principles of Intensive Insulin Therapy. MDText.com, Inc., South Dartmouth (MA); 2000. http://europepmc.org/books/NBK278938.

37. Lu PJ, Hsu PI, Chen CH, et al. Gastric juice acidity in upper gastrointestinal diseases. World J Gastroenterol. 2010;16(43):5496-5501. doi:10.3748/wjg.v16.i43.5496

38. Ulker I, Yildiran H. The effects of bariatric surgery on gut microbiota in patients with obesity: A review of the literature. Biosci Microbiota, Food Heal. **2019**;38(1):3-9. doi:10.12938/bmfh.18-018

39. Sardo P, Walker JH. Bariatric surgery: Impact on medication management. Hosp Pharm. **2008**;43(2):113-120. doi:10.1310/hpj4302-113

40. Geraldo M de SP, Fonseca FLA, Veiga Gouveia MR de F, Feder D. The use of drugs in patients who have undergone bariatric surgery. Int J Gen Med. **2014**;7:219-224. doi:10.2147/IJGM.S55332

41. Kurlan R, Nutt JG, Woodward WR, et al. Duodenal and gastric delivery of levodopa in parkinsonism. Ann Neurol. **1988**;23(6):589-595. doi:10.1002/ana.410230611

42. Lundqvist C. Continuous levodopa for advanced Parkinson's disease. Neuropsychiatr Dis Treat. 2007;3(3):335-348.

43. Bredberg E, Nilsson D, Johansson K, et al. Intraduodenal infusion of a water-based levodopa dispersion for optimisation of the therapeutic effect in severe Parkinson's disease. Eur J Clin Pharmacol. **1993**;45(2):117-122. doi:10.1007/BF00315491

44. Antonini A, Odin P. Pros and cons of apomorphine and l-dopa continuous infusion in advanced Parkinson's disease. Park Relat Disord. **2009**;15(SUPPL. 4):S97-S100. doi:10.1016/S1353-8020(09)70844-2

45. Santos-García D, de Deus T, López-Pazos E, et al. Management of complications related to intraduodenal infusion of levodopa/carbidopa in patients with Parkinson's disease. Rev Neurol. **2014**;58(11):505-515. doi:10.33588/rn.5811.2014067

46. Poyatos-Racionero E, Pérez-Esteve É, Dolores Marcos M, et al. New Oleic Acid-Capped Mesoporous Silica Particles as Surfactant-Responsive Delivery Systems. ChemistryOpen. **2019**;8(8):1052-1056. doi:10.1002/open.201900092

47. Cabrera S, El Haskouri J, Guillem C, et al. Generalised syntheses of ordered mesoporous oxides: The atrane route. Solid State Sci. **2000**;2(4):405-420. doi:10.1016/S1293-2558(00)00152-7

48. Meléndez-Ortiz HI, Perera-Mercado YA, García-Cerda LA, Mercado-Silva JA, Castruita G. Influence of the reaction conditions on the thermal stability of mesoporous MCM-48 silica obtained at room temperature. Ceram Int. **2014**;40(3):4155-4161. doi:10.1016/j.ceramint.2013.08.072

49. Zhao D, Feng J, Huo Q, et al. Triblock Copolymer Syntheses of Mesoporous Silica with Periodic 50 to 300 Angstrom Pores. Science (80-). **1998**;279(5350):548-552. http://science.sciencemag.org/content/279/5350/548.abstract.

50. El Haskouri J, de Zárate DO, Guillem C, et al. Silica-based powders and monoliths with bimodal pore systems. Chem Commun. **2002**;2(4):330-331. doi:10.1039/b110883b

51. Bruschi ML, ed. Mathematical models of drug release. In: Strategies to Modify the Drug Release from Pharmaceutical Systems. Woodhead Publishing; **2015**:63-86. doi:10.1016/b978-0-08-100092-2.00005-9

52. Versantvoort CHM, Oomen AG, Van De Kamp E, Rompelberg CJM, Sips AJAM. Applicability of an in vitro digestion model in assessing the bioaccessibility of mycotoxins from food. Food Chem Toxicol. **2005**;43(1):31-40. doi:10.1016/j.fct.2004.08.007

53. Ritger PL, Peppas NA. A simple equation for description of solute release I. Fickian and non-fickian release from non-swellable devices in the form of slabs, spheres, cylinders or discs. J Control Release. **1987**;5(1):23-36. doi:10.1016/S0168-3659(03)00195-0

54. Huang X, Brazel CS. On the importance and mechanisms of burst release in matrix-controlled drug delivery systems. J Control Release. **2001**;73(2-3):121-136. doi:10.1016/S0168-3659(01)00248-6

55. Choi SJ, Kim YR. Bioinspired layered nanoclays for nutraceutical delivery system. ACS Symp Ser. **2013**;1143:207-220. doi:10.1021/bk-2013-1143.ch012

56. Sgouras D, Duncan R. Methods for the evaluation of biocompatibility of soluble synthetic polymers which have potential for biomedical use: 1 - Use of the tetrazolium-based colorimetric assay (MTT) as a preliminary screen for evaluation of in vitro cytotoxicity. J Mater Sci Mater Med. **1990**;1(2):61-68. doi:10.1007/BF00839070

57. Yazdimamaghani M, Barber ZB, Hadipour Moghaddam SP, Ghandehari H. Influence of Silica Nanoparticle Density and Flow Conditions on Sedimentation, Cell Uptake, and Cytotoxicity. Mol Pharm. **2018**;15(6):2372-2383. doi:10.1021/acs.molpharmaceut.8b00213

Article 3

Gated-organoclays for large biomolecules-controlled release triggered by surfactant stimulus

Elisa Poyatos-Racionero,[a,b] Édgar Pérez-Esteve,[c] Elena Aznar,[b,a,d,e] José M. Barat,[c] Ramón Martínez-Máñez,[a,b,d,e,f] M. Dolores Marcos[a,b,d,e,f]* and Andrea Bernardos[b,a,e]*

[a] Instituto Interuniversitario de Investigación de Reconocimiento Molecular y Desarrollo Tecnológico (IDM). Universitat Politècnica de València, Universitat de València. Camino de Vera s/n, 46022, Valencia (Spain)

[b] CIBER de Bioingeniería, Biomateriales y Nanomedicina (CIBER-BBN) (Spain)

[c] Departamento de Tecnología de Alimentos, Universitat Politècnica de València. Camino de Vera s/n, 46022, Valencia (Spain)

[d] Unidad Mixta de Investigación en Nanomedicina y Sensores. Universitat Politècnica de València, Instituto de Investigación Sanitaria La Fe, Valencia (Spain)

[e] Unidad Mixta UPV-CIPF de Investigación en Mecanismos de Enfermedades y Nanomedicina, Universitat Politècnica de València, Centro de Investigación Príncipe Felipe, Valencia (Spain)

[f] Departamento de Química, Universitat Politècnica de València. Camino de Vera s/n, 46022, Valencia (Spain).

* Correspondence: mmarcos@upv.es (M.D.M.); anberba@upv.es (A.B.)

Submitted to Materials Chemistry Frontiers

Abstract

The low toxicity and high adsorption capacities of clay minerals make them attractive materials for controlled delivery applications. However, the number of studies in the literature focused on active controlled release from these supports is still scarce. In this work, three different clays from the smectite group (Kunipia F, montmorillonite; Sumecton SA, saponite; and Sumecton SWN, hectorite) have been successfully loaded with the rhodamine B dye and functionalized with oleic acid as gatekeeper to produce hybrid organoclays for active and controlled payload-release. Moreover, hematin and cyanocobalamin, biomolecules involved in several metabolic pathways, have also been encapsulated in the hectorite gated-clay. These hybrid organoclays are able to confine the entrapped cargos in aqueous environment, and effectively release them in the presence of surfactants (as bile salts). A controlled delivery of 49 ± 6 μg hematin/mg solid and 32.7 ± 1.5 μg cyanocobalamin/mg solid was reached. The synthesis processes were followed by means of X-ray diffraction, FESEM, N_2 adsorption-desorption isotherms, zeta potential, infrared spectroscopy and thermogravimetric techniques. The cargo release profiles of all the organoclays were adjusted to three different release-kinetic models (i.e. Hill, Higuchi and Korsmeyer – Peppas). The fitting to the Korsmeyer – Peppas model has presented the most enlightening results, demonstrating the release dependence on (i) the organic-inorganic hybrid system, and (ii) the nature of loaded molecules and their interaction with the support. Furthermore, *in vitro* cell viability assays were carried out with Caco-2 cells, demonstrating that the organoclays are well tolerated by cells at particle concentrations of ca. 50 μg/mL.

Keywords: organoclay • hematin • cyanocobalamin • oleic acid • gatekeeper • surfactant • controlled release

1. Introduction

The need of numerous biomolecules to be protected and administrated in a sustained-and-controlled mode has currently stablished a major research area, especially in biomedicine. These requirements are principally due to two main reasons: avoid biomolecule-degradation, and achieve an efficient absorption at site, while unwanted side effects are minimized.[1] Mesoporous materials, and other structures able to be loaded, have become an interesting option for this purpose,[2] with numerous examples not only for biomedicine or pharmacology,[3–6] but also for nutraceutical and food applications,[7,8] or even for sensing and communication protocols. [9–13]

Among the different types of loadable-materials,[10,14–17] clays (hydrated phyllosilicates) have high potential for biological uses, among others, due to their inherent structure.[18] Clays are formed by compiled silica-and-alumina/magnesia layers many of them attached by exchangeable cations. Among all existing clays, minerals from the smectite group (as montmorillonite, hectorite or saponite) have a potential use in food, pharmaceuticals or nutraceuticals.[19] Smectite clays have especially high loading possibilities due to their high cation-exchange-capacity compared with other clay minerals.[20] In addition, clays have a very low oral toxicity, so they have mild side effects derived from their intake.[21] Due to this characteristics, smectite minerals have been traditionally widely employed as excipients, and more recently as carriers for vitamins, drugs or proteins.[22–26] The literature shows that incorporation of these molecules into clay layers can result in their greater stability and an improved release.[21,22,23,24] In fact, there are plenty of works in the literature about adsorbed-biomolecules into smectite clays[22–29] also studying the cargo-mineral interaction.[30] However, almost all the mentioned works with delivery applications are based on a passive release mechanism,[31] which usually consists of the delamination of the material by the solvent and the consequent release of the cargo. In contrast with this general passive mechanism, an active release can also be achieved for instance by functionalizing the external surface of the loaded support with a molecular gate or gatekeeper, which allows

the on-command release of the cargo only when a selected stimulus is present. Although this mechanism has been widely used in mesoporous silica (MS) supports (known as gated MS), as far as the authors know, there are no similar examples using organoclays.

Therefore, it was in our aim to demonstrate that it would be possible to prepare gated organoclays. As proof of concept, we selected smectite clays as supports and oleic acid (OA) as capping ensemble. Our choice of the gatekeeper is based in the fact that OA has demonstrated its ability to act as molecular gate on mesoporous silica materials having different structures and pore sizes.[32] Moreover, it has been reported that OA-gated MS can deliver the entrapped cargo selectively in the presence of surfactants such as for instance bile salts, and are, therefore, excellent candidates to selectively deliver payloads in the small intestine (SI) where bile salts are present.[4]

One group of molecules that could benefit from its protection in organoclay-systems, are biomolecules that are too large to be encapsulated in other loadable-materials, since clays are expandable and have no pore size restrictions.[33] As entrapped molecules we selected the dye rhodamine B (as control system) and the bio-active molecules hematin (*Hem*) and cyanocobalamin (*B12*) which have estimated diameters of ca. 15-20 Å. Although previous works where *B12* is released from clays can be found in the literature,[34,35] they are based on a passive release and do not have defined open-closed states that guarantee a zero-background release in the absence of the stimulus.

Furthermore, *Hem* and *B12* molecules are of special interest from a biochemical point of view. *Hem* molecule contents an iron atom chelated into protoporphyrin IX, and *B12* is a vitamer of vitamin B_{12}. These structural characteristics make the deficit of these molecules to be related to iron deficiency anemias (IDA).[36] In order to treat IDA, oral iron supplementation in the form of ferrous salts is normally the remedy used, but this could be associated with different side effects of varying severity.[37] Smart delivery systems for controlled release of a more-bioavailable-iron-form, like heme iron, could be a valuable option

to effectively regulate iron levels without inducing overdose. Meanwhile, cobalamin (or vitamin B_{12}) has a crucial role in cellular metabolism, and although its clinical deficiency is uncommon, subclinical deficiency affects up to 26% of general population.[38] Its deficit is related with several problems[39–42] and it is usually due to malabsorption, especially in the elderly.[43] There are studies in the literature where high-B12-doses orally administrated have been successful against pernicious anemia, treatment also applicable to supplementation for intake-deficit problems.[44,45] However, the instability of *B12*-molecule under adverse conditions of temperature, pH or light stipulate strict preservation processes, what supposes a clear disadvantage.[46,47] Smart delivery systems for controlled release of *B12* could be a good possibility to protect the *B12* molecule and release it in a controlled manner at its absorption-place, the duodenum.

Based on the above, we report herein the use of Kunipia F (K_F, natural refined montmorillonite), Sumecton SA (S_{SA}, synthetic saponite) and Sumecton SWN (S_{SWN}, synthetic hectorite) clays that were loaded with RhB, and S_{SWN} additionally loaded with Hem and B12*,* and capped with OA. These gated-organoclays display "zero" payload releases in absence of stimulus, yet were able to deliver the cargo in the presence of surfactants such as bile salts. In addition, the release experiments in the presence of bile salts were fitted to different mathematical models for drug release. The potential *in vitro* toxicity of the loaded and functionalized particles was also tested.

2. Materials and methods

2.1. Chemicals and cell culture media

Kunipia F (K_F, natural refined montmorillonite), Sumecton SA (S_{SA}, synthetic saponite), Sumecton SWN (S_{SWN}, synthetic hectorite) were acquired from Kunimine Industries Co. (Tokio, Japan). Rhodamine B (RhB), (3-aminopropyl)triethoxysilane (APTES), oleic acid (OA), N,N'-dicyclohexylcarbodiimide (DCC), hemin, cyanocobalamin (*B12*), cetyltrimethylammonium bromide (CTAB) and bile extract porcine were purchased from Sigma (Sigma-Aldrich Química S.L., Madrid, Spain). Ethanol (extra pure), hexane and dimethyl sulfoxide (DMSO) were acquired from Scharlab (Barcelona, Spain). 3-(4,5-dimethylthiazol-2-yl)-2,5-diphenyltetrazolium bromide (MTT) was provided by ThermoFisher (Madrid, Spain). Phosphate buffered saline (PBS), Dulbecco's Modified Eagle's Medium (DMEM), fetal bovine serum (FBS), penicillin/streptomycin antibiotic (P/S), non-essential aminoacids and all the needed mediums and materials for cell culture were provided by Labclinics (Labclinics S.A., Barcelona, Spain).

2.2. Gated organoclays synthesis

2.2.1. RhB loading

For model molecule (RhB) loading, 1 g of each clay (K_F, S_{SA}, S_{SWN}) was added to 36 mL of a 10 mg/mL solution of RhB in water. Then the mixture was kept under stirring for 24 h. After that, the solids were centrifuged and dried at 40 ℃. The obtained solids, loaded with RhB, were named K_F-RhB, S_{SA}-RhB and S_{SWN}-RhB respectively.

2.2.2. Functionalization

With the aim of controlling payload release from the supports, the loaded clays were functionalized with organic moieties. Solid functionalization was performed in two steps, a preliminary adhesion of APTES as linker molecule, and a final attachment of oleic acid to the APTES-amino groups through an amide bond.

2.2.2.1. 1st step: APTES functionalization

For the 1st step of functionalization, 400 mg of each of the loaded clays (K_F-RhB, S_{SA}-RhB and S_{SWN}-RhB) were resuspended in 15 mL of hexane and 2 mL of APTES were added, allowing the reaction to proceed for 5.5 h. After this process, the solids were isolated by centrifugation and dried under vacuum, obtaining the K_F-RhB-N, S_{SA}-RhB-N and S_{SWN}-RhB-N materials.

2.2.2.2. 2nd step: Oleic acid functionalization

Finally, to perform the last functionalization, 3 mL of OA were added to a solution of DCC in hexane (40 mg in 15 mL). After that, 300 mg of the appropriate APTES-functionalized solid (K_F-RhB-N, S_{SA}-RhB-N or S_{SWN}-RhB-N) were added. The corresponding mixture was stirred for 20 h at room temperature, and the synthesized solid was collected by centrifugation. The precipitate was washed with mixtures of ethanol:water with increasing proportions of water until no coloration was observed, and finally dried under vacuum. The final gated-organoclays, functionalized with OA, were K_F-RhB-OA, S_{SA}-RhB-OA and S_{SWN}-RhB-OA, respectively.

2.3. Characterization methods

Powder X-ray diffraction (PXRD), Field Emission Scanning Electron Microscopy (FESEM), N_2 adsorption-desorption isotherms, zeta (ζ) potential measurements, infrared spectroscopy (FTIR), thermogravimetric analysis (TGA), Fluorescence spectroscopy and UV-Vis spectroscopy were employed to characterize the synthesized supports.

X-ray diffractograms were performed on a Bruker D8 Advance diffractometer (Bruker, Coventry, UK) using Cu Kα radiation. FESEM images were acquired with a Zeiss Ultra 55 (Carl Zeiss NTS GmbH, Oberkochen, Germany) and observed in the secondary electron mode. N_2 adsorption-desorption isotherms were recorded with a Micromeritics TriStar II Plus automated analyzer (Micromeritics Instrument Corporation, Norcross, USA). The samples were degassed at 120 ℃ in vacuum

overnight. The specific surface areas were calculated from the adsorption data in the low-pressure range using the BET model.

The functionalization process of all the solids was followed by FTIR in a Bruker Tensor 27 FTIR spectrometer. To determine ζ potential values of the functionalized organoclays and their bare precursors, a Zetasizer Nano ZS equipment (Malvern Instruments, Malvern, UK) was used. Samples were dispersed in ethanol at 20 ℃, at a concentration of 1 mg/mL. Before each measurement, samples were sonicated for 2 minutes to preclude aggregation. ζ potential was calculated from the particle mobility values by applying the Smoluchowski model. The average of nine recordings was reported as ζ potential, and error bars are given with the standard deviation-value.

The composition of loaded and functionalized clays was determined by TGA. Thermogravimetric analyses were carried out on a TGA/SDTA 851e Mettler Toledo balance (Mettler Toledo Inc., Schwarzenbach, Switzerland), using an oxidant atmosphere (air, 80 mL/min) with a heating program consisting of a heating ramp of 10 ℃ per minute from 20 to 1000 ℃ and two isothermal heating steps at 100 ℃ and 1000 ℃ for 30 min. Fluorescence spectroscopy was carried out on a JASCO FP-8500 Spectrofluorometer (JASCO, Easton, United States) equipped with a FMP-825 Microplate reader, and UV-Visible spectra were recorder with a JASCO V-650 spectrophotometer.

2.4. Cargo delivery

To obtain the cargo release profiles of all the model organoclays, 5 mg of the corresponding solids were placed in 10 mL of PBS (pH 7.5), simulating standard conditions in the gastrointestinal tract (GIT), and in 10 mL of PBS containing 10 mg/mL of bile extract, simulating specific surfactant conditions at the SI. At certain times (0.02, 0.25, 0.5, 1, 2, 4, 6, 8, 24 hours) aliquots of 700 µL were taken and filtered through 0.45 µm PTFE filters. Finally, the RhB content was determined by fluorescence spectroscopy. For the measurement, the employed excitation and emission wavelengths were 555 and 572 nm, respectively.

2.5. Cargo release kinetics

The payload release kinetics from all the gated-organoclays were calculated using different mathematical models. The selected models and their equations were Hill (Eq. [1]); Higuchi (Eq. [2]); Korsmeyer – Peppas (Eq. [3]).

$$\%_{Dye\ release} = F_{max} \cdot [t^{\gamma}/(k^{\gamma} + t^{\gamma})] \quad [1]$$

$$\%_{Dye\ release} = k_H \cdot t^{1/2} \quad [2]$$

$$\%_{Dye\ release} = k' \cdot t^{n} + b \quad [3]$$

2.6. Cell culture conditions

To test the possible toxicity of the different microdevices, Caco-2 human colon adenocarcinoma cells were selected as model of GIT cells. Caco-2 cells were acquired from the American Type Culture Collection (ATCC), and cultured in DMEM medium supplemented with 10% FBS, 1% P/S and 1% non-essential aminoacids. Cells were maintained at 37 ºC in a humidified atmosphere composed of 5% CO_2 and 95% air. The cells underwent passage when they reached 80% confluence.

2.7. MTT cell viability assay

Caco-2 cells were seeded at density of $2 \cdot 10^4$ cells/well in sterile 96-well plates and incubated 24 h in the medium and atmosphere conditions previously reported (see section 2.6). All the solids under study were suspended in the concentrations to be evaluated (50, 100, 250, and 500 μg/mL). Each concentration was tested in 16 wells; being control cells absent of any solid. After 24 h of incubation, cells were washed with PBS in order to remove the remaining particles. Then 100 μL of MTT solution in non-supplemented growing medium (0.5 mg/mL) were added to each well, and the plates were incubated another 2 h. After that, supernatant medium was removed and 100 μL of DMSO were added to each well. Finally, the plate was softly shacked until formazan crystals were completely solved, and the absorbance of the purple samples was measured at λ_{exc} = 550 nm.

3. Results and discussion

3.1. Design, synthesis and characterization of solids

The incorporation of gate-like ensembles into clays is an unexplored approach for controlled delivery applications. The development of responsive gated materials requires the selection of two components: *(i)* a suitable gate-like ensemble reactive to external stimuli and *(ii)* the selection of a structured matrix in which the gate-like assemble is grafted.

Three different materials from the smectite clay-group (K_F, S_{SA}, S_{SWN}) were selected as structured-matrices taking advantage of their natural characteristics. The clay-structure of the smectite clay-group is based on hydrated metallosilicate layers bonded by exchangeable cations (see Scheme 1). For the controlled-delivery intended in this study, we have replaced these cations by different molecules (i.e. a dye and two bioactive molecules). Furthermore, clay-surface is similar to that of mesoporous silica and contains silanol groups that are easily modifiable by means of grafting methods, allowing the possibility of functionalizing clays with gate-like ensembles.[48]

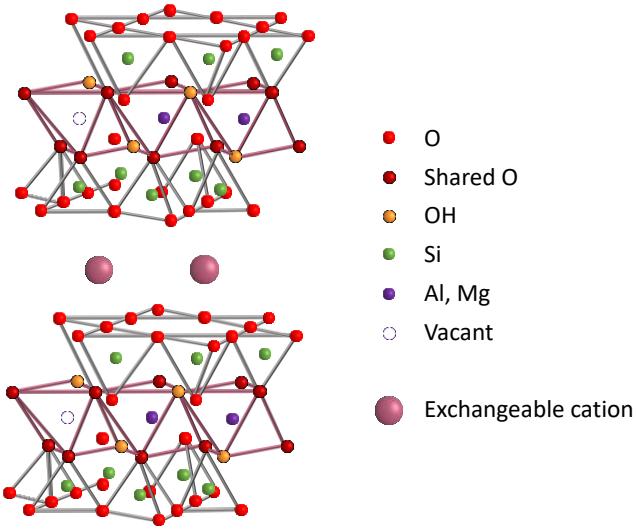

Scheme 1. Representation of the laminar structure of smectite-clays.

For the preparation of the gated materials, the clays K_F, S_{SA}, S_{SWN} were first loaded with rhodamine B (RhB) following an immersion method by means of the exchange-cation capacity of these minerals. The reaction was maintained for 24h to guarantee the clay-delamination needed for cargo loading. In a second step the loaded solids were reacted with APTES, and then oleic acid (OA) was attached to the APTES-amino-terminal group via the formation of an amide-bond. The synthesis procedure is outlined in Scheme 2. We have recently reported that materials gated with fatty acids can be "opened" by interaction with surfactants. It has been suggested, for example, that such gated supports can be used for the controlled delivery of certain biomolecules in the small intestine (SI) due to the presence of bile salts (a natural surfactant). The OA gating mechanism has also been recently described and is due to interaction forces between the hydrophobic tails of OA that act as closing force, preventing cargo release from the system to an aqueous environment. However, in the presence of surfactants (such as bile salts) this interaction is interrupted, and the encapsulated payload can be released. Once the loading and functionalization parameters were optimized with RhB, two more OA-gated S_{SWN} clays loaded with the bioactive molecules *Hem* and *B12* were prepared.

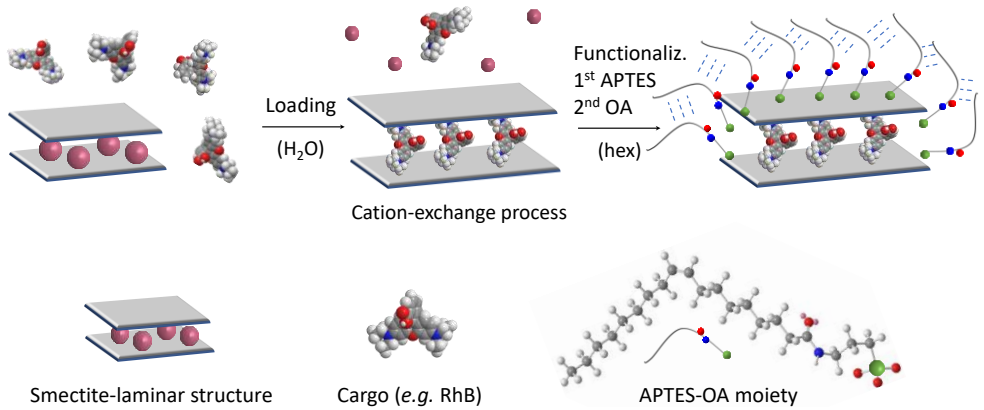

Scheme 2. Representation of the synthesis of the gated clays. Cargo loading was produced by means of cation-exchange process in aqueous medium, whereby the guest molecule is intercalated between the layers of the smectite-clay. In a second step the loaded support is functionalized with APTES and then with OA.

The synthesized particles were characterized by the usual standard techniques. Normalized X-ray diffraction patterns of bare, RhB-loaded and final gated-clays are shown in Figure 1, and “d spacing” values of the more significant peaks in the solids are listed in Table 1.

As it can be seen, these materials do not present very resolved patterns, and the diffraction diagrams are dominated by several intense peaks that correspond with the interlayer spacing. Hence, the first peak in each pattern would correspond with the distance between metallosilicate layers in the clays, and the other intense peaks are the corresponding higher order XRD reflections. Therefore, in all the diffractograms, a low-angle region (3° to 10° 2θ) can be delimited where the intercalation of the different cargo molecules into the clay has its mayor effect. In this region, the most intense peak moves towards smaller 2θ values, i.e. higher d-spacing (see Table 1), when the guest molecule is effectively intercalated in the interlayer spacing, as this action produces the separation of the metallosilicate layers.

However, OA functionalization of the different loaded solids does not produce a further increase but a shrinkage of the interlayer distance that could be related with some leak of the cargo and/or the interaction of OA moieties attached to the metallosilicate layers. Additionally, both the RhB intercalation and the OA functionalization produce a broadening of the other peaks as the intercalation process produces a loss of order in the structure.

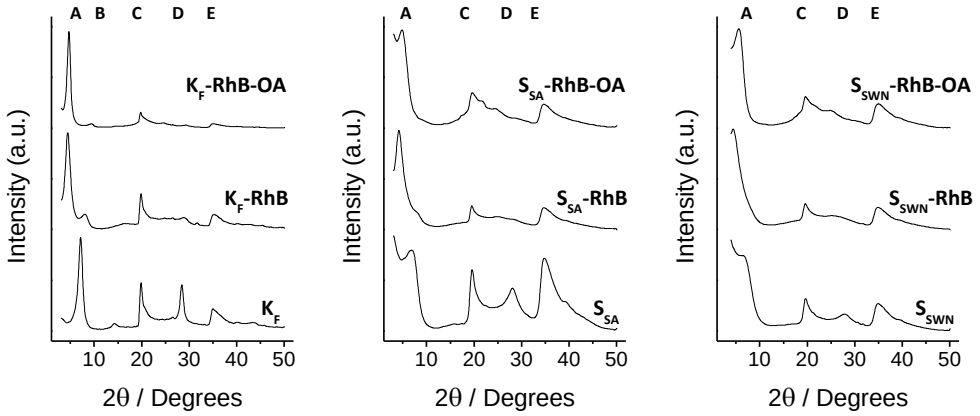

Figure 1. Normalized X-ray patterns of RhB-loaded organoclays in the different synthesis steps, indicated in their respective diffractogram. From bottom to top: bare, loaded and final gated-material, respectively. The main XRD reflections are labelled from left to right as A-E, consecutively.

Table 1. Main reflexions' d-Spacing (Å) values for the RhB-loaded organoclays obtained from Bragg's law ($n\lambda = 2d \cdot \sin(\theta)$, $\lambda = CuK_{\alpha\,av} = 1.54$ Å, n=1).

	A	B	C	D	E
K_F	12.35	6.22	4.48	3.13	2.56
K_F-RhB	19.61	11.47	4.48	3.14	2.54
K_F-RhB-OA	18.79	9.40	4.49	3.13	2.56
S_{SA}	12.35		4.55	3.19	2.58
S_{SA}-RhB	21.71		4.55		2.59
S_{SA}-RhB-OA	18.79		4.57		2.58
S_{SWN}	13.55		4.52	3.21	2.57
S_{SWN}-RhB	19.96		4.54		2.57
S_{SWN}-RhB-OA	15.64		4.55		2.56

FESEM images of all the RhB-loaded final solids in the different synthesis-steps are depicted in Figure 2 (K_F solids are shown in Figure 2A, S_{SA} solids in Figure 2B, and S_{SWN} solids in Figure 2C). Starting from bare materials (Figure 2, 1st row), as observed in the micrographs, the size of bare particles is quite similar for S_{SA} and S_{SWN} (Figure 2B *i* and Figure 2C *i*) that is on average up to 10-20 µm for S_{SA} particles and slightly smaller size for S_{SWN} ones, whereas K_F has a tendency towards much larger agglomerates (Figure 2A *i*). However, the particle's size is not the only difference among the chosen clay materials, as K_F particles show a quite irregular shape, while S_{SA} shows more regular particles and the S_{SWN} is mainly composed of spheres. This external shape of the different particles is related to an also different microscopic arrangement of the metallosilicate plates in each one of the three solids. Thus, K_F particles show a smooth surface (Figure 2A *iii*) that may be related with a microscopic parallel organization of its plaques, while both S_{SA} and S_{SWN} (Figure 2B *iii* and Figure 2C *iii*, respectively) present a microscopic pleated and folded arrangement of the plates to produce the corresponding rounded particle shape. These differences in the microscopic arrangement of the plates for the three solids can be related to the slightly higher crystalline order in the case of the K_F clay, which is shown in the smaller width of its XRD peaks.

After loading of the rhodamine B molecule inside the three host clays (Figure 2, 2nd row), changes in the microstructure are revealed (Figure 2A, K_F-RhB; 2B, S_{SA}-RhB; and 2C, S_{SWN}-RhB). In regard of the particle shape, the biggest changes can be seen for S_{SA} and S_{SWN} materials, as they lose completely the rounded shape and the size homogeneity. In relation to organization of the microscopic plaques, the three cases undergo important changes. While RhB-loaded K_F clay shows a rougher surface, bringing out a disordered arrangement of the microscopic plates, RhB-loaded S_{SA} clay still shows some domains of the pleated and folded microscopic arrangement, and the RhB-loaded S_{SWN} clay shows a quite parallel organization of the microscopic plaques. These changes can be related with a delamination and reorganization process suffered during the immersion-based loading process.

The functionalization processes with APTES (Figure 2, 3rd row) and finally OA (Figure 2, 4th row) do not extremely change the appearance of the particles, but increases the general disorder, making all the materials at the end of the process quite similar in the less homogeneous distribution of particle-sizes and the disordered arrangement of their internal microscopic plaques.

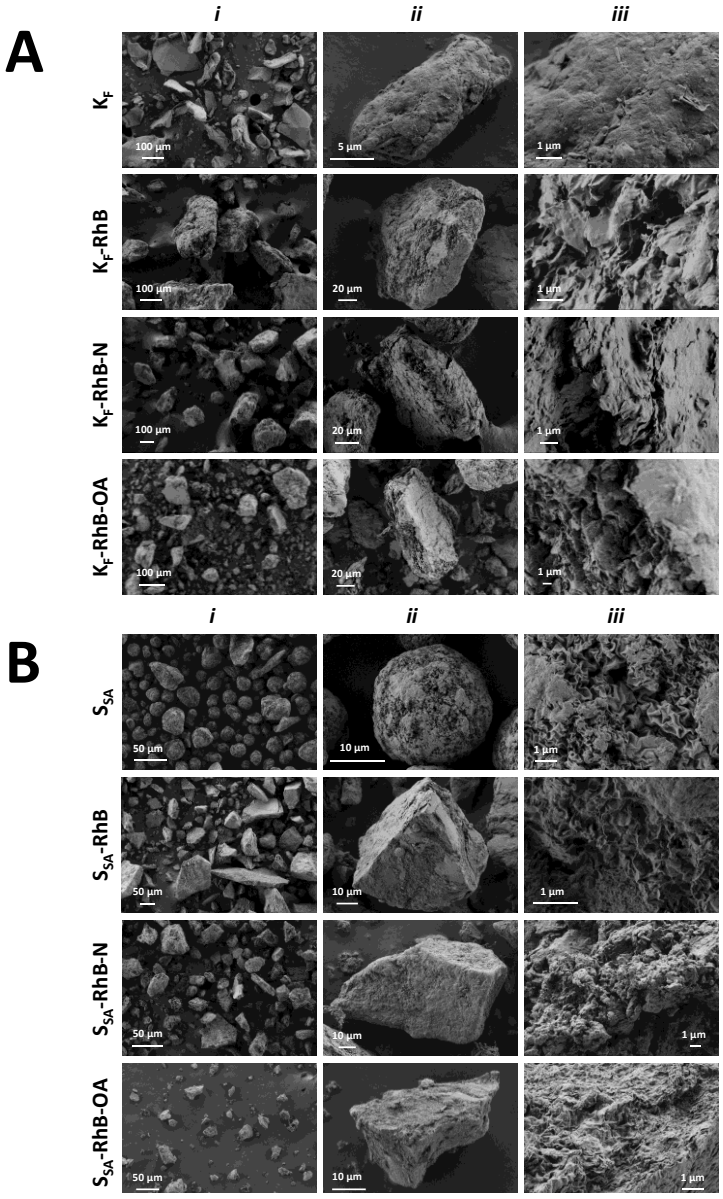

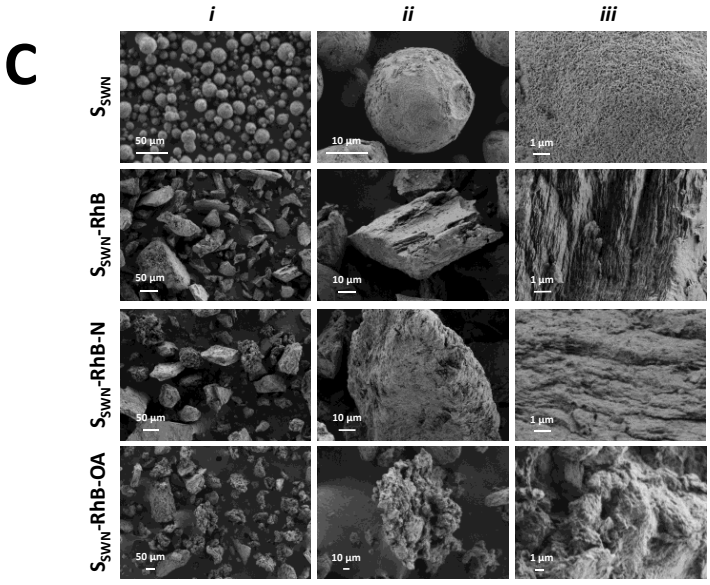

Figure 2. FESEM micrographs of the obtained solids in the different steps of synthesis of **A**, K_F-RhB-OA; **B**, S_{SA}-RhB-OA; and **C**, S_{SWN}-RhB-OA. General view of the particles (***i***), image of a representative particle (***ii***) and surface detail (***iii***).

From the combination of FESEM and XRD data, it can be concluded that despite the changes in size and shape of the obtained particles, the laminar structure of each material is not affected, since the XRD reflections of the initial material are maintained. Also, it can be determined that loading and functionalization processes modify the external appearance of the particles and increase the distance between clay layers due to the organic-matter inclusion into the interlamellar-space of the three materials.

The N_2 adsorption-desorption isotherms of the bare clays and the RhB-loaded final organoclays are shown in Figure 3, and the corresponding values of the specific surface and pore volume are collected in Table 2. Same as in the case of the FESEM analysis, the three bare clays used as support in this work present two differentiated behaviors. In one side, the K_F material presents a type II isotherm[49] that corresponds with a non-porous material. The very small knee at the low P/P_0

values is related to the formation of the adsorbate monolayer, and the thickness of the adsorbed multilayer (region of P/P_0 close to 1) has apparently no limit. Additionally, this support shows a hysteresis loop of type H3, that is typical of non-rigid aggregates of plate-like particles, what is clearly in agreement with the FESEM observations (*vide supra*).

On the other hand, S_{SA} and S_{SWN} empty clays show type IV isotherms with very similar features between them, which can be related to porosity in the mesopore range. Adsorption curves in both materials present a more pronounced knee at the low P/P_0 values than in the case of the K_F clay, corresponding with a higher specific surface (see Table 2). Also, in both cases the increment of the adsorbed N_2 is produced very slowly along the full P/P_0 range, ending only at values close to 1 in a very small plateau, corresponding with a very wide distribution of pore sizes (data not shown). S_{SA} and S_{SWN} clays also present a hysteresis loop of type H2 that could be related to a percolation process of the liquid adsorbate through the clays' structure.

This different behavior between K_F clay in one side and S_{SA} and S_{SWN} on the other can be clearly related to their different microstructure revealed in the FESEM analysis. K_F present smooth surface particles where the metallosilicate layers are quite well ordered one on top of the other. However, S_{SA} and S_{SWN} present particles where the metallosilicate plates are very corrugated, producing the spherical microparticles observed in the FESEM micrographs (Figure 2 A-C, 1st row). The corrugation of the structural layers must be the responsible of this mesoporosity with a very wide pore size distribution. During the loading and functionalization processes, the clays suffer consecutive delamination and reorganization of the metallosilicate layers. Thereof, all the three final materials present similar non-corrugated layers in the FESEM micrographs (see Figure 2) and hence, the three of them only show gas adsorption in the region of high P/P_0 values, which corresponds to intraparticle pores.

Consequently, while an almost negligible change in specific surface area and pore volume is detected for the K_F clay, S_{SA} and S_{SWN} ones suffer an important

decrease in the organoclay N_2 adsorbed volume and surface area reaching the values of the K_F support (see Table 2). Hence, the increase in the value of the d-spacing of the first peak in the three loaded material (Table 1, peak A) is directly related with the loading of the RhB molecule inside the interlayer spacing.

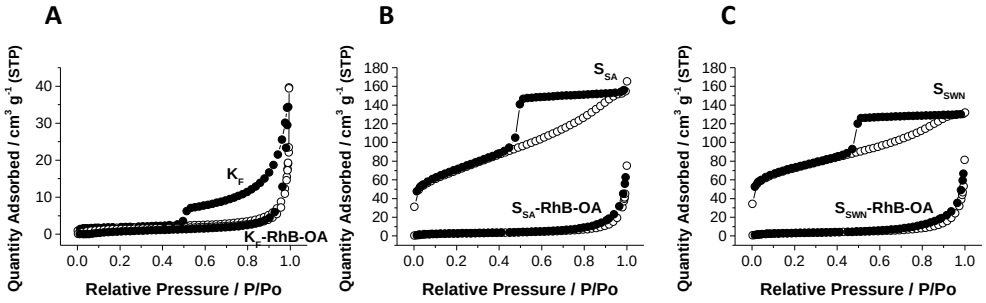

Figure 3. Nitrogen adsorption (○) – desorption (●) isotherms for all the bare clays and final model gated-organoclays. **A**, K_F and K_F-RhB-OA; **B**, S_{SA} and S_{SA}-RhB-OA; **C**, S_{SWN} and S_{SWN}-RhB-OA.

Table 2. BET specific surface values and pore volumes calculated from the N_2 adsorption-desorption isotherms for selected materials.

	S_{BET} ($m^2\ g^{-1}$)	**Pore Volume** [a] ($cm^3\ g^{-1}$)
K_F	5.7	0.04
K_F-RhB-OA	4.8	0.03
S_{SA}	250.5	0.14
S_{SA}-RhB-OA	9.9	0.01
S_{SWN}	242.1	0.10
S_{SWN}-RhB-OA	11.3	0.07

[a]Pore volumes are restricted to intraparticle mesopore area.

Loading and functionalization processes which lead to the final gated-solids were followed by zeta (ζ) potential. The measurement-assay was performed in EtOH at 20 ºC and the obtained values are reported in Figure 4. As it can be observed, the three bare clays (white bars) exhibited negative ζ potential values (between -20 mV and -30 mV). After the loading process, the charge of the materials remained negative (light gray bars) since the external groups of the material were not modified. Then, once the APTES molecule was added, ζ potential values become positive (K_F) or less negative (S_{SA} and S_{SWN}) (dark gray bars), confirming the efficiency of the functionalization process. The neutralization of the charge is a direct consequence of the presence of the amino group of APTES on the surface. Finally, the anchoring of OA to the APTES moieties increases even more the positive charge of the particles, resulting in positive ζ potential values for all the model organoclays.

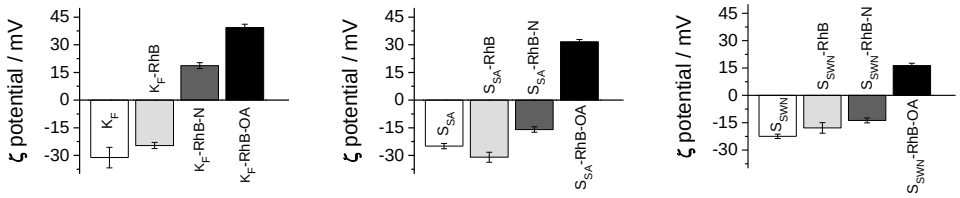

Figure 4. Zeta (ζ) potential values of all the model organoclays. The increasing darkness in bar colors correspond to the progressive synthesis steps: from bare clays to loaded, APTES-functionalized and final OA-functionalized organoclays (white, light gray, dark gray and black bars, respectively).

All the RhB-loaded organoclays in the different synthesis steps were also characterized by infrared spectroscopy (FTIR), and the obtained spectra are depicted in Figure 5. The dominant bands in all the FTIR spectra are those which belong to the silica tetrahedra and metal octahedra which conform the laminar structure of all the phyllosilicates (1050, 600 and 450 cm^{-1}). All the bare-clay precursors are part of the smectite family, and as result of the structural resemblance, the FTIR spectra thereof are similar for the three of them. The broad

band that appears around 3500 cm^{-1} is related to the vibration of the hydration water molecules and it disappears during the functionalization process. The small but sharp band at 3600 cm^{-1} and the sharp one at 1600 cm^{-1} are assigned to the hydroxyl group coordinated to octahedral cations, mainly Al^{3+} in the K_F clay (montmorillonite) and Mg^{2+} in S_{SA} (saponite) and S_{SWN} (hectorite) clays. The clear appearance of two bands at approximately 2900 cm^{-1} and 2850 cm^{-1} in all the spectra of the gated clays is assignable to the bending C–H vibrations. These new bands are related to the presence of APTES and OA.[4]

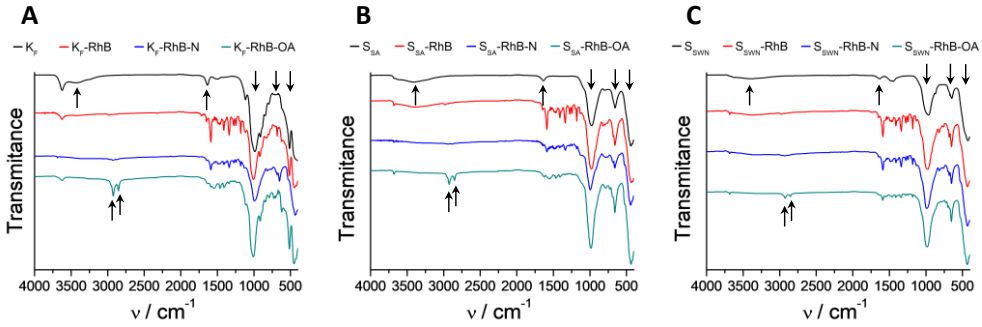

Figure 5. FTIR spectra of the consecutive synthesis steps of the different model organoclays: **A**, K_F-RhB-OA; **B**, S_{SA}-RhB-OA; **C**, S_{SWN}-RhB-OA.

The contents (α_i) in $mmol \cdot g^{-1}$ of remaining residue (metal oxides from the inorganic support) of cargo, APTES and OA in the final RhB loaded organoclays were determined by TGA and are shown in Table 3. As it can be seen, the three materials present similar amount of loaded RhB but different degree of gate functionalization. The relation between organic matter content, functionalization percentage and payload release is explained in section 3.2 (*vide infra*).

Table 3. Content (α) in mmol g^{-1} residue (after calcination) of cargo, APTES and OA in the final organoclays, determined by TGA.

Solid	α_{cargo}	α_{APTES}	α_{OA}
K_F-RhB-OA	0.69	1.3	1.3
S_{SA}-RhB-OA	0.74	0.79	0.61
S_{SWN}-RhB-OA	0.78	0.31	0.30

3.2. Cargo controlled release

In order to evaluate the feasibility of different supports to control the bioaccesibility of the payload, delivery studies of RhB from the three loaded and functionalized clays were carried out in absence and presence of bile salts. RhB concentrations in the different aliquots were measured by means of fluorescence spectroscopy.

Figure 6 shows the release behavior of the three gated-clays loaded with the cited fluorophore and functionalized with OA. For all three systems, a zero baseline was found in release experiments in PBS in absence of bile salts, indicating that RhB remained inside the layers of the clays and it was not released to the solution. In contrast, in the presence of bile salts (conditions of the SI), a progressive delivery of RhB was observed for all of them. This different and remarkable behavior in the presence of the triggering stimulus, when compared to that of the PBS alone, is due to the surfactant effect of bile salts. This fact confirms the ability of OA to act as molecular gate when anchored on these clays, even when they have a layered structure with an expandable interlayer distance, compared with other mesoporous materials typically used for the design of controlled delivery systems. Comparing release curves of the different organoclays, it can be stated that S_{SWN} is the material with the highest delivery capacity, followed by K_F and S_{SA}. To compare the different releasing capacities of the synthesized materials, the maximum payload released must be related with the organic matter content of each solid (Table 3, *vide supra*). Taking into account the data included in Table 3, the different functionalization of the three composites, combined with structural differences of

the host matrices, could be the responsible of the different release presented by the compound materials. Thus, while hectorite (S_{SWN}) and montmorillonite (K_F) clays present substitution in the octahedral (Al/Mg) positions of the metallosilicate layers, saponite clay (S_{SA}) presents substitution in the tetrahedral (Si) positions. This substitution at the tetrahedral sites may produce higher interaction between the metallosilicate layers and the cationic RhB moieties. Then, the material with the highest release (S_{SWN}) is the one with the lowest gate functionalization and octahedral substitution, whereas the one with the lowest release (S_{SA}) corresponds with an intermediate gate functionalization and tetrahedral substitution. Montmorillonite (K_F) clay presents, as hectorite (S_{SWN}) clay, octahedral sites substitution, but a quite higher functionalization what halves the final release for this material compared to the one of the hectorite.

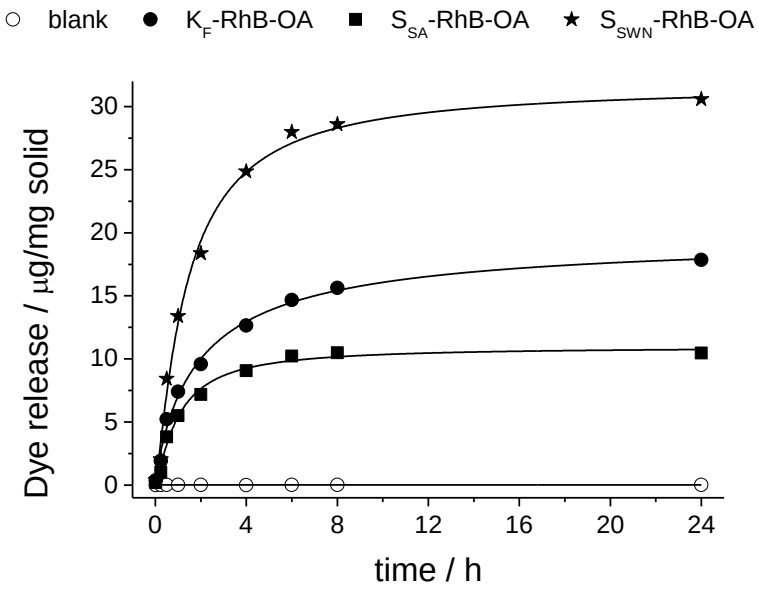

Figure 6: Release profile of RhB dye from all the gated organoclays in PBS (○) and in the presence of bile salts (● K_F-RhB-OA, ■ S_{SA}-RhB-OA, ★ S_{SWN}-RhB-OA).

Once the loading and functionalization parameters were optimized with the model molecule (RhB), the synthesis and release kinetics experiments of clays loaded with bioactive molecules were carried out. Two biomolecules, *Hem* and *B12*, were selected to be encapsulated in the clay with the highest delivery capacity: i.e. S_{SWN}. The synthesis of the bioactive organoclays was followed using XRD, ζ potential, FTIR and TGA techniques (data in Supporting Information). In general, bioactive-loaded clays showed similar results than those found for the RhB-loaded materials. However, it is worthy to point out some differences in the evolution of the XRD diagrams when loading the S_{SWN} clay with both biomolecules. In first place, the intercalation of *Hem* and *B12* in the chosen clay produces a lower displacement of the first peak than the one observed for the S_{SWN}-RhB material, but similar for both biomolecules (from 13.55 Å to 14.52 Å and 14.65 Å for *Hem* and *B12* molecules, respectively). However, the functionalization with OA shows a quite different result for both materials. In the case of the B12-loaded clay the final functionalization with OA produces a quite smaller decrease, almost indiscernible, of the interlayer distance when compared with the RhB-loaded materials, so no leak of the loaded biomolecule during the final functionalization steps has taken place. However, in the case of the Hem-loaded S_{SWN} material not only there is not a decrease in the interlayer distance but also a further increment in the value of the interlayer separation. This different behavior could be related with a possible intercalation of the OA molecules in the interlayer spacing, since hematin molecules are already present in the interlayer spacing of the clay.

Once the S_{SWN}-Hem-OA and S_{SWN}-B12-OA materials were characterized, the procedure followed to obtain the release profiles of the loaded biomolecules was similar to that used in the case of the RhB-loaded organoclays. The details are included in the Supporting Information and the obtained profiles are shown in Figure 7. Both supports have zero or negligible release when they are suspended in PBS media and a marked payload release is produced when surfactant molecules are present (for more information about release kinetics, see section 3.3). This demonstrates that OA-moiety also closes efficiently the phyllosilicate-based system

when large molecules are the entrapped cargo between metallosilicate layers, and that the OA gate allows the release of these big molecules when the appropriate stimulus (e.g. bile salts) is present. However, some differences can be observed between the release profile of these two materials. In the case of the B12-loaded clay, the cargo is quickly released, reaching the maximum payload after 4 hours. In the case of the Hem-loaded solid, the release of the cargo is considerably more sustained in time, and it only reaches its maximum payload after 24 hours. Taking into account the differences in the XRD diagrams of both functionalized materials (see above) we may relate this different behavior to the presence of OA also intercalated in the interlayer spacing what would produce a more complex release process.

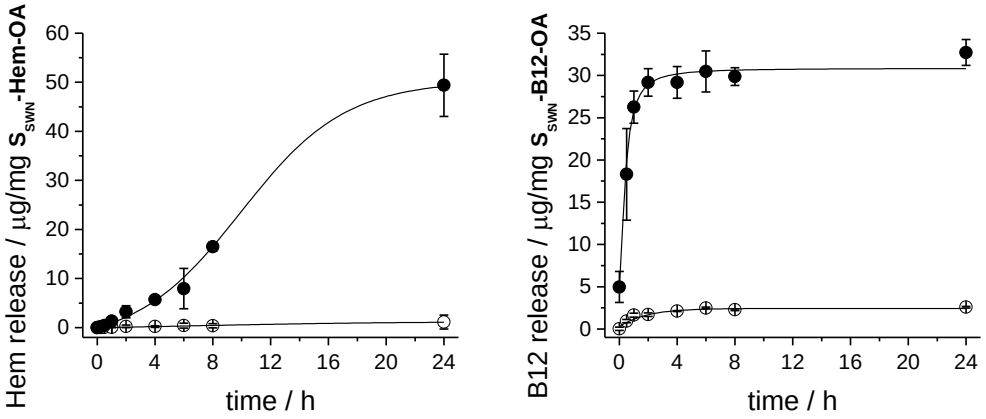

Figure 7: Release profiles of *Hem* (left) and *B12* (right) from S_{SWN}-Hem-OA and S_{SWN}-B12-OA organoclays, respectively. Suspensions of the gated supports in PBS (○), and in a solution containing CTAB-surfactant molecules (●).

Despite the fact that *B12* has previously been encapsulated in similar supports,[34,35] this is the first time that *B12* and *Hem* are protected in a system with a molecular gate that effectively releases them in an active and controlled way. The zero-release achieved by all the synthesized organoclays, regardless of the cargo-molecule-size, constitutes an important outcome in relation to the functionality of OA as molecular gate.

3.3. Cargo release kinetics

Besides achieving a remarkable surfactant-triggered release of the cargo, it was also our aim to evaluate the capability of those systems to control the delivery of the payload molecule over time. With this purpose, data from release experiments in the presence of bile salts were fitted to different mathematical models for drug release: Hill,[50] Higuchi and Korsmeyer-Peppas.[51]

Hill equation has been widely employed to fit data from different physicochemical phenomena as enzymatic reactions or the relation between drug concentration and its effect. The main reason for its success is probably its flexibility and effectiveness in fitting experimental data. In our case, the Hill equation would allow us to simulate a sigmoidal release patterns in which there is an initial slow release, followed by a faster intermediate release, and finally a further slow release. The fitting of the experimental values to this model has allowed us to calculate parameters as the maximum payload release (F_{max}), the sigmoicity coefficient of the curve (γ) and the constant k related with the time needed to get 50% of release, which can help us to compare the different releasing processes.

Higuchi model is based on Fickian diffusion processes taking into account three hypotheses: (i) the initial drug concentration in the matrix is much higher than drug solubility, (ii) the drug diffusion takes place only in one dimension and, (iii) the drug diffusivity is constant. From the fit of the data to this model, the Higuchi's constant K_H related with the velocity of diffusion of the drug from the supporting matrix can be obtained.

The semi-empirical model described by Korsmeyer – Peppas (K-P), denominated also "power law", adds some modifications to the Higuchi model and makes it less restrictive. It is applied for drug release from matrices in which several phenomena occur simultaneously, not only diffusion. Three different parameters are obtained from the mathematical adjustment of the data to the power law that can give us important information about de cargo release process. In first place, *K* is a constant that is directly related with the interaction between the cargo and the

host matrix, i.e. the larger the value of the constant the bigger the interaction. Then, the parameter *b* indicates the presence or not of a phenomenon denominated "burst release" that indicates the immediate release of the load in the corresponding medium. And finally, the parameter *n*, that is the more complex one, is related to the type of diffusion. For a cylindrical geometry of the support the value for this constant should be *n = 0.45* in case of Fickian diffusion, but it would have bigger values if the system presents non-Fickian diffusion. In this last case, there are three possibilities which differ in the velocity of the solvent diffusion (V_{s-d}) respect to the polymeric relaxation process (P_r). The possibilities are (*i*) *0.45 < n < 0.89* if there is anomalous transport, where V_{s-d} and P_r have similar magnitudes; (*ii*) n = 0.89 defines the Case I transport, where $V_{s-d} < P_r$; and (*iii*) n > 0.89 indicate Super Case II transport, where $V_{s-d} >> P_r$ which causes an acceleration of solvent penetration.[51] Although the release process from the organoclays designed in this study is not produced from a polymeric matrix, it is also possible to obtain information about the release mechanism in our materials as the solvent will have to diffuse inside the clay composites to extract the cargo molecules (V_{s-d}), against the gating moieties that should suffer the corresponding relaxation process (P_r) when the external stimulus is present. The values of all the parameters calculated from the release-kinetics-data of all the synthesized organoclays with the aforementioned mathematical models, as well as the obtained coefficients of determination (r^2), are listed on Table 4.

Table 4. Parameters and coefficients of determination (r^2) obtained by adjusting the data to each model equation ([1], [2], [3]).

System	Hill				Higuchi		K-P			
	F_{max}	γ	k min	r^2	K_H $min^{-½}$	r^2	K min^{-n}	n	b	r^2
K_F-RhB-OA	17.85	0.96	86.14	0.991	0.78	0.97	7.75	0.40	0	0.99
S_{SA}-RhB-OA	10.47	1.27	52.54	0.987	0.55	0.94	11.1	0.37	0	0.98
S_{SWN}-RhB-OA	30.57	1.21	73.64	0.995	1.46	0.96	7.83	0.41	0	0.98
S_{SWN}-Hem-OA	49.38	1.83	750.02	0.948	0.50	0.83	0.01	1.21	0.71	0.96
S_{SWN}-B12-OA	32.72	0.79	14.86	0.975	1.79	0.69	3.49	0.42	44.2	0.74

The Hill model is the most flexible of those proposed, and hence it offers the best adjustment of the release kinetics of the five materials, allowing us to get a first comparison among the solids. From the values in Table 4 we can see that the three materials loaded with RhB present quite similar parameters. The material with higher F_{max} value is S_{SWN}-RhB-OA, as it corresponds with the highest cargo loading, followed by K_F-RhB-OA and S_{SA}-RhB-OA, which present similar F_{max} values. In the case of the *B12* release from S_{SWN}-B12-OA, the obtained parameters are similar to those of the RhB loaded solids, but it presents smaller values for k and γ, which would indicate a faster release of the *B12* vitamin. The *Hem*-release curve is the most different of all, showing bigger values for both k and γ parameters, which would indicate a slower and maintained release of the cargo.

The adjustment of the data with the Higuchi model provides worse results, being the coefficients of determination especially low for the S_{SWN}-Hem-OA and S_{SWN}-B12-OA materials ($r^2 < 0.9$). Although the fit of the release kinetics data of these two materials with the Higuchi model is not perfect, the value of the K_H constants obtained indicates that the *B12* release is the fastest process of those studied, while the *Hem* release is the slowest one. These premises are in agreement with the information obtained from the Hill model.

Finally, Korsmeyer – Peppas model shows a very good adjustment of the kinetics for the three RhB loaded materials. The free refinement of the "n" parameter gives values quite close to 0.45, indicating a Fickian diffusion for the RhB release. The three materials present also a zero value for the "b" parameter, indicating a null burst release, and similar values for the "K" parameter which would indicate a similar interaction between the RhB cation and each of the three host matrices. Restricting the "n" value for these materials to the range imposed by the K-P model's definition ($n \geq 0.45$), the adjustment is still quite good, and only small changes in the parameters (b and K) are obtained whereas the relative order of the values is maintained (see supplementary material, Table S2).

Although the application of the K-P model to the release of the *B12* molecule offers poor adjustment, the obtained n and K parameters are similar to the ones of

the RhB composites. This fact would indicate also a Fickian diffusion of the cargo, however in this case a big burst release is produced. On the other hand, when the K-P model is applied to the release of the *Hem* molecule we obtain a better adjustment with a quite different parameters collection. In first place, *n* parameter gets the value of 1.21 which indicates a Super-Case II non-Fickian release ($V_{s\text{-}d} >> P_r$), with a fast solvent penetration and governed by the swelling of the composite. This result would be in agreement with a more complex OA functionalization in the S_{SWN}-Hem-OA material, revealed by its large increment of the interlamellar spacing after the last synthesis step compared with the other materials (see XRD data in Table 1 and Table S1). Additionally, the value of the K parameter is very low, indicating a very small interaction of the *Hem* moiety with the S_{SWN} matrix, markedly lower than the one found in the case of the RhB or *B12* molecules. This can be understood as the anionic charge of the aluminosilicate layers of the three clay materials would interact with higher strength with RhB and *B12* compared with *Hem*, since the first two molecules have cationic character while the *Hem* molecule should present anionic charge at the pH of the loading process.

3.4. In vitro biocompatibility test: interaction with cells of the GIT

In addition to the cargo release experiments from the five different organoclays, it was also aim of this study to assess the biocompatibility of the developed systems. Therefore, cell viability studies with all the bare phyllosilicates and final loaded-and-functionalized solids were performed. Caco-2 human colon carcinoma cells were selected to evaluate a possible toxic effect of the cited microdevices on cells of the GIT. Similar studies found in the literature report low toxicity for this kind of materials at standard concentrations (ca. 50 µg/mL),[19] reason why chronic particle concentrations were tested in the current assay (up to ca. 500 µg/mL). Cells were treated with each one of the prepared systems for 24 h at concentrations of 50, 100, 250 and 500 µg/mL. After this time, a cell viability assay using MTT was performed, which is based in the absorbance measurement of formazan produced by oxidoreductase enzymes of viable cells.[52] The formazan crystals produced by mitochondrial respiration are insoluble in the growing

medium, so DMSO solvent must be added after medium removal in order to solubilize the generated compound. The absorbance of the resulting purple solution was measured at λ_{exc} = 550 nm and compared with the one achieved by control cells.

Figure 8 shows the obtained results from the MTT cell viability assay. First of all, focusing on bare materials toxicity, K_F is the least toxic one, followed by S_{SA} and finally S_{SWN}. If the average-particle-size observed in FESEM micrographs is compared, K_F aggregates were much larger than S_{SA}, and these were slightly larger than S_{SWN} (see section 3.1 for details). Therefore, it can be deduced that the larger the particle size, the lower the material's toxicity. These results agree with multiple data in the literature, because large particle sizes partially prevent their cellular internalization.[53] An increase in the toxicity levels is observed at high particle concentrations, probably because the cell monolayer becomes overspread due to sedimentation of the particles. This fact has been previously described in other works in the literature,[54] and the increased toxicity at high concentrations observed in the present work may be related to this circumstance.

The toxicity of all loaded and functionalized organoclays is comparable between them, which may be related to their similar average size and functionalization. Cell viability values are very similar to each other, and are slightly lower than those of the bare precursors. Focusing on particle-concentrations, standard amounts of the tested organoclays (ca. 50 µg/mL) remain cell viability at high levels (higher than 70%). The results show also that even at particle concentrations as high as 500 µg/mL, S_{SWN} solids (S_{SWN}-RhB-OA, S_{SWN}-Hem-OA and S_{SWN}-B12-OA) are as biocompatible as the starting bare material.

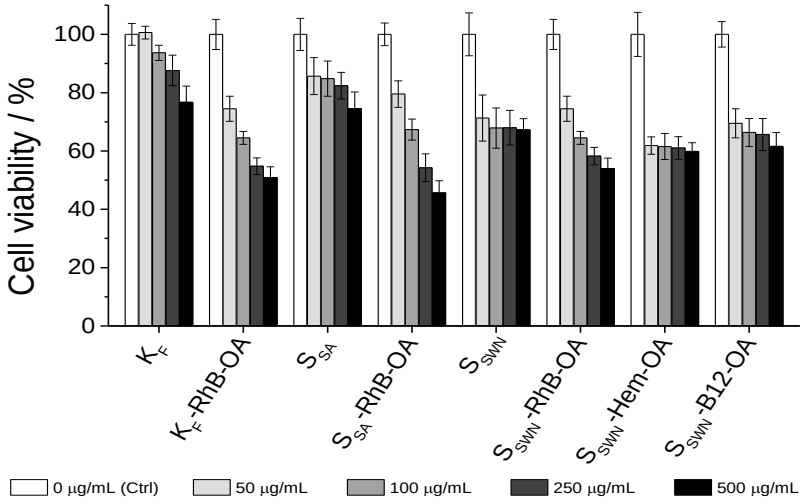

Figure 8. MTT cell viability assay of Caco-2 cells exposed to the indicated materials. Caco-2 cells were treated with the bare clays and the gated organoclays at concentrations of 0 (control), 50, 100, 250 and 500 μg/mL (increasing from light grey to black) for 24 h. Cell viability was quantified by means of DMSO solubilization of the MTT-metabolization crystals.

4. Conclusions

Three different phyllosilicates from the smectite clay-group (montmorillonite, saponite and hectorite) have been successfully loaded with different cargos (rhodamine B, hematin and cyanocobalamin) and functionalized with oleic acid as molecular gate. The new hybrid organoclays are capable of entrapping these molecules and efficiently delivering them in an aqueous environment only when surfactant agents (e.g. bile salts) are present. The cargo release profile of all the synthesized organoclays has been studied by fitting the data with three different release kinetic models: Hill, Higuchi and Korsmeyer - Peppas (K-P) models. The most instructive result was obtained with the K-P model, which highlighted the dependence of release kinetics not only on the organic-inorganic hybrid system but also on the nature of loaded molecules and their interaction with the support. With the aim of testing all the synthesized organoclays as cargo release microdevices, *in*

vitro cell viability assays have been performed with Caco-2 adenocarcinoma cells. The obtained results from this assay show that particle concentrations of ca. 50 μg/mL maintain cell viability at good levels (higher than 70%), demonstrating that the studied organoclays are well tolerated by cells at these concentrations. This work demonstrates the effectiveness of oleic acid as molecular gate for three different clay materials, allowing active and controlled release of the entrapped cargo. Moreover, the zero-release achieved by this molecular gate opens its use to deliver drugs that must be only released in the intestinal endothelium, where bile salts are present, as target tissue and further works will be developed in due course.

Acknowledgments

The authors thank the financial support from the Spanish Government (projects RTI2018-100910-B-C41, RTI2018-101599-B-C22-AR and RTI2018-101599-B-C21-AR (MCUI/FEDER, EU)) and the Generalitat Valenciana (project PROMETEO 2018/024). E.P-R. is grateful to the Generalitat Valenciana for her ACIF/2016/023 PhD. grant. The authors thank the Electron Microscopy Service at the UPV for support. The authors also thank Prof. Pedro Amorós for his explanations and guidance on the knowledge of phyllosilicates.

Bibliography

1 E. Rosado Balmayor, H. Sepulveda Azevedo and R. L. Reis, Controlled delivery systems: From pharmaceuticals to cells and genes, *Pharm. Res.*, 2011, **28**, 1241–1258.

2 M. Moritz and M. Geszke-Moritz, Mesoporous materials as multifunctional tools in biosciences: Principles and applications, *Mater. Sci. Eng. C*, 2015, **49**, 114–151.

3 E. Aznar, R. Villalonga, C. Giménez, F. Sancenón, M. D. Marcos, R. Martínez-Máñez, P. Díez, J. M. Pingarrón and P. Amorós, Glucose-triggered release using enzyme-gated mesoporous silica nanoparticles, *Chem. Commun.*, 2013, **49**, 6391–6393.

4 E. Poyatos-Racionero, É. Pérez-Esteve, M. Dolores Marcos, J. M. Barat, R. Martínez-Máñez, E. Aznar and A. Bernardos, New Oleic Acid-Capped Mesoporous Silica Particles as Surfactant-Responsive Delivery Systems, *ChemistryOpen*, 2019, **8**, 1052–

1056.

5 H. A. Santos, J. Salonen, L. M. Bimbo, V. P. Lehto, L. Peltonen and J. Hirvonen, Mesoporous materials as controlled drug delivery formulations, *J. Drug Deliv. Sci. Technol.*, 2011, **21**, 139–155.

6 M. Manzano and M. Vallet-Regí, New developments in ordered mesoporous materials for drug delivery, *J. Mater. Chem.*, 2010, **20**, 5593–5604.

7 N. W. Clifford, K. S. Iyer and C. L. Raston, Encapsulation and controlled release of nutraceuticals using mesoporous silica capsules, *J. Mater. Chem.*, 2008, **18**, 162–165.

8 A. Bernardos and L. Kourimská, *Czech J. Food Sci.*, 2013, 31, 99–107.

9 À. Ribes, E. Aznar, S. Santiago-Felipe, E. Xifre-Perez, M. ángeles Tormo-Mas, J. Pemán, L. F. Marsal and R. Martínez-Mántild;ez, Selective and Sensitive Probe Based in Oligonucleotide-Capped Nanoporous Alumina for the Rapid Screening of Infection Produced by Candida albicans, *ACS Sensors*, 2019, **4**, 1291–1298.

10 L. E. Santos-Figueroa, C. Giménez, A. Agostini, E. Aznar, M. D. Marcos, F. Sancenón, R. Martínez-Máñez and P. Amorós, Selective and sensitive chromofluorogenic detection of the sulfite anion in water using hydrophobic hybrid organic-inorganic silica nanoparticles, *Angew. Chemie - Int. Ed.*, 2013, **52**, 13712–13716.

11 B. de Luis, A. Llopis-Lorente, P. Rincón, J. Gadea, F. Sancenón, E. Aznar, R. Villalonga, J. R. Murguía and R. Martínez-Máñez, An Interactive Model of Communication between Abiotic Nanodevices and Microorganisms, *Angew. Chemie - Int. Ed.*, 2019, **58**, 14986–14990.

12 A. Llopis-Lorente, P. Díez, A. Sánchez, M. D. Marcos, F. Sancenón, P. Martínez-Ruiz, R. Villalonga and R. Martínez-Máñez, Interactive models of communication at the nanoscale using nanoparticles that talk to one another, *Nat. Commun.*, 2017, **8**, 1–7.

13 C. Giménez, E. Climent, E. Aznar, R. Martánez-Máñez, F. Sancenón, M. D. Marcos, P. Amorós and K. Rurack, Towards chemical communication between gated nanoparticles, *Angew. Chemie - Int. Ed.*, 2014, **53**, 12629–12633.

14 E. Poyatos-Racionero, J. V. Ros-Lis, J.-L. L. Vivancos and R. Martínez-Máñez, Recent advances on intelligent packaging as tools to reduce food waste, *J. Clean. Prod.*, 2018, **172**, 3398–3409.

15 N. Mas, D. Arcos, L. Polo, E. Aznar, S. Sánchez-Salcedo, F. Sancenón, A. García, M. D. Marcos, A. Baeza, M. Vallet-Regí and R. Martínez-Máñez, Towards the development of smart 3D 'gated scaffolds' for on-command delivery, *Small*, 2014, **10**, 4859–4864.

16 E. Perez-Esteve, A. Bernardos, R. Martinez-Manez and J. M. Barat, Nanotechnology in the Development of Novel Functional Foods or their Package. An Overview Based in Patent Analysis, *Recent Pat. Food. Nutr. Agric.*, 2013, **5**, 35–43.

17 C. Coll, R. Casasús, E. Aznar, M. D. Marcos, R. Martínez-Máñez, F. Sancenón, J. Soto

and P. Amorós, Nanoscopic hybrid systems with a polarity-controlled gate-like scaffolding for the colorimetric signalling of long-chain carboxylates, *Chem. Commun.*, 2007, 1957–1959.

18 H. A. Patel, R. S. Somani, H. C. Bajaj and R. V Jasra, Nanoclays for polymer nanocomposites, paints, inks, greases and cosmetics formulations, drug delivery vehicle and waste water treatment, *Bull. Mater. Sci.*, 2006, **29**, 133–145.

19 S. J. Choi and Y. R. Kim, Bioinspired layered nanoclays for nutraceutical delivery system, *ACS Symp. Ser.*, 2013, **1143**, 207–220.

20 S. Gammoudi, N. Frini-Srasra and E. Srasra, Influence of exchangeable cation of smectite on HDTMA adsorption: Equilibrium, kinetic and thermodynamic studies, *Appl. Clay Sci.*, 2012, **69**, 99–107.

21 M. I. Carretero, C. S. F. Gomes and F. Tateo, in *Developments in Clay Science*, eds. F. Bergaya, B. K. . Theng and G. Lagaly, Elsevier, 2006, vol. 1, pp. 717–741.

22 J. F. Lambert and F. Bergaya, in *Developments in Clay Science*, eds. F. Bergaya and G. Lagaly, Elsevier Ltd., 2nd edn., 2013, vol. 5, pp. 679–706.

23 S. Kumaresan, R. Rama Pawar, B. D. Kevadiya and H. C. Bajaj, Synthesis of Saponite Based Nanocomposites to Improve the Controlled Oral Drug Release of Model Drug Quinine Hydrochloride Dihydrate, *Pharmaceuticals*, 2019, **12**, 105.

24 A. Rivera, L. Valdés, J. Jiménez, I. Pérez, A. Lam, E. Altshuler, L. C. De Ménorval, J. O. Fossum, E. L. Hansen and Z. Rozynek, Smectite as ciprofloxacin delivery system: Intercalation and temperature-controlled release properties, *Appl. Clay Sci.*, 2016, **124**–**125**, 150–156.

25 K. A. Block, A. Trusiak, A. Katz, A. Alimova, H. Wei, P. Gottlieb and J. C. Steiner, Exfoliation and intercalation of montmorillonite by small peptides, *Appl. Clay Sci.*, 2015, **107**, 173–181.

26 G. V. Joshi, R. R. Pawar, B. D. Kevadiya and H. C. Bajaj, Mesoporous synthetic hectorites: A versatile layered host with drug delivery application, *Microporous Mesoporous Mater.*, 2011, **142**, 542–548.

27 J. K. Park, Y. Bin Choy, J. M. Oh, J. Y. Kim, S. J. Hwang and J. H. Choy, Controlled release of donepezil intercalated in smectite clays, *Int. J. Pharm.*, 2008, **359**, 198–204.

28 M. C. Hermosin, M. J. Calderón, J. P. Aguer and J. Cornejo, Organoclays for controlled release of the herbicide fenuron, *Pest Manag. Sci.*, 2001, **57**, 803–809.

29 A. Bernardos, M. Bozik, S. Alvarez, M. Saskova, E. Perez-Esteve, P. Kloucek, M. Lhotka, A. Frankova and R. Martinez-Manez, The efficacy of essential oil components loaded into montmorillonite against Aspergillus niger and Staphylococcus aureus, *Flavour Fragr. J.*, 2019, **34**, 151–162.

30 W. H. Yu, N. Li, D. S. Tong, C. H. Zhou, C. X. Lin and C. Y. Xu, Adsorption of proteins

and nucleic acids on clay minerals and their interactions: A review, *Appl. Clay Sci.*, 2013, **80–81**, 443–452.

31 M. Arruebo, Drug delivery from structured porous inorganic materials, *Wiley Interdiscip. Rev. Nanomedicine Nanobiotechnology*, 2012, **4**, 16–30.

32 E. Poyatos-Racionero, I. González-Álvarez, M. González-Álvarez, R. Martínez-Máñez, M. D. Marcos, A. Bernardos and E. Aznar, Surfactant - Triggered Molecular Gate Tested on Different Mesoporous Silica Supports for Gastrointestinal Controlled Delivery, *Nanomaterials*, 2020, **10**, art. 1290 (1-18).

33 V. Anand, R. Kandarapu and S. Garg, *Drug Discov. Today*, 2001, 6, 905–914.

34 M. Akbari Alavijeh, M. N. Sarvi and Z. Ramazani Afarani, Properties of adsorption of vitamin B12 on nanoclay as a versatile carrier, *Food Chem.*, 2017, **219**, 207–214.

35 Z. Ramazani Afarani, M. N. Sarvi and M. Akbari Alavijeh, Modification of montmorillonite nanolayers as a pH-responsive carrier of biomolecules: Delivery of vitamin B12, *J. Taiwan Inst. Chem. Eng.*, 2018, **84**, 19–27.

36 M. E. Conrad, in *Clinical Methods: The History, Physical, and Laboratory Examinations*, eds. H. Walker, W. Hall and J. Hurst, Butterworths, Boston, 3rd editio., 1990, pp. 703–708.

37 R. C. Hider and X. Kong, in *Metal ions in life sciences*, eds. A. Sigel, H. Sigel and R. Sigel, Springer, Dordrecht, 2013, vol. 13, pp. 229–294.

38 R. Green, L. H. Allen, A.-L. Bjørke-Monsen, A. Brito, J.-L. Guéant, J. W. Miller, A. M. Molloy, E. Nexo, S. Stabler, B.-H. Toh, P. M. Ueland and C. Yajnik, Vitamin B12 deficiency, *Nat. Rev. Dis. Prim.*, 2017, **3**, 17040. 1–19.

39 B. H. R. Wolffenbuttel, H. J. C. M. Wouters, M. R. Heiner-Fokkema and M. M. van der Klauw, The Many Faces of Cobalamin (Vitamin B12) Deficiency, *Mayo Clin. Proc. Innov. Qual. Outcomes*, 2019, **3**, 200–214.

40 M. J. Shipton and J. Thachil, Vitamin B12 deficiency - A 21st century perspective, *Clin. Med. (Northfield. Il).*, 2015, **15**, 145–50.

41 R. C. Oh and D. L. Brown, Vitamin B 12 Deficiency Clinical Manifestations of Vitamin B 12 Deficiency, *Am. Fam. Physician*, 2003, **67**, 979–986.

42 R. Kozyraki and O. Cases, *Biochimie*, 2013, 95, 1002–1007.

43 E. Andrès, N. H. Loukili, E. Noel, G. Kaltenbach, M. Ben Abdelgheni, A. E. Perrin, M. Noblet-Dick, F. Maloisel, J. L. Schlienger and J. F. Blicklé, Vitamin B12 (cobalamin) deficiency in elderly patients, *Cmaj*, 2004, **171**, 251–259.

44 S. N. Fedosov, in *Water Soluble Vitamins. Subcellular Biochemistry, vol 56*, ed. O. Stanger, Springer, Dordrecht, 2012, pp. 347–367.

45 E. Andrès, G. Kaltenbach, E. Noel, M. Noblet-Dick, A. E. Perrin, T. Vogel, J. L.

Schlienger, M. Berthel and J. F. Blicklé, Efficacy of short-term oral cobalamin therapy for the treatment of cobalamin deficiencies related to food-cobalamin malabsorption: A study of 30 patients, *Clin. Lab. Haematol.*, 2003, **25**, 161–166.

46 G. Komaromy-Hiller, K. L. Nuttall and E. R. Ashwood, Effect of storage on serum vitamin B12 and folate stability, *Ann. Clin. Lab. Sci.*, 1997, **27**, 249–253.

47 M. Chalella Mazzocato, M. Thomazini and C. S. Favaro-Trindade, Improving stability of vitamin B12 (Cyanocobalamin) using microencapsulation by spray chilling technique, *Food Res. Int.*, 2019, **126**, 1–11.

48 I. I. Slowing, J. L. Vivero-Escoto, B. G. Trewyn and V. S.-Y. Lin, Mesoporous silica nanoparticles: structural design and applications, *J. Mater. Chem.*, 2010, **20**, 7924–7937.

49 M. Thommes, K. Kaneko, A. V. Neimark, J. P. Olivier, F. Rodriguez-Reinoso, J. Rouquerol and K. S. W. Sing, *Physisorption of gases, with special reference to the evaluation of surface area and pore size distribution (IUPAC Technical Report)*, 2015, vol. 87.

50 S. Goutelle, M. Maurin, F. Rougier, X. Barbaut, L. Bourguignon, M. Ducher and P. Maire, The Hill equation: A review of its capabilities in pharmacological modelling, *Fundam. Clin. Pharmacol.*, 2008, **22**, 633–648.

51 M. L. Bruschi, Ed., in *Strategies to Modify the Drug Release from Pharmaceutical Systems*, Woodhead Publishing, Cambridge, UK, 2015, pp. 63–86.

52 D. Sgouras and R. Duncan, Methods for the evaluation of biocompatibility of soluble synthetic polymers which have potential for biomedical use: 1 - Use of the tetrazolium-based colorimetric assay (MTT) as a preliminary screen for evaluation of in vitro cytotoxicity, *J. Mater. Sci. Mater. Med.*, 1990, **1**, 61–68.

53 H. Jaganathan and B. Godin, Biocompatibility assessment of Si-based nano- and micro-particles, *Adv. Drug Deliv. Rev.*, 2012, **64**, 1800–1819.

54 M. Yazdimamaghani, Z. B. Barber, S. P. Hadipour Moghaddam and H. Ghandehari, Influence of Silica Nanoparticle Density and Flow Conditions on Sedimentation, Cell Uptake, and Cytotoxicity, *Mol. Pharm.*, 2018, **15**, 2372–2383.

SUPPORTING INFORMATION

Gated-organoclays for large biomolecules-controlled release triggered by surfactant stimulus

Elisa Poyatos-Racionero,[a,b] Édgar Pérez-Esteve,[c] Elena Aznar,[b,a,d,e] José M. Barat,[c] Ramón Martínez-Máñez,[a,b,d,e,f] M. Dolores Marcos[a,b,d,e,f]* and Andrea Bernardos[b,a,e]*

[g] Instituto Interuniversitario de Investigación de Reconocimiento Molecular y Desarrollo Tecnológico (IDM). Universitat Politècnica de València, Universitat de València. Camino de Vera s/n, 46022, Valencia (Spain)

[h] CIBER de Bioingeniería, Biomateriales y Nanomedicina (CIBER-BBN) (Spain)

[i] Departamento de Tecnología de Alimentos, Universitat Politècnica de València. Camino de Vera s/n, 46022, Valencia (Spain)

[j] Unidad Mixta de Investigación en Nanomedicina y Sensores. Universitat Politècnica de València, Instituto de Investigación Sanitaria La Fe, Valencia (Spain)

[k] Unidad Mixta UPV-CIPF de Investigación en Mecanismos de Enfermedades y Nanomedicina, Universitat Politècnica de València, Centro de Investigación Príncipe Felipe, Valencia (Spain)

[l] Departamento de Química, Universitat Politècnica de València. Camino de Vera s/n, 46022, Valencia (Spain).

* Correspondence: mmarcos@upv.es (M.D.M.); anberba@upv.es (A.B.)

Submitted to Materials Chemistry Frontiers

Bioactive organoclays synthesis

In order to derivatize hemin into hematin, the Cl^- ligand coordinated to the central Fe atom was replaced by an OH^- ligand in aqueous solution. With this aim, 6 mL of 0.5 N NaOH were added to 20 mL of H_2O, and then 650 mg of hemin were dissolved in the basified H_2O. To carry out the loading of S_{SWN} with Hem, 1 g of S_{SWN} was added to the aforementioned solution, and the mixture was stirred overnight. The final solid was collected by centrifugation and dried at 40 ºC (S_{SWN}-Hem). To perform the APTES-functionalization, 400 mg of S_{SWN}-Hem were suspended in 15 mL of hexane and 2 mL of APTES were added. The mixture was stirred at room temperature for 5.5 h, and the final solid (S_{SWN}-Hem-N) was obtained by centrifugation and dried under vacuum. To perform the OA-functionalization, 300 mg of S_{SWN}-Hem-N were added to a previous solution composed by 3 mL of OA in hexane (15 mL) and 40 mg of DCC. The mixture was stirred overnight, and the precipitate was collected by centrifugation and washed with EtOH:H_2O mixtures with increasing amounts of H_2O until colorless-supernatant was obtained. The final solid (S_{SWN}-Hem-OA) was centrifuged and dried in vacuum.

The procedure followed to obtain the second bioactive microdevice, loaded with *B12*, was similar to the one used for Hem. For the cargo loading, 1 g of S_{SWN} was added to a solution of *B12* in water (100 mg in 10 mL) to obtain S_{SWN}-B12 solid. The APTES-functionalization and posterior OA-functionalization procedures, as well as the reagents proportions, were the same as the employed with the Hem-loaded-solids (*vide supra*). Accordingly, S_{SWN}-B12-N solid (APTES functionalized) and S_{SWN}-B12-OA solid (OA functionalized) were obtained.

Bioactive organoclays cargo delivery

The procedure followed to obtain cargo delivery profiles of the bioactive molecules was similar to the one used for the model solids (see section 2.4). However, as it was done in previous works,[28] bile salts were replaced by another surfactant that had no background signal in the range where the bioactive molecules have their maximum absorption. For this reason, 5 mg of the

corresponding solid were placed in 10 mL of PBS as blank (simulating conditions in absence of bile salts) and a solution of surfactant agent in PBS ($5 \cdot 10^{-3}$ M CTAB in PBS) as stimulus. At certain times (0.02, 0.25, 0.5, 1, 2, 4, 6, 8, 24 h) aliquots of 700 µL were centrifuged and the bioactive molecule content determined by means of its absorbance in a UV-Vis spectrophotometer. For the measurement, the employed excitation wavelengths for *Hem* and *B12* were 385 and 361 nm, respectively.

Bioactive organoclays characterization

The synthesized bioactive organoclays were characterized with the usual techniques. X-ray diffraction (XRD), infrared spectroscopy (FTIR), zeta (ζ) potential measurements and thermogravimetric analysis (TGA) were performed.

Normalized X-ray patterns of bare, loaded and final gated-clay are shown in Figure S1. These materials present low resolution patterns dominated by the intense peaks related to the metallosilicate interlayer spacing. The "d spacing" values of the more significant peaks are listed in Table S1.

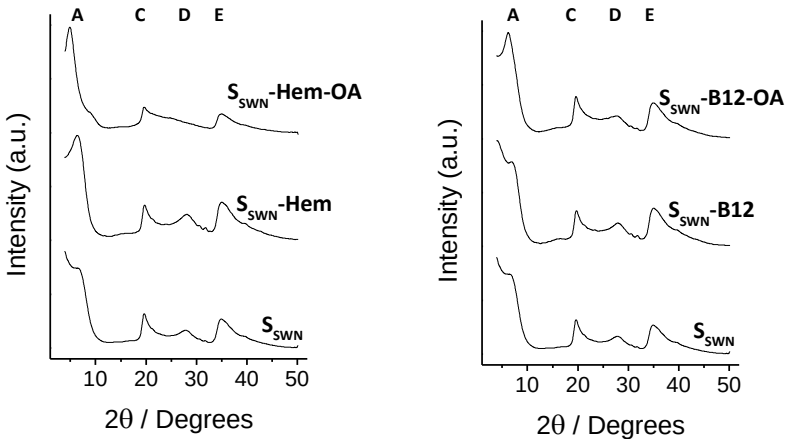

Figure S1. Normalized X-ray patterns of the bioactive organoclays (indicated in their respective diffractogram). From bottom to top: bare, loaded and final gated-organoclay, respectively. The main XRD reflections are labelled from left to right as A-E, consecutively. B-peak is omitted in order to correlate the peaks with the previously obtained for model-solids (Figure 1).

Table S1. Main reflexions' d-Spacing (Å) values for the bioactive organoclays obtained from Bragg's law (nλ = 2d · sin(θ), λ=CuK$_{\alpha\,av}$ = 1,54 Å, n=1).

	A	*B*	C	D	E
S_{SWN}	13.55		4.52	3.21	2.57
S_{SWN}-Hem	14.52		4.52	3.17	2.55
S_{SWN}-Hem-OA	18.03		4.53		2.54
S_{SWN}-B12	14.65		4.51	3.20	2.57
S_{SWN}-B12-OA	14.24		4.53	3.21	2.56

Loading and functionalization processes which lead to final gated-solids were followed by zeta (ζ) potential. The obtained values are reported in Figure S2, and they were measured in EtOH at 20 ℃. As it can be observed, the bare S_{SWN} clay exhibited a negative ζ potential value (around -20 mV). After the loading process, the charge of the materials remains negative. Once the APTES molecule was added, ζ potential values become less negative, confirming the efficiency of the functionalization process, being the charge-neutralization a direct consequence of the presence of the APTES-amine group on the surface. Finally, the anchoring of OA to the particles increased the positivity in the ζ potential values of the particles.

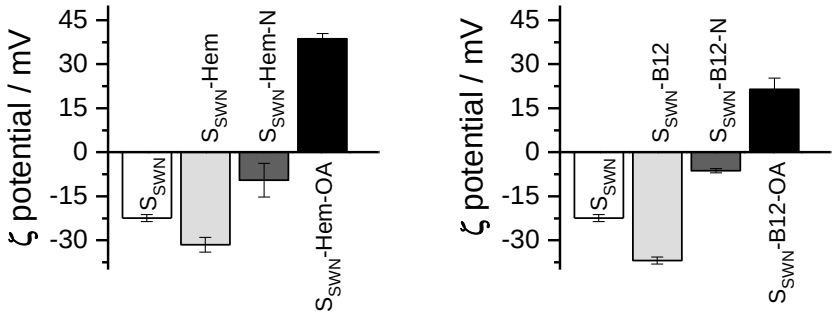

Figure S2. Zeta (ζ) potential values of all the bioactive organoclays. The increasing darkness in bar colors correspond to the progressive synthesis steps: from bare S_{SWN} to loaded, APTES-functionalized and final OA-functionalized organoclays (white, light gray, dark gray and black bars, respectively).

The bioactive organoclays in the different synthesis steps were also characterized by infrared spectroscopy (FTIR), and the obtained spectra are depicted in Figure S3. The dominant bands in all the FTIR spectra are those which belong to the silica tetrahedra and metal octahedra which conform the laminar structure of all the phyllosilicates (1050, 600 and 450 cm^{-1}). The broad band that appears around 3500 cm^{-1} is assigned to the vibration of the hydration water molecules. The hydroxyl group coordinated to octahedral cations, typically Mg^{2+}, show a small and sharp band at 3600 cm^{-1} and another sharp one at 1600 cm^{-1}. The clear appearance of two bands at approximately 2900 cm^{-1} and 2850 cm^{-1} in all the spectra of the gated clays is assignable to the bending C–H vibrations. These new bands are related with the presence of organic matter from the APTES or OA.[28]

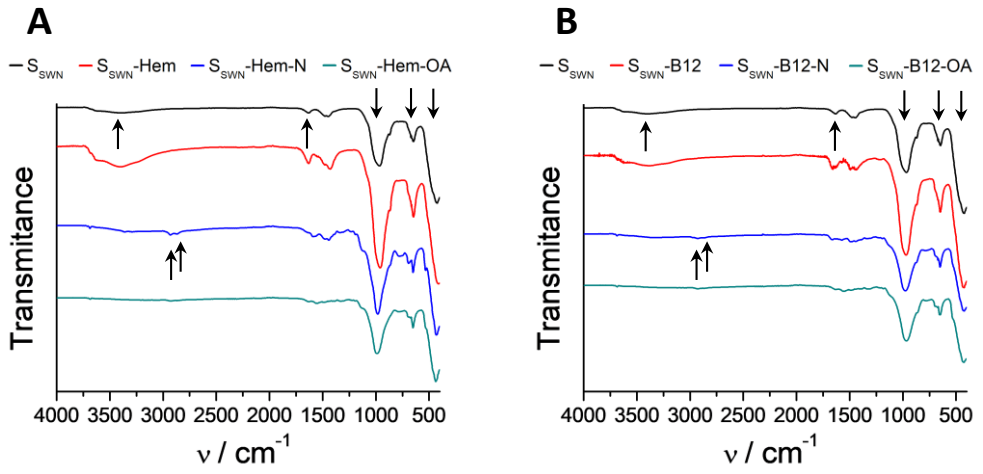

Figure S3. FTIR spectra of the consecutive synthesis steps of the bioactive organoclays: **A**, S_{SWN}-Hem-OA; **B**, S_{SWN}-B12-OA

Table S2. Parameters and coefficients of determination (r^2) obtained by adjusting the data with the K-P model (equation [3]) fixing the value of the *n* parameter ($n \geq 0.45$).

System	K-P			
	K min^{-n}	n	b	r^2
K_F-RhB-OA	7.75	0.40	0	0.99
S_{SA}-RhB-OA	11.1	0.37	0	0.98
S_{SWN}-RhB-OA	7.83	0.41	0	0.98
S_{SWN}-Hem-OA	0.01	1.21	0.71	0.96
S_{SWN}-B12-OA	3.49	0.42	44.2	0.74

4. CHAPTER 2

Protein-gated microdevices

Article 4

Towards the Enhancement of Essential Oil Components Antimicrobial Activity Using New Zein-Protein-Gated Mesoporous Silica Microdevices

Elisa Poyatos-Racionero,[a,b] Gemma Guarí-Borràs,[a] María Ruiz-Rico,[c] Elena Aznar[a,b,d,e] José M. Barat,[c] Ramón Martínez-Máñez,[a,b,d,e,f] M. Dolores Marcos[a,b,d,e,f]* and Andrea Bernardos[a,b,e]*

[a] Instituto Interuniversitario de Investigación de Reconocimiento Molecular y Desarrollo Tecnológico (IDM), Universitat Politècnica de València, Universitat de València. Camino de Vera s/n, 46022, Valencia (Spain).

[b] CIBER de Bioingeniería, Biomateriales y Nanomedicina (CIBER-BBN) (Spain)

[c] Departamento de Tecnología de Alimentos, Universitat Politècnica de València. Camino de Vera s/n, 46022, Valencia (Spain)

[d] Unidad Mixta de Investigación en Nanomedicina y Sensores Universitat Politècnica de València, IIS La Fe de Valencia. 46026, Valencia (Spain)

[e] Unidad Mixta UPV-CIPF Invest Mecanismos Enfermedad, Universitat Politècnica de València, Centro de Investigación Príncipe Felipe. 46100, Valencia (Spain).

[f] Departamento de Química, Universitat Politècnica de València. Camino de Vera s/n, 46022, Valencia (Spain).

* Correspondence: mmarcos@upv.es (M.D.M.); anberba@upv.es (A.B.)

Submitted to International Journal of Molecular Sciences

Abstract

The development of new food preservatives is essential to prevent foodborne outbreaks or food spoilage due to microbial growth, enzymatic activity or oxidation. Also new compounds that substitute the commonly used synthetic food preservatives are needed to strive the rising trouble of microbial resistance. In this scenario, we report herein as far as we know for the first time, the use of Zein protein as gating moiety and its application for the controlled release of Essential Oil Components (EOCs). The design of microdevices consist of mesoporous silica particles, loaded with essential oils components (thymol, carvacrol and cinnamaldehyde) and functionalized with the zein prolamin protein found in maize or corn as molecular gate. Zein protein grafted on the synthesized microdevices is degraded by the proteolytic action of bacterial enzymatic secretions with the consequent release of the loaded essential oil components efficiently inhibiting bacterial growth. The results allow us to conclude that the new microdevice presented here, loaded with the essential oil component cinnamaldehyde improved the antimicrobial properties of the free compound by decreasing volatility and increasing local concentration.

Keywords: mesoporous silica particles • zein • corn • molecular gate • protease secretion • *E. coli* • foodborne illnesses • food preservative • essential oil components • cinnamaldehyde

1. Introduction

Foodborne outbreaks caused by ingestion of food contaminated with pathogenic microorganisms are one of the main threats to public health, and one of the biggest impediments to socioeconomic development all over the world. Food poisoning caused by pathogens or their produced toxins have been stablished as the main source of foodborne illnesses in both developing and developed nations. Although some viruses, prions or protozoa can be the cause of these illnesses, most of them are caused by fungi and bacteria. Some examples of foodborne germs are specific strains of *Salmonella enterica, Listeria monocytogenes, Clostridium botulinum, or Escherichia coli*, among others [1].

Pesticides, food preservatives and antibiotics have been generally used with the aim of fighting the pathogenic microorganisms that cause foodborne outbreaks. Occasionally, this use has been made indiscriminately, generating an even greater problem; i.e. antimicrobial resistance [2,3]. In this context, the development of new alternatives is necessary to solve this increasing problem of public health. With this aim, numerous researches have been developed in the potential use of natural compounds, due to the problems derived from common preservatives and their rejection by consumers [4–6].

As a suitable option, general attention has been turned on the study of the versatile properties of essential oil components (EOCs) as a possible alternative to synthetic antimicrobial agents [7,8]. EOCs are a wide group of bioactive chemical components found naturally in essential oils [9]. These essential oils are complex mixtures of 20-60 molecules produced during secondary metabolism of aromatic and medicinal plants, with important antioxidant, bactericidal, fungicidal or antiparasitic effects [10]. Due to their numerous properties, EOCs have been used since the beginning of humankind, and are still being used nowadays as an alternative to other synthetic chemical compounds in the pharmaceutical and food industry [11,12].

The antimicrobial action of EOCs can be attributed to a set of cascade reactions that results in the destruction of the bacterial cell [13]. Several mechanisms have been described to explain the antimicrobial action of EOCs, being one of the most relevant the destabilization of lipids of the cell membrane and the mitochondria due to the hydrophobic character of EOCs [14]. However, other mechanisms can also occur that finally result in the microorganism death, such as damage of membrane proteins or inhibition of the electron transport chain, among others [13].

However, EOCs' high volatility, high reactivity and low solubility in water limit their application [15,16]. Several strategies have been investigated to improve the use of EOCs, most of them aiming to reduce their volatility and increase their solubility. Among these strategies, the use of encapsulation protocols has been explored [14,17,18]. Among materials for EOCs encapsulation, mesoporous silica particles (MSPs) present several advantages, such as high pore volume for loading molecules, easy chemical functionalization and low toxicity levels [19]. In fact, MSPs have been used for the protection and controlled release of (i) bioactive molecules for the improvement of organoleptic or nutritional properties of foods [20] or (ii) antimicrobial agents to design novel preservatives [18,21,22]. Moreover, given the easy chemical modification of the MSPs' surface, a wide variety of organic moieties have been used as molecular gates (also known as gatekeepers or nanovalves) to develop advanced delivery systems [23]. In these systems, the gated materials show an ideally "zero" payload release, yet the presence of predefined physical, chemical or biochemical stimuli induce pore opening and cargo delivery. This concept has been widely applied for drug delivery [24,25], sensing [26,27] and communication protocols [28–30]. Among gating moieties, proteins have been employed as blocking-pore agents in hybrid MSPs materials, allowing entrapped cargo release when proteolytic enzymes are present [31–38]. However, considering the inherent presence of bacterial protease secretion as a potential stimulus for cargo release, studies in the literature aiming to develop protein-capped antimicrobial carriers are still scarce [39,40]. Moreover, protease secretion is a key

factor in the virulence of pathogen growth [41], so the greater the pathogen virulence, the larger the protease secretion and therefore the higher the triggering stimulus. Based on aforementioned premises, the attainment of a protein able to act as capping-moiety is preeminent to develop alternative MSPs antimicrobial systems. In this scenario, a low-cost, industrially produced and widely studied protein is α-zein, the most abundant protein in corn [42–45]. α-zein (onwards, zein) is an approximately 22 kDa prolamin protein with a complex tertiary structure which strongly depends on the solvent, but based on nine repeating α-helices and with an elongated proposed shape [45]. Although zein is a widely described protein, and it has even been studied as a matrix for the preparation of antibacterial nanocomposite including essential oil-loaded MSPs [46], its use specifically as gatekeeper for MSPs has not been reported yet. However, its own characteristics make zein a viable option to block the pores in MSPs, and, therefore to prepare enzyme-responsive particles to protect and actively release different EOCs. Furthermore, as zein protein is a food grade compound, it can be applied for fortification in food systems. Thus, EOCs volatility can be reduced through their encapsulation into MSPs, and their active controlled-release triggered by proteolytic enzymes will enhanced their antimicrobial action, improving EOCs bioavailability, with the aim of increasing food safety while extending the shelf life of food.

Based on the above, we report herein for the first time, as far as the authors know, the application of the zein protein as gating moiety and its application for the controlled release of EOCs (thymol, carvacrol and cinnamaldehyde). Additionally, we evaluate here the antimicrobial activity of the prepared zein-gated MSPs against *E. coli* as common foodborne bacteria.

2. Materials and methods

2.1. Reagents, bacterial strain and culture media

Tetraethylortosilicate (TEOS), triethanolamine ($TEAH_3$), sodium hydroxide (NaOH), *N*-cetyltrimethylammonium bromide (CTAB), (3-aminopropyl)triethoxysilane (APTES), *N*-(3-dimethylaminopropyl)-N'-ethylcarbodiimide (EDC), rhodamine B (RhB), thymol (Thy), carvacrol (Car) and cinnamaldehyde (Cin) were provided by Sigma (Sigma-Aldrich Química S.L., Madrid, Spain). α-zein corn-protein (zein), ethanol (extra pure) and dimethyl sulfoxide (DMSO) were purchased from Scharlab (Barcelona, Spain). *Escherichia coli* K12 (CECT 433) was obtained from the Spanish Type Culture Collection (CECT, Burjassot, Spain). The bacterial strain was reconstituted accordingly to the CECT instructions. After that, the bacterial stock was maintained at 4 ℃ in plate count agar before its use. *E. coli* inoculum was prepared by placing one single colony of the *E. coli* strain into 10 mL of tryptic soy broth (TSB). The mixture was incubated at 37 ℃ for 24 h in order to obtain an inoculum with a density of approximately 10^8 cells/mL of broth. All culture media were supplied by Scharlab S.A. (Barcelona, Spain).

2.2. Inorganic support synthesis

The synthesis of mesoporous material was performed according to the protocol described by Bernardos et al [47]. The synthesis process was carried out following the "atrane route" [48] in which the structure-directing agent is composed of an intermediate species between CTAB and $TEAH_3$. The molar ratio between the reagents was: 7 $TEAH_3$: 2 TEOS: 0.52 CTAB: 0.5 NaOH: 180 H_2O.

For the microparticle synthesis, 0.49 g of NaOH were added to 25.79 g of $TEAH_3$ and the mixture was heated to 120 ℃ in order to evaporate ethanol generated in the condensation reaction. Then, the mixture was cooled to 70 ℃. 11 mL of TEOS were added dropwise and the reaction was heated again until 120 ℃ under stirring. Once the temperature was reached, 4.68 g of CTAB were added, and the mixture was cooled again to 70 ℃. Finally, 80 mL of distilled H_2O were added, and the

mother liquor was stirred vigorously for 1 h at room temperature. The final mixture was transferred to a Teflon flask and kept at 100 ℃ for 24 h. After this time, the suspension was filtered under vacuum and washed until neutral pH. The material was dried and finally calcined at 550 ℃ to completely remove the surfactant molecules that conformed the nanotubular template. Following this procedure, the final MCM-41 microparticles, bare and unloaded (solid M41) were obtained.

2.3. Synthesis of the gated microdevices

2.3.1. Synthesis of the M41-RhB gated system

RhB was encapsulated into M41 microparticles by the immersion method, following a similar loading procedure to the carried out in previous works [49]. With that purpose, 1 g of M41 was added to a solution of RhB (0.8 mmol in 40 mL of H_2O) and stirred during 24 h. The mixture was filtered and the resulting solid, M41-RhB, was dried under vacuum. Once M41 was loaded with RhB, the surface of the support was functionalized with zein protein. For the protein bonding, a previous surface-functionalization with APTES as linker between the protein and the MSPs-silanol groups was necessary. Functionalization was performed by adding 8 mL APTES to a suspension of 1.2 g of the loaded solid in 25 mL of H_2O. The reaction was stirred for 5.5 h at room temperature. The resulting APTES-functionalized particles (M41-RhB-N) were collected by centrifugation and dried under vacuum. Finally, the binding of corn protein zein on the surface of M41-RhB-N was performed through a covalent amide bond between carboxylate moieties in the protein and amino groups from APTES following similar protocols to those described in the literature with slight modifications [32]. In a typical procedure, a suspension of 1 g of zein in 30 mL of H_2O and 200 mg of EDC was prepared and stirred for 30 min. Then, 700 mg of M41-RhB-N were added and the mixture was stirred at room temperature overnight. The final solid was collected by centrifugation and washed 3 times with mixtures of ethanol:water with gradually increasing proportions of water. Finally, the protein-functionalized solid (M41-RhB-Z) was dried under vacuum.

2.3.2. Synthesis of the M41-EOC gated systems

Three different EOCs, thymol, carvacrol and cinnamaldehyde (Thy, Car and Cin, respectively) were loaded into the mesoporous material by steam adsorption by mixing 250 mg of M41 solids and 250 mg of each EOC in a perfectly closed vial. The mixtures were shaken at 40 ℃ for 24 h, until the added amount of EOC was completely adsorbed and the solids (i.e. M41-EOC: *M41-Thy*, *M41-Car* and *M41-Cin,* respectively) looked completely dry. Once M41 was loaded with the different cargo molecules, the surface of the support was functionalized with zein protein following a similar procedure as described above. In a typical procedure, 8 mL APTES were added to a suspension of 1.2 g of the loaded solid in 25 mL of H_2O. The reaction was stirred for 5.5 h at room temperature. The resulting APTES-functionalized particles (M41-EOC-N) were collected by centrifugation and dried under vacuum. A suspension of 1 g of zein in 30 mL of H_2O and 200 mg of EDC was prepared and stirred for 30 min. Then, 700 mg of M41-EOC-N were added to the mixture and stirred at room temperature overnight. The final solids were collected by centrifugation, and washed 3 times with mixtures of ethanol:water gradually increasing proportions of water. Finally, the protein-functionalized solids (M41-EOC-Z: *M41-Thy-Z*, *M41-Car-Z* and *M41-Cin-Z*) were dried under vacuum.

2.3.3. Synthesis of unloaded gated system

Additionally, a solid without loaded molecules but gated with the zein protein (M41-Z) was synthesized and used as negative control in the microbiological tests. For this purpose, 500 mg of M41 were functionalized with APTES (3 mL) as described above obtaining the M41-N solid. The final unloaded gated system, M41-Z, was obtained by binding the zein protein (150 mg) to the amino-terminal groups in M41-N (50 mg) following the same procedure previously described.

2.4. Characterization methods

Powder X-ray diffraction (PXRD), transmission electron microscopy (TEM), N_2 adsorption–desorption isotherms, ζ potential, thermogravimetric analysis (TGA) and fluorescence spectroscopy were used to characterize the synthesized solids.

PXRD was performed on a Bruker D8 Advance diffractometer (Bruker, Coventry, UK) using Cu Kα radiation. TEM images were obtained with a JEOL JEM-1010 (JEOL Europe SAS, Croissysur-Seine, France). N_2 adsorption–desorption isotherms were recorded with a Micromeritics TriStar II Plus automated analyzer (Micromeritics Instrument Corporation, Norcross, USA). Inorganic samples were degassed at 120 ℃ in vacuum overnight. Samples with organic content were degassed at 70 ℃ overnight. The specific surface areas were calculated from the adsorption data in the low-pressure range using the BET model. Pore size was determined following the BJH method. To determine ζ potential of all the solids, a Zetasizer Nano ZS equipment (Malvern Instruments, Malvern, UK) was used. Samples were dispersed in distilled water at a concentration of 1 mg/mL. Before measuring, each sample was sonicated for 5 minutes to preclude aggregation. ζ values were calculated from the particle mobility values by applying the Smoluchowski model. Each sample was measured in triplicate at 25 ℃, performing three recordings per measurement. The average of the 9 obtained values was reported as ζ potential, and error bars represent the standard deviation-value. Fluorescence spectroscopy measurements were performed with a JASCO FP-8300 Spectrofluorometer (JASCO, Easton, United States).

2.5. Cargo release assay

For the cargo release experiment, 5 mg of final solids (M41-RhB-Z) were placed in 10 mL of H_2O at pH 8, and other 5 mg of M41-RhB-Z were placed in 10 mL of a pronase enzyme solution (0.12 mg/mL of pronase in H_2O at pH 8). At certain times, aliquots were taken and filtered. The RhB-delivery from the pore voids to both solutions was quantified via the fluorescence emission band of this molecule at 572 nm (excitation at 555 nm). The release assay was performed in triplicate.

2.6. EOCs payload quantification

In order to determine the maximum payload released from the M41-EOC-Z microdevices, a DMSO extraction process was performed. For this purpose, 2 mg of the corresponding solid were suspended in 2 mL of DMSO and the mixture was kept

under stirring for 24 h. After this time, the EOC payload released was quantified by measuring the absorbance of the sample at 280 nm.

2.7. Microbiological analysis

2.7.1. Antimicrobial susceptibility assays

The minimum bactericidal concentration (MBC) of the antimicrobial compounds was obtained by the macrodilution method [50]. The MBC was defined as the lowest concentration of the antimicrobial compound that could kill 99.9% of *E. coli* cells. The antimicrobial assay was performed in liquid medium to allow the contact between bacteria and the free or encapsulated antimicrobials during incubation, followed by plating to enumerate the remaining viable colony forming units (CFUs). Different compound concentrations were prepared in Erlenmeyer flasks with 15 mL of TSB for each free EOC in accordance with previous studies, considering the obtained MBC values in these works [51,52]. The tested concentrations were 50, 100, 150, 200 and 250 μg/mL for Thy and Car, and 125, 250, 500, 750 and 1000 μg/mL for Cin. Then Erlenmeyer flasks, including controls containing only TSB medium, were inoculated with 10 μL of *E. coli* suspension to obtain a final concentration of 10^6 cells/mL. Finally, all the flasks were incubated with orbital stirring (150 rpm) at 37 ℃ for 24 h. In order to enumerate the viable cells after the antimicrobial treatment, decimal serial dilutions were prepared in sterile distilled water and 100 μL-aliquots of them were spread on Tryptone Bile X-glucuronide (TBX) plates. After plate incubation at 37 ℃ for 24 h, colonies were counted, and the obtained results were expressed as log CFU/mL. To perform the M41-EOC-Z antimicrobial assays, the synthesized particles were added directly to the TSB contained in the Erlenmeyer flasks to obtain suspensions of each M41-EOC-Z microdevice at concentrations of 0, 1, 2, 4, 8 and 12 mg/mL, and the subsequent procedure was the same as that followed for free antimicrobials (*vide supra*). Positive controls, where the *E. coli* inoculum was allowed to grow without alterations, and negative controls, where the non-treating system M41-Z was added at maximum particle concentration (12 mg/mL), were also performed. All

the treatments (which include controls, free EOCs and M41-EOC-Z microdevices) were tested in triplicate.

2.7.2. Determination of bacterial viability and agglomeration by fluorescence assay

To develop this experiment, suspensions of bacteria-inoculated-TSB with a final concentration of 10^6 cells/mL were prepared and incubated under different conditions for 5 h. The studied conditions included bacteria treated with free Cin (400 µg/mL) or M41-Cin-Z (4 mg/mL), and also positive and negative controls (non-treated bacteria or treated with M41-Z at 4 mg/mL, respectively). Treatment concentrations were chosen based on the microbial count results (see section 2.7.1) with the aim of testing concentrations where both live and dead cells could be visualized in the same sample. The cells in each suspension where stained with a two-color fluorescent kit, LIVE/DEAD® BacLight™ (Invitrogen, (ThermoFisher Scientific, UK), used for visualizing the viable and remaining-dead bacteria according to membrane cell integrity. The two-color kit is composed by SYTO 9 (green-fluorescent nucleic acid stain) that labels all the microbial cells with either intact or damaged membranes, and propidium iodide (red-fluorescent nucleic acid stain) that passes only across damaged membranes, so it labels only the dead cells that remain present in the media. Propidium iodide reduces SYTO 9 fluorescence when both dyes coexist in the same cell, resulting in red labelling. This results in a green/red labeling of the living/dead cells, respectively. For that, 0.8 µL of the aforementioned kit (SYTO 9 and propidium iodide mixed at a ratio 1:1) were added to 500 µL of each studied suspension. The mixture was incubated in the dark for 10 min to allow the penetration of dyes. Then 5 µL of stained cells were placed over poly-L-lysine-covered slides (Sigma-Aldrich, Madrid, Spain) and sealed with a coverslip. The samples were finally observed under a Motic BA310E trinocular microscope equipped with an Epi-Led module with a 3W Led 470 nm illuminator bulb, MB barrier filter (AT480/30x, AT505DC and AT515LP fluorescence filters) and a Moticam 3+ camera. The obtained fluorescence images were acquired in dark field with a 100x objective, and have a pixel size of 0.156 µm (64 px = 10 µm).

3. Results and discussion

3.1. Design, synthesis and characterization of the gated systems

The design of smart delivery systems is based on three components: (i) a porous support, (ii) bioactive compounds with antimicrobial properties and (iii) a biomolecule as molecular gate or gatekeeper. MCM-41 mesoporous silica material was selected as inorganic support due to its loading capacity and easy-to-functionalize surface [19]. Essential oil components (EOCs) were chosen as cargo because they are naturally-occurring antimicrobial compounds considered as safe in the food industry [53]. In addition, the corn protein zein [45] was selected as gatekeeper. Following this approach three materials were prepared (M41-EOC-Z solids) all of them using mesoporous silica microparticles loaded with three different EOCs (i.e. Thy, Car and Cin) and capped with the zein protein (Scheme 1). The preparation of the materials was carried out in three consecutive stages. The first step consists of cargo loading of the mesoporous material by EOC steam adsorption. Next, a functionalization of the silica surface with the linker APTES was carried out, which was used to finally link the zein protein to the particle's surface via the formation of amide bonds (Scheme 1). An additional zein-capped material loaded with the dye Rhodamine B (M41-RhB-Z) was also prepared.

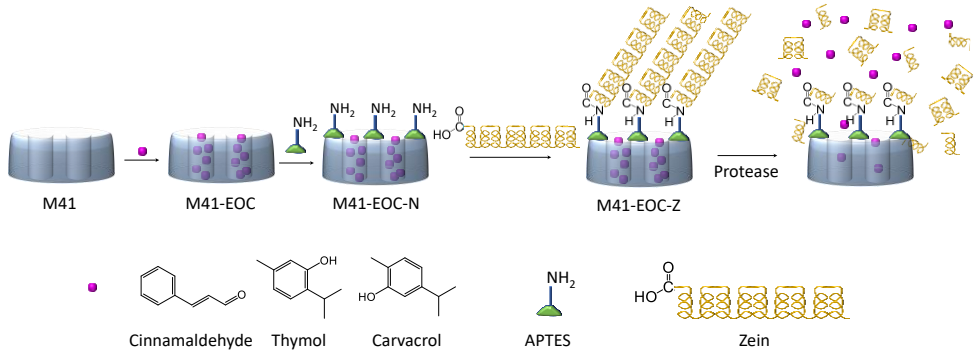

Scheme 1. Representation of M41-EOC-Z synthesis and cargo release. Cargo loading (EOCs) is followed by APTES-functionalization, and finally zein is attached to the amino groups. The cargo is actively released due to the hydrolyzing action of protease enzymes.

The synthesized solids were characterized using standard techniques. Normalized X-ray patterns of all the solids (MCM-41 "as made", calcined M41, M41-RhB-Z, M41-Thy-Z, M41-Car-Z and M41-Cin-Z) are shown in Figure 1a. The diffractogram of the MCM-41 "as made" shows four low-angle peaks characteristic of a hexagonal pore-arrangement. The peaks were indexed from left to right as (1 0 0), (1 1 0), (2 0 0) and (2 1 0) Bragg reflections, respectively. After calcination, a notable shift towards higher 2θ values compared with the as made material can be observed. This phenomenon is related with cell contraction due to the condensation of silanol groups in the calcination process. It also can be appreciated that in the curves corresponding to all the gated solids the reflections (1 1 0), (2 0 0) and (2 1 0) have almost disappeared. This fact is due to the large amount of organic matter contained in the final solids, which causes partial loss of the structural order. However, the clear presence of the (1 0 0) peak in all the diffractograms demonstrates that neither the calcination nor the loading and functionalization processes modify the mesoporous structure.

The expected porous structure of the starting solid M41 was also confirmed through TEM micrographs (Figure 1b). In these images, the typical matrix of the MCM-41 material, composed of narrow channels with hexagonal arrangement, can be appreciated. This structure is visualized as alternating white and black stripes, and the pore stacking is visible when the pores are seen frontally in the image. Comparing the images of the final solids (Figure 1b *ii*-*v*) with the M41 one (Figure 1b *i*), it is possible to see the structure-preservation after the loading and functionalization processes, even despite the loss of contrast in the images due to the presence of organic matter.

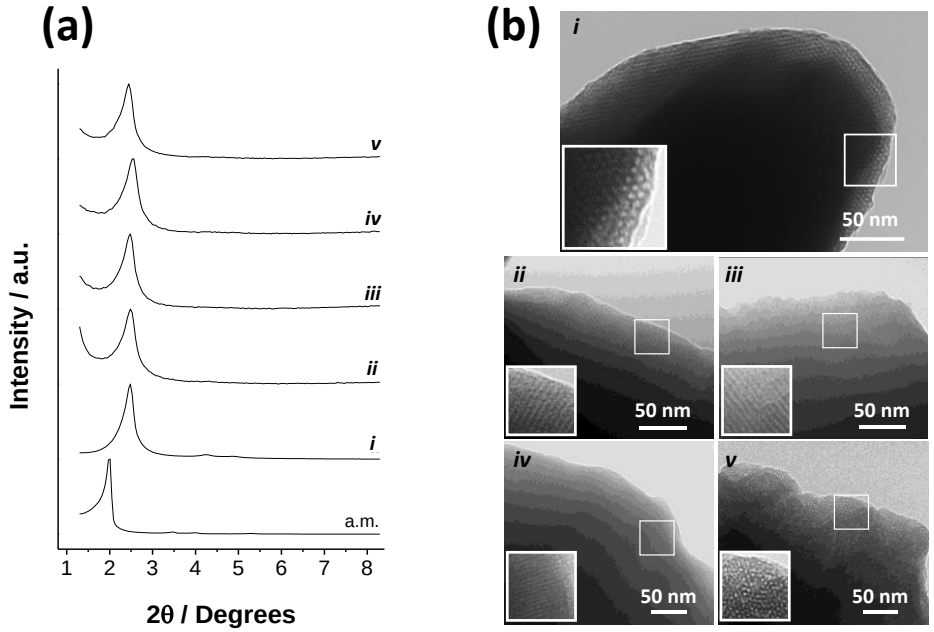

Figure 1. (**a**) Normalized X-ray patterns of all the synthesized solids. From bottom to top, the reported solids are: as made material (a.m.), calcined support M41 (*i*) and final materials: M41-RhB-Z (*ii*), M41-Thy-Z (*iii*), M41-Car-Z (*iv*), M41-Cin-Z (*v*). (**b**) TEM images of solids M41 (*i*), M41-RhB-Z (*ii*), M41-Thy-Z (*iii*), M41-Car-Z (*iv*), M41-Cin-Z (*v*). Insets correspond to a 2x magnification of the framed areas.

The N_2 adsorption-desorption isotherms of the calcined support (M41) are shown in Figure 2a. A typical curve for this mesoporous solid consisting of an adsorption step in the interval of P/P_0 values between 0.1–0.3 can be observed. The curve fits with a type IV isotherm, in which the increase produced in the gas absorption corresponds to a condensation of the N_2 molecules within the mesopores of the inorganic structure [54]. The absence of hysteresis loop in this interval and the narrow BJH distribution of pore diameter (Figure 2b) suggest the existence of uniformly cylindric mesopores, in which gas adsorption and desorption processes are carried out by the same mechanisms. The N_2 adsorption-desorption isotherm of M41-RhB-Z solid is typical of mesoporous systems with practically filled mesopores (see Figure 2a). The high amount of organic matter in the solid avoids

the adsorption of gas molecules, so the registered curve is completely flat when compared with the one of the empty starting material. Consequently, an absence of appreciable mesoporosity is observed (see Figure 2c), and relatively low quantity of adsorbed N_2 and low surface area (see Table 1) were obtained. Solids containing EOCs loaded into the pores could not be analyzed by this technique due to the previous degassing process under high vacuum and high temperature applied to the samples that would extract the encapsulated molecules.

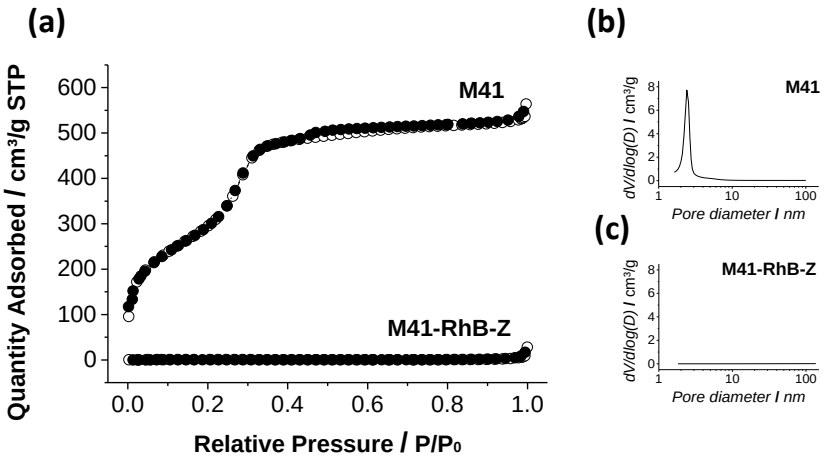

Figure 2. (**a**) Nitrogen adsorption (○) – desorption (●) isotherms of the calcined solid M41 and M41-RhB-Z final solid; (**b**) pore distribution graph of M41 and (**c**) pore distribution graph of M41-RhB-Z.

Table 1. BET specific surface values, pore volumes and pore sizes calculated from the N_2 adsorption–desorption isotherms for selected materials.

	S_{BET} ($m^2\ g^{-1}$)	Pore Volume [a] ($cm^3\ g^{-1}$)	Pore size [a, b] (nm)
M41	1108.27	0.91	2.50
M41-RhB-Z	1.71	0.01	-

[a]Pore volumes and pore sizes are restricted to intraparticle mesopores. [b]Pore size was estimated by using the BJH model applied on the adsorption branch of the isotherm.

The different stages of the synthesis process were followed by ζ potential. The obtained values are shown in Figure 3. As it can be observed, a starting negative ζ value was obtained for the bare material (M41), which is related with the deprotonated silanol groups on the particle's surface. The negative charge of M41 particles was maintained after loading process with Thy and Car. A remarkable fact was the slightly positive value of the solid M41-Cin, possibly due to the formation of hemiacetal groups between the aldehyde of Cin and the silanolate groups on the MSPs surface, which compensates the negative charge on the M41 surface. This process did not occur with the other two EOCs (Thy and Car) since their active groups are alcohols, which do not react with silanolates. The hemiacetal formation is a pH-dependent reversible phenomenon [55], so the interaction of Cin with the silanolates can be reverted when APTES is added. The APTES-functionalization occurred effectively as it can be seen in the value of ζ potential reached by M41-Cin-N, which is comparable to the other M41-EOC-N values. Finally, only small changes in the ζ potential values were observed when zein protein was attached to the external surface of the particles.

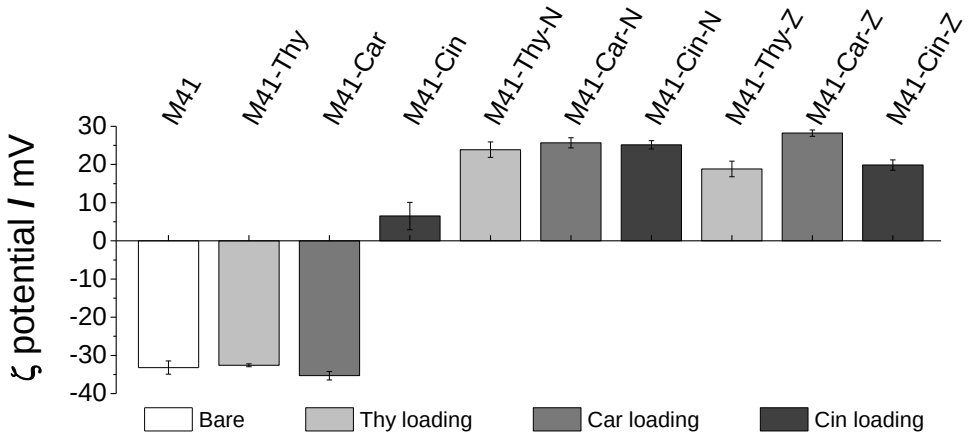

Figure 3. ζ potential values of the solids in the different synthesis steps.

In order to determine the maximum EOC-payload released from M41-EOC-Z, a DMSO cargo-extraction was performed. This procedure allowed the determination of the payload within the different supports (μg EOC mg^{-1} M41-EOC-Z) and the obtained values are shown in Table 2. As can be seen, the encapsulation efficiency of the M41-Cin-Z solid was greater than that obtained with the other employed EOCs, i.e. Thy and Car.

Table 2. Extracted content of cargo in each solid (μg EOC mg^{-1} M41-EOC-Z).

	M41-Thy-Z	M41-Car-Z	M41-Cin-Z
μg EOC mg^{-1} M41-EOC-Z	11.5	6.2	18.1

The differences in cargo loading efficiency may be due to the different structure of the studied molecules. The three-dimensional structure of the loaded EOCs is evidenced by the MM2 energy minimized ChemDraw 3D model shown in Figure 4. As it can be seen in this figure, Thy and Car molecules are isomers with notably higher steric hindrance than the Cin molecule, which is flat. This flat structure in aromatic compounds favors π-π interactions, which permits the accommodation of a greater number of molecules in a given space and might explain the larger loading of Cin in comparison with Thy and Car.

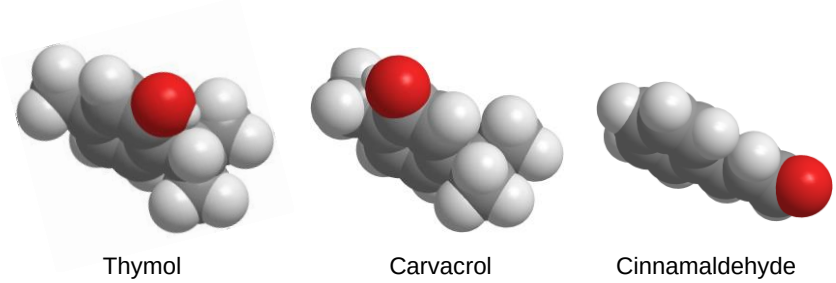

Figure 4. ChemDraw 3D MM2 energy minimized model showing 3D structure of thymol, carvacrol and cinnamaldehyde.

3.2. Cargo controlled release

Release assays were carried out with M41-RhB-Z, to confirm the mechanism of the protein-gated support to modulate cargo release, according to the presence of proteolytic enzymes in the medium. Delivery studies from M41-RhB-Z were performed in H_2O at pH 8 in the absence and in the presence of pronase, as a generic cocktail of proteolytic enzymes. As it can be seen in Figure 5, the cargo released from the system, when no proteolytic enzymes were present, is relatively low compared to the cargo delivered in the presence of pronase. This confirms that cargo delivery is hindered by the zein protein anchored to the surface of the mesoporous silica particles while the presence of proteolytic enzymes favors the sustained release of the entrapped molecule over time.

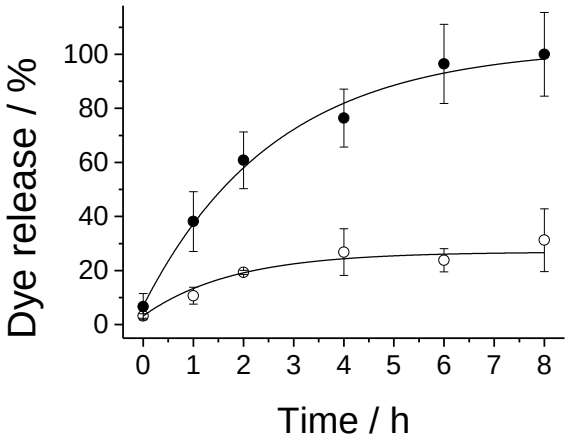

Figure 5. Cargo release profiles of RhB from M41-RhB-Z in H_2O at pH 8 (○) and when proteolytic enzymes (pronase) are present (●). Release assays were performed in triplicate, and error bars correspond to standard deviation.

3.3. Antimicrobial activity of free and encapsulated EOCs

The antimicrobial activity of free and encapsulated EOCs against *E. coli* as model foodborne strain was evaluated by *in vitro* assays. The effectiveness of the studied systems, evaluated by means of *E. coli* microbial counts after 24 h of treatment with the antimicrobials, is shown in Figure 6. Different concentration ranges were tested for each EOC in accordance with previous reported studies [52]. All free EOCs were able to completely inhibit bacterial growth in the tested concentration ranges (50-250 µg/mL for Thy and Car, and 125-1000 µg/mL for Cin), specifically, the MBC obtained for the free EOCs was found in the following concentration ranges: 100-150 µg/mL for Thy, 150-200 µg/mL for Car and 250-500 µg/mL for Cin. These results are in agreement with previously described data in the literature, where the studied EOCs were reported to have MBC values of 240-300.5 µg/mL for Thy, 244.2-366.4 µg/mL for Car and 262.5 µg/mL for Cin, against *E. coli* [51]. It can be observed that among the tested free EOCs, the least active was cinnamaldehyde since more concentration was needed to obtain the same inhibitory effect (see Figure 6d for Thy, 6e for Car and 6f for Cin antimicrobial activities).

In the case of the M41-EOC-Z microdevices, a maximum concentration of 12 mg/mL was chosen, since higher particle concentration would not be feasible in a real application. In Figure 6.a, 6.b and 6.c the bactericidal effect of the M41-EOC-Z solids is shown. In order to relate the bactericidal effects of the microdevices to those of the free EOCs, the coincident concentration data in the Figure 6 top and bottom graphs have been highlighted with red dots.

In Figure 6.a. and 6.b it can be appreciated that the systems M41-Thy-Z and M41-Car-Z did not reach MBC at any of the tested concentrations. This circumstance might be explained by the fact that the released payload by these gated microdevices is below the MBC of the corresponding free compound. In contrast, the cinnamaldehyde-loaded solid shows a clear bactericidal effect, achieving a maximum effect at a particle concentration of 8 mg/mL, which corresponds to a Cin payload of 145 µg/mL. The figure also shows that the M41-

Cin-Z solid was able to decrease significantly the microbial population at a concentration as low as 4 mg/mL, which corresponds to a Cin payload of 73 µg/mL. These results indicated that the M41-Cin-Z system is not only better than the other studied M41-EOC-Z, but also has a greater bactericidal effect than free Cin. The MBC of the M41-Cin-Z system falls within the 73-145 µg of Cin/mL range. This concentration was much lower than the MBC of free Cin, which, as stated before, was in the 250-500 µg/mL range. This MBC value obtained was also much lower than those reported in other previous works in which this compound was tested against different microorganisms [51,56–58]. This MBC improvement can be related with the advantages offered by the encapsulation and the active release of this volatile compound from the gated-MSP system. Thereby, the designed microdevice increases the local concentration of EOC and prevents its evaporation from the medium, achieving the same antimicrobial effect with lower active compound concentration.

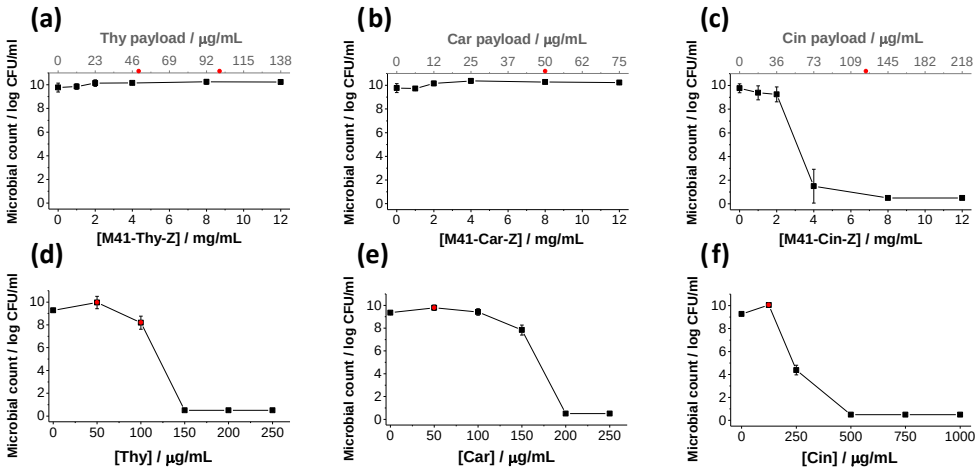

Figure 6. E. coli counts after incubation with M41-EOC-Z systems (top) and free EOCs (bottom) according to particle and EOC concentration. Red dots mark the coincident concentrations between the encapsulated EOC and the free molecule. Antimicrobial assays were performed in triplicate, and error bars correspond to standard deviation.

Besides plate counting results, the bacterial viability of the cells treated with the free and encapsulated Cin was analyzed with a two-color fluorescent LIVE/DEAD® *Bac*Light™ kit, in order to visualize the remaining viable cells (see section 2.7.2 for details). As an outline of the kit's performance, living cells become green-stained, and dead bacteria that remain physically intact in the medium are red-stained, thus allowing to qualitatively visualize cell viability. With this aim, cells incubated under different conditions (without treatment -positive control-, with unloaded M41-Z particles -negative control-, with free Cin and with M41-Cin-Z) were stained with the aforementioned kit (see section 2.7.2 for details). Afterwards, fluorescence microscopy images were obtained. The resulting micrographs are shown in Figure 7. As it can be seen, there was no difference between positive (Figure 7a) and negative controls (Figure 7b) on the *E. coli* viability (green cells). In contrast, the number of living cells (shown in green color) was practically reduced to zero when free Cin (Figure 7c) or M41-Cin-Z (Figure 7d) were added to the medium at tested concentrations. The absence of red-stained cells is related to the absence of intact dead cells. This suggests cell-envelope-disruption and leakage of intracellular content, resulting in loss of cellular structure and the inability of the red fluorophore to stain these cells. These results are in accordance with previous studies using essential oil components as antimicrobials [59,60].

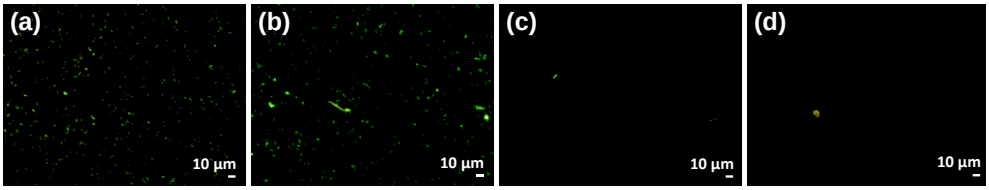

Figure 7. Fluorescence images of untreated *E. coli* (**A**) and cells treated with M41-Z (**B**) as negative control, free Cin (**C**) and M41-Cin-Z (**D**) after 5 h of incubation. The study was performed by the 2-color fluorescent LIVE/DEAD® *Bac*Light™ assay, used to visualize viable (green) and dead (red) bacteria. Red-stained bacteria are not visible when dead cells do not remain intact after treatment.

4. Conclusions

In this work, a new antimicrobial device applying for the first time the zein protein as gating moiety, and based on MSPs loaded with essential oil components, is developed for the controlled release of natural antimicrobial compounds (essential oil components (EOCs) thymol, carvacrol and cinnamaldehyde). The antimicrobial action of cinnamaldehyde encapsulated inside the microdevice against *E. coli* is demonstrated by culturability and viability assays. Indeed, the results show not only a good inhibitory effect of cinnamaldehyde when encapsulated in gated MSPs but also the enhancement of the cinnamaldehyde bactericidal effect when compared with the corresponding free compound. The accomplishment of this microdevice is based on the bacteria proteolytic secretion acting as triggering stimulus that allows the sustained release of the entrapped EOC. In this way, the developed microdevice improves the antimicrobial properties of the essential oil component by decreasing its volatility and hence, increasing its local concentration. The developed antimicrobial system, based on the combination of food-grade molecules and a biocompatible support, might be used as new preservative in the food industry.

Authors contribution: Conceptualization, E.P-R., M. R-R., M.D.M. and A.B.; methodology, E.P-R., G.G-B, M.R-R and A.B.; validation, E.P-R, G.G-B., M.R-R, E.A., J.M.B., R.M-M., M.D.M. and A.B.; formal analysis, E.P-R., G.G-B. and M.R-R.; investigation, E.P-R., G.G-B. and M.R-R.; data curation, E.P-R.; writing—original draft preparation, E.P-R. and A.B.; writing—review and editing, E.P-R., M.R-R., R.M-M., M.D.M. and A.B.; visualization, E.P-R., M.R-R., E.A., J.M.B., R.M-M., M.D.M. and A.B.; supervision, E.A., R.M.M., M.D.M. and A.B.; project administration, M.D.M.; funding acquisition, E.A., J.M.B., R.M-M. and M.D.M. All authors have read and agreed to the published version of the manuscript.

Funding: This research was funded by the Spanish Government (projects RTI2018-100910-B-C41, RTI2018-101599-B-C22-AR and RTI2018-101599-B-C21-AR (MCUI/FEDER, EU)) and the Generalitat Valenciana (project PROMETEO 2018/024, grant numbers ACIF/2016/023 and APOSTD/2019/118).

Acknowledgments: The authors want to thank the Electron Microscopy Service at the UPV for support.

Conflicts of Interest: The authors declare no conflict of interest

References

1. Martinović, T.; Andjelković, U.; Gajdošik, M.Š.; Rešetar, D.; Josić, D. Foodborne pathogens and their toxins. *J. Proteomics* 2016, *147*, 226–235, doi:10.1016/j.jprot.2016.04.029.
2. Capeletti, L.B.; De Oliveira, L.F.; Gonçalves, K.D.A.; De Oliveira, J.F.A.; Saito, Â.; Kobarg, J.; Santos, J.H.Z. Dos; Cardoso, M.B. Tailored silica-antibiotic nanoparticles: Overcoming bacterial resistance with low cytotoxicity. *Langmuir* 2014, *30*, 7456–7464, doi:10.1021/la4046435.
3. World Health Organization *Antimicrobial resistance*; WHO Fact Sheet, 2018;
4. Gokoglu, N. Novel natural food preservatives and applications in seafood preservation: a review. *J. Sci. Food Agric.* 2019, *99*, 2068–2077, doi:10.1002/jsfa.9416.
5. Adelakun, O.E.; Oyelade, O.J.; Olanipekun, B.F. Use of essential oils in food preservation. In *Essential Oils in Food Preservation, Flavor and Safety*; Preedy, V.R., Ed.; Academic Press: San Diego, 2016; pp. 71–84 ISBN 9780124166448.
6. Appendini, P.; Hotchkiss, J.H. Review of antimicrobial food packaging. *Innov. Food Sci. Emerg. Technol.* 2002, *3*, 113–126, doi:10.1016/S1466-8564(02)00012-7.
7. Savoia, D. Plant-derived antimicrobial compounds: Alternatives to antibiotics. *Future Microbiol.* 2012, *7*, 979–990, doi:10.2217/fmb.12.68.
8. Chávez-González, M.L.; Rodríguez-Herrera, R.; Aguilar, C.N. Essential Oils: A Natural Alternative to Combat Antibiotics Resistance. In *Antibiotic Resistance: Mechanisms and New Antimicrobial Approaches*; Kon, K., Rai, M., Eds.; Academic Press: Boston, 2016; pp. 227–237 ISBN 9780128036686.
9. Tajkarimi, M.M.; Ibrahim, S.A.; Cliver, D.O. Antimicrobial herb and spice compounds in food. *Food Control* 2010, *21*, 1199–1218, doi:10.1016/j.foodcont.2010.02.003.

10. Lingan, K. A Review on Major Constituents of Various Essential Oils and its Application. *Transl. Med.* 2018, *8*, 1–5, doi:10.4172/2161-1025.1000201.

11. Bakkali, F.; Averbeck, S.; Averbeck, D.; Idaomar, M. Biological effects of essential oils - A review. *Food Chem. Toxicol.* 2008, *46*, 446–475, doi:10.1016/j.fct.2007.09.106.

12. Inoue, M.; Hayashi, S.; E. Craker, L. Role of Medicinal and Aromatic Plants: Past, Present, and Future. *Pharmacogn. - Med. Plants* 2019, 1–13, doi:10.5772/intechopen.82497.

13. Nazzaro, F.; Fratianni, F.; De Martino, L.; Coppola, R.; De Feo, V. Effect of essential oils on pathogenic bacteria. *Pharmaceuticals* 2013, *6*, 1451–1474, doi:10.3390/ph6121451.

14. Chouhan, S.; Sharma, K.; Guleria, S. Antimicrobial Activity of Some Essential Oils—Present Status and Future Perspectives. *Medicines* 2017, *4*, 58, doi:10.3390/medicines4030058.

15. Suhr, K.I.; Nielsen, P. V. Antifungal activity of essential oils evaluated by two different application techniques against rye bread spoilage fungi. *J. Appl. Microbiol.* 2003, *94*, 665–674, doi:10.1046/j.1365-2672.2003.01896.x.

16. Laird, K.; Phillips, C. Vapour phase: A potential future use for essential oils as antimicrobials? *Lett. Appl. Microbiol.* 2012, *54*, 169–174, doi:10.1111/j.1472-765X.2011.03190.x.

17. Asbahani, A. El; Miladi, K.; Badri, W.; Sala, M.; Addi, E.H.A.; Casabianca, H.; Mousadik, A. El; Hartmann, D.; Jilale, A.; Renaud, F.N.R.; et al. Essential oils: From extraction to encapsulation. *Int. J. Pharm.* 2015, *483*, 220–243, doi:10.1016/j.ijpharm.2014.12.069.

18. Bernardos, A.; Piacenza, E.; Sancenón, F.; Hamidi, M.; Maleki, A.; Turner, R.J.; Martínez-Máñez, R. Mesoporous Silica-Based Materials with Bactericidal Properties. *Small* 2019, *15*, 1–34, doi:10.1002/smll.201900669.

19. Arruebo, M. Drug delivery from structured porous inorganic materials. *Wiley Interdiscip. Rev. Nanomedicine Nanobiotechnology* 2012, *4*, 16–30, doi:10.1002/wnan.132.

20. Bernardos, A.; Kourimská, L. Applications of mesoporous silica materials in food - A review. *Czech J. Food Sci.* 2013, *31*, 99–107.

21. Melendez-Rodriguez, B.; Figueroa-Lopez, K.J.; Bernardos, A.; Martínez-Máñez, R.; Cabedo, L.; Torres-Giner, S.; Lagaron, J.M. Electrospun antimicrobial films of poly(3-hydroxybutyrate-co-3-hydroxyvalerate) containing eugenol essential oil encapsulated in mesoporous silica nanoparticles. *Nanomaterials* 2019, *9*, 227, doi:10.3390/nano9020227.

22. Bernardos, A.; Marina, T.; Žáček, P.; Pérez-Esteve, É.; Martínez-Mañez, R.; Lhotka, M.; Kouřimská, L.; Pulkrábek, J.; Klouček, P. Antifungal effect of essential oil

components against Aspergillus niger when loaded into silica mesoporous supports. *J. Sci. Food Agric.* 2015, *95*, 2824–2831, doi:10.1002/jsfa.7022.

23. García-Fernández, A.; Aznar, E.; Martínez-Máñez, R.; Sancenón, F. New Advances in In Vivo Applications of Gated Mesoporous Silica as Drug Delivery Nanocarriers. *Small* 2020, *16*, 1–62, doi:10.1002/smll.201902242.

24. Aznar, E.; Villalonga, R.; Giménez, C.; Sancenón, F.; Marcos, M.D.; Martínez-Máñez, R.; Díez, P.; Pingarrón, J.M.; Amorós, P. Glucose-triggered release using enzyme-gated mesoporous silica nanoparticles. *Chem. Commun.* 2013, *49*, 6391–6393, doi:10.1039/c3cc42210k.

25. Poyatos-Racionero, E.; Pérez-Esteve, É.; Dolores Marcos, M.; Barat, J.M.; Martínez-Máñez, R.; Aznar, E.; Bernardos, A. New Oleic Acid-Capped Mesoporous Silica Particles as Surfactant-Responsive Delivery Systems. *ChemistryOpen* 2019, *8*, 1052–1056, doi:10.1002/open.201900092.

26. Ribes, À.; Aznar, E.; Santiago-Felipe, S.; Xifre-Perez, E.; Tormo-Mas, M. ángeles; Pemán, J.; Marsal, L.F.; Martínez-Mántild;ez, R. Selective and Sensitive Probe Based in Oligonucleotide-Capped Nanoporous Alumina for the Rapid Screening of Infection Produced by Candida albicans. *ACS Sensors* 2019, *4*, 1291–1298, doi:10.1021/acssensors.9b00169.

27. Santos-Figueroa, L.E.; Giménez, C.; Agostini, A.; Aznar, E.; Marcos, M.D.; Sancenón, F.; Martínez-Máñez, R.; Amorós, P. Selective and sensitive chromofluorogenic detection of the sulfite anion in water using hydrophobic hybrid organic-inorganic silica nanoparticles. *Angew. Chemie - Int. Ed.* 2013, *52*, 13712–13716, doi:10.1002/anie.201306688.

28. de Luis, B.; Llopis-Lorente, A.; Rincón, P.; Gadea, J.; Sancenón, F.; Aznar, E.; Villalonga, R.; Murguía, J.R.; Martínez-Máñez, R. An Interactive Model of Communication between Abiotic Nanodevices and Microorganisms. *Angew. Chemie - Int. Ed.* 2019, *58*, 14986–14990, doi:10.1002/anie.201908867.

29. Llopis-Lorente, A.; Díez, P.; Sánchez, A.; Marcos, M.D.; Sancenón, F.; Martínez-Ruiz, P.; Villalonga, R.; Martínez-Máñez, R. Interactive models of communication at the nanoscale using nanoparticles that talk to one another. *Nat. Commun.* 2017, *8*, 1–7, doi:10.1038/ncomms15511.

30. Giménez, C.; Climent, E.; Aznar, E.; Martánez-Máñez, R.; Sancenón, F.; Marcos, M.D.; Amorós, P.; Rurack, K. Towards chemical communication between gated nanoparticles. *Angew. Chemie - Int. Ed.* 2014, *53*, 12629–12633, doi:10.1002/anie.201405580.

31. Xu, J.H.; Gao, F.P.; Li, L.L.; Ma, H.L.; Fan, Y.S.; Liu, W.; Guo, S.S.; Zhao, X.Z.; Wang, H. Gelatin-mesoporous silica nanoparticles as matrix metalloproteinases- degradable drug delivery systems in vivo. *Microporous Mesoporous Mater.* 2013, *182*, 165–172, doi:10.1016/j.micromeso.2013.08.050.

32. Popat, A.; Jambhrunkar, S.; Zhang, J.; Yang, J.; Zhang, H.; Meka, A.; Yu, C. Programmable drug release using bioresponsive mesoporous silica nanoparticles for site-specific oral drug delivery. *Chem. Commun.* **2014**, *50*, 5547–5550, doi:10.1039/c4cc00620h.

33. Llopis-Lorente, A.; Lozano-Torres, B.; Bernardos, A.; Martínez-Máñez, R.; Sancenón, F. Mesoporous silica materials for controlled delivery based on enzymes. *J. Mater. Chem. B* **2017**, *5*, 3069–3083, doi:10.1039/c7tb00348j.

34. Thornton, P.D.; Heise, A. Highly specific dual enzyme-mediated payload release from peptide-coated silica particles. *J. Am. Chem. Soc.* **2010**, *132*, 2024–2028, doi:10.1021/ja9094439.

35. Candel, I.; Aznar, E.; Mondragón, L.; De La Torre, C.; Martínez-Máñez, R.; Sancenón, F.; Marcos, M.D.; Amorós, P.; Guillem, C.; Pérez-Payá, E.; et al. Amidase-responsive controlled release of antitumoral drug into intracellular media using gluconamide-capped mesoporous silica nanoparticles. *Nanoscale* **2012**, *4*, 7237–7245, doi:10.1039/c2nr32062b.

36. Pang, J.; Zhou, G.; Liu, R.; Li, T. Esterification of oleic acid with methanol by immobilized lipase on wrinkled silica nanoparticles with highly ordered, radially oriented mesochannels. *Mater. Sci. Eng. C* **2016**, *59*, 35–42, doi:10.1016/j.msec.2015.09.088.

37. Radhakrishnan, K.; Gupta, S.; Gnanadhas, D.P.; Ramamurthy, P.C.; Chakravortty, D.; Raichur, A.M. Protamine-capped mesoporous silica nanoparticles for biologically triggered drug release. *Part. Part. Syst. Charact.* **2014**, *31*, 449–458, doi:10.1002/ppsc.201300219.

38. Mondragón, L.; Mas, N.; Ferragud, V.; De La Torre, C.; Agostini, A.; Martínez-Máñez, R.; Sancenón, F.; Amorós, P.; Pérez-Payá, E.; Orzáez, M. Enzyme-responsive intracellular-controlled release using silica mesoporous nanoparticles capped with ε-poly- L -lysine. *Chem. - A Eur. J.* **2014**, *20*, 5271–5281, doi:10.1002/chem.201400148.

39. Zhao, G.; Chen, Y.; He, Y.; Chen, F.; Gong, Y.; Chen, S.; Xu, Y.; Su, Y.; Wang, C.; Wang, J. Succinylated casein-coated peptide-mesoporous silica nanoparticles as an antibiotic against intestinal bacterial infection. *Biomater. Sci.* **2019**, *7*, 2440–2451, doi:10.1039/c9bm00003h.

40. Song, Y.; Zhu, P.; Wu, Y.; Tan, L.; Wei, W.; Liu, S.; Huang, Q.; Chen, J. Epsilon-poly-L-lysine decorated ordered mesoporous silica contributes to the synergistic antifungal effect and enhanced solubility of a lipophilic drug. *Mater. Sci. Eng. C* **2019**, *99*, 231–240, doi:10.1016/j.msec.2019.01.077.

41. Frees, D.; Brøndsted, L.; Ingmer, H. Bacterial Proteases and Virulence. In *Regulated Proteolysis in Microorganisms. Subcellular Biochemistry*; Dougan, D., Ed.; Springer: Dordrecht, 2013; Vol. 66 ISBN 978-94-007-5939-8.

42. Momany, F.A.; Sessa, D.J.; Lawton, J.W.; Selling, G.W.; Hamaker, S.A.H.; Willett, J.L.

Structural characterization of α-zein. *J. Agric. Food Chem.* 2006, *54*, 543–547, doi:10.1021/jf058135h.

43. Tatham, A.S.; Field, J.M.; Morris, V.J.; I'Anson, K.J.; Cardle, L.; Dufton, M.J.; Shewry, P.R. Solution conformational analysis of the alpha-zein proteins of maize. *J. Biol. Chem.* 1993, *268*, 26253–26259.

44. Li, Y.; Li, J.; Xia, Q.; Zhang, B.; Wang, Q.; Huang, Q. Understanding the dissolution of α-zein in aqueous ethanol and acetic acid solutions. *J. Phys. Chem. B* 2012, *116*, 12057–12064, doi:10.1021/jp305709y.

45. Shukla, R.; Cheryan, M. Zein: The industrial protein from corn. *Ind. Crops Prod.* 2001, *13*, 171–192, doi:10.1016/S0926-6690(00)00064-9.

46. Liu, X.; Jia, J.; Duan, S.; Zhou, X.; Xiang, A.; Lian, Z.; Ge, F. Zein/MCM-41 nanocomposite film incorporated with cinnamon essential oil loaded by modified supercritical CO2 impregnation for long-term antibacterial packaging. *Pharmaceutics* 2020, *12*, 169, doi:10.3390/pharmaceutics12020169.

47. Bernardos, A.; Aznar, E.; Coll, C.; Martínez-Mañez, R.; Barat, J.M.; Marcos, M.D.; Sancenón, F.; Benito, A.; Soto, J. Controlled release of vitamin B2 using mesoporous materials functionalized with amine-bearing gate-like scaffoldings. *J. Control. Release* 2008, *131*, 181–189, doi:10.1016/j.jconrel.2008.07.037.

48. Cabrera, S.; El Haskouri, J.; Guillem, C.; Latorre, J.; Beltrán-Porter, A.; Beltrán-Porter, D.; Marcos, M.D.; Amorós, P. Generalised syntheses of ordered mesoporous oxides: The atrane route. *Solid State Sci.* 2000, *2*, 405–420, doi:10.1016/S1293-2558(00)00152-7.

49. Poyatos-Racionero, E.; González-Álvarez, I.; González-Álvarez, M.; Martínez-Máñez, R.; Marcos, M.D.; Bernardos, A.; Aznar, E. Surfactant - Triggered Molecular Gate Tested on Different Mesoporous Silica Supports for Gastrointestinal Controlled Delivery. *Nanomaterials* 2020, *10*, art. 1290 (1-18), doi:10.3390/nano10071290.

50. Clinical and Laboratory Standards Institute (CLSI) *Methods for Dilution Antimicrobial Susceptibility Tests for Bacteria That Grow Aerobically*; 11th ed.; Wayne, PA, 2018;

51. Mith, H.; Duré, R.; Delcenserie, V.; Zhiri, A.; Daube, G.; Clinquart, A. Antimicrobial activities of commercial essential oils and their components against food-borne pathogens and food spoilage bacteria. *Food Sci. Nutr.* 2014, *2*, 403–416, doi:10.1002/fsn3.116.

52. Ruiz-Rico, M.; Pérez-Esteve, É.; Bernardos, A.; Sancenón, F.; Martínez-Máñez, R.; Marcos, M.D.; Barat, J.M. Enhanced antimicrobial activity of essential oil components immobilized on silica particles. *Food Chem.* 2017, *233*, 228–236, doi:10.1016/j.foodchem.2017.04.118.

53. Burt, S. Essential oils: Their antibacterial properties and potential applications in foods - A review. *Int. J. Food Microbiol.* 2004, *94*, 223–253.

54. Thommes, M.; Kaneko, K.; Neimark, A. V.; Olivier, J.P.; Rodriguez-Reinoso, F.; Rouquerol, J.; Sing, K.S.W. *Physisorption of gases, with special reference to the evaluation of surface area and pore size distribution (IUPAC Technical Report)*; 2015; Vol. 87;.

55. Ouellette, R.J.; Rawn, J.D. Aldehydes and Ketones. In *Principles of Organic Chemistry*; Ouellette, R.J., Rawn, J.D., Eds.; Elsevier: Boston, 2015; pp. 259–286 ISBN 9781118834015.

56. Didry, N.; Dubreuil, L.; Pinkas, M. Activity of thymol, carvacrol, cinnamaldehyde and eugenol on oral bacteria. *Pharm. Acta Helv.* 1994, *69*, 25–28, doi:10.1016/0031-6865(94)90027-2.

57. Firmino, D.F.; Cavalcante, T.T.A.; Gomes, G.A.; Firmino, N.C.S.; Rosa, L.D.; De Carvalho, M.G.; Catunda, F.E.A. Antibacterial and Antibiofilm Activities of Cinnamomum Sp. Essential Oil and Cinnamaldehyde: Antimicrobial Activities. *Sci. World J.* 2018, *2018*, doi:10.1155/2018/7405736.

58. Malheiro, J.F.; Maillard, J.Y.; Borges, F.; Simões, M. Evaluation of cinnamaldehyde and cinnamic acid derivatives in microbial growth control. *Int. Biodeterior. Biodegrad.* 2019, *141*, 71–78, doi:10.1016/j.ibiod.2018.06.003.

59. Ruiz-Rico, M.; Moreno, Y.; Barat, J.M. In vitro antimicrobial activity of immobilised essential oil components against Helicobacter pylori. *World J. Microbiol. Biotechnol.* 2020, *36*, 1–9, doi:10.1007/s11274-019-2782-y.

60. Orhan-Yanıkan, E.; da Silva-Janeiro, S.; Ruiz-Rico, M.; Jiménez-Belenguer, A.I.; Ayhan, K.; Barat, J.M. Essential oils compounds as antimicrobial and antibiofilm agents against strains present in the meat industry. *Food Control* 2019, *101*, 29–38, doi:10.1016/j.foodcont.2019.02.035.

5. CHAPTER 3

Saccharide-gated microdevices

Article 5

Lactose-gated mesoporous silica particles for controlled intestinal delivery of essential oil components: an *in vitro* and *in vivo* study

Elisa Poyatos-Racionero,[a,b] Isabel González-Álvarez,[c] Paola Sánchez-Moreno,[d] Leopoldo Sitia,[e,f] Francesca Gatto,[e] Pier Paolo Pompa,[e] Elena Aznar,[a,b,g,h] Marta González-Álvarez,[c] Ramón Martínez-Máñez,[a,b,g,h,i] María Dolores Marcos,[a,b,g,h,i]* Andrea Bernardos[a,b,h]*

[a] Instituto Interuniversitario de Investigación de Reconocimiento Molecular y Desarrollo Tecnológico (IDM), Universitat Politècnica de València, Universitat de València. Camino de Vera s/n, 46022, Valencia (Spain).

[b] CIBER de Bioingeniería, Biomateriales y Nanomedicina (CIBER-BBN) (Spain).

[c] Departamento de Ingeniería, Sección de Farmacia y Tecnología Farmacéutica, Universidad Miguel Hernández. 03550, Alicante (Spain).

[d] Department of Applied Physics, Faculty of Sciences, University of Granada, Avenida Fuente Nueva s/n, 18071 Granada (Spain).

[e] Nanobiointeractions & Nanodiagnostics. Istituto Italiano di Tecnologia (IIT). Via Morego, 30, 16163 Genova (Italy).

[f] Nanomedicine Laboratory, Department of Biomedical and Clinical Sciences "Luigi Sacco", University of Milano, Milan (Italy).

[g] Unidad Mixta de Investigación en Nanomedicina y Sensores. Universitat Politècnica de València, Instituto de Investigación Sanitaria La Fe, Valencia (Spain).

[h] Unidad Mixta UPV-CIPF de Investigación de Mecanismos Enfermedades y Nanomedicina. Universitat Politècnica de València, Centro de Investigación Príncipe Felipe. Valencia (Spain).

[i] Departamento de Química, Universitat Politècnica de València. Camino de Vera s/n, 46022, Valencia (Spain).

* Correspondence: M.D. M: mmarcos@upv.es; A. B: anberba@upv.es

Submitted to Journal of Controlled Release

Abstract

In this work, we present the synthesis and characterization of hybrid M41-EOC-L materials for the specific release of essential oil components (ECOs) in the small intestine, based on the ability of lactose to act as molecular gate on mesoporous silica microparticles. Different techniques are presented here to validate the designed microdevices, including *in vitro* and *in vivo* intestinal models in which the presence of lactase enzyme acts as the triggering stimulus for the controlled release of the encapsulated EOCs. Significant particle internalization was observed in Caco-2 cells and, among the different microdevices prepared (containing EOCs thymol (*Thy)*, eugenol (*Eug*), and cinnamaldehyde (*Cin*)), the one loaded with *Cin* showed the more significant cell viability reduction. On the other hand, interaction of the loaded and functionalized particles with enterocyte-like monolayers showed the reduction of EOCs permeability when protected into the designed microdevices. Based on these results, the M41-Cin-L microdevice was chosen to be applied in the *in vivo* model of Wistar rat. The results showed a reduction in cinnamaldehyde plasma levels and an increase in its concentration in the lumen of the gastrointestinal tract (GIT). The absence of payload release in the stomach, the progressive release throughout the intestine thanks to the triggering action of the secreted lactase, and the prolonged stay of the payload in the GIT-lumen increased the bioavailability of the encapsulated compound at the site of the desired action. These results suggest that the M41-payload-L could be a potential hybrid microdevice for the protection and administration of bioactive molecules whose site of action is the small intestine and colon.

1. Introduction

Hybrid systems based on Mesoporous Silica Particles (MSPs) as inorganic support, coated with molecular gates (also known as gatekeepers or nanovalves), have been widely described and applied in several research fields such as sensing,[1,2] chemical communication[3–5] or drug controlled release for biomedical or food technology applications.[6–15] The versatility of these systems lies not only in the use of molecular gates for on-command payload delivery, but also in the great variety of molecules they can harbor in their porous structure. Various examples of molecules encapsulated in MSPs can be found in the literature, including vitamins,[16–18] antioxidants,[19,20] antibiotics, [21,22] anti-inflammatories[23,24] or anti-tumor compounds.[25–27]

Focusing on this field, several examples of MSPs for controlled delivery of bioactive molecules into the gastrointestinal tract (GIT) have been reported.[28–33] The multiple conditions present along the digestive system provide a wide variety of stimuli able to trigger the controlled release of the payload lodged into MSPs.[30] Among these stimuli, differences in pH values or redox potential can be highlighted, as well as specific enzymes secreted by the GIT tissues and their sheltered microbiota.[34] In fact different MSPs have been used to effectively reach the GIT and deliver their cargo through pH-, redox- or enzyme-responsive molecular gates.[16,23,35–38]

From another point of view, one example of bioactive molecules that are gaining great interest, are essential oil components (EOCs). Essential oils (EO) are complex mixtures of about 20-60 components, generated by aromatic and medicinal plants in their secondary metabolism, in order to protect themselves against tissue damage (as pests or oxidative stress, among others).[39] Broadly, EOCs have important nutritional and medicinal properties: antimicrobial,[40] antioxidant,[41] anti-inflammatory and anticancer.[42] Due to the aforementioned properties, EOCs have traditionally been used as naturally occurring alternative to other synthetic chemical compounds in food and pharmaceutical industries as preservatives and antioxidant molecules.[43,44] Their proven anti-inflammatory[41,45–53] and/or anti-

cancer properties,[54–57] in addition to their natural origin, have been a crucial combination to put the focus on their study. Furthermore, their weak points as drug molecules,[58,59] such as low water solubility due to their lipophilic nature, or their general high volatility, could be mitigated using controlled release systems.[12] Furthermore, their lipophilic nature entails a too high passive permeability through cell tissues,[60,61] which also could be mitigated by the sustained administration provided by controlled release devices. Among them, some reports describe the use of gated MSPs to deliver EOCs.[62] In fact, the development of smart MSP-systems, loaded with EOCs and functionalized with specific molecular gates, could be a promising combination for enhancing the EOCs applications in a number of diseases.

To move forwards and validate the applications of gated MSPs loaded with EOCs, it is essential to study their interaction with biological systems and evaluate their possible toxicity by means of *in vitro* and/or *in vivo* models. The toxicity of MSPs-based materials has been extensively studied in numerous works found in the literature.[63–65] Their particle size,[66] the presence of organic moieties onto the external surface and their chemical nature,[64,67–69] the particle concentration and stability,[70] the administration route into the organism[71] and the inner toxicity of the host molecules, are factors that can modify the toxicity of MSP-systems, from harmless to highly toxic, including intermediate possibilities. Focusing on the oral route of administration into the GIT, several useful models to study the particle integrity and their interaction/toxicity with the involved tissues can be found. On one hand, since the degradation of the particles can modify their toxicity for cells, it is important to emulate their passage through the GIT to know their behavior under these changes to evaluate the particles degradation along the digestion process, and to assess their inalterability from the ingestion to the excretion stage.[72] In this scenario, *in vitro* digestion models that simulate changes in pH and ionic strength, as well as the presence of biomolecules (including enzymes) in the different organs of the GIT have been widely applied.[73,74]

On the other hand, more complex *in vitro* test, such as GIT cellular models have also been employed to evaluate the MSPs toxicity. Several cell lines have been used for this purpose, among which the immortalized Caco-2 cell line of human colon adenocarcinoma stands out, since its simplicity and reproducibility allows the interlaboratory results-comparison.[34] Furthermore, under certain conditions, this line spontaneously differentiates into enterocyte-like monolayers that closely simulates the epithelium of the small intestine (SI).[75–77] This system, also denominated intestinal barrier, is a very appropriate model to mimic and study the interaction of nano and microparticles with intestinal enterocytes, as well as to get an initial understanding of the internalization and permeability processes through the intestinal membrane. In addition, more complex *in vivo* animal models, which provide more truthful information as they consider factors that cannot be simulated in the *in vitro* test, such as feedback mechanisms, peristaltic movements, gastric emptying or changes in pH and secretion flow rates, as well as intestinal microflora and liver metabolism can also be used to study the effect of encapsulated EOCs.[73]

Based on the above, we report herein the preparation of EOC-loaded MSPs functionalized with lactose as molecular gate, which allows EOCs on-command delivery in SI conditions (lactase secretion). Despite lactose (*Lac*) molecule has previously been used as molecular gate,[78] its behavior as gatekeeper in MSPs under GIT conditions for delivering EOCs has not been reported yet. The aim of the EOC-loaded lactose-capped MSPs developed in the present work is to increase the bioavailability of EOCs throughout the intestinal lumen. This is expected to be achieved by the combination of different factors that simultaneously occur, such as (*i*) the increase in the EOCs-local concentration thanks to the encapsulation process; (*ii*) the dependence of the EOCs release on the enzymatic activity of the enterocytes-secreted lactase, which makes it a controlled and sustained process over time; and (*iii*) the reduction of the high EOCs permeability due to their progressive administration through the SI, thus favoring a sustained administration and a more prolonged effect throughout the entire intestinal lumen. The system's

effectiveness and the accomplishment of the aforementioned characteristics have been evaluated in this work using *in vitro* and *in vivo* biological models in which the secretion of lactase, a β-galactosidase enzyme (β -gal),[79–81] acts as trigger stimulus for the hydrolysis of the molecular gate and the payload's release. The integrity of the system subjected to changes in pH, ionic strength and presence of biomolecules has been studied in an *in vitro* digestion model, and its GIT-interaction has been assessed with cellular models of Caco-2 and enterocyte-like monolayers (intestinal barriers). The toxicity of the gated particles, internalization, cell viability, inflammatory response and cell permeability, are evaluated. Additionally, lactose-gated MSPs loaded with cinnamaldehyde have been tested in an *in vivo* model of Wistar rat to evaluate the effectiveness of the microdevice in prolonging the EOC-presence throughout the intestinal lumen, measurements of the EOC concentration in plasma as well as in the different areas of the GIT.

2. Materials and methods

2.1. Chemicals and cell-culture media

Tetraethylortosilicate (TEOS), triethanolamine ($TEAH_3$), sodium hydroxide (NaOH), N-cetyltrimethylammonium bromide (CTAB), (3-aminopropyl)triethoxysilane (APTES), N-(3-dimethylaminopropyl)-N'-ethylcarbodiimide (EDC), lucifer yellow (LY), coumarin 6 (C6), rhodamine B (RhB), lipopolysaccharide (LPS, from *Escherichia coli*), trifluoroacetic acid (TFA), thymol (*Thy*), eugenol (*Eug*), cinnamaldehyde (*Cin*), lactose (*Lac*), paraformaldehyde (PAF), bovine serum albumin (BSA), β-galactosidase (β-gal) from *Aspergillus oryzae* and all the components of the simulated fluids for the *in vitro* digestion were provided by Sigma (Sigma-Aldrich Química S.L., Madrid, Spain). Ethanol (extra pure), methanol (MeOH) and dimethyl sulfoxide (DMSO) were purchased from Scharlab (Barcelona, Spain). 3-(4,5-dimethylthiazol-2-yl)-2,5-diphenyltetrazolium bromide (MTT) and Hanks' Balanced Salt solution (HBSS) were supplied by ThermoFisher (Madrid, Spain). Dulbecco's modified Eagles Medium (DMEM), fetal bovine serum (FBS), 1%

nonessential aminoacids and 100 U/mL penicillin/streptomycin were purchased from Labclinics (Labclinics S.A., Barcelona, Spain).

2.2. Synthesis of mesoporous silica

The synthesis of the mesoporous silica material was performed according to the protocol described in previous authors´ works.[16] The synthesis process was carried out following the "atrane route"[82] in which the molar ratio between the reagents was: 7 $TEAH_3$: 2 TEOS: 0.52 CTAB: 0.5 NaOH: 180 H_2O. In a typical synthesis NaOH was added to $TEAH_3$ and the mixture was heated to 120 ℃. Then, the mixture was cooled to 70 ℃ and 11 mL of TEOS were added dropwise. The reaction was heated under stirring until 120 ℃ and once the temperature was reached, CTAB was added and the mixture was cooled again to 70 ℃. Finally, deionized H_2O was added, and the mother liquor was stirred vigorously for 1 h at room temperature. The final mixture was transferred to a Teflon flask and kept at 100 ℃ for 24 h. After this time, the suspension was filtered under vacuum and washed until neutral pH. The material was dried and finally calcined at 550 ℃ to completely remove the surfactant molecules which conformed the template, thus obtaining the final MCM-41 solid (M41) in the form of microparticles.

2.3. Synthesis of the gated materials

A fluorophore and three EOCs (*Thy*, *Eug* and *Cin*) were loaded in the M41 microparticles (solids M41-#). RhB was encapsulated into M41 following the immersion method. With that purpose, 1 g of M41 was added to a solution of RhB (0.8 mmol in 40 mL of H_2O) and stirred for 24 h. The mixture was filtered and the resulting solid (M41-RhB) was dried under vacuum. EOCs (*Thy*, *Eug* and *Cin*) were loaded into the mesoporous material by steam adsorption. For that, 250 mg of M41 was mixed with 250 mg of each EOC in a perfectly closed vial. The mixtures were shaken at 40 ℃ for 24 h to obtain the loaded solids (named M41-EOC (i.e. M41-Thy, M41-Eug and M41-Cin)). In a second step, the loaded microparticles were reacted with APTES. APTES functionalization was performed by mixing 1.2 g of M41-# with 1.68 mL of APTES in 16 mL of H_2O for 5.5 h at room temperature. The obtained

materials (M41-EOC-N (i.e. M41-Thy-N, M41-Eug-N and M41-Cin-N) and M41-RhB-N, or in general M41-#-N) were collected by centrifugation and dried under vacuum. Finally, the lactose molecule was reacted with the amine groups of the M41-#-N solids following a similar protocol previously described with slight modifications.[83] In a typical synthesis of 2 g of lactose in 40 mL of H_2O was stirred for 30 min. Then, 1 g of the corresponding M41-#-N solid was added, and the reaction was stirred at room temperature overnight. The final solids were collected by centrifugation and washed three times with deionized H_2O. Finally, the lactose-functionalized solids (M41-RhB-L and M41-EOC-L (i.e. M41-Thy-N-L, M41-Eug-N-L and M41-Cin-N-L) or M41-#-L in general) were dried under vacuum and stored at 5 ºC until their use. Additionally, three EOCs-loaded lactose-capped materials with an additional hydrophilic fluorophore (coumarin 6, C6) were synthesized to carry out microscopy experiments. With this aim, C6 was dissolved in the corresponding EOC in melted state (10 mg C6/100 µL EOC) and mixed with 100 mg M41, the loaded solid was reacted with APTES and capped with lactose following a similar procedure to that shown above to obtain the final M41-EOC_{C6}-L (i.e. M41-Thy_{C6}-N-L, M41-Eug_{C6}-N-L and M41-Cin_{C6}-N-L) fluorescent materials (also included in the M41-#-L denomination).

2.4. Characterization techniques

X-ray diffractograms were carried out on a Bruker D8 Advance diffractometer (Bruker, Coventry, UK) using Cu Kα radiation. TEM images were obtained with a JEOL JEM-1010 (JEOL Europe SAS, Croissysur-Seine, France). N_2 adsorption–desorption isotherms were recorded with a Micromeritics TriStar II Plus automated analyzer (Micromeritics Instrument Corporation, Norcross, USA). The samples were degassed at 120 °C in vacuum overnight. The specific surface areas were calculated from the adsorption data in the low-pressure range using the BET model. Pore dimensions (size and volume) were determined following the BJH method. The functionalization process was followed by ζ potential with a Zetasizer Nano ZS equipment (Malvern Instruments, Malvern, UK). Samples (bare and functionalized microdevices) were dispersed in deionized H_2O at neutral pH, at a concentration of

1 mg/mL. Before each measurement, samples were sonicated for 2 min to preclude aggregation. Values were calculated from the particle mobility values by applying the Smoluchowski model. Each measurement was performed in triplicate at 25 ℃, and the average of three recordings per measurement was reported as ζ potential (error bars correspond to the standard deviation-value). The organic content in loaded and functionalized particles was determined by TGA. Thermogravimetric analyses were carried out on a TGA/SDTA 851e Mettler Toledo balance (Mettler Toledo Inc., Schwarzenbach, Switzerland), using an oxidant atmosphere (air, 80 mL/min) with a heating program consisting of a heating ramp of 10 ℃ per minute from 25 ℃ to 1000 ℃ with three isothermal heating steps of 30 min at 37 ℃, 100 ℃ and 1000 ℃. Fluorescence spectroscopy measurements were performed with a JASCO FP-8300 Spectrofluorometer equipped with an FMP-825 microplate reader (JASCO, Easton, United States). UV-Visible spectra were recorder with a JASCO V-650 spectrophotometer. EOCs quantification was performed by HPLC with Novapack C18 column (Waters Alliance® e2695, Milford, MA, USA).

2.5. In vitro digestion assay

The employed artificial fluids for the *in vitro* digestion assays and the residence times in each organ were based on the protocol described by Versantvoort et al.[84] The pH of the fluids was adjusted to the appropriate value (6.8 ± 0.1 for saliva, 1.3 ± 0.1 for stomach, 8.1 ± 0.1 for duodenal and 8.2 ± 0.1 for bile) with NaOH (1M) or HCl (37%). All the experiment was performed at 37 ℃. In a typical experiment, four samples of 10 mg of M41-RhB-L were placed in different vials and the simulated fluids were added in temporary order mimicking the transit of food along the intestinal tract. Each sample was used to reach a subsequent stage of the digestion and samples were taken from each of the phases of the digestion process. Hence, 3 mL of simulated saliva were added to the first sample in order to simulate the mouth stage. The second sample was also suspended in 3 mL of simulated saliva, and after 5 min of incubation, 6 mL of gastric juice were added. Finally, the two remaining samples were treated as the previous one and, to simulate the intestinal stage, after 120 min stirring with gastric juices, 3 mL of bile, 6 mL of duodenal fluid

and 1 mL of 1 M $NaHCO_3$ were added to both, plus 5 mg/mL of β-gal to only one of them, and these mixtures were shaken until completing the theoretical time of intestinal stay (5 h). The aliquots taken from each digestion-step were separated by centrifugation and the released RhB from the pore voids of M41-RhB-L to the supernatant was determined by means of its fluorescence signal (λ_{exc} = 555 nm, λ_{em} = 572 nm). The pellets were collected for further characterization. In order to remove the major part of the salts and proteins present in the simulated fluids, the M41-RhB-L particles in each sample were collected by centrifugation, separated from the supernatant, washed with deionized H_2O until neutral pH and dried under vacuum.

For the observation of the fluorescence-confinement of the RhB into the M41-RhB-L during the *in vitro* digestion process, different aliquots were taken directly from each *in vitro* digestion fluid without β-gal. 5 µL of each digestion steps were taken and dropped onto glass coverslips, and confocal laser scanning microscopy (CLSM) images were acquired in a Leica TCS-SP5 confocal microscope with an oil-immersion 63x objective, and excitation wavelength λ_{ex} = 546 nm. Also, images of a suspension of 1 mg/mL of M41-RhB-L in deionized H_2O at neutral pH were taken as control.

2.6. Cargo release experiments

To perform the payload release experiments from M41-EOC-L materials (M41-Thy-L, M41-Eug-L and M41-Cin-L), a batch mode experiment was carried out. Hence, 14 samples of 2 mg for each M41-EOC-L were placed in microtubes, and suspended half of them in 1 mL of PBS (pH 7.4), and the other half in 1 mL of β-gal solution in PBS (5 mg/mL) and were kept under stirring at 37 ℃. At scheduled times (2 min, 30 min, 1 h, 3 h, 6 h, 9 h and 24 h), aliquots were taken and centrifuged in order to remove the suspended microparticles. Proteins present in the supernatants were precipitated with MeOH (1 mL) at -14 ℃, and the mixture was centrifuged. EOC delivery from M41-EOC-L to the supernatant solution was analyzed by HPLC (see below).

2.7. EOCs quantification

The EOC concentration in the aliquots of each specific section ((i) cargo release experiments, section 2.6; (ii) EOCs permeability across the Intestinal barriers, section 2.13; and (iii) *in vivo* pharmacokinetic assays, section 2.17) was analyzed by HPLC. For *Thy* and *Eug* molecules, the mobile phase used was ACN:H_2O 50:50 v/v with 0.05% of TFA and absorbance detector using λ_{ex} = 280 nm. For *Cin*, the mobile phase was ACN:H_2O 85:15 v/v with 0.05% of TFA and λ_{ex} = 254 nm. 200 mL of volume injection were used and a flow of 1 mL/min was fixed. The methods were previously validated with adequate linearity, precision and accuracy (R > 0.99 and coefficient of variation < 5%).

2.8. Caco-2 cell culture conditions

Human colon adenocarcinoma Caco-2 cells were acquired from the American Type Culture Collection (ATCC), and they were grown in DMEM medium supplemented with 10% FBS, 1% penicillin/streptomycin antibiotic and 1% nonessential aminoacids. Cells were maintained at 37 ℃ in incubator, with a humidified controlled atmosphere composed of 5% CO_2 and 95% air and underwent passage when 80% confluence was reached.

2.9. MTT cell viability assay

Caco-2 cell viability was determined by means of the MTT method. With this aim, Caco-2 cells were seeded in 96-well plates at a density of $2 \cdot 10^4$ cells/well and they were incubated for 24 h. Then, all the tested M41-EOC-L particles were suspended in concentrations corresponding to payloads of 50, 100 and 200 µM. The M41-RhB-L system was used as control ($control_{part}$), in particle concentrations of 250, 500 and 750 µg/mL (to match the maximum concentrations tested in each M41-EOC-L). Each particle-concentration was tested in 8 wells and compared with cells absent of any MSP as negative control. Two independent experiments were performed to assess the assay-repeatability. After 24 h and 48 h of incubation, cells were washed with PBS in order to remove MSPs, and then 100 µL of MTT solution

in non-supplemented DMEM (0.5 mg/mL) were added to each well. The plates were incubated for 2 h, after what the supernatant was removed, and 100 µL of DMSO were poured into each well. The plate was softly shaken until complete solution of formazan crystals, and its absorbance was finally measured at λ_{exc} = 550 nm.

2.10. Caco-2 cell monolayer culture

To obtain intestinal epithelium membranes, Caco-2 cells were seeded in 6-well plates onto PET porous Millicell hanging cell culture inserts (Merck Millipore) (area 4.2 cm^2; pore size 0.4 µm) in 2 mL of medium at a seeding density of $2.5 \cdot 10^5$ cells per insert in the apical side. Then, 3 mL of medium were added in the basolateral compartment. Culture medium was changed every 2-3 days and the seeded cells were grown for 21 days, to allow cell differentiation into enterocyte-like cells, characteristic enzymes production and tight junctions formation.[72] Before starting all the experiments, transepithelial electrical resistance (TEER) of each insert was measured to confirm the correct formation of confluent intestinal monolayers.

2.11. Transepithelial Electrical Resistance (TEER) Measurements

The integrity of the monolayer formed by differentiated Caco-2 cells was evaluated by means of TEER measurements, before and after 24 h incubation for all the treatments, using a chop-stick electrode device (Millicell-ERS voltmeter, Millipore). TEER values were expressed as $\Omega \cdot cm^2$ and were calculated according to the equation [1]:

$$TEER = [\Omega_{\text{cell monolayer}} - \Omega_{\text{insert (cell-free)}}] \times \text{insert area (4.2 cm}^2\text{)} \quad [1]$$

Inserts with TEER value > 600 $\Omega \cdot cm^2$ were considered valid for conducting the corresponding experiments.

2.12. Intestinal barriers treatment with M41-#-L and free EOCs

The Caco-2 cell epithelia were incubated in cell culture medium with each treatment, free EOCs (200 µM) and M41-#-L solids (concentration of particles corresponding to a 200 µM EOC-payload), during the time required to perform the

assay: 90 min for EOCs permeability (see section 2.13) and 24 h for the other interaction studies (Lucifer yellow, section 2.14, and inflammatory response measurement, section 2.15). Also, some cell inserts were incubated with free medium at the same conditions as negative controls. TEER measurements were performed before and after each treatment, to ascertain the validity of the membranes before the assay, and to know the treatment's effect on them.

2.13. EOCs permeability across the Intestinal barriers

Permeability assays were performed by using Caco-2 cell monolayers. EOCs-permeability across the membranes was performed in the apical-to-basolateral direction for the M41-EOC-L materials and the free EOCs. The transport experiments were performed in HBSS at 37 ℃ using an orbital shaker (50 rpm). The calculated concentration of particles corresponding to a 200 µM EOC-payload ((750 µg/mL for M41-Thy-L; 500 µg/mL for M41-Eug-L; 300 µg/mL for M41-Cin-L) and 200 µM free EOC) were pipetted in the apical (*ap*) side of the inserts in 2 mL of HBSS. Then, 100 µL samples were taken from the basolateral (*bl*) side of inserts after certain times of incubation (15, 30, 45 and 90 min), and the withdrawn volume was replaced with 100 µL of fresh HBSS buffer. EOC-concentrations of each sample were quantified by HPLC (see section 2.7), and the accumulated amounts were plotted vs time (up to 90 min). The EOCs' permeability from *ap* to *bl* (P_{ab}) values were calculated as the slope of the obtained line.

2.14. Lucifer Yellow (LY) Assay

The integrity of the enterocyte-like-layer after 24 h of treatment with free EOCs and M41-#-L was evaluated by means of LY assay. This test measures the ability of this paracellular marker to cross the cell monolayer. After 24 h of incubation with the different treatments (M41-#-L, free-EOCs and non-treated controls), apical and basolateral media were collected and cell layers were washed twice with HBSS. *Bl* compartments were filled with HBSS, and the *ap* side with a LY solution in HBSS (0.4 mg/mL). Cell layers were incubated for 2 h at 37 ℃, and then, 100 µL aliquots were taken from each insert at the *bl* side (including cell-free

inserts). The aliquots were added into a black 96-well plate and their LY content was determined by fluorometric measurements (λ_{ex} = 428 nm, λ_{ex} = 536 nm). The transported LY percentage from-*ap*-to-*bl* side after treatment was compared to the transported LY in the control monolayers.

2.15. Inflammatory response measurement

Inflammatory cytokine and chemokine release (IL-8, MCP-1) was measured in the apical media from the enterocyte layers after 24 h of treatment with the corresponding M41-EOC-L and free EOCs. For the measurement, a Bio-Plex 1 MAGPIX TM Multiplex Reader (Bio-Rad) was employed according to the manufacturer-described-procedure. The cells were stimulated with 10 µg/mL LPS as positive control.

2.16. Cell Staining and Confocal Microscopy

For the observation of the microdevices' interaction with cells, Caco-2 cells and enterocyte-like layers were incubated for 244 h with M41-RhB-L and M41-EOC_{C6}-L. After the incubation, both single Caco-2 cells and monolayers were washed twice with PBS and fixed with 4% PAF for 30 min at room temperature. After washing, cells were permeabilized with 0.1% Triton ×100 for 5 min, and the process was stopped with blocking buffer solution (1% BSA in PBS) for 20 min. Cells were then stained with 0.1 nM Alexa Fluor 488 Phalloidin (M41-RhB-L treated cells) or Alexa Fluor 594 Phalloidin (M41-EOC_{C6}-L treated cells) for 30 min to localize actin microfilaments. In order to localize cell nuclei, all the cells were stained with Hoechst 33342 at a concentration of 5 µg/mL for 5 min. CLSM images were acquired using excitation wavelengths λ_{ex} = 405, 488, and 546 nm. To investigate the subcellular localization, living Caco-2 cells treated with M41-EOC_{C6}-L and M41-RhB-L were incubated for 1 h at 37 °C with LysoTracker Red DND-99 and LysoTracker Green DND-26 in DMEM, respectively, at a concentration of 75 nM. Nuclei and cell membranes were stained following the procedure previously described, excluding cell fixation.

2.17. In vivo pharmacokinetic assays

In vivo experiments with M41-Cin-L in a Wistar rat model were carried out in order to study the concentration of cinnamaldehyde, free and encapsulated, in plasma and in the different gastrointestinal sections. The animal study was approved by the Scientific Committee of the Faculty of Pharmacy Universidad Miguel Hernández, Elche (project reference DI-MBS-02-15) and followed the guidelines described in the EC Directive 86/609, the Council of the Europe Convention ETS 123 and Spanish national laws governing the use of animals in research (Real Decreto 223/ 1988, BOE 67, 18-3-98:8509-8511). To perform the *in vivo* assays, 12 male Wistar rats were previously fasted for 4 h. Subsequently, 6 animals were assigned to the trial group (g_T), who was orally administered 150 mg of M41-Cin-L (containing 13.6 mg of *Cin*). The other 6 animals were assigned to the control group (g_C), who was administered an equivalent dose of free *Cin* (13.6 mg). To carry out the experiments, both groups were organized into two batches with 3 subjects per batch (n = 3), one in which the assay was finished at 2 h (b_{2h}), and another in which the digestive process was allowed to complete for up to 4 h (b_{4h}). Plasma samples were collected at 30, 45, 60, 90 and 120 min from the b_{2h} batch of each group, and at 30, 45, 60, 90, 120, 180 and 240 min from the b_{4h} batch, and then the animals were sacrificed. The GIT of all the animals were excised, and divided into their corresponding physiological segment (stomach, duodenum, jejunum, ileum and colon). The tissues were washed with PBS, in a three-fold volume of the tissue's weight, and finally homogenized using a glass homogenizer with Teflon pestle. Both blood samples and homogenized tissues were centrifuged (8000 rpm, 10 min), and deproteinized with cold methanol. The concentration of *Cin* in each sample was determined by HPLC following the methodology described in section 2.7.

3. Results and Discussion

3.1. Design, synthesis and characterization of the prepared solids

Mesoporous silica microparticles (M41) were prepared by the "atrane route" following previously described procedures.[16] A fluorophore (rhodamine B, RhB) and three EOCs (*Thy*, *Eug* and *Cin*) were loaded in the M41 microparticles (solids M41-#). M41-# supports were then reacted with APTES (solids M41-#-N) and lactose was attached to the solids by a condensation reaction between the saccharide's anomeric carbon and the APTES-amino group to give the final capped solids (M41-#-N-L). As the pores are first loaded with RhB or EOCs the functionalization process with APTES and lactose is expected to occur mainly on the external surface of the M41 microparticles as shown in Scheme 1. In addition, EOCs-loaded lactose-capped materials with an additional hydrophilic fluorophore (coumarin 6, C6) were also prepared to carry out microscopy experiments.

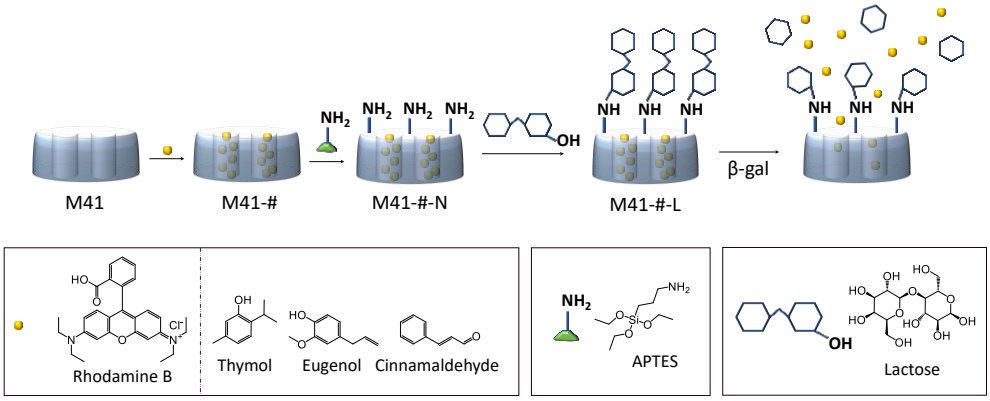

Scheme 1. Representation of the M41-EOC-L synthesis process and subsequent cargo delivery performance under β-gal enzymatic action.

The synthesized solids were characterized by standard techniques. Normalized X-ray diffractograms of all the solids (MCM-41 "as made", calcined particles (M41) and loaded-and-functionalized solids) are shown in Figure 1A. Four low-angle peaks can be observed in all the patterns, which are characteristic of a hexagonal channels-arrangement, and indexed from left to right as (1 0 0), (1 1 0), (2 0 0) and (2 1 0) Bragg reflections, respectively. Once the as made material was calcined, it can be observed that the (1 0 0) peak of the M41 particles is shifted to higher 2θ values compared with the as made one, phenomenon related with cell contraction due to the condensation of silanols in the calcination process. It also can be appreciated that in the curves corresponding to all the final loaded and functionalization solids, the reflections (1 1 0), (2 0 0) and (2 1 0) are vanished because of the high amount of organic matter which fills the pores. Although the increase in organic matter of the solids decreases the definition of their peaks, the clear presence of the peak (1 0 0) in all the diffractograms demonstrates that neither the calcination nor pore filling and functionalization processes modify the initial MCM-41 structure.

The mesoporous structure of the starting solid M41, and its persistence in the final solids after the loading and functionalization steps, was also confirmed through TEM images (Figure 1B). In these images, the typical matrix of the MCM-41 particles could be appreciated and visualized as alternating white and black stripes corresponding to the hexagonally-arranged channels characteristics of the material's structure. Moreover, the hexagonal stacking was visible when the pores were frontally seen in the image. Furthermore, an estimation of the particles' size was made by means of cited images, by measuring 68 particles randomly chosen and obtaining from the majority population an average of 2.2 ± 0.8 μm (figure 1B f).

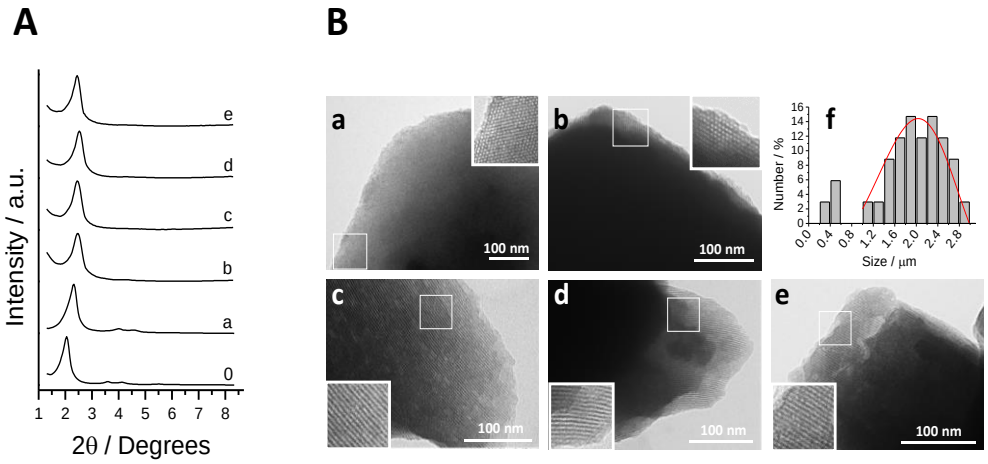

Figure 1. Normalized powder X-ray patterns of all the synthesized solids. From bottom to top, the reported solids are the as made material (0), the calcined support M41 (a) and the loaded and functionalized final materials: M41-RhB-L (b), M41-Thy-L (c), M41-Eug-L (d) and M41-Cin-L (e). **B**) TEM micrographs of starting bare material M41 (a), and loaded and functionalized solids M41-RhB-L (b), M41-Thy-L (c), M41-Eug-L (d) and M41-Cin-L (e), and particle size estimation (f). Insets correspond to a 2x magnification of the selected areas.

The N_2 adsorption-desorption isotherm of the calcined support (M41) is shown in Figure 2. A typical curve of a mesoporous solid consisting of an adsorption step at P/P_0 values between 0.1 – 0.3 is observed. The curve fits with a type IV isotherm, in which the increase produced in the gas absorption corresponds to a condensation of the N_2 molecules within the mesopores of the inorganic structure.[85] The absence of hysteresis loop in this interval ($0.1 < P/P_0 < 0.3$) and the narrow pore diameter distribution suggest the existence of cylindrical mesopores with a uniform structure, in which the processes of gas adsorption and desorption are developed following the same mechanism. The N_2 adsorption-desorption isotherm of M41-RhB-L solid is typical of mesoporous systems with practically filled mesopores (Figure 2). The high amount of organic matter in M41-RhB-L avoids the adsorption of gas molecules, and consequently, the registered curve is completely flat. Accordingly, an absence of appreciable mesoporosity is observed and relatively low N_2 adsorbed quantity and surface area values were obtained (see Table 1).

Solids containing EOCs loaded into the pore voids could not be analyzed by this technique due to the EOCs volatility that would clog the porosimeter during the degassing pretreatment of the samples.

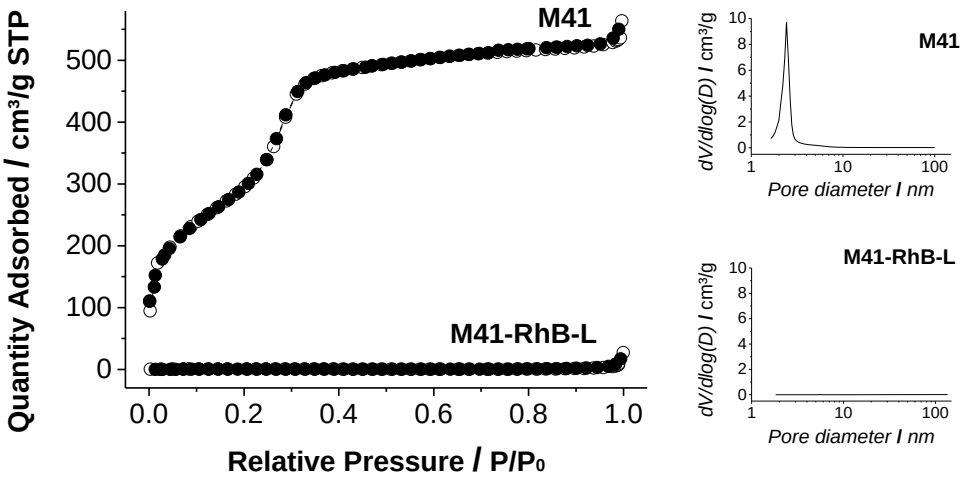

Figure 2: Left: Nitrogen adsorption (○) – desorption (●) isotherms of the calcined starting material M41 and M41-RhB-L. Right: pore distribution graphs of M41 (top) and M41-RhB-L (bottom).

Table 1. BET specific surface values, pore volumes and pore sizes calculated from the N_2 adsorption–desorption isotherms for selected materials.

	S_{BET} ($m^2\ g^{-1}$)	Pore Volume [a] ($cm^3\ g^{-1}$)	Pore size [a, b] (nm)
M41	1098.3	1.0	2.5
M41-RhB-L	2.6	0.0	-

[a]Pore volumes and pore sizes are restricted to intraparticle mesopores. [b]Pore size was estimated by using the BJH model applied on the adsorption branch of the isotherm.

The different stages of the synthesis process, from loading to final functionalization with lactose through prior functionalization with APTES were followed by ζ potential measurements. ζ potential (Figure 3) of the starting M41 solid is negative due to the presence of silanolate groups. This negative value is reduced for the loaded materials M41-Thy and M41-Eug. Moreover, a positive ζ potential for M41-Cin is observed, possibly due to the formation of some hemiacetal groups between the aldehyde group present in the *Cin* molecule and the silanolate groups in the M41-surface present at neutral pH, which compensates their initial negative charge. The alcohol which form the active groups of *Thy* and *Eug* does not react with the M41 surface, ergo no important modifications of the surface's charge is observed. Following with the next functionalization step, it can be appreciated how the APTES-moiety makes the external charge of the particles more positive due to the primary amines. Functionalization with lactose results in final solids still with a positive ζ potential.

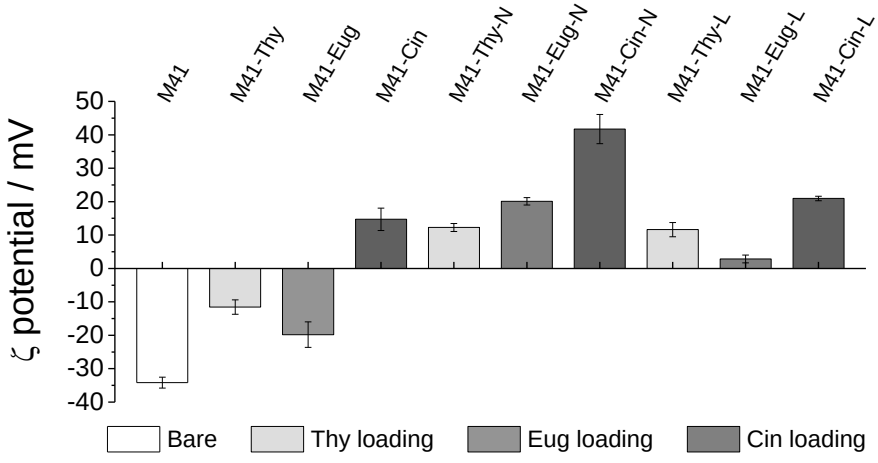

Figure 3. ζ potential values for solids in the different synthesis-stages. From left to right, bare material (M41), loaded supports (M41-EOC), APTES-functionalized materials (M41-EOC-N) and final gated microdevices (M41-EOC-L).

The contents of organic matter of all the loaded and functionalized M41-EOC-L solids were determined by TGA, and they are listed in Table 2 as function of the remaining SiO_2 residue (μg_{OM}/mg SiO_2). In addition, in order to compare the maximum payload of EOC released from M41-EOC-L (see section 3.3) with the loaded amount of EOC, the amount of EOC released per mg of solid (μg_{EOC}/mg M41-EOC-L) are included in Table 2.

Table 2. Organic matter content (μg_{OM}/mg SiO_2) and EOC payload released (μg/mg of M41-EOC-L) for each M41-EOC-L microdevice

Solid	μg_{OM}/mg SiO_2	μg_{EOC}/mg M41-EOC-L released
M41-Thy-L	311	37.5[a]
M41-Eug-L	446	79.0[a]
M41-Cin-L	758	89.3[a]

[a]Maximum payload released (μg_{EOC}/mg M41-EOC-L) from data in section 3.3.

3.2. In vitro digestion: release profile and structure-integrity

As previously stated, the performance of *Lac* moiety as gatekeeper triggered by the enzymatic action of β-gal was reported previously by some of us.[78] Based on this knowledge, this work aims to validate the performance of the *Lac* molecular gate in biological conditions. To achieve this goal, an *in vitro* digestion assay simulating GIT conditions[84] with the M41-RhB-L model material was accomplished. This procedure not only simulates the GIT by reproducing the oral, gastric, and SI environment (Figure 4A), but also considers all the important parameters during digestion process, such as pH changes, salinity, the most relevant enzymes or the residence times (section 2.5). The obtained cargo release profiles from M41-RhB-L in the different GIT fluids are shown in Figure 4B. The procedure started with a stay of solid M41-RhB-L in the simulated saliva for 5 min (data not shown) followed by the gastric digestion step, where the gastric fluid was added. M41-RhB-L remained for 2 h in the stomach fluid, during which no release of RhB was observed. Finally, two different routes were followed to obtain the intestinal release profiles, a first

route with addition of the β-gal enzyme (5 mg/mL) in the SI simulated fluid, and a second one without β-gal addition. While the first process showed a marked cargo release to the digestive fluid, for the latter no dye release was observed. The RhB release behavior of M41-RhB-L is similar to that reported in the literature under simplified conditions (water suspensions in the absence and in the presence of added β-gal),[78] thus demonstrating that the gating mechanism is equally efficient under simulated GIT conditions.

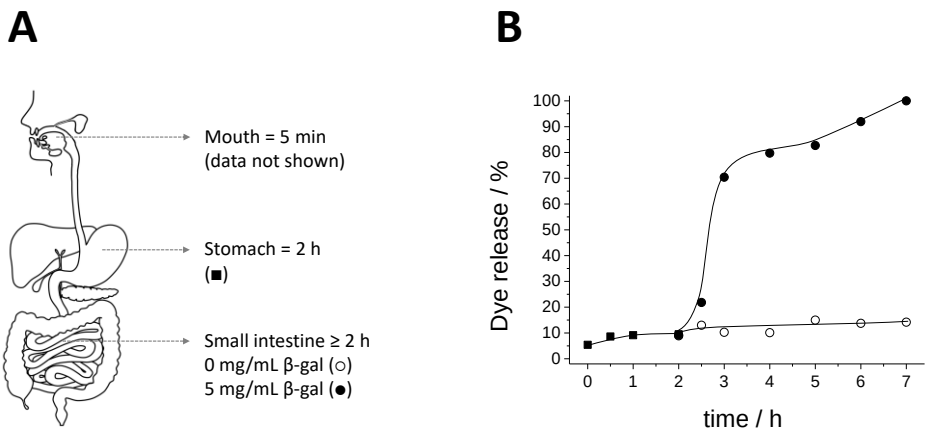

Figure 4. **A**) *In vitro* digestion scheme and retention times. **B**) *In vitro* digestion release profiles from M41-RhB-L in simulated gastric (■), and intestinal fluids in the absence (○) or in the presence of β-gal at a concentration of 5 mg/mL (●).

To study the possible degradation of the mesoporous support due to the aggressive environment of the digestive fluids (regardless of the triggering stimulus), the M41-RhB-L particles after each gastrointestinal step were studied using TEM and CLSM, and the obtained images are shown in Figure 5. The CLSM images were taken directly from the digestion fluids, while the samples for the TEM analysis were previously collected, washed and dried (for further details, see section 2.5 for TEM and section 2.15 for CLSM). TEM micrographs (Figure 5A) showed no significant changes in the M41 characteristic structure during the *in vitro* digestion. The typical striped structure was preserved from the initial material

suspended in water (a) to the particles in the presence of saliva (b), gastric fluid (c) and finally all digestive fluids in the intestinal step (d), including duodenal fluid and bile salts. A loss of contrast was observed in the final micrograph (Figure 5A (d)), possibly due to the high amount of organic matter involved in this assay.

To support the results shown in the dye release graph (Figure 4B), aliquots of the different *in vitro* digestion steps were also subjected to CLSM (see figure 5B and 5C). In these figures, the fluorescence of RhB inside the M41-RhB-L particles can be observed, both in particles suspended in water (Figure 5B (a)) and during all the digestion steps (Figure 5B, from (b) to (d)). Furthermore, complementary transmitted light of CLSM images (Figure 5C) confirmed that the cited fluorescence co-located with the particles.

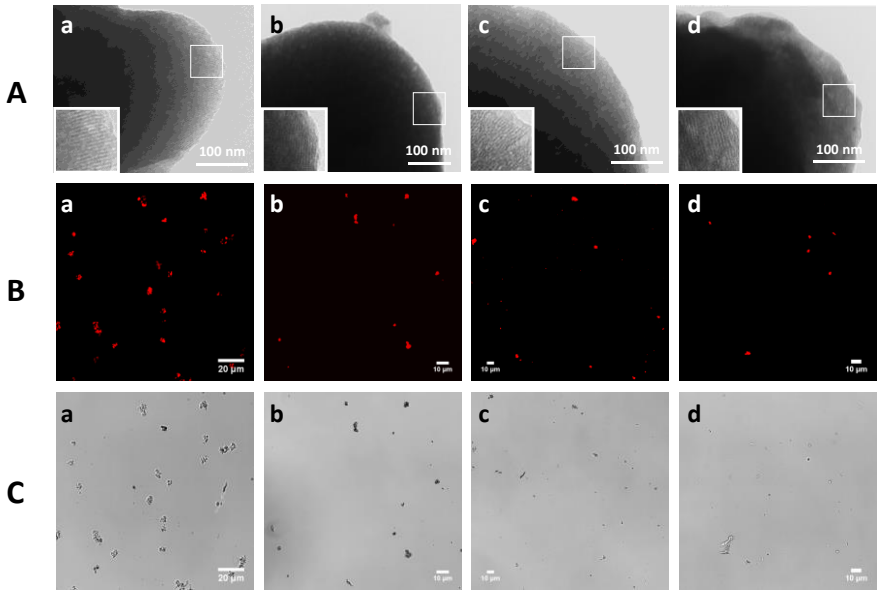

Figure 5. TEM (**A**), CLSM (**B**) and CLSM transmitted light (**C**) micrographs of M41-RhB-L suspended in water (**a**), and in the different simulated saliva (**b**), gastric fluid (**c**) and intestinal fluid (**d**), showing no degradation of the structured-material. TEM micrographs (**A**) were acquired after collecting, washing and drying several times the particles.

This result is in agreement with the release profile shown in Figure 4B, and together demonstrates the cargo-confinement into the M41 pores in absence of β-gal and the structure conservation after the *in vitro* digestion process. This result is in line with previous studies that demonstrated the stability of functionalized micro-sized M41 materials during *in vitro* digestion assays.[86]

3.3. Cargo release experiments

Once the *in vitro* control releasing ability the gated microparticles under GIT simulated conditions was demonstrated, cargo-delivery assays from M41-EOC-L were carried out in the presence and in the absence of β-gal (5 mg/mL) in PBS at 37 °C. The cargo-delivery profiles were determined by HPLC, and are shown in Figure 6.

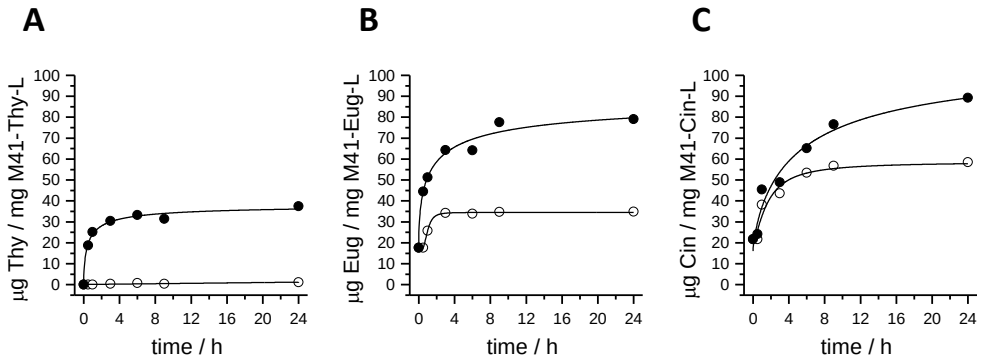

Figure 6. **A**) *Thy*, **B**) *Eug* and **C**) *Cin* release profiles from their respective M41-EOC-L solids at 37 °C, in PBS in the absence (○) and in the presence of 5 mg/mL of β-gal (●) in PBS.

M41-Thy-L shows a zero release in the absence of β-gal and reach a delivery of 37.5 µg/mg of solid in the presence of the enzyme. The amount of *Thy* released is lower than that of M41-Eug-L and M41-Cin-L, yet it is also the EOCs that is loaded in a lower amount (see Table 2). In comparison, the M41-Eug-L system (Figure 6B) presents a higher payload release than *Thy* (79.0 µg/mg solid at 24 h in the presence

of β-gal) although is this case the lactose molecular gate is not able to completely inhibit cargo release in the absence of the enzyme. A similar situation is observed for M41-Cin-L. Cargo release in the absence of β-gal is of 58 μg/mg of solid, whereas this value increases to 89 μg/mg of solid with the enzyme. Moving to the payload's delivery rate, both *Thy* and *Eug* molecules outflow from their respective M41-EOC-L solids more abruptly than *Cin*. In fact, after 3 h both M41-Thy-L and M41-Eug-L released ca. 81% of the maximum-released-payload in the presence of β-gal, while this value was only 55% for M41-Cin-L. This fact could be explained, by the formation of a hemiacetal group between a fraction of the *Cin* molecules and the silanolates present in the M41-walls, which also affects to the ζ potential of the M41-Cin-L support (see section 3.1). Even with the differences present in the M41-EOC-L solids, from their release profiles it can be concluded that *Lac* molecule was able to act as molecular gate, allowing triggering cargo delivery (this is especially so for M41-Thy-L) or allow enhanced delivery (for M41-Cin-L and M41-Eug-L) in the presence of β-gal.

3.4. In vitro Interaction studies between Caco-2 cells and M41-#-L materials

With the aim of investigating the interaction between the M41-#-L materials with the tissues present in the GIT, two different studies involving Caco-2 cells were performed: in the first one we used a simple model of undifferentiated Caco-2 cells and in the second an intestinal barrier model established from Caco-2 cells differentiation into enterocyte-like monolayers.

3.4.1. Caco-2 cell viability assays (MTT)

The viability of Caco-2 cells treated with the M41-#-L systems and free EOCs was determined by using the MTT method. The conversion of MTT (yellow-colored compound) into formazan (purple-colored compound) is directly proportional to the number of living cells, and can be spectroscopically quantified. EOCs antioxidant capacity has been reported to result in anti-inflammatory properties at low concentrations,[87–89] and with anti-cancer effects at high concentrations,[55–57,90,91] EOC concentrations in the cell assays were chosen from data reported in the

literature[55–57,87–90] and were fixed at 50, 100 and 200 μM, whereas M41-EOC-L particles were added to finally have at equivalent concentrations of EOCs (i.e. 75, 150 and 300 μg/mL for M41-Cin-L; 125, 250 and 500 μg/mL for M41-Eug-L; 190, 375 and 750 μg/mL for M41-Thy-L). Non-treated cells were used as negative control and M41-RhB-L (at concentrations of 300, 500, and 750 μg/mL) was tested to check the support-toxicity *per se* ($control_{part}$). Caco-2 cells were exposed to free EOCs and M41-#-L for 24 and 48 h, and the obtained results are shown in Figure 7.

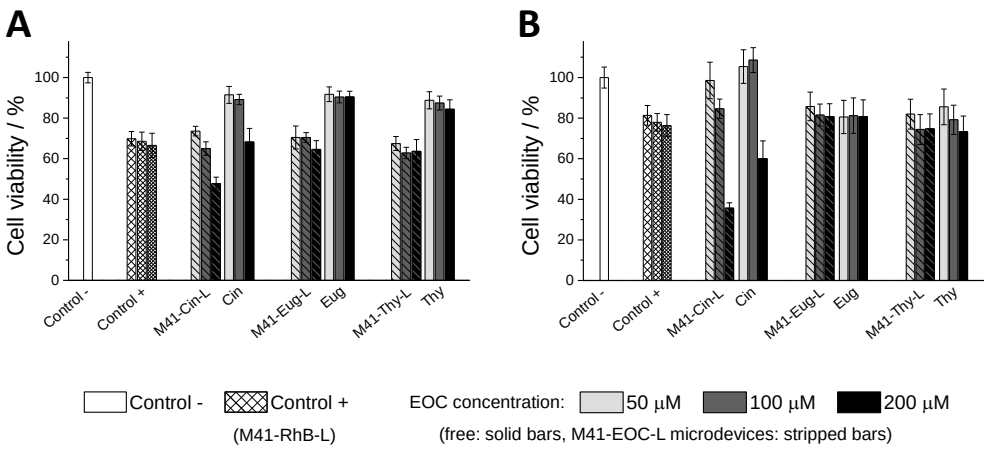

Figure 7. Cell viability of Caco-2 cells treated with the free EOCs and M41-EOC-L for **A**) 24 h and **B**) 48 h. Cell viability of free-EOCs treated cells (solid bars) and M41-EOC-L treated cells (striped bars) was compared with non-treated cells as negative control (empty white bars) and cells treated with the M41-RhB-L (striped white bars). Positive control (M41-RhB-L) bars have increasing density-mesh for increasing particle-concentration: 300, 500 and 750 μg/mL. EOCs concentration, both as free compounds or as the microdevices' released payload, was increased from 50 μM (light gray bars) to 100 μM (dark gray bars) and finally 200 μM (black bars). To achieve this payload concentration, the tested particle concentration of the different M41-EOC-L microdevices was: 75, 150 and 300 μg/mL for M41-Cin-L; 125, 250 and 500 μg/mL for M41-Eug-L; and 190, 375 and 750 μg/mL for M41-Thy-L. Data correspond to the average of two different experiments (8-well per experiment), and error bars represent their standard deviation.

Despite the exposure to critical particle concentrations such as 750 µg/mL, the high cell viability obtained for Caco-2 cells treated with M41-RhB-L (Figure 7, positive control) indicates that the lactose-functionalized M41 solid is not toxic. The slight viability-reduction that can be observed when compared with control cells could be related with cell coating due to particle sedimentation, which can increase the cellular uptake and consequently, the measured cytotoxicity.[70,92] Cell viability after 24 h upon treatment (Figure 7A) shows that free EOCs at the tested concentrations are not toxic. Only *Cin* at the highest concentration (200 µM) slightly reduces cell-viability. Toxicity assays with M41-EOC-L are similar to those found for M41-RhB-L except for M41-Cin-L at high concentration that significantly reduced cell viability to values as low as ca. 30% at 48h.

3.4.2. CLSM imaging of the Caco-2 cells' interaction with M41-#-L

The M41-#-L capability to be internalized by Caco-2 cells was investigated by CLSM. The experiments were carried out with M41-RhB-L and with solids loaded with the lipophilic fluorophore Coumarin 6 in addition to the pertinent EOC (M41-EOC_{C6}-L). Since some M41-#-L particles at high concentrations have shown to compromise Caco-2 cells viability, lower concentrations of particles (50 µg/mL) were selected. Representative photographs are shown in Figures 8 and 9. CLSM images obtained from the M41-RhB-L treated cells show high particle-internalization within the Caco-2 cells at 4 h (Figure 8A). Longer incubation times (24 h) exhibit a larger internalization of the particles (Figure 8B). Frontal and orthogonal views in the figure show the presence of particles (in red) that are localized into the cells (delimited by the cell membrane, shown in green), next to the cell nucleus (shown in blue).

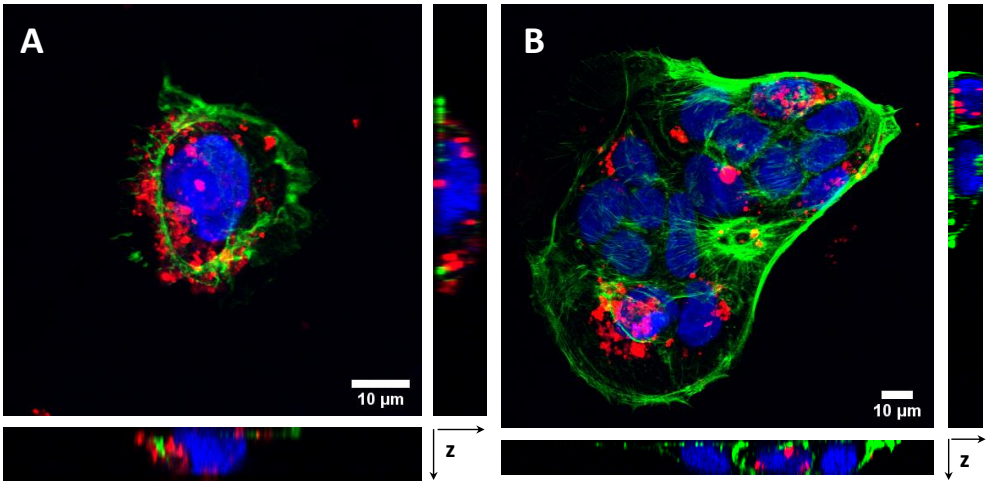

Figure 8. CLSM images of fixed Caco-2 cells after 4 h (**A**) and 24 h (**B**) of incubation with M41-RhB-L particles. Actin microfilaments are shown in green, cell nuclei in blue and microparticles in red. Lateral boxes represent z-stack projections along x–z and y–z axis.

The particles' internalization process can be carried out by cells through different mechanisms, such as phagocytosis, macropinocytosis, or clathrin- and non-clathrin-mediated endocytosis.[93] A common mechanism of internalization is phagocytosis, which ends with the fusion of the generated phagosomes with lysosomes. Entry into lysosomes generally leads to the degradation of the particles and/or the encapsulated drugs due to the acidification and enzymolysis performed in these organelles.[94] In order to know if the M41-#-L particles were or not incorporated into the lysosomes, CLSM experiments with living cells and a specific lysosomal marker (LysoTracker, see section 2.16 for details) were carried out. The obtained CLSM micrographs are shown in Figure 9, where lysosomes are shown in green and particles in red, whereas cell membranes and nuclei are shown in purple and blue respectively. As it can be seen in all the micrographs, neither M41-RhB-L (Figure 9A), M41-Thy$_{C6}$-L (Figure 9B), M41-Eug$_{C6}$-L (Figure 9C) nor M41-Cin$_{C6}$-L (Figure 9D) particles co-localize with the lysosomes.

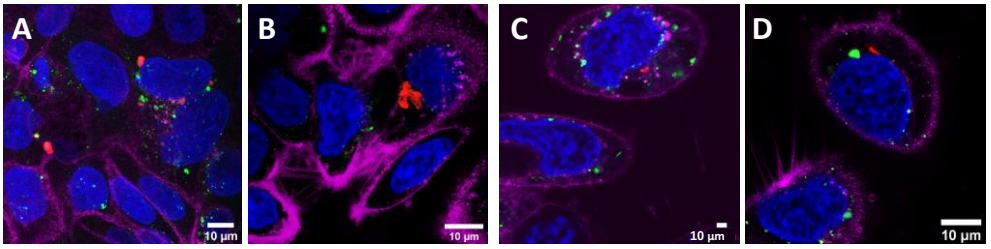

Figure 9. CLSM images of living Caco-2 cells treated for 24 h with M41-RhB-L (**C**), M41-Thy-L (**D**), M41-Eug-L (**E**), and M41-Cin-L (**F**) particles. Lysosomes and the respective microparticles were shown in green and red, respectively, in order to clearly visualize their location, whereas actin microfilaments and cell nuclei were shown in purple and blue, respectively.

Despite the high particle uptake qualitatively observed in this work, neither cell viability nor cell's shape were affected by the treatment with the studied solids at low particle concentration (Figures 7, 8 and 9).

3.5. In vitro Interaction studies between Intestinal barriers and M41-#-L

As stated before, one of the most important objectives of this work was to study the interaction of the designed microdevices with the GIT (both with *in vitro* and *in vivo* models), especially with the intestinal epithelium, since it is one of the most important cellular barriers in the mammalian organism. This barrier comprises various vitally important functions, from the nutrient uptake to the protection against pathogenic organisms, including the shelter of the intestinal microbiota.[95] Homeostasis of the intestinal barrier is compromised by numerous diseases of the digestive system, such as inflammatory bowel diseases or some types of cancer.[96–101] Alterations in the intestinal barrier, whether profitable to induce treatment or damaging due to pathologies or drug side effects, end up affecting the entire organism.[101] Therefore, the study of the interaction of drug carriers with an intestinal barrier model, either *in vitro* or *in vivo*, is essential to validate its oral administration. The *in vitro* model of intestinal epithelium generated by Caco-2 cells differentiated into enterocyte-like cells is a versatile tool for these studies.[102] It is a

low-cost assay without ethical impact, which allows evaluating the effectiveness of systems in an early stage of development. Furthermore, and as a key fact for the performance of the particles studied here, the intestinal barrier model is capable of producing β-gal with an activity similar to that of the human intestine.[34,76,79]

This *in vitro* model of intestinal barrier was obtained establishing a cell layer by seeding and growing human intestinal epithelial cells for 21 days onto porous inserts.[76] The procedure is detailed in section 2.10 and outlined in Scheme 2. Transepithelial electrical resistance (TEER) measurements were performed before each assay (see section 2.11 for details), and they verified the complete membrane formation to ensure the development of its characteristic structures, such as microvilli and tight junctions between cells. Intestinal barriers were exposed to the maximum particle concentrations necessary to release an EOC payload of 200 µM, as it was done with undifferentiated Caco-2 cells (section 3.4, *vide supra*), to perform the assays described below.

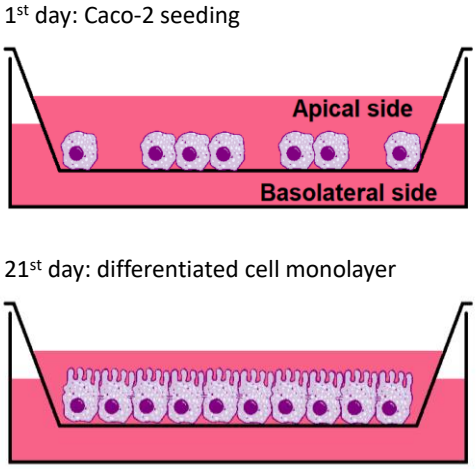

Scheme 2. Representation of the Caco-2 seeding and differentiation after 21 days to intestinal barrier *in vitro* model.

3.5.1. EOCs permeability through the Intestinal barriers

The permeability assay measures the speed of passage of a compound through the intestinal membrane, from the apical (*ap*) compartment to the basolateral (*bl*) side, during the assay time (90 min). Apical to basolateral permeability (P_{ab}) values of EOCs were determined using the Caco-2 monolayers as an *in vitro* model able to predict human absorption, simulating the passage of compounds from the intestinal lumen (*ap*) to the plasma (*bl*) across the intestinal membrane.[92,102] To perform the assay, EOCs (free or encapsulated into M41-EOC-L microdevices) were placed in the *ap* side, and during the 90 min of incubation, different samples were taken from the *bl* side. Calculated P_{ab} values of the different EOCs, both free and encapsulated into the M41-EOC-L microdevices, are shown in Figure 10, where also the P_{ab} value of Metropolol has been included as permeability reference standard.

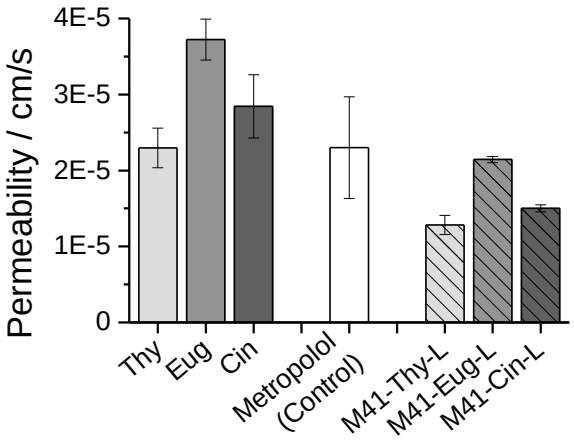

Figure 10. Apical to basolateral permeability (P_{ab}) values obtained from the intestinal membrane treatment with the three different EOCs, both free (solid bars) or encapsulated into the M41-EOC-L microdevices (striped bars). Metropolol's permeability values were also added as standard permeability reference (white bar). Provided data represent the average of three different experiments measured in triplicate, and the error bars represent the standard deviation.

The depicted data in Figure 10 show high P_{ab} values for the free EOCs compared to the reference standard, thus being able to define them as high permeability compounds. These results are consistent with the lipophilic nature of these EOCs,[60,61] which causes them to rapidly diffuse through the epithelial membrane. However, when EOCs were encapsulated into the M41-EOC-L microdevices, their P_{ab} values become lower for the three EOCs tested, even lower than the standard reference. This result indicates that the EOCs loading and protection in the designed system slows down the payload's release transport across the monolayer. This reduction of P_{ab} values is especially interesting as it would mean that the designed carriers could produce *(i)* the prevention of drug access to systemic circulation, *(ii)* the improvement of the therapeutic efficacy in the colon, *(iii)* the reduction of systemic toxicity and *(iv)* the minimization of adverse side effects.

3.5.2. Intestinal membrane treatment with free EOCs and M41-#-L

Once studied the effect of encapsulation on EOCs' permeability, the next step to study the interaction of microdevices with the intestinal membranes was to evaluate the effect of their treatment during longer exposure times. The enterocyte-like membranes were exposed for 24 h to a critical particle concentration, necessary to release a payload's concentration of 200 µM. The integrity of the membranes after treatment was determined by TEER (*Transepithelial electric resistance*) measurement and by the percentage of transported LY (*Lucifer yellow*) from *ap* to *bl* side (Figure 11A and 11B, respectively).

As it can be observed in the graphs, TEER values of monolayers treated with free-EOCs, and treated with the M41-Thy-L and M41-Eug-L supports did not differ from those obtained from the negative control (untreated membranes, white bar) or the $control_{part}$ (M41-RhB-L, black bar). However, the TEER values of the monolayers treated with M41-Cin-L were much lower than the control ones, which could be related with an alteration produced in the intestinal epithelium.

Focusing on the transport of LY, a paracellular marker that manifests membrane-alterations, it can be seen that the values of all the treatments were similar to the control, with the same exception of the M41-Cin-L system. From the obtained data, it can be deduced that the M41-#-L system does not alter the intestinal-membranes-viability *per se*. Only the M41-Cin-L system causes a response in the epithelial membranes, which is consistent with the Caco-2 cell viability data obtained in section 3.4 and also with the EOCs permeability study (section 3.5.1, *vide supra*). The increased cytotoxicity for Caco-2 cells of *Cin* when it is encapsulated and its reduced permeability trough the membranes (increasing its residence time in the *ap* side of membranes) may explain both the TEER and LY results.

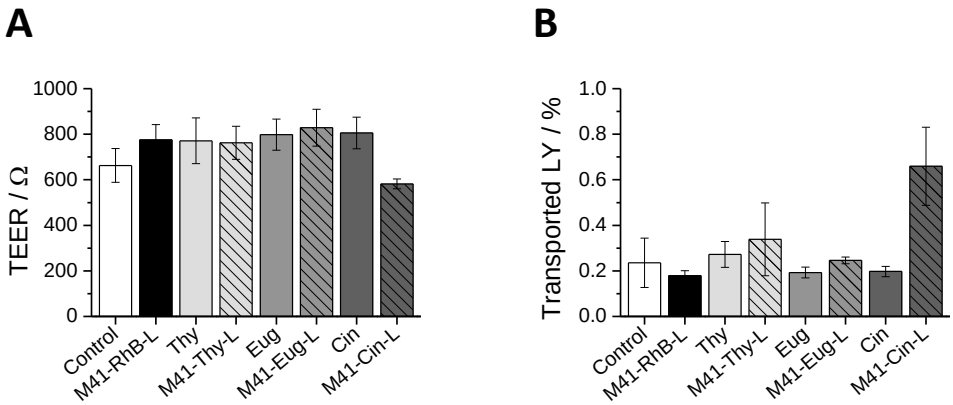

Figure 11. **A**) TEER measurement values of non-treated intestinal barriers as negative control (white bar), treated with M41-RhB-L non-active microdevice as positive control (black bar) and intestinal barriers after 24 h of exposure to free EOCs (solid bars) or encapsulated into the M41-EOC-L microdevices (striped bars). **B**) Transported LY (%) through the intestinal barrier after 24 h of exposure to free EOCs (solid bars) or encapsulated into the M41-EOC-L microdevices (striped bars) compared with non-treated membranes as negative control (white bar) or treated with M41-RhB-L (black bar). Data correspond to the average of three different experiments measured in triplicate, and error bars represent their standard deviation.

3.5.3. *Inflammatory Response of Intestinal Epithelium to M41-EOC-L and free EOCs*

It has been reported in the literature that an inflammation response of the intestinal epithelium can be triggered by its exposure to different materials, depending on their physicochemical characteristics.[103–105] Focusing on studies with silica particles, micro-sized silica particles have been proved to be less aggressive than nano-sized ones, and furthermore, the inflicted damaged is reduced when their surface was functionalized with organic moieties.[103] The present section aims to know the existence of an inflammatory reaction produced in the intestinal membranes exposed to free EOCs or M41-EOC-L. Hence, the secretion of two inflammatory cytokines, IL-8 and MCP-1, in the *ap* media was measured to evaluate the monolayer inflammatory response. IL-8 and MCP-1 were selected as monitored cytokines due to their frequent increase in both Caco-2 cultures subjected to inflammatory agents[106,107] and in patients with inflammatory diseases.[108,109]

The cytokine production values of the treated-membranes with the different treatments in an EOC concentration of 200 µM (both free and in M41-EOC-L) for 24 h was measured. The obtained values are shown in Figure 12, which also shows data obtained from untreated-cells and cells treated with lipopolysaccharide (LPS) as negative and positive controls, respectively. The IL-8 levels of cells treated with free EOCs and M41-EOC-L (Figure 12A) are slightly higher than the negative control, but considerably lower than that measured in LPS-treated membranes. Furthermore, the M41-Cin-L support has the highest IL-8 production among all the performed treatments, closely followed by the M41-Thy-L.

In relation with the MCP-1 cytokine it can be observed in Figure 12B that *Eug* treatment of the membranes increases its levels, both in the free and the encapsulated administrations. Moreover, in the case of the *Cin* the treatment with the M41-Cin-L produces very high values of MCP-1, comparable with the secretion of LPS-stimulated membranes, and quite higher than the treatment with free-*Cin*. From a general view, EOCs encapsulated in M41-EOC-L promote a greater

inflammatory response than the corresponding free compounds. This is especially so for is M41-Cin-L.

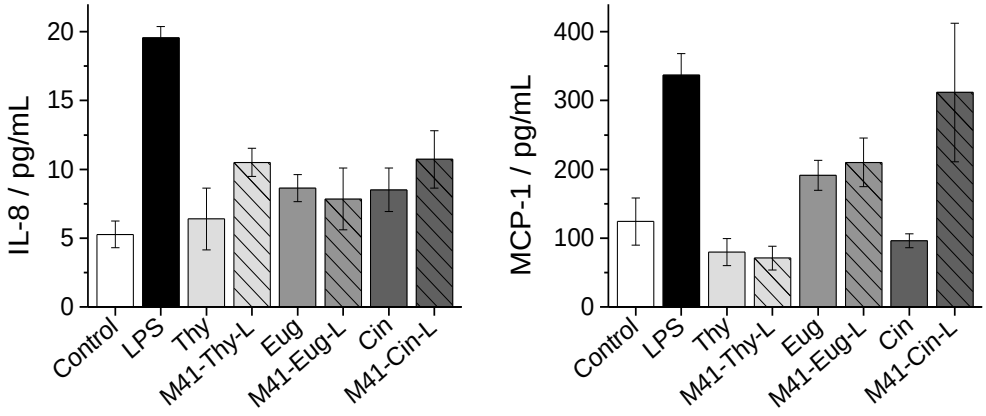

Figure 12. **A**) IL-8 and **B**) MCP-1 cytokine production in the apical compartment as inflammatory response of intestinal barriers exposed to the quoted treatments. Non-treated control intestinal barriers (white bar), treated with LPS as inflammatory control (black bar) and intestinal barriers after 24 h of exposure to free EOCs (solid bars) or released from M41-EOC-L (striped bars). Provided data represent the average of three different experiments measured in triplicate, and the error bars represent the standard deviation.

3.5.4. CLSM imaging of the intestinal barrier's interaction with M41-#-L

In addition to the previous assays, the M41-#-L interaction with enterocyte-like membranes was also investigated by means of CLSM. Since M41-Cin-L particles at high concentrations produce membrane alterations, a low particle concentration (50 μg/mL) was selected to perform microscopy assays. Figure 13 shows CLSM micrographs of enterocyte membranes treated with M41-RhB-L (Figure 13A) and M41-Cin_{C6}-L (Figure 13B), after 24 h. Microscopy assays were performed with the other two M41-EOC_{C6}-L systems, but due to the results similarity and the images-redundancy, data are not shown.

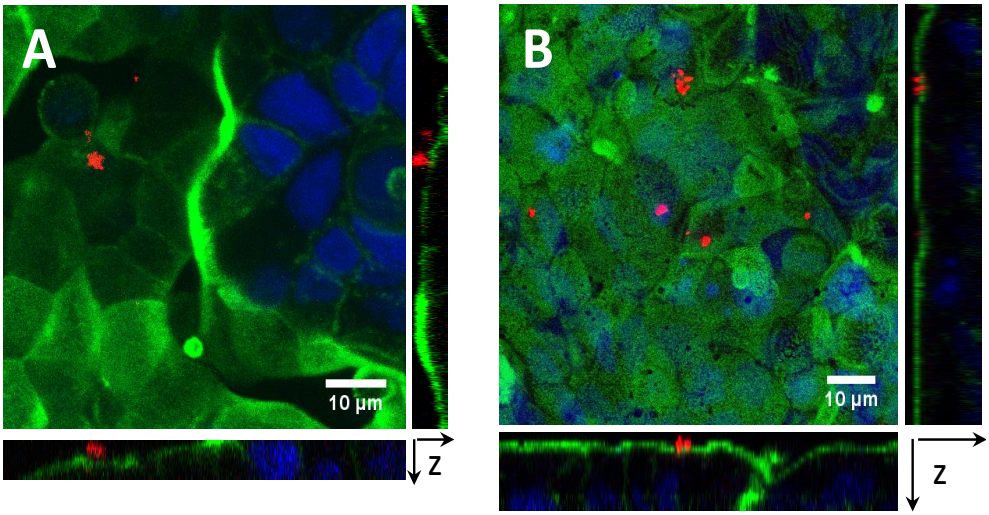

Figure 13. CLSM images of confluent intestinal barriers after 24 h of exposure to M41-RhB-L (**A**) and M41-Cin_{C6}-L (**B**). Actin microfilaments (stained with Alexa Fluor Phalloidin)) in green, cell nuclei (stained with Hoechst 33342) in blue, and M41-#-L particles in red (see section 2.16 for details). Lateral boxes represent z-stack projections along x–z and y–z axis.

As it can be seen in Figure 13, few spots corresponding to the silica particles can be seen. The images confirm, qualitatively and from a morphological point of view, that the treatment with this particle-concentration do not affect the membrane integrity. Moreover, CLSM z-sectioning of the intestinal membrane demonstrate the extracellular particle-localization. As expected from comparison with similar studies in the literature,[110] the particle-internalization by the enterocyte membranes was much lower than the observed in undifferentiated Caco-2 cells (see Figure 8A and 8B). As it has been reported in multiple studies, the particle-uptake by the intestinal endothelium is reduced due to the existence of tight junctions between cells and a dense brush border of microvilli.[102,110,111] Therefore, the non-internalization of the microdevices by the intestinal membranes would favor their permanence in the intestinal lumen that jointly with the triggering action of the β-gal secreted by the microvilli may to extend the effect of the encapsulated EOC-payload even reaching the large intestine.

3.6. In vivo pharmacokinetic assays

Due to the existing constraints of *in vitro* models, where certain parameters are difficult to simulate (*e.g.* exact enzymatic action, real composition of fluids and their pH, gastric emptying and digestive motility, exact mechanisms of internalization across membranes, etc.) we carried out an *in vivo* pharmacokinetic study with M41-Cin-L as *(i)* it exhibited the highest EOC-loading efficiency, *(ii)* it reduced Caco-2 cell viability to the lowest values and with the lowest particle concentration, *(iii)* it achieved the greater pro-inflammatory response in the enterocyte monolayers, necessary for a regenerative action, and *(iv)* the *Cin*-transport through the membrane was twice slowed when compared with free-*Cin*.

To perform the pharmacokinetic studies, male Wistar rats were divided into two groups (n = 6 in each group). Subjects in control group (g_C) were orally administered 2 mL of *Cin* solution (13,8 mg *Cin* in 2 mL PBS), and subjects from the second group (g_T) were orally administered with 150 mg of M41-Cin-L (equivalent *Cin* payload of 13,8 mg) suspended in 2 mL of PBS. Additionally, both groups were organized into two batches (n = 3 in each group), one in which digestion assay was stopped after 2 h (b_{2h}), and a second group in which the digestion was allowed to complete for 4 h (b_{4h}). These two batches were stablished for the experiment since GIT samples were needed in short times where the animals had not excreted the treatments (2 h), but plasma samples were needed up to longer times (4 h) for the pharmacokinetic profile of *Cin*.

After the treatments' administration and subsequent plasma sampling, animals were sacrificed (batch b_{2h} at time = 2 h, and batch b_{4h} at time = 4 h) and their GIT were excised to quantify the *Cin* concentration in the different GIT sections. The experiment's design is outlined in Scheme 3, and although the GITs of subjects from b_{4h} were also excised, only data from b_{2h} have been represented.

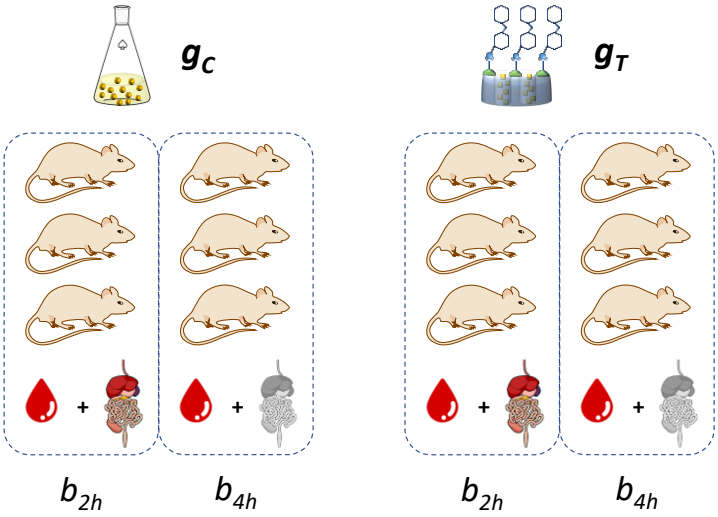

Scheme 3. Representation of the *in vivo* experiment's design. Animals were divided into two groups, one for free-*Cin* administration as control (g_C) and a second one for M41-Cin-L administration as trial group (g_T). Additionally, both groups were subdivided into two batches, in which digestion assay was stopped after 2 h (b_{2h}), and a second group where the digestion was allowed to complete during 4 h (b_{4h}). Plasma samples of all the subjects were considered, but only GIT sections of the b_{2h} group were considered, since they still maintain the treatments into the intestinal lumen (non-excreted).

3.6.1. Cin quantification in plasma samples: pharmacokinetic parameters

The variation with time of the *Cin* concentration in plasma for both groups of animals is shown in Figure 14, and the calculated values of different pharmacokinetic parameters are listed in Table 3. From the data shown in Figure 14 and Table 3, it can be seen that subjects from g_C group (animals treated with free *Cin*) showed maximum concentration of *Cin* molecule (C_{max}) at 45 min after dose administration (Figure 14, black line). However, the C_{max} value of subjects from g_T group (animals treated with M41-Cin-L) appears at 60 min, slightly more delayed (Figure 14, gray line). This difference can be related with the decrease in *Cin* permeability thanks to its protection into the hybrid system M41-Cin-L. As already mentioned above, and demonstrated with the results in section 3.5.1, *Cin* is a

lipophilic molecule with high permeability, whose absorption is produced almost immediately after gastric emptying. However, compound's protection in the M41-Cin-L system delays its release until the action of intestinal β-gal, which is also consistent with the *in vitro* permeability results described in section 3.5.1. Moreover, C_{max} obtained in the plasma samples for the M41-Cin-L system was 20% lower than the peak obtained for the free compound (0.22 and 0.15 mg/mL respectively), which in a possible co-administration of several drugs reduces the potential risk of adverse effects derived from drugs interaction.

The other two pharmacokinetic parameters are: the area under the curve (AUC), which is related to the total amount of compound in plasma, and the time at which half of cited compound has been metabolized ($t_{½}$). Based on these parameters, it can be seen that the amount of compound in the plasma is practically the same (almost identical AUC values, 31.02 and 30.76 for free *Cin* and M41-Cin-L, respectively), although the incorporation is faster for the free compound (lower $t_{½}$ value, 81.55 min compared with 93.67 min for M41-Cin-L). This again corroborates the decrease of the *Cin*-permeability when it is encapsulated inM41-Cin-L.

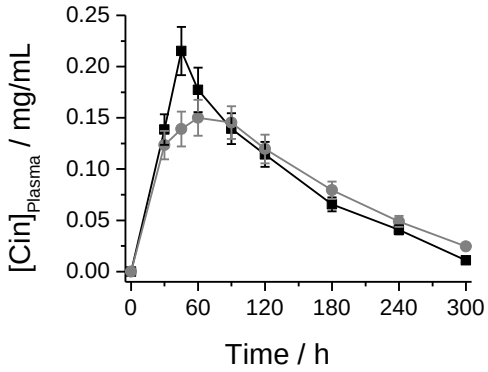

Figure 14. Cinnamaldehyde (*Cin*) concentrations in plasma and after oral administration of a dose of 13,6 mg *Cin* in the different formulations: free (black ■) or encapsulated into the M41-Cin-L microdevice (gray ●). The number of individuals in the groups were n = 6 up to 120 min, and n = 3 up to 240 min. Provided data represent data average, and error bars represent the standard deviation.

Table 3. Pharmacokinetic parameters calculated from plasma samples after oral administration of a Cin dose of 13.6 mg both free and encapsulated into M41-Cin-L microdevice.

Parameter	***Cin* free**	**M41-Cin-L**	**% Relative** (M41-Cin-L/Cin free)
t_{max}	45 min	60 min	↑ 33.3 %
C_{max}	0.22 mg/mL	0.17 mg/mL	↓ 31.8 %
AUC	31.02	30.76	↓ 0.8 %
$t_{½}$	81.55 min	93.67 min	↑ 14.9 %

3.6.2. Cin quantification in the GIT lumen

Finally, *Cin* concentration in the different intestine sections from the excised GIT was quantified. After 4 h of oral administration *Cin* levels in all the GIT sections (b_{4h}) were undetectable, both for the free-Cin and M41-EOC-L (data not shown). On the other hand, the obtained results after 2 h of digestion (b_{2h}) (Figure 15) show that although *Cin* levels are also negligible in almost all the GIT-sections when the compound was administered free, it's much higher when the treatment administration is performed with the M41-Cin-L system: until 20-fold higher in duodenum, 6-fold higher in jejunum, and 2-fold higher in ileum and colon.

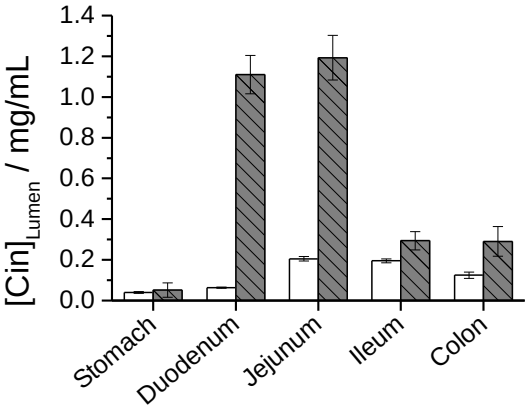

Figure 15. Cinnamaldehyde (*Cin*) concentrations in the detailed GIT sections after 2 h from an oral administration of a dose of 13,6 mg *Cin* in the different formulations: free (white bars) or encapsulated into the M41-Cin-L microdevice (gray stripped bars). The subjects' number was n = 3, provided data represent the data average, and error bars represent the standard deviation.

This distribution profile in the different sections of the GIT shows that the M41-Cin-L system is capable of prolonging the *Cin*-presence along the intestinal lumen compared to the administration of the free compound. This fact benefits the administration of *Cin* as potential antitumor drug to treat intestinal tract tumors in a more effective way, since the greater permanence in the intestinal lumen and the progressive action of the β-gal secreted along the SI would maintain the *Cin*-bioavailability. Furthermore, this microdevice may be suitable for other types of drugs intended to exert their effects in the intestine, such as other antitumor drugs, antiparasitic, anti-inflammatories, immunosuppressant, corticosteroids or any other bioactive compound whose target were the gut itself.

4. Conclusions

In this work, the ability of lactose of capping mesoporous silica particles (MSPs) loaded with essential oil components (EOCs) for controlled delivery specifically in small intestine conditions was investigated. The effects of the digestive process on the lactose-capped systems were studied using an *in vitro* digestion assay, after which no structural changes in the essayed solids were observed. Then, the interaction of lactose-gated systems with different *in vitro* and *in vivo* intestinal models was studied. Interaction with Caco-2 cells resulted in particle-internalization by the cells, and in a greater cell-viability-reduction by the cinnamaldehyde-loaded microdevice (M41-Cin-L) compared with the free compound. Interaction with an intestinal membrane model stablished from Caco-2 differentiation into enterocyte-like monolayers, demonstrated a Cin permeability decrease across the membrane by means of its encapsulation in M41-Cin-L. This permeability-reduction involves a progressive action of the M41-Cin-L system, in which a more sustained payload bioavailability is achieved compared with the obtained with the free EOC administration. Moreover, a pro-inflammatory effect of M41-Cin-L on the intestinal membranes, that could be a needed cell response to promote a curative action, was observed. Finally, the effect of M41-Cin-L was studied in an *in vivo* model of Wistar rat. Through these assays, the permeability reduction observed *in vitro* was confirmed. A reduction in cinnamaldehyde plasma levels was observed. Moreover, the distribution profile shows that the M41-Cin-L system is capable of prolonging the *Cin*-presence along the intestinal lumen compared to the administration of the free compound. This effect, together with the reported anti-cancer properties of Cin, makes the M41-Cin-L microdevice a system with potential use to treat tumors in distant sections of the small intestine and even the colon. The obtained results suggest that the M41-payload-L could be a potential hybrid microdevice for the protection and administration of other bioactive molecules whose action place is the small intestine and colon, such as anti-inflammatory, antiparasitic or other antitumor drugs.

Acknowledgements

The authors thank the financial support from the Spanish Government (projects RTI2018-100910-B-C41 and RTI2018-101599-B-C22-AR (MCUI/FEDER, EU)), the Agencia Estatal de Investigación and European Union through FEDER (Fondo Europeo de Desarrollo Regional, AEI/FEDER EU, project SAF2016-78756) and the Generalitat Valenciana (project PROMETEO 2018/024 and E.P-R. predoctoral grant ACIF/2016/023). The authors also thank the Electron Microscopy Service at the UPV for support.

References

1 À. Ribes, E. Aznar, S. Santiago-Felipe, E. Xifre-Perez, M. ángeles Tormo-Mas, J. Pemán, L. F. Marsal and R. Martínez-Mántild;ez, *ACS Sensors*, 2019, **4**, 1291–1298.

2 M. Oroval, C. Coll, A. Bernardos, M. D. Marcos, R. Martínez-Máñez, D. G. Shchukin and F. Sancenón, *ACS Appl. Mater. Interfaces*, 2017, **9**, 11332–11336.

3 C. Giménez, E. Climent, E. Aznar, R. Martánez-Máñez, F. Sancenón, M. D. Marcos, P. Amorós and K. Rurack, *Angew. Chemie - Int. Ed.*, 2014, **53**, 12629–12633.

4 B. de Luis, A. Llopis-Lorente, P. Rincón, J. Gadea, F. Sancenón, E. Aznar, R. Villalonga, J. R. Murguía and R. Martínez-Máñez, *Angew. Chemie - Int. Ed.*, 2019, **58**, 14986–14990.

5 A. Llopis-Lorente, P. Díez, A. Sánchez, M. D. Marcos, F. Sancenón, P. Martínez-Ruiz, R. Villalonga and R. Martínez-Máñez, *Nat. Commun.*, 2017, **8**, 1–7.

6 A. García-Fernández, E. Aznar, R. Martínez-Máñez and F. Sancenón, *Small*, 2020, **16**, 1–62.

7 J. W. Steed, J. L. Atwood and P. A. Gale, in *Supramolecular Chemistry: From Molecules to Nanomaterials*, eds. P. A. Gale and J. W. Steed, 2012, pp. 3–8.

8 C. Giménez, C. De La Torre, M. Gorbe, E. Aznar, F. Sancenón, J. R. Murguía, R. Martínez-Máñez, M. D. Marcos and P. Amorós, *Langmuir*, 2015, **31**, 3753–3762.

9 L. Pascual, C. Cerqueira-Coutinho, A. García-Fernández, B. de Luis, E. S. Bernardes, M. S. Albernaz, S. Missailidis, R. Martínez-Máñez, R. Santos-Oliveira, M. Orzaez and F. Sancenón, *Nanomedicine Nanotechnology, Biol. Med.*, 2017, **13**, 2495–2505.

10 J. Liu, B. Zhang, Z. Luo, X. Ding, J. Li, L. Dai, J. Zhou, X. Zhao, J. Ye and K. Cai, *Nanoscale*, 2015, **7**, 3614–3626.

11 V. Mamaeva, C. Sahlgren and M. Lindén, *Adv. Drug Deliv. Rev.*, 2013, **65**, 689–702.

12 M. Van Speybroeck, R. Mellaerts, J. A. Martens, P. Annaert, G. Van den Mooter and P. Augustijns, in *Controlled Release in Oral Drug Delivery*, eds. C. G. Wilson and P. J. Crowley, Springer US, New York, 2011, pp. 203–219.

13 S. Wang, *Microporous Mesoporous Mater.*, 2009, 117, 1–9.

14 M. Vallet-Regí, F. Balas and D. Arcos, *Angew. Chemie - Int. Ed.*, 2007, **46**, 7548–7558.

15 C. M. Sabliov and C. E. Astete, in *Delivery and Controlled Release of Bioactives in Foods and Nutraceuticals*, ed. N. B. T.-D. and C. R. of B. in F. and N. Garti, Woodhead Publishing, 2008, pp. 297–330.

16 A. Bernardos, E. Aznar, C. Coll, R. Martínez-Mañez, J. M. Barat, M. D. Marcos, F. Sancenón, A. Benito and J. Soto, *J. Control. Release*, 2008, **131**, 181–189.

17 Z. Mai, J. Chen, Y. Hu, F. Liu, B. Fu, H. Zhang, X. Dong, W. Huang and W. Zhou, *J. Colloid Interface Sci.*, 2017, **508**, 184–195.

18 L. Rashidi, E. Vasheghani-Farahani, K. Rostami, F. Gangi and M. Fallahpour, *Iran. J. Biotechnol.*, 2013, **11**, 209–213.

19 N. Gargiulo, I. Attianese, G. G. Buonocore, D. Caputo, M. Lavorgna, G. Mensitieri and M. Lavorgna, *Microporous Mesoporous Mater.*, 2013, **167**, 10–15.

20 M. Popova, A. Szegedi, V. Mavrodinova, N. Novak Tušar, J. Mihály, S. Klébert, N. Benbassat and K. Yoncheva, *J. Solid State Chem.*, 2014, **219**, 37–42.

21 V. Nairi, L. Medda, M. Monduzzi and A. Salis, *J. Colloid Interface Sci.*, 2017, **497**, 217–225.

22 X. Shi, Y. Wang, L. Ren, N. Zhao, Y. Gong and D. A. Wang, *Acta Biomater.*, 2009, **5**, 1697–1707.

23 A. H. Teruel, É. Pérez-Esteve, I. González-Álvarez, M. González-Álvarez, A. M. Costero, D. Ferri, M. Parra, P. Gaviña, V. Merino, R. Martínez-Mañez and F. Sancenón, *J. Control. Release*, 2018, **281**, 58–69.

24 A. García-Fernández, G. García-Laínez, M. L. Ferrándiz, E. Aznar, F. Sancenón, M. J. Alcaraz, J. R. Murguía, M. D. Marcos, R. Martínez-Máñez, A. M. Costero and M. Orzáez, *J. Control. Release*, 2017, **248**, 60–70.

25 C. A. Cheng, T. Deng, F. C. Lin, Y. Cai and J. I. Zink, *Theranostics*, 2019, 9, 3341–3364.

26 X. Xu, C. Wu, A. Bai, X. Liu, H. Lv and Y. Liu, *J. Nanomater.*, , DOI:10.1155/2017/2069685.

27 C. Murugan, K. Rayappan, R. Thangam, R. Bhanumathi, K. Shanthi, R. Vivek, R. Thirumurugan, A. Bhattacharyya, S. Sivasubramanian, P. Gunasekaran and S. Kannan, *Sci. Rep.*, 2016, **6**, 1–22.

28 A. Bernardos and L. Kourimská, *Czech J. Food Sci.*, 2013, 31, 99–107.

29 J. Florek, R. Caillard and F. Kleitz, *Nanoscale*, 2017, **9**, 15252–15277.

30 É. Pérez-Esteve, M. Ruiz-Rico, R. Martínez-Máñez and J. M. Barat, *J. Food Sci.*, 2015, **80**, E2504–E2516.

31 N. Garti, Ed., *Delivery and Controlled Release of Bioactives in Foods and Nutraceuticals*, Woodhead Publishing, Cambridge, England.

32 N. W. Clifford, K. S. Iyer and C. L. Raston, *J. Mater. Chem.*, 2008, **18**, 162–165.

33 É. Pérez-Esteve, M. Ruiz-Rico, R. Martínez-Máñez and J. M. Barat, in *Nanotechnology in Nutraceuticals: Production to Consumption*, eds. S. Sen and Y. Pathak, CRC Press, Boca Raton, 1st Editio., 2016, pp. 397–438.

34 T. Lea, in *The Impact of Food Bioactives on Health: In Vitro and Ex Vivo Models*, eds. K. Verhoeckx, P. Cotter, I. López-Expósito, C. Kleiveland, T. Lea, A. Mackie, D. Swiatecka, T. Requena and H. Wichers, Springer International Publishing, New York, 2015, pp. 103–111.

35 É. Pérez-Esteve, A. Fuentes, C. Coll, C. Acosta, A. Bernardos, P. Amorós, M. D. Marcos, F. Sancenón, R. Martínez-Máñez and J. M. Barat, *Microporous Mesoporous Mater.*, 2015, **202**, 124–132.

36 E. Poyatos-Racionero, É. Pérez-Esteve, M. Dolores Marcos, J. M. Barat, R. Martínez-Máñez, E. Aznar and A. Bernardos, *ChemistryOpen*, 2019, **8**, 1052–1056.

37 M. González-Alvarez, C. Coll, I. Gonzalez-Alvarez, C. Giménez, E. Aznar, M. C. Martínez-Bisbal, I. Lozoya-Agulló, M. Bermejo, R. Martínez-Máñez and F. Sancenón, *Mol. Pharm.*, 2017, **14**, 4442–4453.

38 A. H. Teruel, C. Coll, A. M. Costero, D. Ferri, M. Parra, P. Gaviña, M. González-Álvarez, V. Merino, M. D. Marcos, R. Martínez-Máñez and F. Sancenón, *Molecules*, 2018, **23**, 1–13.

39 M. M. Tajkarimi, S. A. Ibrahim and D. O. Cliver, *Food Control*, 2010, **21**, 1199–1218.

40 A. Bernardos, E. Piacenza, F. Sancenón, M. Hamidi, A. Maleki, R. J. Turner and R. Martínez-Máñez, *Small*, 2019, **15**, 1–34.

41 M. G. Miguel, *Molecules*, 2010, **15**, 9252–9287.

42 K. Lingan, *Transl. Med.*, 2018, **8**, 1–5.

43 F. Bakkali, S. Averbeck, D. Averbeck and M. Idaomar, *Food Chem. Toxicol.*, 2008, **46**, 446–475.

44 M. Inoue, S. Hayashi and L. E. Craker, *Pharmacogn. - Med. Plants*, 2019, 1–13.

45 F. Nazzaro, F. Fratianni, L. De Martino, R. Coppola and V. De Feo, *Pharmaceuticals*, 2013, **6**, 1451–1474.

46 Y. Hagenlocher, S. Satzinger, M. Civelek, K. Feilhauer, J. Köninger, S. C. Bischoff and A. Lorentz, *Mol. Nutr. Food Res.*, 2017, **61**, 1–9.

47 J. S. Muhammad, S. F. Zaidi, S. Shaharyar, A. Refaat, K. Usmanghani, I. Saiki and T. Sugiyama, *Biol. ^|^ Pharm. Bull.*, 2015, **38**, 109–115.

48 D. Bujňáková, Š. Juhás and Š. Faix, *Biol.*, 2013, **68**, 1000–1003.

49 R. D. C. Da Silveira E Sá, L. N. Andrade, R. D. R. B. De Oliveira and D. P. De Sousa, *Molecules*, 2014, **19**, 1459–1480.

50 L. K. Chao, K. F. Hua, H. Y. Hsu, S. S. Cheng, I. F. Lin, C. J. Chen, S. T. Chen and S. T. Chang, *Food Chem. Toxicol.*, 2008, **46**, 220–231.

51 A. Bukovská, Š. Čikoš, Š. Juhás, G. Il'ková, P. Rehák and J. Koppel, *Mediators Inflamm.*, , DOI:10.1155/2007/23296.

52 Š. Juhás, D. Bujňáková, P. Rehák, Š. Čikoš, S. Czikková, J. Veselá, G. Il'ková and J. Koppel, *Acta Vet. Brno*, 2008, **77**, 327–334.

53 X. Huang, Y. Liu, Y. Lu and C. Ma, *Int. Immunopharmacol.*, 2015, **26**, 265–271.

54 S. H. Hong, I. A. Ismail, S. M. Kang, D. C. Han and B. M. Kwon, *Phyther. Res.*, 2016, **30**, 754–767.

55 M. Thompson, E. M. Schmelz and L. Bickford, *J. Nutr. Food Sci.*, , DOI:10.4172/2155-9600.1000750.

56 M. T. Islam, A. B. R. Khalipha, R. Bagchi, M. Mondal, S. Z. Smrity, S. J. Uddin, J. A. Shilpi and R. Rouf, *IUBMB Life*, 2019, **71**, 9–19.

57 D. P. Bezerra, G. C. G. Militão, M. C. De Morais and D. P. De Sousa, *Nutrients*, 2017, **9**, 1–15.

58 K. I. Suhr and P. V. Nielsen, *J. Appl. Microbiol.*, 2003, **94**, 665–674.

59 K. Laird and C. Phillips, *Lett. Appl. Microbiol.*, 2012, **54**, 169–174.

60 X. J. Tian, X. W. Yang, X. Yang and K. Wang, *Int. J. Pharm.*, 2009, **367**, 58–64.

61 O. H. Chan and B. H. Stewart, *Drug Discov. Today*, 1996, **1**, 461–473.

62 A. Janatova, A. Bernardos, J. Smid, A. Frankova, M. Lhotka, L. Kourimská, J. Pulkrabek and P. Kloucek, *Ind. Crops Prod.*, 2015, **67**, 216–220.

63 H. Jaganathan and B. Godin, *Adv. Drug Deliv. Rev.*, 2012, **64**, 1800–1819.

64 E. Rascol, C. Pisani, C. Dorandeu, J. L. Nyalosaso, C. Charnay, M. Daurat, A. Da Silva, J. M. Devoisselle, J. C. Gaillard, J. Armengaud, O. Prat, M. Maynadier, M. Gary-Bobo, M. Garcia, J. Chopineau and Y. Guari, *Biomimetics*, , DOI:10.3390/biomimetics3030022.

65 B. Fadeel and A. E. Garcia-Bennett, *Adv. Drug Deliv. Rev.*, 2010, 62, 362–374.

66 I. Y. Kim, E. Joachim, H. Choi and K. Kim, *Nanomedicine Nanotechnology, Biol. Med.*, 2015, **11**, 1407–1416.

67 S. P. Hudson, R. F. Padera, R. Langer and D. S. Kohane, *Biomaterials*, 2008, **29**, 4045–4055.

68 R. Narayan, U. Y. Nayak, A. M. Raichur and S. Garg, *Pharmaceutics*, 2018, 10.

69 A. Yildirim, E. Ozgur and M. Bayindir, *J. Mater. Chem. B*, 2013, **1**, 1909–1920.

70 M. Yazdimamaghani, Z. B. Barber, S. P. Hadipour Moghaddam and H. Ghandehari, *Mol. Pharm.*, 2018, **15**, 2372–2383.

71 C. Fu, T. Liu, L. Li, H. Liu, D. Chen and F. Tang, *Biomaterials*, 2013, **34**, 2565–2575.

72 D. Guarnieri, P. Sánchez-Moreno, A. E. Del Rio Castillo, F. Bonaccorso, F. Gatto, G. Bardi, C. Martín, E. Vázquez, T. Catelani, S. Sabella and P. P. Pompa, *Small*, 2018, **14**, 1–11.

73 A. Alegría, G. Garcia-Llatas and A. Cilla, in *The Impact of Food Bioactives on Health: In Vitro and Ex Vivo Models*, eds. K. Verhoeckx, P. Cotter, I. López-Expósito, C. Kleiveland, T. Lea, A. Mackie, D. Swiatecka, T. Requena and H. Wichers, Springer International Publishing, 2015, pp. 3–12.

74 A. Mackie and N. Rigby, in *The Impact of Food Bioactives on Health: In Vitro and Ex Vivo Models*, eds. K. Verhoeckx, P. Cotter, I. López-Expósito, C. Kleiveland, T. Lea, A. Mackie, D. Swiatecka, T. Requena and H. Wichers, Springer International Publishing, 2015, pp. 13–22.

75 Y. Sambuy, I. De Angelis, G. Ranaldi, M. L. Scarino, A. Stammati and F. Zucco, *Cell Biol. Toxicol.*, 2005, **21**, 1–26.

76 I. J. Hidalgo, T. J. Raub and R. T. Borchardt, *Gastroenterology*, 1989, **96**, 736–749.

77 V. Meunier, M. Bourrié, Y. Berger and G. Fabre, *Cell Biol. Toxicol.*, 1995, **11**, 187–194.

78 A. Bernardos, E. Aznar, M. D. Marcos, R. Martínez-Máñez, F. Sancenón, J. Soto, J. M. Barat and P. Amorós, *Angew. Chemie - Int. Ed.*, 2009, **48**, 5884–5887.

79 E. H. Van Beers, R. H. Al, E. H. H. M. Rings, A. W. C. Einerhand, J. Dekker and H. A. Buller, *Biochem. J.*, 1995, **308**, 769–775.

80 M. I. M. Fernandes, L. C. Galvão, M. F. Bortolozzi, W. P. Oliveira, S. Zucoloto and M. L. P. Bianchi, *Disaccharidases and cell proliferation in anemic rats*, 1997, vol. 30.

81 T. D. Bolin, A. McKern and A. E. Davis, *Gastroenterology*, 1971, **60**, 432–437.

82 S. Cabrera, J. El Haskouri, C. Guillem, J. Latorre, A. Beltrán-Porter, D. Beltrán-Porter, M. D. Marcos and P. Amorós, *Solid State Sci.*, 2000, **2**, 405–420.

83 A. Popat, S. Jambhrunkar, J. Zhang, J. Yang, H. Zhang, A. Meka and C. Yu, *Chem. Commun.*, 2014, **50**, 5547–5550.

84 C. H. M. Versantvoort, A. G. Oomen, E. Van De Kamp, C. J. M. Rompelberg and A. J. A. M. Sips, *Food Chem. Toxicol.*, 2005, **43**, 31–40.

85 M. Thommes, K. Kaneko, A. V. Neimark, J. P. Olivier, F. Rodriguez-Reinoso, J. Rouquerol and K. S. W. Sing, *Physisorption of gases, with special reference to the evaluation of surface area and pore size distribution (IUPAC Technical Report)*, 2015, vol. 87.

86 É. Pérez-Esteve, M. Ruiz-Rico, C. De La Torre, E. Llorca, F. Sancenón, M. D. Marcos, P. Amorós, C. Guillem, R. Martínez-Máñez and J. M. Barat, *Microporous Mesoporous Mater.*, 2016, **230**, 196–207.

87 S. Mateen, M. T. Rehman, S. Shahzad, S. S. Naeem, A. F. Faizy, A. Q. Khan, M. S. Khan, F. M. Husain and S. Moin, *Eur. J. Pharmacol.*, 2019, **852**, 14–24.

88 F. A. Omonijo, S. Liu, Q. Hui, H. Zhang, L. Lahaye, J. C. Bodin, J. Gong, M. Nyachoti and C. Yang, *J. Agric. Food Chem.*, 2019, **67**, 615–624.

89 D. M. Liu, C. Y. Zhou, X. L. Meng, P. Wang and W. Li, *Trop. J. Pharm. Res.*, 2018, **17**, 1803–1810.

90 S. K. H. Huan, K. T. Wang, S. Der Yeh, C. J. Lee, L. C. Lin, D. Z. Liu and C. C. Wang, *Molecules*, 2012, **17**, 6277–6289.

91 L. M. Coussens and Z. Werb, *Nature*, 2002, **420**, 860–867.

92 B. Halamoda-Kenzaoui, M. Ceridono, P. Colpo, A. Valsesia, P. Urbán, I. Ojea-Jiménez, S. Gioria, D. Gilliland, F. Rossi and A. Kinsner-Ovaskainen, *PLoS One*, , DOI:10.1371/journal.pone.0141593.

93 J. Rejman, V. Oberle, I. S. Zuhorn and D. Hoekstra, *Biochem. J.*, 2004, **377**, 159–169.

94 L. Kou, J. Sun, Y. Zhai and Z. He, *Asian J. Pharm. Sci.*, 2013, **8**, 1–10.

95 D. C. Baumgart and A. U. Dignass, *Curr. Opin. Clin. Nutr. Metab. Care*, 2002, **5**, 685–694.

96 R. Goll and A. Van Beelen Granlund, *Scand. J. Gastroenterol.*, 2014, **50**, 3–12.

97 E. A. Alhinai, G. E. Walton and D. M. Commane, *Int. J. Mol. Sci.*, 2019, **20**, 1–12.

98 L. Antoni, S. Nuding, J. Wehkamp and E. F. Stange, *World J. Gastroenterol.*, 2014, **20**, 1165–1179.

99 M. G. Laukoetter, P. Nava and A. Nusrat, *World J. Gastroenterol.*, 2008, **14**, 401–407.

100 K. J. Maloy and F. Powrie, *Nature*, 2011, **474**, 298–306.

101 L. Thoo, M. Noti and P. Krebs, *Cell Death Dis.*, 2019, 10.

102 P. Artursson, K. Palm and K. Luthman, *Adv. Drug Deliv. Rev.*, 2001, **46**, 27–43.

103 T. Morishige, Y. Yoshioka, H. Inakura, A. Tanabe, S. Narimatsu, X. Yao, Y. Monobe, T.

Imazawa, S. I. Tsunoda, Y. Tsutsumi, Y. Mukai, N. Okada and S. Nakagawa, *Arch. Toxicol.*, 2012, **86**, 1297–1307.

104 S. Fritsch-Decker, Z. An, J. Yan, I. Hansjosten, M. Al-Rawi, R. Peravali, S. Diabaté and C. Weiss, *Nanomaterials*, , DOI:10.3390/nano9081172.

105 H. Chen, R. Zhao, B. Wang, C. Cai, L. Zheng, H. Wang, M. Wang, H. Ouyang, X. Zhou, Z. Chai, Y. Zhao and W. Feng, *NanoImpact*, 2017, **8**, 80–88.

106 T. Kucharzik, N. Lügering, H. G. Pauels, W. Domschke and R. Stoll, *Clin. Exp. Immunol.*, 1998, **111**, 152–157.

107 A. Georgantzopoulou, T. Serchi, S. Cambier, C. C. Leclercq, J. Renaut, J. Shao, M. Kruszewski, E. Lentzen, P. Grysan, S. Eswara, J. N. Audinot, S. Contal, J. Ziebel, C. Guignard, L. Hoffmann, A. T. J. Murk and A. C. Gutleb, *Part. Fibre Toxicol.*, , DOI:10.1186/s12989-016-0117-9.

108 M. Uguccioni, P. Gionchetti, D. F. Robbiani, F. Rizzello, S. Peruzzo, M. Campieri and M. Baggiolini, *Am. J. Pathol.*, 1999, **155**, 331–336.

109 U. P. Singh, N. P. Singh, E. A. Murphy, R. L. Price, R. Fayad, M. Nagarkatti and P. S. Nagarkatti, *Cytokine*, 2016, **77**, 44–49.

110 K. Sakai-Kato, M. Hidaka, K. Un, T. Kawanishi and H. Okuda, *Biochim. Biophys. Acta - Gen. Subj.*, 2014, **1840**, 1171–1180.

111 D. Ye, M. Bramini, D. R. Hristov, S. Wan, A. Salvati, C. Åberg and K. A. Dawson, *Beilstein J. Nanotechnol.*, 2017, **8**, 1396–1406.

6. GENERAL DISCUSSION

The present work can be simplified in two main facets. The first one is to design robust but simple controlled release systems, by using easily available biomolecules to take advantage of nature and the capacity of the human body to proceed with them. In this way, it is possible to design simple molecular gates that respond to stimuli naturally present in the gastrointestinal tract, in order to regulate the delivery of the payload loaded in the microdevice. The second facet is to focus on bioactive molecules present in nature and in food, to protect them through this technology while enhancing their intrinsic activity (antimicrobial activity, antioxidant or even anticancer capacity).

To achieve this double goal, inorganic silica materials (mesoporous particles and clays) have been used as supports due to their high load capacity and the ease chemical modification. Different (bio)molecules have been lodged into their cavities, and then the systems have been functionalized with gatekeepers of different nature: lipid, protein and disaccharide molecules. These three types of molecular gates define the three chapters into which this PhD thesis is divided. Also, the nature of the payload or the potential use of the corresponding microdevice is different in each chapter.

The presence of different biochemical conditions in the digestive processes has been the driving force for the selection of different gatekeepers. In order of appearance (and development) in this work these biochemical conditions are: bile salts, proteolytic enzymes, and lactase secretion.

First, bile salts are poured into the small intestine by the gallbladder, in the first intestinal stage, the duodenum. Although its lipid-emulsifier action has been known since ancient times, its use as a triggering stimulus for payload release has not been exploited in the literature. Therefore, a comprehensive study of a lipid moiety, oleic acid, has been carried out to verify its release control ability. The hydrophobic interactions between the hydrocarbon-tails of the anchored lipids are the closing force that maintain the cargo molecules confined. The bile salts surfactant action is the disrupting agent that break these interactions, thus allowing the payload's release in the duodenum. In **Article 1**, oleic acid demonstrated the

ability of entrapping the cargo in aqueous environments (H_2O, PBS) and even under the action of nonspecific enzymes (pronase, pepsin, pancreatin or esterase), while an effective payload's release was achieved in the presence of surfactant agents (SDS, CTAB, bile salts, etc.) This oleic acid-functionalization has managed to close the pores of materials with very diverse structures (**Article 2**), such as cylindrical mesopores (MCM-41, SBA-15), bimodal pores (UVM-7), three-dimensional pores (MCM-48) and interlaminar spacings of three different clays (saponite, hectorite and montmorillonite, **Article 3**). Thanks to this, different biomolecules have been protected and released in a controlled way, from small photolabile vitamins (vitamin B_2, **Article 1**) to complex and sensitive cofactors (vitamin B_{12} or iron coordinated to protoporphyrin IX -*heme* iron-, **Article 3**).

Secondly, in **Article 4**, the proteolytic action of the secretions produced in bacterial growth has been used as a stimulus that hydrolyzes the second designed gatekeeper, the zein protein of corn. Since the ultimate goal of the designed microdevice was to improve the antimicrobial action of different encapsulated essential oil components (EOCs), the secretion of bacterial proteases was the selected stimulus. Additionally, this system could also be used for gastrointestinal release of the loaded (bio)molecules, using as stimulus the proteolytic enzymes present in the gastrointestinal tract as pepsin or pancreatin. Returning to the objective of the work, different microdevices were synthesized with encapsulated EOCs, obtaining an efficient system for encapsulation of cinnamaldehyde. The encapsulation and controlled release processes performed with the EOC increased its antimicrobial capacity, decreasing its MBC from 250-500 ug/mL when it was free, to 73-145 ug/mL when it was incorporated into the designed microdevice.

Lastly, the secretion of lactose by the intestinal microvilli throughout the entire small intestine was chosen as the triggering stimulus of the last designed microdevice in **Article 5**. The objective of this microdevice was to release EOCs throughout the intestinal lumen, in order to improve their properties as possible anticancer drugs. In this way, the protection of the compounds inside the hybrid system reduces their volatility and increases their concentration, slowing down the

EOCs release, only through the action of lactose that hydrolyzes the gatekeeper, and decreasing their permeability through the membrane, lengthening their presence in the lumen. The microdevice design especially enhances the activity of cinnamaldehyde, since its interaction with *in vitro* models caused a greater pro-inflammatory response of the intestinal membranes (sometimes necessary for subsequent tissue recovery). Moreover, a decrease of the EOC permeability when it was encapsulated in the microdevice was also observed in the *in vivo* model, hence confirming the results obtained with the *in vitro* membranes. These results demonstrated a greater presence of the compound along the GIT of the subjects, thus enhancing the action of the encapsulated molecules.

Therefore, the compilation of the works developed here indicates that it is possible to use simple molecules available in nature as gatekeepers in organic-inorganic hybrid systems. These systems allow the protection and controlled release of active molecules from nature, or nutraceuticals, thus increasing their bioavailability. Although further research is necessary to verify the effectiveness of these systems, this work makes a contribution to the ongoing search for new drugs or systems with fewer side effects for several therapeutic applications.

7. CONCLUSIONS AND FUTURE PERSPECTIVES

Conclusions

In this PhD Thesis, different microdevices for cargo-controlled release have been developed. Several cargoes have been protected into the designed systems, such as model fluorophores (dyes) or natural biomolecules like vitamins or natural volatile compounds from plants. Moreover, the loaded molecules have been delivered upon the triggering action of a specific external stimulus.

In the **first chapter** of this PhD Thesis, the use of a new molecular gate of lipid nature has been described: oleic acid. This chapter has been subdivided into three articles. In the first one, the use of oleic acid as gatekeeper of controlled delivery systems based on Mesoporous Silica Particles (MSPs) loaded with cargo molecules has been reported. The hydrophobic interactions between the oleic acid-moieties are the closing force that maintain the cargo molecules entrapped into the pore voids. Different cargo molecules (rhodamine B and vitamin B_2) have been protected into the system, and delivered in a controlled way upon the triggering action of surfactant molecules, such as bile salts. The system has shown zero-release under different tested stimuli (pH variations, salting force and enzymatic action), whereas a markedly payload release has been produced when surfactant molecules were present.

Once oleic acid was validated as gatekeeper, it has been used in a second article to synthesize a set of four delivery systems by functionalizing different MSPs (MCM-41, MCM-48, SBA-15, UVM-7) with oleic acid. The rhodamine B release profiles from the microdevices, triggered by the bile salts' surfactant action, have been studied using four different mathematical models, demonstrating the dependence of the release-rate on the inorganic support. *In vitro* cell viability assays of Caco-2 cells treated with the microdevices have demonstrated the non-toxicity of the systems even at high particle concentrations. Finally, the rhodamine B absorption from the system with the fastest release kinetics (based on the UVM-7 support) has been compared with the absorption of the free compound in an *in vivo* model of Wistar rat. In this assay, a delay in the cargo absorption from the gated-microdevice has been observed compared with the administration of the

loaded compound (rhodamine B) in its free form, demonstrating that the triggering action of bile salts controls (and delays) the cargo's bioavailability.

In the third article of this chapter, oleic acid has been successfully used as gatekeeper of three different clays (montmorillonite, saponite and hectorite), benefiting from their ability as natural loadable materials. Different molecules have been protected into the synthesized organoclays, including two large biomolecules (hematin and cyanocobalamin). Oleic acid has demonstrated the ability of entrapping the cargo molecules also into the studied clays, and selectively release them under the action of surfactant molecules. The obtained release profiles have been studied using three different mathematical models, highlighting the dependence of the release kinetics on *(i)* the organic-inorganic hybrid system, *(ii)* the nature of loaded molecules and *(iii)* the cargo-support interaction. *In vitro* cell viability assays with Caco-2 cells have been performed, showing that standard organoclay concentrations are well tolerated by cells.

In the **second chapter**, the hydrolytic action of protease enzymes has been selected as triggering stimulus of a new controlled delivery system functionalized with a protein-gatekeeper. Here, a new antimicrobial microdevice based on MSPs loaded with essential oil components (EOCs) and gated with zein, a prolamin from corn, has been developed. For the microdevice's antimicrobial action, the bacterial proteolytic secretion has demonstrated to be the payload's release stimulus. The antimicrobial action of cinnamaldehyde (*Cin*) encapsulated inside the synthesized microdevice against *E. coli* has been enhanced when compared with the free compound. The developed microdevice, based on the combination of food-grade molecules and a biocompatible support, improves the antimicrobial properties of the loaded EOC by decreasing its volatility and increasing its local concentration.

Finally, in the **third chapter**, the ability of lactose of capping MSPs loaded with EOCs for their intestinal delivery has been investigated. The steric hindrance offered by the saccharide gatekeeper maintains the cargo molecules into the MSPs pore voids, which is disrupted by the hydrolyzing action of the lactase (β-galactosidase) secreted by the intestinal microvilli that allows the payload's release.

In vitro digestion assays have confirmed the absence of structural changes in to the system after the digestion process. *In vitro* cell culture assays have demonstrated *(i)* the particles' internalization by Caco-2 cells (human colorectal adenocarcinoma cells), *(ii)* the contact between particles and the intestinal brush border, and *(iii)* the EOC's permeability reduction across the intestinal membrane thanks to their encapsulation in the gated-microdevices. The greater Caco-2 cell-viability-reduction has been achieved by the *Cin*-loaded microdevice (M41-Cin-L), which also has produced a pro-inflammatory response from the intestinal membranes. For these reasons, the effect of M41-Cin-L has been studied in an *in vivo* model of Wistar rat, where a reduction in *Cin*-plasma levels and a *Cin*-lengthened stay into the intestinal lumen has been achieved thanks to the system's design. These features allow the potential use of *Cin* in the treatment of tumors in distant sections of the small intestine or the colon, or the use of the proposed design for the protection and administration of other bioactive molecules in the aforementioned action places.

As general conclusion of this PhD Thesis, different simple molecules from natural origin have been described as effective molecular gates of inorganic materials with several structures for controlled release applications. The designed systems have exemplary protected different nutraceuticals, and the controlled release of the payload has allowed the increase of its bioactivity. All the microdevices developed in this work are biocompatible, and their design can be extrapolated to other (bio)molecules whose action must be focused in different places of the gastrointestinal tract.

Future Perspectives

The side effects associated with different drugs, as well as pathogen's resistance to many others, are two major problems which tries to solve the biomedical research. New active compounds are continuously required to improve the existing treatments, or to replace them with other more effective or with less adverse effects.

The spotlight has shifted back to one of the sources that humans have been using since our origin, the Nature. Numerous compounds that have traditionally been used as home remedies around the world, today are studied through the tools of Science to take benefit of their active components. This is how a new branch of bioactive compounds has appeared to try to solve the aforementioned problems, the nutraceuticals. Naturally present in food, these compounds contribute to maintaining or improving the state of health, since they help directly or indirectly to balance the dysregulated metabolism of a sick individual.

On the other hand, a more sophisticatedly designed tool that aims to improve the properties of existing treatments is Nanotechnology. Several controlled release systems aiming to increase the bioavailability of bioactive compounds are proposed as potent alternatives. The encapsulation of these compounds in mesoporous silica particles is the proposal detailed in this Thesis as one of the possible solutions for the protection and controlled release of several compounds, both traditional drugs and nutraceuticals.

There are still some steps to take in order to ensure the implementation of this nanotechnological solution, where research plays a fundamental role. To increase the knowledge on the biological behavior of these systems in the body, how the organism degrades or excretes them, and how to make them 100% biocompatible and bioavailable can offer an incredibly versatile therapeutic tool to solve many of the biomedical problems that blame humanity.

Therefore, aiming to unite Nature, Nanotechnology and Knowledge, this PhD Thesis project has sought to contribute to the understanding of simple, resistant

and more biocompatible nutraceutical-controlled release systems. From the trajectory drawn by this work, different research works could be followed in future, such as *(i)* applying the molecular gates designed to other inorganic materials different from the used in this work, *(ii)* encapsulating different compounds such as drugs or other nutraceuticals, or *(iii)* selecting other different gastrointestinal stimuli as triggers for controlled release. Furthermore, in the field of systems-testing, (*iv*) other cellular and/or tissue models could be used, such as other cell lines different from Caco-2, or (*v*) 3D cultures or organoids to further strengthen the biocompatibility of the designs.

8. APPENDICES

Appendix I. List of publications included in this thesis

E. Poyatos-Racionero, É. Pérez-Esteve, M. Dolores Marcos, J. M. Barat, R. Martínez-Máñez, E. Aznar, A. Bernardos. New Oleic Acid-Capped Mesoporous Silica Particles as Surfactant-Responsive Delivery Systems. *ChemistryOpen* **2019**, *8*, 1052. *doi: 10.1002/open.201900092*

Poyatos-Racionero, E.; González-Álvarez, I.; González-Álvarez, M.; Martínez-Máñez, R.; Marcos, M.D.; Bernardos, A.; Aznar, E. Surfactant-Triggered Molecular Gate Tested on Different Mesoporous Silica Supports for Gastrointestinal Controlled Delivery. *Nanomaterials* **2020**, *10*, 1290. *doi: 10.3390/nano10071290*

E. Poyatos-Racionero, É. Pérez-Esteve, E. Aznar, J. M. Barat, R. Martínez-Máñez, M. Dolores Marcos, A. Bernardos. Gated-organoclays for large biomolecules-controlled release triggered by surfactant stimulus. *Submitted to Acta Biomaterialia*.

E. Poyatos-Racionero, G. Guarí-Borràs, M. Ruiz-Rico, E. Aznar, J. M. Barat, R. Martínez-Máñez, M. Dolores Marcos, A. Bernardos. Towards the Enhancement of Essential Oil Components Antimicrobial Activity Using New Zein-Protein-Gated Mesoporous Silica Microdevices. *Submitted to Journal of Molecular Sciences*.

E. Poyatos-Racionero, I. González-Álvarez, P. Sánchez-Moreno, L. Sitia, F. Gatto, P.P. Pompa, E. Aznar, M. González-Álvarez, R. Martínez-Máñez; M.D. Marcos, A. Bernardos. Lactose-gated mesoporous silica particles for essential oil components-controlled delivery along the intestine. A study of their *in vitro* and in vivo interaction. *Submitted to Journal of Controlled Release*.

Appendix II. Other scientific publications

Poyatos-Racionero E, Ros-Lis JV, Vivancos J-L, Martínez-Máñez R. Recent advances on intelligent packaging as tools to reduce food waste. *J Clean Prod*. **2018**; 172:3398-3409. *doi: 10.1016/j.jclepro.2017.11.075*